Terms and Conditions of Use of Digitised Theses from Trinity College Library Dublin

Copyright statement

All material supplied by Trinity College Library is protected by copyright (under the Copyright and Related Rights Act, 2000 as amended) and other relevant Intellectual Property Rights. By accessing and using a Digitised Thesis from Trinity College Library you acknowledge that all Intellectual Property Rights in any Works supplied are the sole and exclusive property of the copyright and/or other IPR holder. Specific copyright holders may not be explicitly identified. Use of materials from other sources within a thesis should not be construed as a claim over them.

A non-exclusive, non-transferable licence is hereby granted to those using or reproducing, in whole or in part, the material for valid purposes, providing the copyright owners are acknowledged using the normal conventions. Where specific permission to use material is required, this is identified and such permission must be sought from the copyright holder or agency cited.

Liability statement

By using a Digitised Thesis, I accept that Trinity College Dublin bears no legal responsibility for the accuracy, legality or comprehensiveness of materials contained within the thesis, and that Trinity College Dublin accepts no liability for indirect, consequential, or incidental, damages or losses arising from use of the thesis for whatever reason. Information located in a thesis may be subject to specific use constraints, details of which may not be explicitly described. It is the responsibility of potential and actual users to be aware of such constraints and to abide by them. By making use of material from a digitised thesis, you accept these copyright and disclaimer provisions. Where it is brought to the attention of Trinity College Library that there may be a breach of copyright or other restraint, it is the policy to withdraw or take down access to a thesis while the issue is being resolved.

Access Agreement

By using a Digitised Thesis from Trinity College Library you are bound by the following Terms & Conditions. Please read them carefully.

I have read and I understand the following statement: All material supplied via a Digitised Thesis from Trinity College Library is protected by copyright and other intellectual property rights, and duplication or sale of all or part of any of a thesis is not permitted, except that material may be duplicated by you for your research use or for educational purposes in electronic or print form providing the copyright owners are acknowledged using the normal conventions. You must obtain permission for any other use. Electronic or print copies may not be offered, whether for sale or otherwise to anyone. This copy has been supplied on the understanding that it is copyright material and that no quotation from the thesis may be published without proper acknowledgement.

Design, Synthesis and Physical Evaluation of Luminescent Lanthanide-based Supramolecular Systems

Floriana Stomeo
October 2006

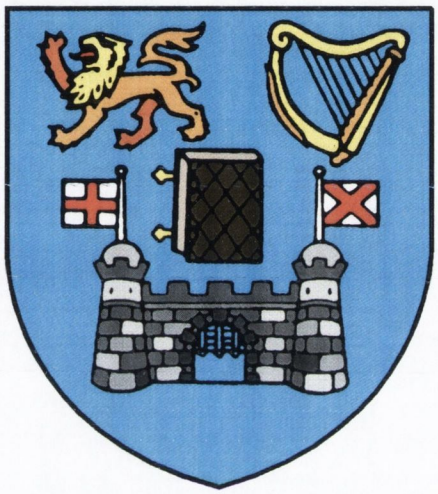

University of Dublin Trinity College

Based on research carried out under the direction of
Prof. Thorfinnur Gunnlaugsson (TCD)
and Dr. Colin P. McCoy (QUB)

A thesis submitted to the School of Chemistry, University of Dublin, Trinity College for the degree of Doctor of Philosophy

DECLARATION

This thesis has not been submitted as an exercise for a degree at any other university. Except where stated, the work described therein was carried out by me alone.

I give permission for the Library to lend or copy this thesis upon request.

Signed:

Floriana Stomeo

Declaration

This thesis is submitted for the degree of Doctor of Philosophy to the University of Dublin, Trinity College and has not been submitted for any degree or examination to this or any other University. Other than where acknowledged, all work described herein is original and carried out by the author.

Floriana Stomeo

Floriana Stomeo

Abstract

This thesis entitled "Design, Synthesis and Physical Evaluation of Luminescent Lanthanide-based Supramolecular Systems" is divided into five chapters, and is in two parts. The first part, Chapter 2, deals with the synthesis and characterisation of naphthalimide-based and lanthanide-based luminescent pH sensors, for incorporation into hydrogels. The second part, Chapters 3 and 4, describes the design and the physical studies of chiral Eu^{III}-based triple helicates, in partially aqueous and organic media.

Chapter 1 introduces the field of lanthanide-based supramolecular systems, giving an overview of the advances made in this area in recent times. The principles and advantages of lanthanide luminescent sensing are illustrated and a review of various lanthanide luminescent supramolecular assemblies is presented. Finally, a description of the main features and applications of hydrogels, in the field of molecular recognition and sensing, is outlined.

Chapter 2 is divided in two sections; the first part deals with the synthesis and characterisation of fluorescent naphthalimide-based pH sensors in solution and incorporated into water permeable soft materials. The pK_a values obtained for these naphthalimide-based sensors indicate that both sensors are suitable for monitoring the pH changes in the physiological range. The fluorescent sensors are incorporated into a hydrogel matrix without being covalently bound to the hydrogel polymeric network. The emission properties of the resulting polymeric films, investigated using confocal laser-scanning microscopy, are switched "*on*" or "*off*" as a function of pH, mirroring the behaviour in aqueous solution. The second section of Chapter 2 covers the study, in solution and in soft materials, of a Eu^{III}-cyclen based luminescent pH sensor. The synthesis and characterisation of the cyclen-based ligand and the corresponding Eu^{III} complex are described. Potentiometric and spectroscopic techniques are used to monitor the behaviour of both ligand and complex in aqueous solution. The protonation constants of both ligand and Eu^{III} complex and the metal complex ion stability constants are dependent on the choice of the Eu^{III} counteranion. The Eu^{III} emission of the complex exhibits high pH sensitivity, with the emission being reversibly switched '*off-on*' as a function of pH in solution. The non-covalent incorporation of the Eu^{III} complex into three compositions of hydrogel is detailed. The emission of these water-permeable materials is also highly pH sensitive and reversible.

Chapter 3 discusses the synthesis, characterisation, potentiometric and photophysical studies of two chiral bis-tridentate ligands and their corresponding Eu^{III} complexes in a partially aqueous solution of CH_3CN/H_2O (80:20; v/v). Molecular mechanics calculations followed by geometry optimisation are consistent with the proposed dinuclear triple helicate model for the two Eu^{III} complexes. ^{1}H-NMR spectroscopy also confirmed that the complexes exist in solution in their *rac*-form (helical). Potentiometric titrations of the ligands and determination of the metal complex ions stability constants in CH_3CN/H_2O (80:20; v/v) are described. UV-Vis, fluorescence and lanthanide luminescence pH titrations highlight the importance of the deprotonation of the metal bound water molecules and that of the amide moieties in the photophysical properties of the complexes.

Chapter 4 presents the study of the dinuclear triple helical Eu^{III} complexes in CH_3CN and in $CH_3CN/CHCl_3$ (50:50) solution. Several spectroscopic techniques, ^{1}H-NMR, CD, CPL, UV-Vis and luminescence spectroscopy, are used in order to gain insight in the formation of the desired dinuclear triple helical species, Eu_2L_3, in solution. The analysis of these data highlights the importance of the time scale of the experiment, the polarity of the solvent, the counterion and the chirality of the ligands in the formation of the helical Eu_2L_3 complexes.

Finally, Chapter 5 outlines the experimental procedures used in Chapters 2, 3, and 4, and presents the characterisation of the novel compounds prepared.

Acknowledgements

I would like to sincerely thank both my supervisors, Prof. Thorri Gunnlaugsson and Dr. Colin McCoy, for all their time, support and advice during my PhD, and for their enthusiasm throughout the whole adventure!

A huge GRAZIE to my TG family! Thanks Andrew, Ann Marie, Celine, Cidalia, Claire, Danny, Debbie, Doireann, Emma, Eoin, Fred, Gary, Jilly, Joe, Julie, Julien, Katell, Lin, Lisa, Niamh, Raman, Rebecca, Sally, Susan, and all the new entries, Christophe, Jennifer, Célia! Thanks for all your help and patience, the good times and good fun!

A big thankyou to Joe for being my guide over the past four years and for I know that I can always count on you! Thanks Josephino! Thanks to Lin and Céline for their friendship, for listening to me, for always being there! Thanks to Debbie and Eoin for being my office mates over the last two months, for all your help and for always answering to my "How do I say this?" Thanks very much guys! A very special THANKYOU goes to Sally; I really don't know what I would have done without you! Thanks for all your time, in the lab, in our penthouse, in the pub; thanks for your optimism, your encouragement, your motivation! Thanks Sally!

I would also like to thank Dr. Paul Kruger for his help with the MM studies and for clearing up the fog on helicates!!! Thanks to Dr. Peacock in Glasgow for the use of the CPL machine. Thanks must go to all the staff in the Chemistry department, including Dr. John O'Brien and Dr. Manuel Ruether for all their help with the NMRs. Thanks to Martin, for all the assistance with the mass spec. To Sandrine and Tom McCabe for all the attempts to get a crystal structure, as well as the technicians Fred, Ed, Patsy, Brendan, Mark and Peggy. Thanks to Theresa Mc Donald for all her assistance. And thank you to the secretaries Corrine, Tess and Helen.

Grazie Roberta for your vitality and for all the good times together! Grazie Silvia for all our chats and for all your advice! Thanks to the Ahern family for their warm welcome to my irish life! Grazie mille to everybody in Caffé di Napoli; it's great to have a piece of Italy just around the corner! Thanks to all my Italian friends….. Faraway, so close!

I really can't find the words to thank my fantastic family! Grazie mamma, papá, Marco e Maria Teresa, Checca, Antonio, nonno Rocco, nonnina, zia Maria and our new treasure Matilda! I couldn't have asked for more! Grazie a tutti!

And finally, thanks to the love of my life, for his encouragement, his positive vibes, his love; thanks for inspiring my days! Grazie Blessing!

Abbreviations

Abs	absorbance
β	overall stability constant
bipy	bipyridine
br	broad
$CHCl_3$	chloroform
CH_2Cl_2	dichloromethane
CH_3CN	acetonitrile
Cyclen	1,4,7,10-tetraazacyclododecane
χ^2	chi squared
[ ]	concentration
δ	chemical shift
d	doublet
DCM	dichloromethane
DMF	*N,N*-dimethyl formamide
DMSO	dimethyl solfoxide
DNA	deoxyribonucleic acid
ε	molar extinction coefficient
EDTA	ethylenediamine tetraacetic acid
ES	electrospray
ES-MS	electrospray mass spectrometry
Et	ethyl
EtOH	ethanol
h	hour
HCl	hydrochloric acid
$HClO_4$	perchloric acid
HEPES	4-(2-hydroxyethyl)-1-piperazineethanesulfonic acid
HMQC	hetronuclear multiple quantum correlation
HOMO	highest occupied molecular orbital
HPLC	high performance liquid chromatography
IR	infra red
ISC	inter system crossing
J	coupling constant

K	apparent stability constant
K_a	acid dissociation constant
Khphthalate	potassium hydrogen phthalate
L	unspecified ligand
Lit.	literature
Ln	lanthanide
Ln^*	lanthanide excited state
log	logarithm (base 10)
LUMO	lowest unoccupied molecular orbital
m	multiplet
M^{n+}	unpecified metal ion
m/z	mass to charge ratio
MeOH	methanol
NEt_4Br	tetraethylammonium bromide
NEt_4ClO_4	tetraethylammonium perchlorate
NMR	nuclear magnetic resonance
PET	photo induced electron transfer
Ph	phenyl
pH	$-\log[H_3O^+]$
pKa	$-\log[K_a]$ where K_a is the acidity constant
pM	-log[M]
Phen	phenanthroline
ppm	parts per million
S^0	singlet ground state
S^1	first excited singlet state
T^1	first excited triplet state
THF	tetrahydofuran
TLC	thin layer chromatography
TRIS	tris(hydroxymethyl)aminomethane
Trif	triflate (trifluorosulfonate)
UV	ultra violet
ν	frequency
μ	micro (x 10^{-6})
λ	wavelenght

1 INTRODUCTION

1.1 Lanthanide metal ions

The unique magnetic and photophysical properties of the metals in the lanthanide series have attracted large interest over the past years, due to their potentials in medical diagnostics,[1] optical imaging,[2] and high technological applications.[3] The importance of lanthanides for magnetic and optical materials has long drawn attention to their physical properties and solid-state chemistry, which have been extensively studied.[4] More recently however, the development of contrast agents for medical magnetic resonance imaging (MRI) and luminescent chemosensors for optical imaging of cells[5] has shifted the focus towards their coordination chemistry in solution.

Within this chapter an overview of the features of the lanthanide ions will be presented along with some salient examples of their use in the field of supramolecular chemistry.

1.1.1 Properties and advantages

Despite their name "*rare earth elements*", lanthanides are in fact not especially rare: each is more common in the earth's crust than silver, gold or platinum. They possess characteristic 4*f* open-shell configurations and exhibit a close chemical resemblance across the periodic series due to the small and regular decrease in their ionic radii. This decrease in radii is known as the lanthanide contraction.[5] Their most stable oxidation state is +3, particularly in water, with a [Xe]$4f^n$ configuration. The lanthanide ions possess relatively high charge densities and have a strong electrostatic nature in their bonding, as the ions are polarising and hard Lewis acids. They can coordinate to a variety of ligands with different coordination numbers, most typically eight to ten. The hard Lewis acidity of the lanthanide ions results into a specific preference towards ligands incorporating atoms which can act as hard Lewis bases or can be easily polarised. Therefore, combinations of amines and carboxylic groups are commonly used in lanthanide complexation.[2] Indeed, one of the most popular ligands in the complexation of lanthanides is 1,4,7,10-tetrakiscarboxymethyl-1,4,7,10-tetraazacyclododecane (commonly known as DOTA). Its popularity is largely due to its use as a magnetic resonance contrast agent with gadolinium,[6,7] where the ion

coordinates to the four nitrogens of the cyclen ring and the four carboxylates of the pendent arms, giving rise to an octa-coordination environment.

The role played by the lanthanide ions in many supramolecular systems is mostly based on their optical features and coordination requirements. Lanthanides present special spectroscopic properties due to the shielding of the 4*f* orbitals, with forbidden intraconfiguration *f-f* electronic transitions resulting in very low extinction coefficients (ε typically 0.1 $mol^{-1}dm^3cm^{-1}$)[8] and characteristic narrow line-like emission bands, mostly in the visible and near infrared ranges. Most of the lanthanide ions are luminescent, some more than others. Their emission depends on how efficiently their excited state(s) can be populated and their non-radiative deactivation pathways minimised. The main advantage is that the *f-f* electronic transitions are easily recognisable for they are independent from the chemical environment of the ion. They can be either fluorescent (*e.g.* Pr^{III}, Nd^{III}, Ho^{III}, Er^{III}, and Yb^{III}) or phosphorescent (*e.g.* orange Sm^{III}, red Eu^{III}, Gd^{III} which emits in the UV, green Tb^{III}, yellow Dy^{III} and blue Tm^{III}),[4] following the IUPAC rules regarding molecular luminescence spectroscopy.[9] According to these rules, the term "fluorescence" refers to processes which occur without change in spin, typically $S_1 \rightarrow S_0$ or $Yb(^2F_{5/2} \rightarrow {}^2F_{7/2})$ transitions, and the term "phosphorescence" to transitions involving a change in spin, typically $T_1 \rightarrow S_0$ or Eu ($^5D_4 \rightarrow {}^7F_J$, J = 0-4) transitions.[5] Two ions, La^{III} and Lu^{III}, have no *f-f* transitions and are therefore not luminescent. Typical luminescence spectra of Sm^{III}, Eu^{III}, Tb^{III}, and Dy^{III} are shown in Figure 1.1.

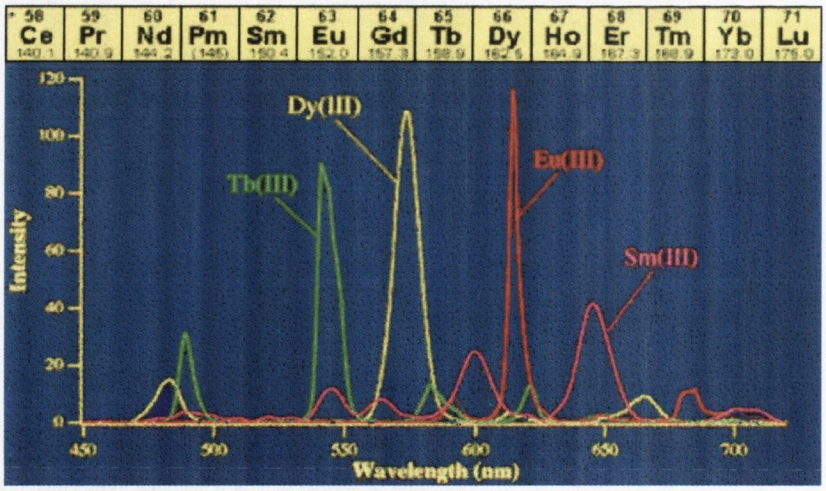

Figure 1.1 Typical emission spectra of luminescent lanthanide complexes of Sm^{III}, Eu^{III}, Tb^{III}, and Dy^{III}.[10] Inset: the lanthanide series.

The intrinsic luminescence quantum yields are highly dependent on the energy gap between the lowest lying excited state and the highest sublevel of the ground state (Figure 1.2). The smaller this gap the higher the possibility for the metal ion to undergo non-radiative deactivation processes, for instance through high energy vibrations such as O-H.

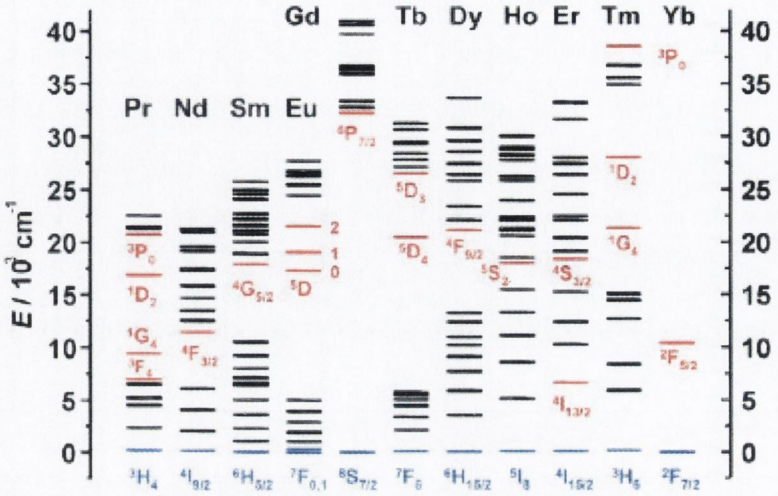

Figure 1.2 Partial energy diagram for the lanthanide aquo ions showing the ground state (blue) and the most luminescent excited states (red).[11]

In terms of energy gap, Eu^{III} (ΔE = 12300 cm^{-1}, $^5D_0 \rightarrow {}^7F_6$), Gd^{III} (ΔE = 32200 cm^{-1}, $^6P_{7/2} \rightarrow {}^8S_{7/2}$) and Tb^{III} (ΔE = 14800 cm^{-1}, $^5D_4 \rightarrow {}^7F_0$) are the best ions for an efficient population of their excited states. However, while Eu^{III} and Tb^{III} emit in the visible region of the spectrum, Gd^{III} emits in the UV. This makes the latter unsuitable as a luminescent probe for bio-analyses due to the absorption and emission interference (light scattering, *etc.*) from the organic part of the complexing molecule. The sizable energy gap displayed by Eu^{III} and Tb^{III} explains why luminescent probes containing these ions have been so popular during the last decade. Besides Sm^{III} (ΔE = 7400 cm^{-1}, $^4G_{5/2} \rightarrow {}^6F_{11/2}$) and Dy^{III} (ΔE = 7850 cm^{-1}, $^4F_{9/2} \rightarrow {}^6F_{3/2}$), which have been employed in dual luminescent time-resolved immunoassays,[12,13] the other lanthanide ions have not found similar applications, due to their very low quantum yield in aqueous solution.[5] Pr^{III} emits both in the visible and near-infrared (NIR) ranges[14] and is often a component of solid state optical materials. This is due to its blue up-conversion, that is the blue emission from $^3P_0$ upon two- or three-photon pumping into the $^1G_4$ or $^1D_2$ states.[15] Thulium is a blue emitter from its $^3P_0$, $^1D_2$, and $^1G_4$ levels and is used as such in electroluminescent devices;[3] it is known to be one of the first ions having shown up-conversion.[15] The ions Nd^{III}, Dy^{III}, Ho^{III}, and Er^{III} also display up-conversion processes.[5] Moreover, Nd^{III}, Ho^{III}, Er^{III}, and Yb^{III} have stirred particular interest in the design of lasers (especially Nd^{III}) and telecommunication devices owing to

their ability to emit in the NIR part of the electromagnetic spectrum.[16] In addition, Nd^{III}, Er^{III}, and Yb^{III} have been recently employed in the development of luminescent probes for time-resolved imaging of biological tissues, as they are able to efficiently transmit light in the NIR spectral range.[17-19]

The lanthanide(III) ions have the advantage of possessing long excited state lifetimes, provided that deactivations by non-radiative pathways are minimised. The lifetime of emission from the excited state of the lanthanide ions falls in the range of microseconds (*e.g.* Yb, Nd) to sub-milliseconds (*e.g.* Eu and Tb).[20] Such long-lived emissions have led to numerous applications of lanthanide-based systems as luminescent probes and sensors.[2,4,20] This is due to the possibility of time-resolved detection, which allows a relatively easy discrimination between the desired luminescent signal and the autofluorescence of the background. Such methods are based on a delay set between the excitation of the probe and the measurement of the lanthanide luminescence, so that the shorter-lived (ns time frame) fluorescence and light scattering of the biological background (autofluorescence) , decay to negligible levels (Figure 1.3).[8] This provides good signal to noise ratio, which enables more accurate determination of the analyte in real-time.

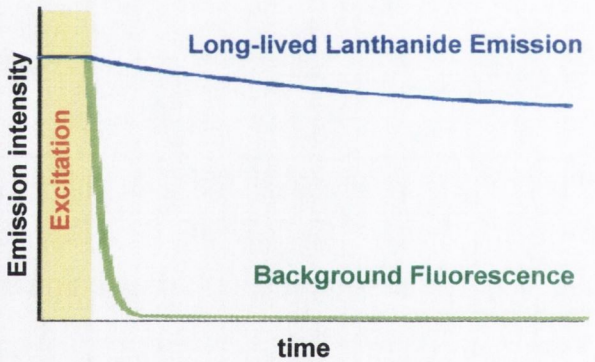

Figure 1.3 Lanthanide ions possess a long lived excited state which continues to emit long after background fluorescence has dispersed.

The main drawback to the use of the lanthanide ions for such assays is their low absorption coefficients, resulting in inefficient direct excitation,[21] unless a very intense light source is used. Laser radiation is suitable, provided that the radiation matches closely the energy gap between the ground state and the emissive excited state of the lanthanide ion. The two most widely-used emissive lanthanide ions, Tb^{III} and Eu^{III}, may be excited in this way by the 488 nm line of an argon ion laser (which matches the $^7F_6 \rightarrow {}^5D_4$ energy

transition) and by rhodamine 110 in a dye laser (*e.g.* the $^7F_0 \rightarrow {}^5D_0$ transition at 580 nm or the $^7F_2 \rightarrow {}^5D_1$ at 557 nm), respectively.[8]

The alternative and most versatile way to address this problem is to use appropriate chromophores (*e.g.* polyaromatics) as sensitisers or *antennae*, which can pass on their excited state energy to the lanthanide excited state. Such indirect excitation takes advantage of the generally high extinction coefficients of the employed chromophore/antenna. The sensitisation process, schematically represented in Figure 1.4, can be summarised as follows:

- The antenna (denoted Ar in Figure 1.4 a) absorbs the excitation energy producing a singlet-excited state (^{1}Ar).
- The energy is passed to the triplet state of the antenna (^{3}Ar) *via* inter system crossing (ISC).
- The energy is transferred to the lanthanide ion (*Ln) by means of an intramolecular energy transfer (ET).
- The excited state of the Ln^{III} relaxes to the ground state with characteristic emission bands.

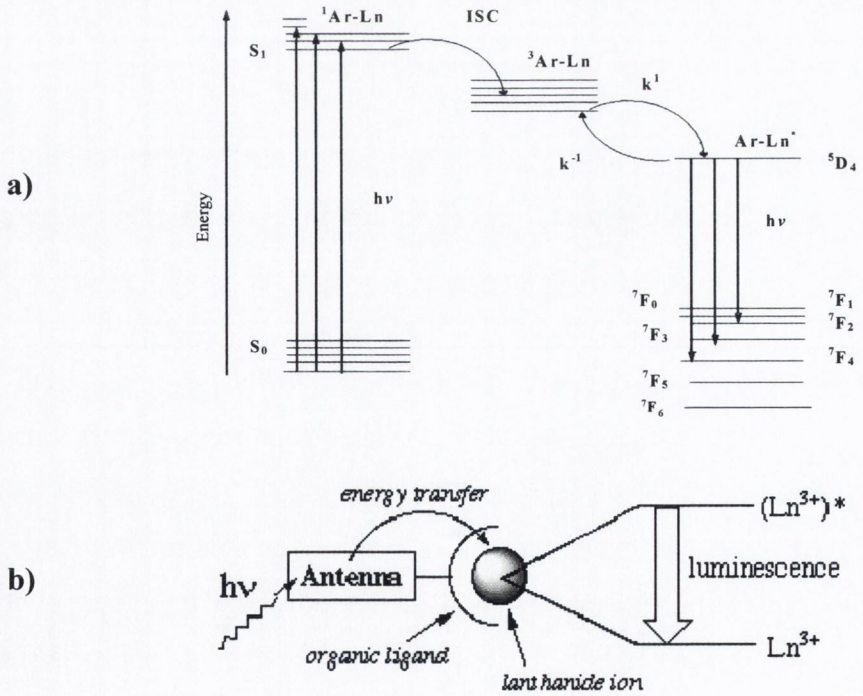

Figure 1.4 a) Jablonski diagram illustrating sensitisation of a lanthanide ion. b) Schematic representation of the sensitisation process.[10]

Singlet and triplet excited states share a common geometry where their potential curves intersect (Figure 1.5); however, intersystem crossing from an S_1 to a T_1 is a spin forbidden process. Nevertheless, singlet-triplet transitions may occur in the presence of spin-orbit coupling which is largely promoted by the presence of heavy atoms (*e.g.* lanthanides).[22]

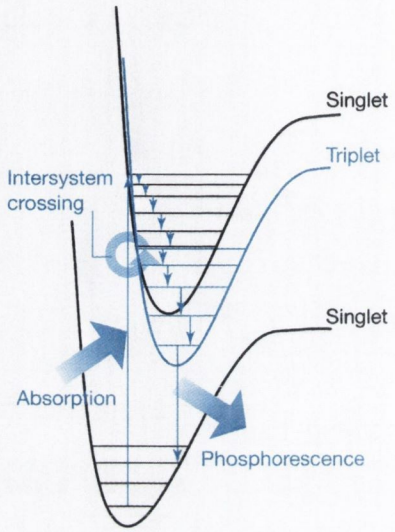

Figure 1.5 Potential energy wells showing vibrational levels. Note the overlapping of the T_1 and S_1 states. Intersystem crossing (ISC) from a singlet to a triplet excited state is made possible by spin-orbit coupling.[22]

As for the energy transfer from the triplet state of the antenna to the lanthanide centre ($^3Ar \rightarrow {}^*Ln$), two possible mechanisms exist: the Förster energy transfer mechanism[23] and the Dexter mechanism.[24,25] The former involves overlap of energy levels and it is described in terms of an interaction between the transition dipole moments (a dipolar mechanism). The energy transfer occurs through space and has r^{-6} distance dependence, where r is the distance between the metal ion and the excited chromophore/*antenna*. Consequently, the energy transfer process can be made more efficient by minimising the distance between the lanthanide ion and the *antenna*. In the Dexter mechanism, the energy transfer occurs as a result of an electron exchange between the excited chromophore and the metal ion in a through-bond interaction with an e^{-r} dependency. Again the process can be made more efficient by minimising the distance r.

The sensitisation process can be achieved by either covalently attaching the sensitiser molecules to an organic ligand, which is able to complex a lanthanide ion,[26] or by the direct coordination of sensitiser molecules to the lanthanide ion.[27] When population

occurs, the luminescence efficiency of a lanthanide ion depends on several factors: (1) efficiency of the $S_1 \rightarrow T_1$ intersystem crossing; (2) efficiency of energy transfer from the triplet state to the lanthanide centre ($T_1 \rightarrow Ln^*$); (3) radiation efficiency of the lanthanide complex (Φ_{Ln}); and (4) quenching efficiency by non-radiative means.[28]

Among these factors, the non-radiative quenching process is the most important in determining the luminescence quantum yield. Non-radiative deactivation may occur through energy transfer to vibrational modes which match the energy of the excited state of the lanthanide ion. High frequency vibrations, such as those of O-H, N-H, and even C-H oscillators, strongly dissipate the energy of the lanthanide excited state resulting in quenching of the lanthanide luminescence.[29,30] The lower the excited state energy of the lanthanide earth ion, the more efficient the energy dissipation process. Therefore, direct coordination of water and other solvent molecules to the lanthanide centre has a large effect on the deactivation of the excited state through non-radiative paths, and on the efficiency and lifetime of the emission process.[8]

In order to minimise vibration-induced deactivation processes, a rigid metal-ion environment is needed which is free of high energy vibrations and which can protect the Ln^{III} ion from solvent coordination. As required by both the Förster and the Dexter mechanisms, the lanthanide centre must be in close proximity to the *antenna* for efficient population of the excited state. Moreover, the energy of T_1 must be above the energy level of the lanthanide excited states. A variety of ligands bearing aromatic sensitising chromophores has been devised for such sensitisation, including bipyridines,[31] terpyridines,[32] substituted phenyls,[33] and naphthyl groups.[34] All of the chromophores employed as *antennae* show a common requirement: the energy of their triplet excited state needs to lie at least 1700 cm^{-1} above the energy of an accepting lanthanide energy level (often the emissive state).[20] If this energy gap is less than 1500 cm^{-1}, then thermally activated back-energy transfer competes to re-populate the triplet state of the *antenna*. Conversely, if the energy gap is too big the efficiency of the energy transfer is compromised. Hence, a balance needs to be reached between these opposing factors. The next section shall detail some examples of molecular systems utilising the magnetic and photophysical properties of lanthanide ions and a multitude of different sensitisers.

1.1.2 Efficient ligands for lanthanides

The requirements for the Ln^{III} environment in a lanthanide-containing luminescent system are dictated not only by the energy transfer process and the minimisation of non-radiative pathways, but also by the thermodynamic stability as well as the kinetic inertness of the resulting complex. As a consequence, the design of a ligand meeting all these prerequisites plays a key role in view of the success of the lanthanide molecular system. Moreover, the lability of the rare earth ions and their high coordination numbers has rendered the overall strategy a challenge for synthetic chemists over the last decades.

In aqueous solution, the driving force of the complexation process is mainly related to dehydration of both cation and ligand(s) and a consequent positive entropy change. Given that the dehydration process is endothermic and often this unfavourable thermodynamic contribution is not compensated by the bond formation between the cation and the ligand(s), the overall process is generally entropy driven.[5] Therefore, the best strategy is to insert the lanthanide ion into functional architectures using polydentate ligands. In summary, the main features that a lanthanide complex should possess are:

- ✓ High thermodynamic stability and kinetic inertness;
- ✓ A chromophore, either inbuilt to the ligand or coordinated to the metal ion, which is only a short distance from the lanthanide ion, absorbs light efficiently (high ε), and possesses a triplet excited state that is efficiently populated.
- ✓ The lanthanide complex should be shielded from the deactivating effect of energy-matched X-H oscillators, suggesting that octa- and/or nonadentate ligands should be preferably used.[20]

Common examples of organic ligands which have been employed in lanthanide supramolecular chemistry are: macrocycles, either pre-disposed (*e.g.* cyclen derivatives and calixarenes fitted with functionalised pendant arms), or pre-organised (*e.g.* crown ethers or cryptands), polyaminocarboxylates, β-diketonates, and podands.[4] The next sections shall detail some examples of macrocyclic and acyclic ligands and their use in self-assembly processes.

1.1.2.1 Lanthanide macrocyclic complexes

Macrocyclic ligands have been extensively studied as receptors for lanthanide ions due to their ability to completely enclose the metal ion centre and to fulfill the high

coordination requirement. As such, they protect the ion from solvation effects, thus providing kinetically inert and thermodynamically stable complexes, which often have high luminescence quantum yields. Due to their pre-organised and suitably sized cavity, macrocyclic receptors require the minimum amount of reorganisation energy upon complexation. The most important property that macrocycles possess is the *macrocyclic effect*. A macrocycle has donor atoms arranged in fixed positions and thus there is less of an entropic effect in the binding energy of macrocycles than that observed for polydentate acyclic ligands with an equal number of donor atoms. Therefore, lanthanide complexes of macrocyclic ligands are usually more stable than those with polydentate ligands. The increased thermodynamic stability of macrocyclic complexes over their linear analogues having the same number of chelate rings is the aforementioned *macrocyclic effect*.[35] The kinetic macrocyclic effect refers to the slow kinetics of dissociation of macrocyclic compounds as compared to their open chain analogues.[36]

Aza-macrocycles, such as 1,3,7,10-tetraazacyclododecane (more commonly known as cyclen), have been extensively used in the field of lanthanide coordination chemistry. Cyclen and analogue aza-macrocycles provide a good base for the design of efficient luminescent lanthanide complexes.[8] Numerous aza-macrocycles have been derivatised through functionalisation of the ring nitrogen atoms with a variety of groups (pendent arms) bearing hard donor atoms. Such functionalisation also offers the possibility to easily incorporate aromatic chromophores as sensitisers. Bünzli *et al.* designed tetraamide cyclen frameworks fitted with phenacyl (**1a**) and 4-phenylphenacyl (**1b**) chromophores, which are known to induce efficient energy transfers onto Tb^{III} and Eu^{III} ions.[37] These ligands form stable 1:1 complexes with lanthanide trifluoromethanesulfonate salts in water; the stability constant for **Eu.1a** was determined as $\log K = 12.86 \pm 0.15$ at 298 K. The crystal structure of **Tb.1a** showed the metal ion lying on a C_4 axis and being 9-coordinate, with one water molecule in its inner coordination sphere. The absolute quantum yields of Sm^{III}, Eu^{III}, Tb^{III}, and Dy^{III} complexes of both **1a** and **1b** were measured, with values of 23.1% for $\mathbf{[Tb(H_2O)1a]^{3+}}$ and 24.7% for $\mathbf{[Eu.(H_2O)1b]^{3+}}$ upon excitation of phenacyl and 4-phenylphenacyl, respectively.

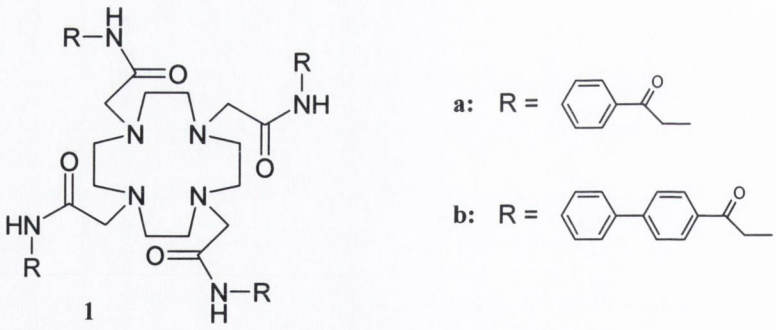

1

Although cationic substrates do not directly interact with the lanthanide metal ions, due to coulombic repulsion, they can interact with the ligands. Such interactions induce changes in their absorbance, redox potentials, and excited states configuration. These changes can consequently affect the efficiency of the lanthanide emission, signalling the occurred interaction. Therefore, protonation or metal ion complexation of the ligand in a lanthanide complex could result in detectable photophysical changes of the metal luminescence. Lanthanide pH sensors are contained in this category and a variety of them have been reported. [16,38,26,39] In the Eu^{III} complex **2** the luminescence emission is enhanced upon protonation due to suppression of the intramolecular electron transfer from the phenanthridine moiety to the lanthanide centre, thus preventing its reduction to Eu^{II}.[8]

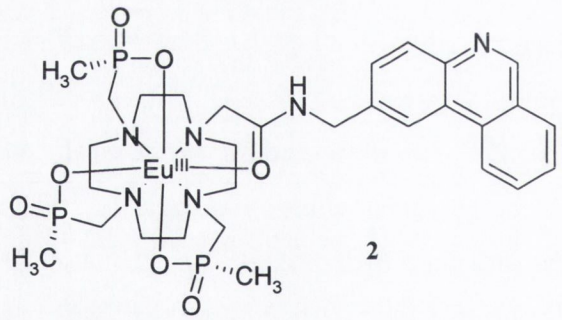

2

The reduction of the lanthanide ion to its bivalent oxidation state may occur to a significant extent in complexes of europium and ytterbium, by means of electron transfer from the excited singlet state of the sensitising chromophore to the complexed lanthanide ion.[20] The likelihood of this event can be predicted by the adapted Weller equation for photoinduced electron transfer (PET) processes (Equation 1.1).[40]

$$\Delta G_{eT} = nF([E_{ox} - E_{red}] - E_s - e^2/\varepsilon_r)\ J{\cdot}mol^{-1} \qquad (1.1)$$

where E_{ox} is the oxidation potential of the electron donor (*e.g.* electron rich aromatic group, N lone pair), E_{red} is the reduction potential of the acceptor (*e.g.* Ln^{III} centre or electron poor

aryl group), E_s is the singlet excited state energy, and e^2/ε_r is the energy term related to the formation of a radical ion pair (usually < 0.2 eV).[20] Thus, when the phenanthridine moiety in **2** is unprotonated (E_{ox} ~ 1.1 V) the electron transfer is highly favourable (ΔG_{eT} = -1.5 eV); whereas upon protonation the oxidation potential of the chromophore increases (> + 2.6 V) to such an extent as to inhibit the reduction of Eu^{III} to Eu^{II}. Correspondingly, the excited singlet state of the phenanthridine can undergo intersystem crossing more efficiently and transfer its energy to the lanthanide excited state, hence enhancing the luminescence intensity.[8]

Similarly, Woods and Sherry have developed pH responsive probes which are independent from probe concentration.[41] The europium luminescence pattern of $[Eu(\mathbf{3})]^{3+}$ has been shown to be significantly dependent on the ligand structural arrangements triggered by changes in pH (Scheme 1.1).

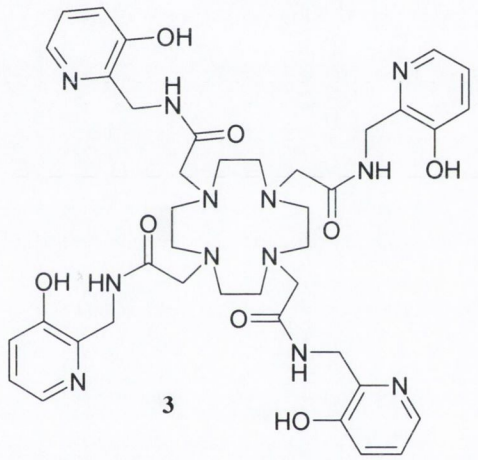

3

The most intense of the europium $^5D_0 \rightarrow {}^7F_J$ emission bands are commonly the ΔJ = 1 and ΔJ = 2 bands centred at 593 and 615 nm, respectively. The $^5D_0 \rightarrow {}^7F_1$ transition is considered to be unaffected by the coordination environment of the lanthanide centre, *i.e.* by the ligand field, whereas the $^5D_0 \rightarrow {}^7F_2$ band is known to be hypersensitive to the coordination environment. The ratio between the intensity of these two bands has been proven to change as a function of pH.

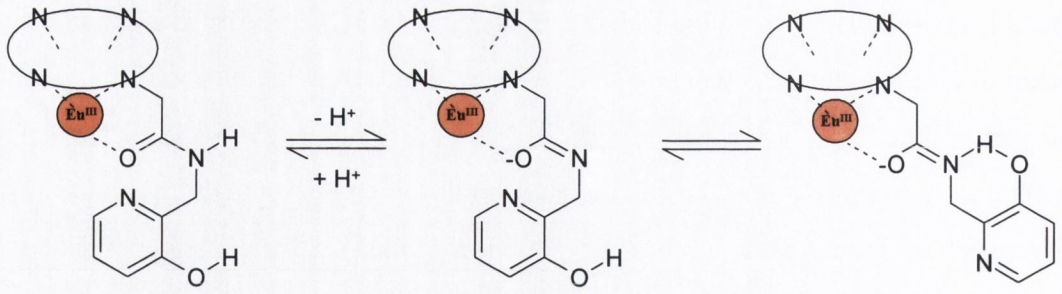

Scheme 1.1 Schematic representation of the deprotonation of the coordinating amides in $[Eu(4)]^{3+}$ showing the intramolecular acid-base paring with the phenolic protons.[42]

Incorporation of potential metal ion binding sites into the macrocyclic ligand can yield metal-specific luminescent probes. In the Tb^{III} complex **4**, for instance, the selective zinc ion binding at pH 7.4 in a competitive ionic background resulted in a luminescence enhancement of the terbium emission by 26 %.[43]

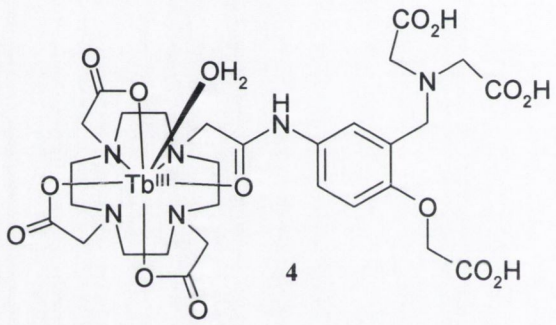

In 2004, Gunnlaugsson *et al.* designed a cationic cyclen based Eu^{III} complex as a luminescent copper sensor (**5**).[44] In this system, a 1,10-phenanthroline group is conjugated to the macrocycle playing a dual role: it serves as the antenna for the complex as well as being a potential coordination site for transition metal ions. Indeed, **5** forms a tetranuclear polymetallic Cu^{II} – Eu^{III} supramolecular complex in aqueous solution where Cu^{II} is bound by three europium conjugates **5**. This can be considered as one of the first examples of supramolecular self-assembly of mixed *f-d* metal ion conjugates. Further examples of such supramolecular systems shall be detailed in the next section. The recognition of Cu^{II} in water at pH 7.4 gives rise to the quenching of the Eu^{III} luminescence showing good selectivity over other ions such as Co^{II}, Fe^{II}, and Fe^{III}.

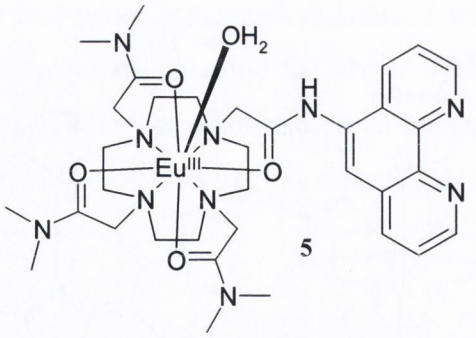

5

The same research group investigated the effect on the ground, singlet excited states and the Tb^{III} emission of **6a** and **6b** as a function of pH and concentration of alkali metal cations.[45] By analysing the photophysical properties of the complexes in water, upon excitation at 300 nm, it was established that both their ground and excited states were modulated by changes in pH and by the presence of ions such as Na^+ and K^+. Both **6a** and **6b** were found to be pH independent between pH 4 and 8, where their luminescence was "switched off". However, in buffered pH 7.4, the Tb^{III} emission was highly modulated by either Na^+ and K^+, **6b** showing higher sensitivity due to the more suitable size of the receptor. In all cases, the photophysical changes were attributed to the modulation of the antenna-receptor moiety and of the energy transfer process from the antenna to the lanthanide centre.

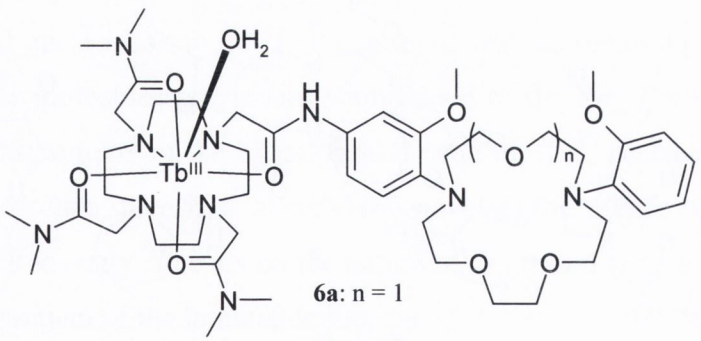

6a: n = 1

6b: n = 2

A palladium porphyrin has been covalently linked to a chiral Yb^{III} complex (**7**) by Parker *et al.*[46] In this hetero-metallic system the quenching of the excited triplet state of the Pd^{II} porphyrinate by molecular oxygen is suppressed upon DNA binding resulting in an enhancement of the NIR Yb^{III} luminescence.

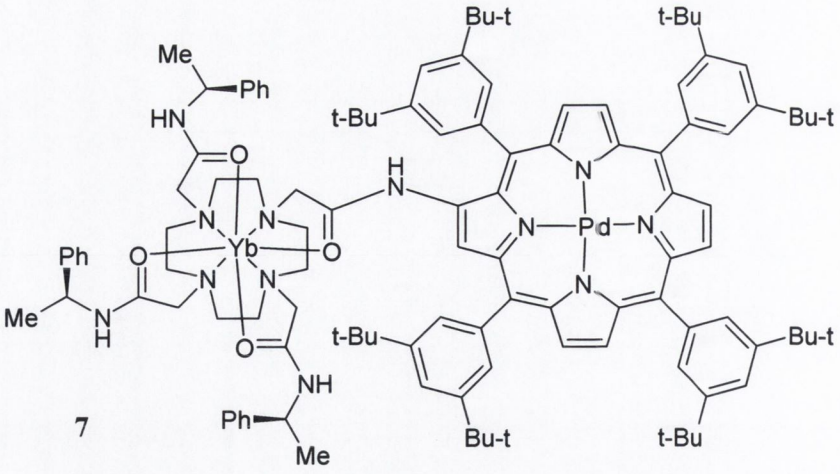

7

Faulkner and Pope investigated the synthesis and luminescence properties of a hetero-trimetallic lanthanide complex containing two terbium ions and one ytterbium ion (**8**).[47] In this system, the Yb^{III} centred NIR emission at 980 nm is sensitised via energy transfer from the terbium centres when excited at 488 nm. It is worth noting that neither ytterbium nor the aryl chromophore of the aminobenzyl group possess any absorption bands at 488 nm. Therefore, it was deduced that ytterbium sensitisation occurred by means of energy transfer from the terbium ions. This is one of the first examples of a lanthanide centred NIR emission sensitised by a lanthanide ion.

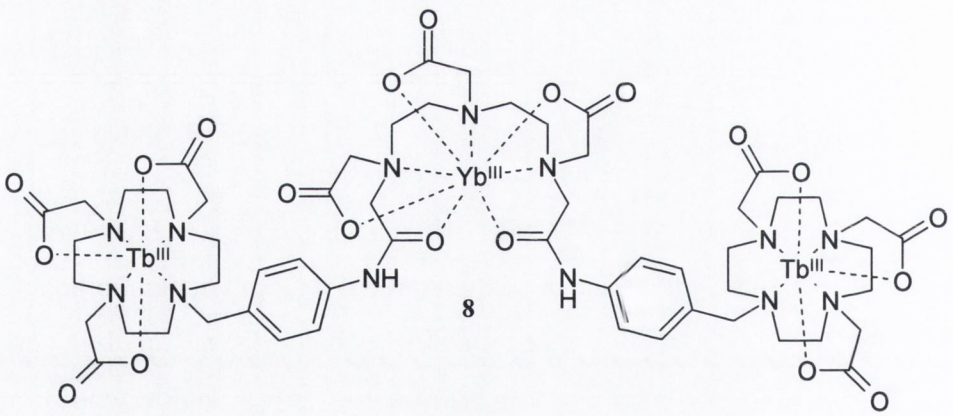

8

Other examples of cyclen derivatised lanthanide complexes have shown how the coordination number of the metal ion plays a very important role in the design of luminescent sensors. Gunnlaugsson *et al.* developed kinetically stable heptadentate tri-amide Tb^{III} cyclen complexes (**9a** and **9b**) for the recognition of aromatic carboxylates in water.[48,27] The lanthanide ion is coordinatively unsaturated and in water at pH 7.4 the

corresponding complexes have two water molecules associated with their structure, thus fulfilling the metal coordination requirement (nine for Tb^{III}). These water molecules are labile and can be removed upon binding of anions, such as bicarbonate, acetate, lactate, citrate, phosphate and halides to the lanthanide ion, as reported by Parker *et al.* for related systems.[49,50]

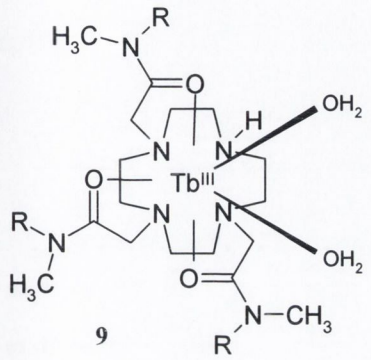

9

9a R = H

9b R = CH_3

In **9a** and **9b** no antenna is incorporated in the cyclen structure and the complexes are "photophysically silent"; hence the idea here was to displace the two water molecules with aromatic carboxylates which can act as sensitisers, in order to "switch on" the Tb^{III} emission *via* energy transfer. This proved to be the case for the formation of ternary complexes between both **9a** and **9b** with *N,N*-dimethylaminobenzoic acid and between **9b** and salicylic acid. On all occasions, the lanthanide luminescence was greatly enhanced upon recognition of the analytes. The complexation promotes efficient energy transfer from the photo-excited guest anion to the Tb^{III} centre, as well as removing the quenching process from the water molecules previously coordinated to the ion. Furthermore, anion coordination alters the symmetry of the ligand field around the Tb^{III} centre as indicated by the ratio of the luminescence intensities at different wavelengths. Hence, the intensity of the luminescence bands strongly depends on the nature of the bound aromatic guest and on the coordination environment of the lanthanide ion.

Along with the multitude of cyclen-based ligands, other macrocyclic ligands have been employed in the development of lanthanide complexes, such as crown ether derivatives.[51] Structural and photophysical studies on the lanthanide complexes of the di-deprotonated form of the bibracchial lariat ethers **10a-c** as luminescent tags, have been reported by de Blas and co-workers.[52] In the X-ray crystal structures of [Ho(**10c**-2H)]ClO_4 and [Er(**10c**-2H)]ClO_4, the metal ion is eight coordinate in the cavity of the dianionic receptor. Both pendant arms of **10c** are on the same side of the crown ether moiety,

resulting in a *syn* conformation. Attempts to isolate complexes of the lightest members of the lanthanide series were unsuccessful, suggesting a certain degree of selectivity towards the heaviest lanthanide ions.

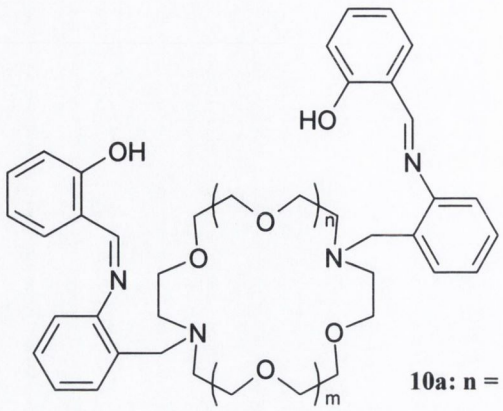

10a: n = 1, m = 1

10b: n = 1, m = 0

10c: n = 0, m = 0

X-ray quality crystals could not be obtained for the lanthanide complexes derived from ligands **10a** and **10b**. Nevertheless, theoretical calculations on the bond distance between the metal ion and the coordinated ligand atoms, allowed the authors to conclude that the related systems $[Ln(\mathbf{10a}\text{-}2H)]^+$ and $[Ln(\mathbf{10b}\text{-}2H)]^+$ are specially adapted for the complexation of lighter lanthanide ions. From the photophysical point of view, the Er^{III} and Yb^{III} complexes of **10c** have been shown to be emissive in the near-IR in both methanol and acetonitrile upon excitation of the ligand band at 373 nm. The luminescence in acetonitrile was more intense and longer-lived than in methanol. Conversely, the luminescence properties measured in acetonitrile were comparable to those in deuterated methanol, as a result of the more effective non-radiative quenching of the excited states from the O-H oscillators. In all cases, time-resolved studies of the complexes confirmed that solvent was excluded from the inner coordination sphere, which makes them suitable for use as luminescent tags.

Calixarenes represent another example of macrocycles pre-disposed to coordinate lanthanide ions. Beer and co-workers synthesised and studied the photophysical properties of luminescent ruthenium(II) bipyridyl complexes containing one, two (**11**) or six lower rim acid-amide modified calix[4]arene moieties covalently linked to the bipyridine groups.[53] The Ru-calixarene complex **11** is able to coordinate Nd^{III}, Eu^{III} and Tb^{III} in a 2 : 1 Ln^{3+} : complex ratio. Addition of lanthanide ions (as nitrate salts) to acetonitrile solutions

of the ruthenium complex **11** caused noticeable changes in the absorption and emission spectra allowing the evaluation of the association constants (Table 1.1).

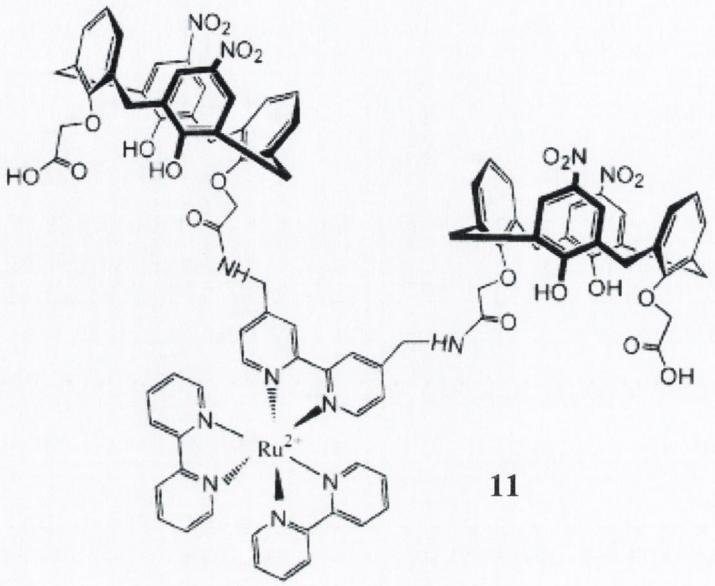

11

$2(PF_6^-).2H_2O$

Table 1.1 Log *K* values for the association constants of the lanthanide adducts with the ruthenium bipyridyl-calix[4]arene complex 11. [53]

	Abs Measurements			*Emission Measurements*		
adducts	**Nd^{3+}**	**Eu^{3+}**	**Tb^{3+}**	**Nd^{3+}**	**Eu^{3+}**	**Tb^{3+}**
11 · Ln^{3+}	7.0	7.4	8.1	8.0	*a*	8.0
11 · $2Ln^{3+}$	13.1	13.7	13.4	13.4	*a*	12.5

[a] Unsuitable fitting

The luminescence studies upon excitation of the tris(bipyridine)-ruthenium(II) complex at 452 nm, show that the adduct formation affects the ruthenium luminescence, which is strongly quenched by Nd^{III} and increased by Tb^{III} and Eu^{III}.

In the case of Nd^{III}, the excitation spectra show that (i) the quenching of the ruthenium luminescence occurs *via* energy transfer to the Nd^{III} centre and (ii) the electronic energy of the excited calixarene is not transferred to the $Ru(bpy)_3$ but again to Nd^{III}, owing to its proximity to the calixarene moiety. As a consequence, the neodymium emission at 1064 nm is greatly enhanced. In the case of Tb^{III}, the emission intensity and the lifetime of the ruthenium bipyridine moiety increase. This behaviour was ascribed to the electric field

created by the lanthanide ion around the ruthenium-calixarene complex by comparison with the Gd^{III} ion, which behaves identically and can affect ruthenium only through its charge. Another contribution may have come from the decrease of vibrational motions (therefore of non-radiative processes) upon complexation with Tb^{III} due to the rigidification of the structure. Finally, in the case of Eu^{III}, it was found that the ruthenium bipyridine emission intensity and lifetime increase if the lanthanide ion was added as a nitrate salt; whereas the addition of Eu^{III} as a triflate salt does not affect the ruthenium luminescence. This lead to the conclusion that the luminescence behaviour is strongly dependent on the lanthanide counterion. Moreover, the electron transfer (*Ru → Eu) quenching process, although thermodynamically allowed, does not occur due to kinetic reasons. Most probably the quenching process is rendered inefficient by the specific geometry/conformation of the [**11** · $2Eu^{3+}$] adduct, where the nitrate plays a very important role.

All these examples give an idea of how macrocycles can be successfully employed in the formation of very stable lanthanide complexes; in the next section, a few examples of acyclic ligands used in lanthanide complexation shall be detailed.

1.1.2.2 Acyclic complexes

In order to shield the metal from inner sphere solvation, thus preventing the quenching of metal-based luminescence through solvent X-H oscillators, another approach, along with the use of macrocyclic ligands, consists of using polydentate or multifunctional ligands bearing appropriate donor units.

The terpyridyl derivatives **12a-c** have been used as ligands by de Silva *et al.* in the development of pH sensors based on long-lived lanthanide luminescence.[32]

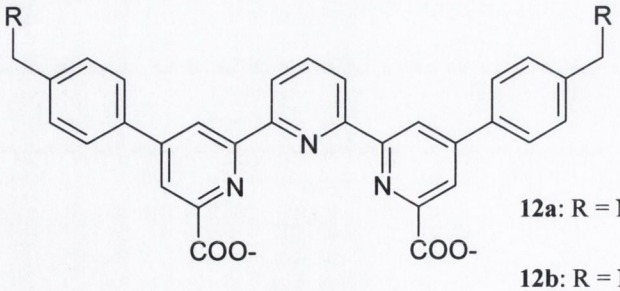

12a: R = NEt_2

12b: R = $N[(CH_2)_2]_2O$

12c: R = N^+Me_3

The bi-carboxylate terpyridine moiety is particularly suitable to coordinate the lanthanide ion and can also serve as an *antenna* owing to its near-ultraviolet absorption. On

the other hand, the amino groups in the side chains can function as proton receptors and electron donors in the Photoinduced Electron Transfer (PET) quenching of the terpyridine electron-deficient π-system. The Tb^{III} and Eu^{III} complexes of ligands **12** were prepared *in situ* by mixing the ligands and the lanthanide ion salt in hundredfold excess. The pK_a values for the side chain amino groups were calculated from the absorbance data upon pH titration, yielding the following values: 7.2 (Tb.**12a**), 7.6 (Eu.**12a**), 5.3 (Tb.**12b**), and 5.5 (Eu.**12b**). The luminescence emission of Tb.**12a** and Tb.**12b** was enhanced by a factor of 16 and 10, respectively, upon protonation, due to proton-induced suppression of the PET process. Conversely, Tb.**12c** showed pH-independent luminescence over the pH range 3-8. These sensors, with relatively long emission lifetimes (in the millisecond range), could therefore be used in real-time proton monitoring, even in intrinsically fluorescent environments. The europium complexes did not participate as strongly in the PET processes, mainly due to the fact that the π-system is less electron deficient than in the terbium analogues, as inferred by the pK_a values, thus rendering the PET less efficient.

In the case of the methyl diester derivatives of ligands **12**, when the appropriate monoazacrown ether is present in the side chain (**13a** and **13b**), the europium complexes, but not the terbium analogues, behave as PET sensors for alkali cations.[54]

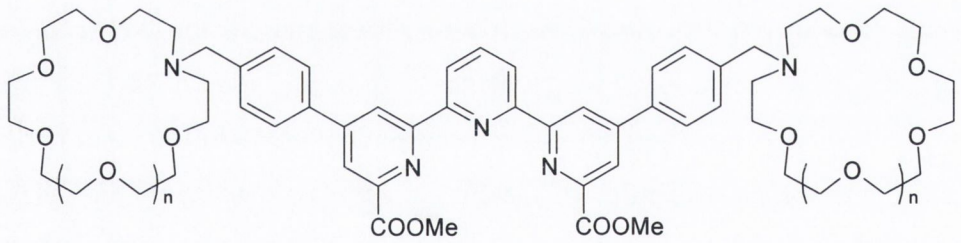

13a: n = 0

13b: n = 1

The complexation processes of both Tb^{III} and Eu^{III} with **13a** and **13b**, were monitored by UV-vis absorption spectroscopy, yielding a 1:1 binding isotherm in all cases. Upon addition of alkali cations, the delayed luminescence of Eu.**13a** and Eu.**13b** was enhanced by an order of magnitude due to the alkali-induced suppression of the PET from the azacrown to the *antenna* (terpyridine moiety), in a manner described for **12**. The switching efficiency of Eu.**13b** was stronger with K^+ than Na^+, probably because the smaller and harder Na^+ is closer to the oxygen atoms in the crown ether, which reduces the

PET efficiency. The weak emission of the Tb^{III} complexes can be ascribed to the back energy transfer to the triplet excited state of the *antenna*. The triplet level of the complexed ligand lies only 1434 cm^{-1} above the terbium emissive state ($^5D_4$), rendering the back energy transfer process feasible even at room temperature (*cf.* section 1.1.1).

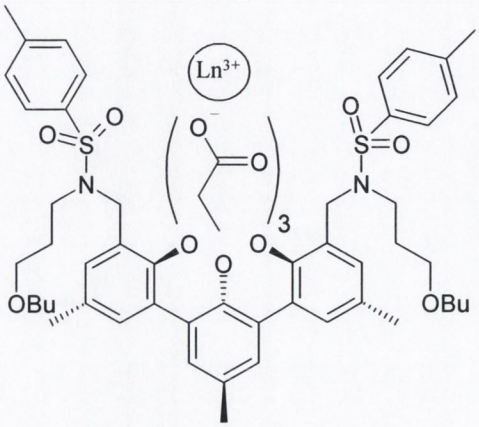

Ln.14

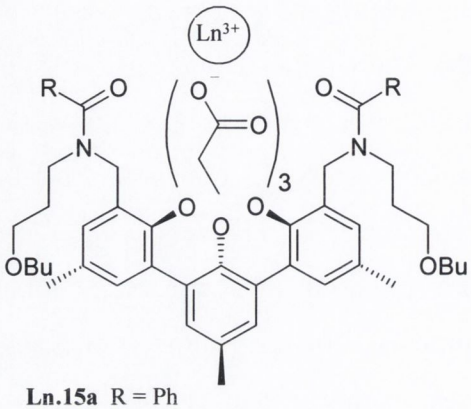

Ln.15a R = Ph

Ln.15b R = Me

A series of oxyacetate-functionalised *m*-terphenyl-based ligands incorporating sulfonamido (**14**) and amide groups (**15a** and **15b**) have been reported and the structures of their corresponding neutral lanthanide complexes have been studied by ^{1}H-NMR and luminescence experiments.[55] In **Eu.14**, **Eu.15a-b**, **Tb.14**, and **Tb.15a** the ligand occupies eight coordination sites of the metal ion by means of three chelating oxyacetate groups and two amide or sulfonamide oxygens. A solvent molecule completes the inner coordination sphere. The luminescence properties of the Eu^{III}, Tb^{III}, Dy^{III}, and Sm^{III} complexes were investigated through excitation of the terphenyl moiety using methanol as a solvent in the first two cases and DMSO for the Dy^{III} and Sm^{III} complexes; the choice of the solvent was dictated by the higher sensitivity of the latter two ions to quenching by solvent hydroxyl groups compared to Eu^{III} and Tb^{III}. Laser excitation at 350 nm of **Er.15a**, **Nd.15a**, and **Yb.15a** also resulted in metal-based luminescence demonstrating that Er^{III}, Nd^{III} and Yb^{III} can accept energy even from high lying ligand centred triplet states (Figure 1.6).[55]

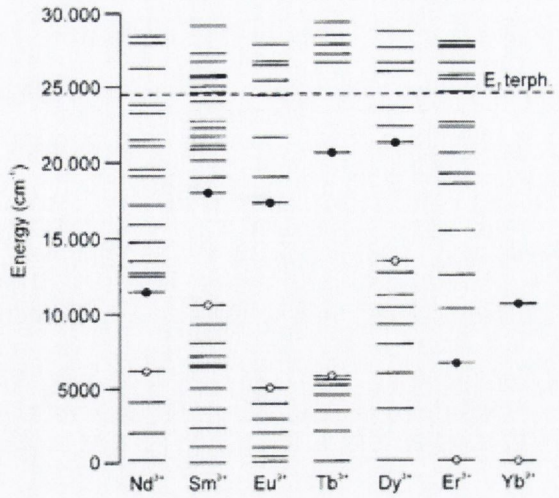

Figure 1.6 Energy diagram of the 4f energy levels responsible for the lanthanide luminescence. (•) = lowest luminescent excited state; (◦) = highest non luminescent state.[55]

Organic dyes with a lower energy excited triplet state (around 14000-17000 cm^{-1}) have been employed as *antennae* for the near-infrared luminescent Yb^{III}, Nd^{III}, and Er^{III} complexes of **16** and **17**.[56] The 1:1 complexes can be efficiently excited with visible light, λ_{exc} = 488 nm for both fluorescein (in **16**) and eosin (in **17**) derivatives, displaying intense lanthanide luminescence at low concentration ($\approx 10^{-6}$ mol l^{-1}) in D_2O as a result of energy transfer from the chromophore. However, this process occurs rather slowly, as indicated by measurements on the effects of quenching by molecular oxygen.

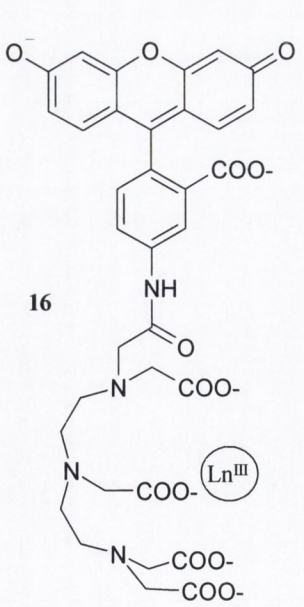

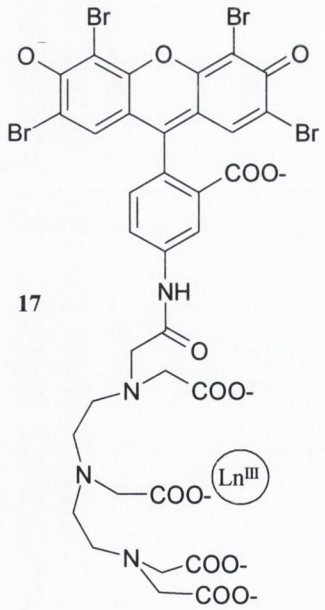

A hairpin-shaped heterotrimetallic luminescent neodinium complex (**18**) has been designed for sensing biological substrates, such as DNA.[57] In this system, the ligand can wrap around the lanthanide ion through a hard binding core, *i.e.* the diethylenetriaminepentaacetic acid derivative moiety, as well as providing two soft thiol sites available for binding transition metal ions, such as Pt^{II}. The two planar Pt^{II} complexes act as strong DNA intercalators and also as sensitisers for Nd^{III} NIR luminescence. The lanthanide unit does not interact with DNA, thus acting as a luminescent "reporter".

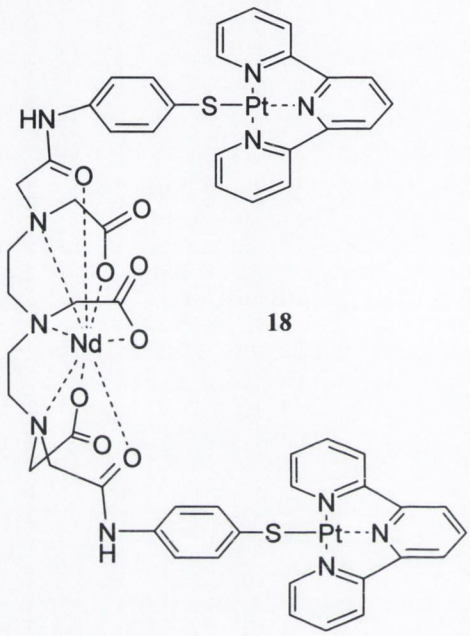

Tsukube and co-workers prepared the Eu^{III} complex of tris(2-pyridylmethyl)amine **19**, as a luminescent sensor for nitrate, NO_3^-, while the corresponding Tb^{III} complex displayed Cl^- selectivity.[58] The Eu^{III} complexes of **19** and **20** possess 1:1 stoichiometry and are stable enough for use in solution. In this case, the pyridine units fulfil the role of the sensitising antenna, absorbing at 260 nm before transferring their excited state energy to the lanthanide ion. However, the complexes are coordinatively unsaturated and hence the metal bound solvent molecules effectively quench the luminescence. Nevertheless, upon addition of three equivalents of NO_3^- to **Eu.19**, or Cl^- in the case of **Tb.19**, in CH_3CN, the solvent molecules are displaced and the luminescence is increased by factors of 4.9 and 5.4, respectively. Conversely, anions such as I^-, Br^-, Fl^-, ClO_4^-, SCN^-, HSO_4^-, and $H_2PO_4^-$ do not show the same response. The achiral ligand **20** displayed similar anion selectivity in CH_3CN, although to a lesser extent than the chiral analogue.

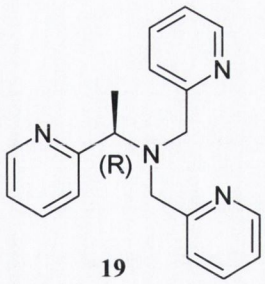

19

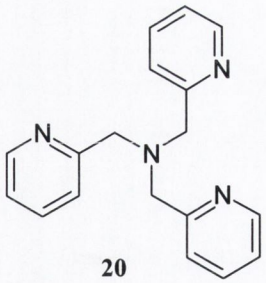

20

Charbonnière *et al.* reported on the time-resolved luminescent properties of a nona-coordinated Eu^{III} complex (Figure 1.7).[59] The ligand comprises of a podand incorporating bipyridine arms, each of which bears a carboxylate unit (**21**).

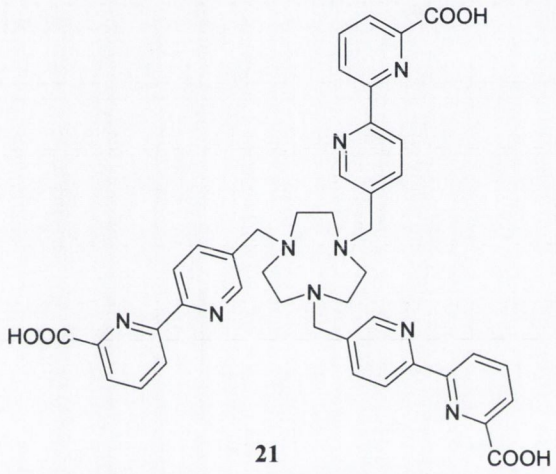

21

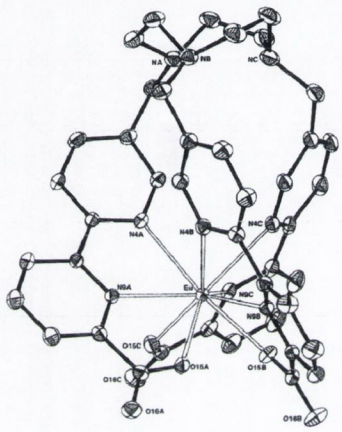

Figure 1.7 Ligand 21 and the X-ray crystal structure of [Eu(21-2H)]Cl·10H_2O showing an ORTEP view of the $[Eu(21\text{-}2H)]^+$ complex along the pseudo-C_3 axis with 30% probability thermal ellipsoids and H atoms omitted for clarity.[59]

In the resulting Eu^{III} complex, the metal ion coordinates to six nitrogen atoms from the three bipy subunits together with three oxygen atoms of the carboxylate groups, providing an overall coordination number of 9. The ^{1}H-NMR spectrum of the Eu^{III} complex in d_6-DMSO shows unambiguously a C_3 symmetry in solution. From the analysis of its photophysical properties in water at room temperature, the Eu^{III} complex exhibited a long excited state lifetime (τ = 1.85 ms) and a relatively high quantum yield (Φ = 0.12). The stability constant of the complex was proven to be of the same order of magnitude as the corresponding EDTA complex, under the same conditions ($\log K$ = 14.3 ± 0.8). Bioaffinity assays based on time-resolved luminescence were carried out using the Eu^{III} complex, suggesting that suitable $[Eu(\mathbf{21}\text{-}2H)]^+$ derivatives could be used as luminescent labels in time-resolved luminescence microscopy.

1.1.2.3 Self-assembly processes

An alternative strategy for engineering elaborate multimetallic edifices and devices with predetermined luminescent or magnetic properties is to turn to self-assembly processes.[5] Trivalent lanthanide ions have the advantage of having both high electric fields and weak intermolecular interactions. This offers the opportunity to self-assemble sizeable coordinating units around the metal centre, hence yielding mono- or multi-metallic functional architectures. Bünzli and co-workers designed a new class of highly stable and luminescent dimetallic carboxylates which self-assemble in water forming lanthanide helicates.[60] Ligand **22** yields neutral triple-stranded dimetallic helicates with the entire series of lanthanide ions $[Ln_2(\mathbf{22}\text{-}2H)_3]$; such complexes are stable in water in the pH range 4-13, with stability comparable to that of DOTA-derived complexes (pLn ≈ 21-22; where pLn = $-\log[Ln^{III}(aq)]^{3+}$ when $[Ln^{III}]_t = 10^{-6}$ M and [DOTA] = 10^{-5} M, at pH = 7.4).[4] This indicates that the large hydration energy of the trivalent lanthanide ions is adequately compensated by the favourable thermodynamic contribution of the self-assembly process.

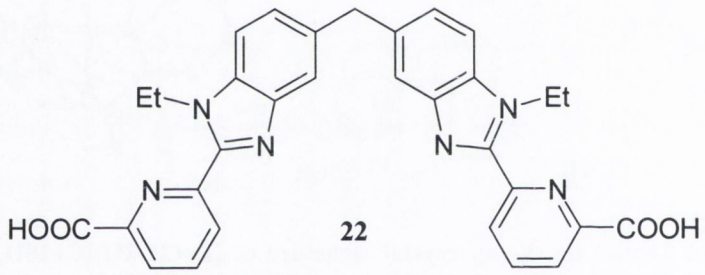

In the case of the Ln^{III} complexes of **22**, the three ligand strands are wrapped around the two nine-coordinate Ln^{III} ions in a helicate shaped structure with a pseudo-D_3 symmetry around the metal; a stereoview of $[Tb_2(\mathbf{22}\text{-}2H)_3]\cdot 20.5\ H_2O$ is shown in Figure 1.8. Similar systems will be discussed in more detail in Chapter 3.

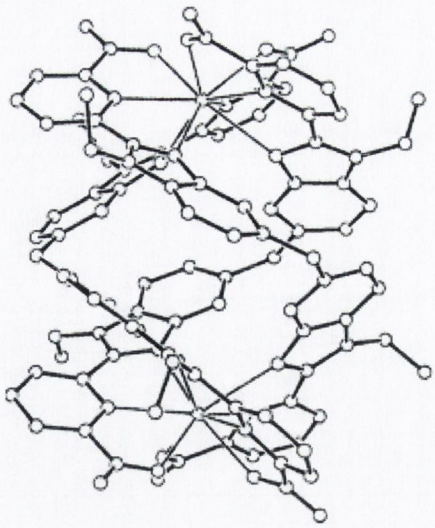

Figure 1.8 View of $[Tb_2(22\text{-}2H)_3]\cdot 20.5\ H_2O$.[60]

A remarkable example of self-assembly is represented schematically in Figure 1.9. The supramolecular system **23** consists of a heterotrimetallic complex, in which the photoexcitation of the Eu^{III} occurs *via* energy transfer from a transition-metal-based antenna.[61] In such a system, the Ir^{III}-based moiety acts as a sensitiser for the Eu^{III} red emission. Interestingly, the emission of almost-white light can be observed if there is only partial energy transfer from the excited Ir^{III}-based chromophore. If this occurs, the Eu^{III} red emission combined with the residual blue emission from the iridium complex gives rise to a global white light emission (Figure 1.9).

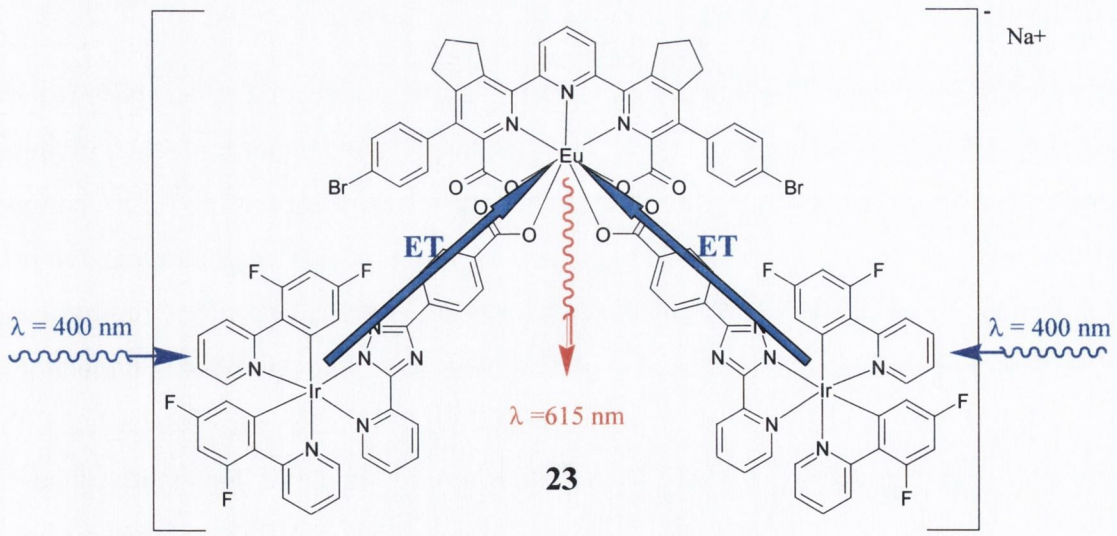

Figure 1.9 Schematic representation of the intramolecular *d→f* energy transfer processes responsible for the sensitising of Eu^{III} in a heterotrimetallic $[IrEuIr]^-$ assembly.[61]

In the trimetallic $RuLn_2$ complex **24**, the near-infrared luminescence of neodymium and ytterbium was sensitised by energy transfer from the triplet excited state of the ruthenium-tris(bipyridine) complex.[62] The transition metal-based antenna absorbs in the visible part of the electromagnetic spectrum. The luminescent nature of the donating state (the ^{3}MLCT state) has allowed a detailed study of the energy transfer process to the lanthanide centres. The rate of the sensitisation process measured for both Nd^{III} and Yb^{III} complexes are 1.1×10^6 s^{-1} and $\leq 10^5$ s^{-1}, respectively.

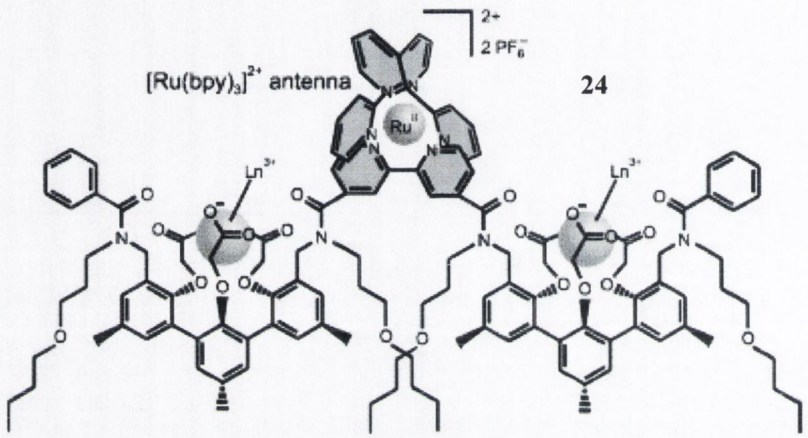

A mixed linear trimetallic *f-d* supramolecular self-assembly was also developed by Gunnlaugsson and co-workers through modification of complex **5,** previously described. A Eu^{III} cyclen derivative appended with a terpyridine (**25**), in which the terpyridine moiety acts as a sensitiser for the lanthanide centre as well as a suitable ligand for transition metal ions, such as Fe^{II} and Ni^{II}, was reported.[63] The hydration state of the complex (q) was found to be 1.2 indicating that complex **25** had one metal-bound water molecule, giving an overall nine-coordinate environment. The lanthanide luminescence of the Eu^{III} complex was monitored as a function of pH resulting in the emission being switched on above pH 3 and switched off above pH 9. The UV-vis, fluorescence and europium luminescence spectra were then measured at neutral pH upon addition of a series of transition metal ions. The changes in the ground state of **25** showed the formation of a ternary complex with a new MLCT band appearing at *ca.* 570 nm upon coordination of Fe^{II} and Ni^{II} to the terpyridine moiety. As for the fluorescence, the emission band at 422 nm was quenched upon titration with both Fe^{II} and Ni^{II}. The coordination of these metal ions to the antenna also caused the quenching of the delayed europium luminescence, probably due to back energy transfer from the lanthanide emissive state ($^5D_0$) to the excited triplet state of the

antenna. The Eu^{III} ion can therefore be used as an "impartial luminescent reporter" for the formation of the self-assembly complex, as it is not directly involved in the binding of the transition metal ions.

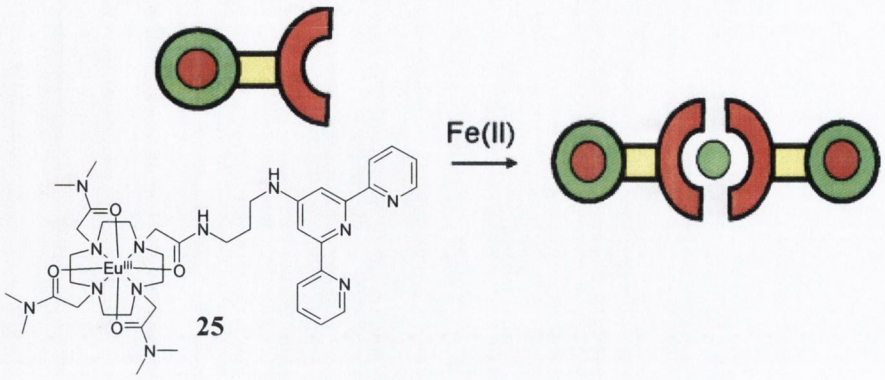

Figure 1.10 Schematic representation of the linear self-assembly

Pikramenou and co-workers prepared the bis(*β*-diketone) ligands **26** and **27** (shown in their enolic forms) which bind to Ln^{III} or Y^{III} ions to form neutral homodimetallic triple-stranded complexes $[M_2(\mathbf{26}\text{-}2H)_3]$ where M = Eu, Nd, Sm, Y, Gd and $[M_2(\mathbf{27}\text{-}2H)_3]$, where M = Eu, Nd or anionic quadruple-stranded dinuclear lanthanide units, $[Eu_2(\mathbf{26}\text{-}2H)_4]^{2-}$.[64]

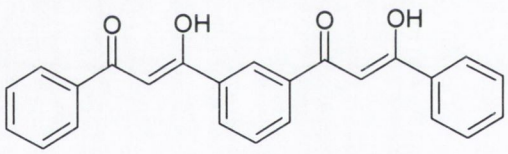

26

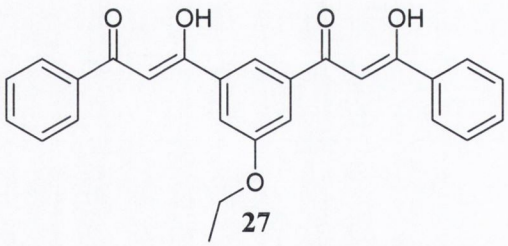

27

The complexes have been thoroughly investigated by NMR confirming the formation of a single complex species with high symmetry and chiral nature (see molecular model in Figure 1.11), as demonstrated by the splitting of the NMR signals upon addition of Pirkle's reagent. The absorption spectra of both **26** and **27** exhibit an intense band centred at 357 nm, attributed to the π–π^* enol absorption. This is typical of the enol form of *β*-diketones. The complexes have high molar absorption coefficients (*ca.* 13×10^4 M^{-1}

cm^{-1}) and display strong visible or NIR luminescence, depending on the chosen lanthanide, upon excitation of the ligand band at 350 nm. The bis-diketonate ligand proved to be an efficient sensitiser, particularly for Sm^{III} and Nd^{III}. Compared with the triple stranded Eu^{III} complex in the solid state, the quadruple-stranded complex displays a more intense luminescence with a distinct emission pattern indicating its higher symmetry.

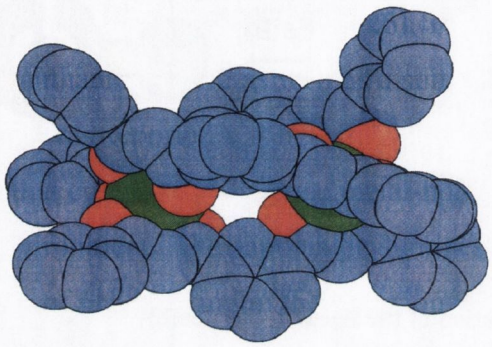

Figure 1.11 Molecular model of the $[Eu_2(26\text{-}2H)_3]$ complex.[64]

The challenging development of heteropolymetallic *f-f'* complexes has been achieved by Piguet *et al.* by assembling the tris-tridentate ligand **28** and two different lanthanide metal ions (Ln^1 and Ln^2).[65] In acetonitrile, the self-assembly under stoichiometric conditions yields a mixture of heterotrimetallic triple stranded helicates $[(Ln^1)_x(Ln^2)_{3-x}(\mathbf{28})_3]^{9+}$ (x = 0-3) with Ln^1, Ln^2 = La^{III}, Nd^{III}, Sm^{III}, Eu^{III}, Yb^{III}, Lu^{III}, Y^{III}. The statistical analysis of the thermodynamic data obtained through qualitative (ESI-MS) and quantitative (^{1}H-NMR) investigations highlighted the importance of the different affinities of each specific lanthanide for the terminal sites (N_6O_3) and the central one (N_9). These parameters depend on the ionic radius, thus providing size-discriminating effects which favour the formation of heterotrimetallic helicates with the central site occupied by the larger metal (Figure 1.12).

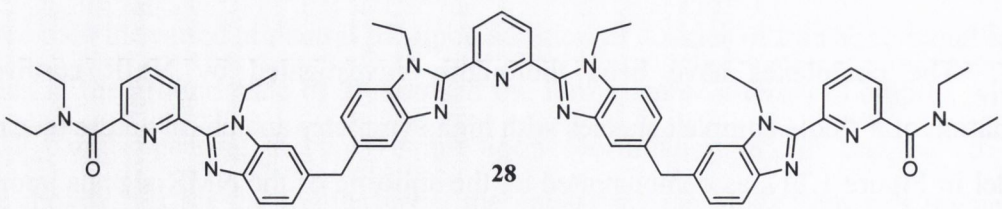

28

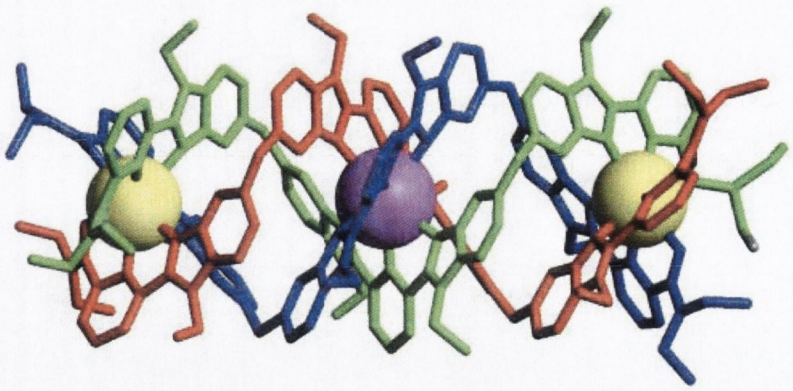

Figure 1.12 Molecular structure of $[EuLaEu(28)_3]^{9+}$

The diastereoselective self-assembly of a trinuclear Eu^{III} array has been presented by Mamula *et al.*, which exhibits a supramolecular helical chirality related to the arrangement of the ligands **29** around the metallic core.[66]

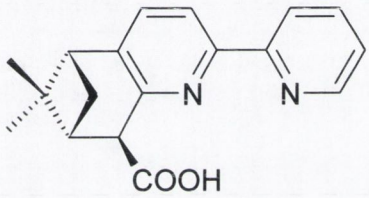

(+)-H**29**

The crystal structure of the trinuclear assembly shown in Figure 1.13 revealed that the ligands adopt a left-handed helical configuration, which was also proven by the circular dichroism (CD) spectrum of the complex. Preliminary investigations were conducted, which showed that the trinuclear assembly persists in the solution state. Upon UV irradiation, the Eu^{III} array displays bright red luminescence in both solution and solid state. The properties of the assembly in the excited state were therefore investigated by circularly polarised luminescence (CPL) spectroscopy. The excitation of the organic chromophore at 315 nm in CH_3CN gave rise to polarised emission bands corresponding to the Eu^{III}-centered $^5D_0 \rightarrow {}^7F_J$ transitions.

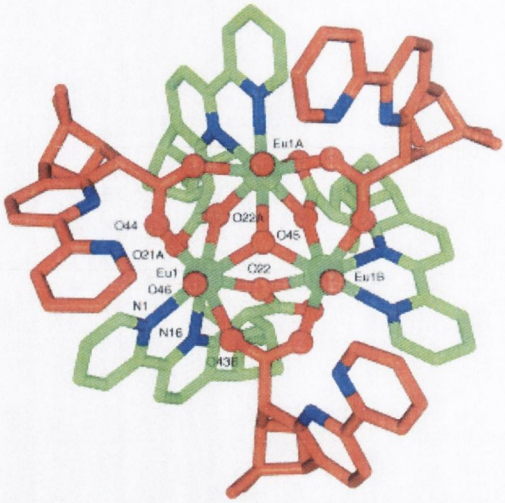

Figure 1.13 Crystal structure of $[Eu_3\{(+)\text{-}29\}_6(\mu_3\text{-}OH)(H_2O)_3](ClO_4)_2 \cdot 3\ H_2O$ (O red, Eu turquoise, N dark blue; O-coordinated pinene-bipyridyl groups orange, N,O-coordinated pinene-bipyridyl groups green). View parallel to the crystallographic C_3 axis with a simplified labelling scheme. Hydrogen atoms, perchlorate counterions, and water molecules of crystallization have been omitted for clarity.[66]

In this part of the introduction, the synthesis, characterisation and use of several lanthanide systems have been discussed, in order to highlight their potential as sensors and luminescent molecular devices in solution. As one of the aims of this work is to study the photophysical properties of such lanthanide systems when incorporated into hydrogels, the next section shall detail the main features and applications of these 'soft materials'.

1.2 Chemistry in soft-matter: hydrogels

Hydrogels are three-dimensional, hydrophilic, polymeric networks that swell, but do not dissolve in water.[67] The idea of using hydrogels as biomaterials dates back to the landmark work of Wichterle and Lím (1960),[68] which described the rational design of hydrophilic polymer networks for biological uses.

A hydrogel can be considered as a container of water consisting of a three-dimensional mesh. Polymeric structures are termed hydrogels when the amount of water retained is between 20-100% of the total weight; when the water content exceeds 100% they are classified as super-adsorbent hydrogels.[69] Hydrogels are said to possess both the cohesive properties of a solid and the diffusive transport properties of a liquid.[70] A detailed study of the relationship between the structure of hydrogels and their biocompatibility[71] has resulted in their widespread use in the medical and pharmaceutical sectors. Hydrogels are generally found to be very well tolerated when implanted *in vivo* since they resemble natural living tissue more than any other class of synthetic biomaterials.[72] This is due to

their high water content and soft consistency which is similar to natural tissue. Additional advantages of hydrogels are their non-toxicity, non-antigenicity, non-irritability and chemical stability. The relatively high water content makes them permeable to small molecules such as oxygen, nutrients and metabolites. It is thus not difficult to understand why hydrogels have been used as surgical sutures, artificial organs, hemodialysis membranes, drug delivery systems and soft contact lenses over the past decades.[67,73-75]

1.2.1 Preparation of Hydrogels

The literature on the synthesis of new polymer materials has exploded since the first biomedical application of poly(hydroxyethyl methacrylate), known also as pHEMA, by Wichterle and Lím.[68] Hydrogels are typically synthesised by one of two well-established procedures: (*a*) polymerisation and simultaneous or postpolymerisation cross-linking of hydrophilic monomers, and (*b*) modification of hydrophilisation of existing polymers with potential hydrogel properties.[69]

The main property of hydrogels is their ability to swell in the presence of water and to shrink in the absence of it. The two most important factors controlling the extent of swelling are the hydrophilicity of the polymer chains and the cross-link density. A detailed description of these features shall be given in section 1.2.2. Hydrogels can be homopolymeric or copolymeric networks, depending on the methods of preparation. Additionally, they can be classified as either neutral or ionic depending on the nature of the side groups (Figure 1.14).

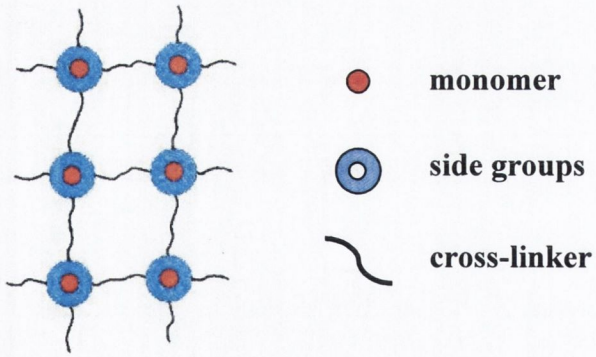

Figure 1.14 Schematic representation of a hydrogel structure.

The most common neutral hydrophilic monomers from which hydrogels have been prepared are listed in Table 1.2. The copolymerisation of these neutral hydrophilic monomers with monomers bearing ionic moieties gives the opportunity to prepare a greater variety of hydrogels. However, polymerisation of the ionic monomers alone can also yield

successful homopolymeric hydrogels. Examples and classifications of basic cationic and acidic anionic monomers are given in Table 1.3.

Table 1.2 Hydrophilic monomers for hydrogel synthesis. [76]

Monomer	Structure	Properties
Hydroxyalkyl methacrylates *e.g.* 2-hydroxyethyl methacrylate (HEMA)	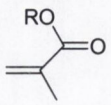	Neutral, Hydrophilic
N-Substituted acrylamides *e.g.* N-isopropylacrylamide (NIPAAm)	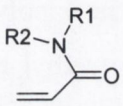	Neutral, Hydrophilic
N-vinyl-2-pyrrolidone (NVP)	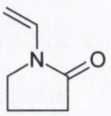	Neutral, Hydrophilic
N-Acryloylpyrrolidine	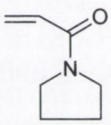	Neutral, Hydrophilic

Table 1.3 Ionic monomers for hydrogel synthesis.[76]

Monomer	Structure	Properties
Vinylpyridinium	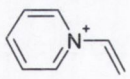	Cationic, Basic
Ethylammonium methacrylates	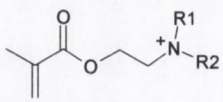	Cationic, Basic
Methacrylic acid	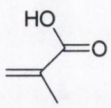	Anionic, Acidic
Sodium styrene sulfonate	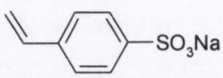	Anionic, Acidic

In order to provide hydrogels with a different range of mechanical and physical properties, it is possible to copolymerise and crosslink the hydrophilic monomers with hydrophobic ones, Table 1.4. However, the latter do not yield water swellable materials upon polymerisation, thus providing harder and less elastic hydrogels. Using chemical

cross-linking it is then possible to provide network structure to the hydrogel maintaining its integrity with swelling. Ethylene glycol dimethacrylate has become one of the most popular cross-linkers, while other commonly used cross-linkers include *N,N'*-methylenebisacrylamide, divinylbenzene, triallylamine, methylene bis(4-phenyl isocyanate), Table 1.5.

Table 1.4 Hydrophobic monomers for hydrogel synthesis.[76]

Monomer	Structure	Properties
Acrylics	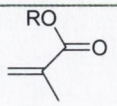	Nonionic, Hydrophobic
Methacrylics	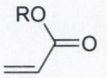	Nonionic, Hydrophobic
Vinyl Acetate	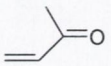	Nonionic, Hydrophobic
Acrylonitrile		Nonionic, Hydrophobic
Styrene		Nonionic, Hydrophobic

Table 1.5 Cross-linkers used in the preparation of hydrogels.[76]

Cross-linker	Structure
Ethylene glycol dimethacrylates	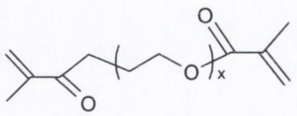
Divinylbenzene	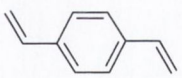
Triallylamine	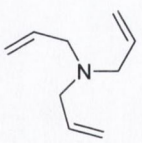
Methylene *bis*(4-phenyl isocyanate)	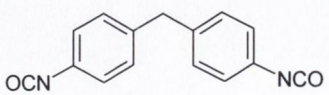

By incorporating some stimuli-responsive co-monomers either into the backbone of the network structure or as pendant groups, it is possible to prepare hydrogels with responsive properties.[67] Such method can also be addressed to incorporate molecules, such as luminescent sensors and switches, into soft materials for potential applications in medical devices (*e.g.* monitoring of electrolytes in the blood, during surgical operations). Furthermore, when the composition of the hydrogels is appropriately chosen, they do not require the sensor or the receptor to be covalently bonded to the polymeric matrix.[77] In this case, the analysis of the hydrogel properties must take into consideration the solute transport through the macroporous network of the hydrogel. Solute transport occurs primarily within the water-filled regions in the space delineated by the polymer chains. Any factor which reduces the size of these spaces will have an effect on the movement of the solute, hence on the response time of the polymeric system. In general, the diffusion of a solute through a hydrogel decreases as crosslinking density increases, as the size of the solute increases, and as the volume fraction of the water within the gel decreases.[78]

1.2.2 Hydrogel properties: swelling degree

One of the most remarkable properties of hydrogels is that they can undergo substantial swelling and collapsing depending on their environment.[79] The swelling degree of a polymer gel directly influences all other properties and is controlled by two major factors:

- hydrophilicity of the polymer chains,
- crosslink density.

1.2.2.1 Hydrophilicity of polymer chains

Hydrogels containing hydrophilic groups take up higher volumes of water than those incorporating hydrophobic groups.[72] In the presence of water, hydrophobic groups collapse and the exposure to water molecules is minimised, reducing the swelling ability of the gel. The swelling capacity of a gel can therefore be increased by the addition of higher amounts of hydrophilic monomer. The same result can also be achieved by the incorporation of an ionic monomer. In neutral hydrogels the driving force for swelling arises from the water-polymer thermodynamic mixing contribution, *i.e.* the spontaneous mixing of the fluid with the polymer chains, to the overall free energy. This contribution is coupled with an elastic polymer contribution, which is the result of the elastic retractive forces developed inside the gel.[72] For hydrogels containing ionic groups the swelling

process has a third contributor which is the electrostatic interactions between the charges on the polymer and also between the charged polymer and counterions.

1.2.2.2 Crosslink density

One of the major disadvantages of hydrogels is their relatively low mechanical strength. However, this can be overcome by increasing the crosslink density between the polymer chains. The crosslinking ratio is one of the most important factors that affect the swelling of hydrogels. It is defined as the ratio of moles of crosslinking agent to the moles of polymer repeating units. The higher the crosslinking ratio, the more crosslinking agent is incorporated in the hydrogel structure. Highly crosslinked hydrogels have a tighter structure and swell less compared to the same hydrogel with a lower crosslinking ratio.[72] The structure of an idealised hydrogel is shown schematically in Figure 1.15, whereby two of the most important parameters defining the structure and properties of a swollen hydrogel, M_c and ξ are indicated. M_c is the *effective molecular weight* of the polymer chain between crosslinks and ξ is the *networks mesh* or the *pore size*.

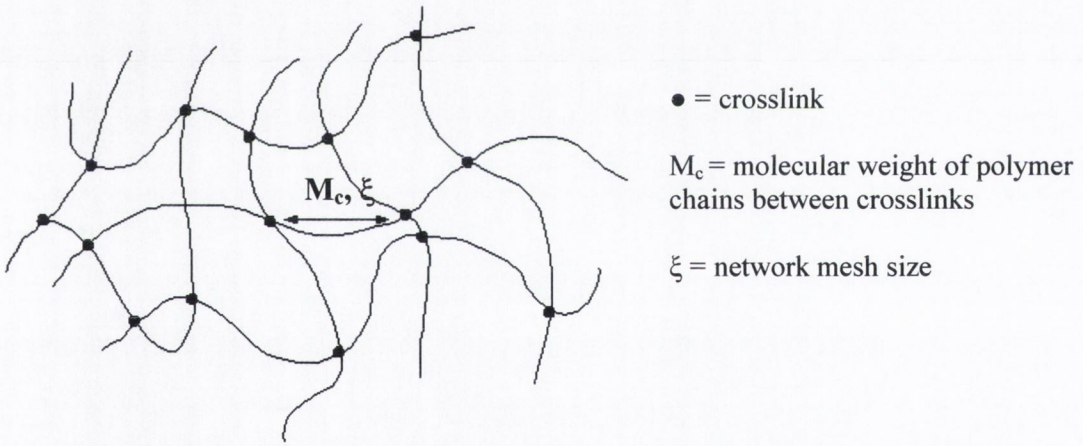

Figure 1.15 Schematic representation of a crosslinked hydrogel structure.[80]

The polymer volume fraction after equilibrium swelling (*i.e.* the swollen polymer volume fraction), $\upsilon_{2,s}$, gives an indication of the amount of solution that a hydrogel can integrate into its structure (Equation 1.2):[81]

$$\upsilon_{2,s} = \frac{V_d}{V_s} \qquad (1.2)$$

where V_d is the volume of the initially dry hydrogel and V_s is the volume of the swollen hydrogel. From the molecular weight between crosslinks (M_c), the number of links between two crosslinks, *n*, is calculated as:

$$n = \frac{2M_c}{M_r} \tag{1.3}$$

where M_r is the average molecular weight of the repeating unit.[81]

The network mesh size gives some indication of the degree of porosity of the gel which can be experimentally measured through techniques such as electron microscopy.

Depending on the pore size, hydrogels can be classified as

1) macro-porous;
2) micro-porous;
3) non-porous.[72]

Although convenient for speculating on the network properties, this idealised image of the polymer network does not take into consideration defects which occur during the process of cross-linking, such as pendant links, entanglements or loops.[82] Hydrogels are generally non-homogeneous, containing regions of low water swelling as a result of high crosslink density, known as clusters, dispersed within regions of high swelling and lower crosslink density.[83]

1.2.3 Content/State of water

When a dry hydrogel begins to absorb water, the most polar and hydrophilic groups, *i.e.* the ionic (if present) and H-bonding groups, are the first to be hydrated upon submersion. This type of water is referred to as "primary bound water".[83] After this initial absorption, the polymer chains begin to expand and the exposure of the hydrophobic groups to water molecules occurs leading to hydrophobic interactions and the subsequent formation of a "coating" around these groups. This kind of water is often called "secondary bound water". These two types of water are generally combined to form the "bound water". When these short-range interactions of water with polymer backbone groups are satisfied, the network may absorb more water, thus expanding to an equilibrium swelling level. Such additional water is referred to as "free water" or "bulk water".

Covalently crosslinked networks, described as "permanent" or "chemical" gels, maintain their shape upon swelling. When the networks are held together by molecular

entanglements or secondary forces including ionic, H-bonding or hydrophobic interactions, they are called "reversible" or "physical" gels, and can be disrupted by changes in physical conditions or the application of stress.[83] Some examples of physical forces present in reversible hydrogels are depicted in Figure 1.16.

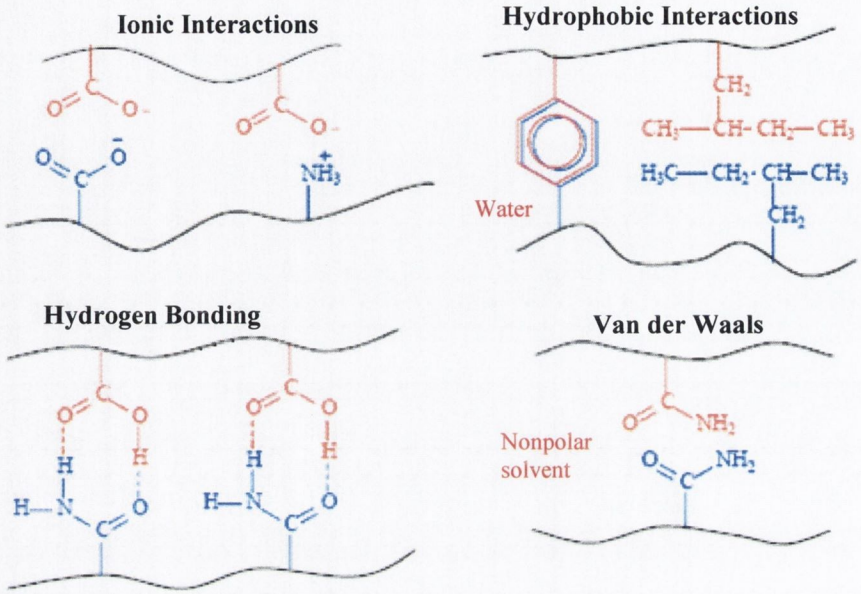

Figure 1.16 Four fundamental forces which can physically cross-link hydrogels and are subject to disruption by an external stimulus.[84]

1.2.4 Biocompatibility and permeability

Since the development of pHEMA (**30**) in the early 1960s, hydrogels have been considered for use in a wide range of biomedical and pharmaceutical applications.[68,72,82] Hydrogel properties can be engineered for biocompatibility, selective permeability, mechanical and chemical stability.[85] For the successful use of hydrogels as biomaterials, they must be conducive to cell viability and function (biocompatibility). They must also possess proper permeability to allow sufficient transport of oxygen and essential nutrients across the hydrogel network. They must be non-toxic and relatively inert, without interfering with cell functions. The hydrophilicity of hydrogels renders most of them biocompatible. Hydrogels also possess a high dergree of flexibility similar to natural tissue which, when used as an implant material, minimises irritation to surrounding tissue and membranes.[86] This resemblance to natural tissue is greater than that of any other class of synthetic biomaterials, which can be attributed to their high water content and soft, rubbery consistency.[72]

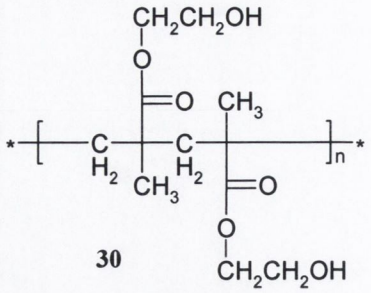

30

The most widely used hydrogel in biomaterial applications is water swollen crosslinked pHEMA (**30**) due to its inertness to normal biological processes, resistance to degradation, metabolite permeability, its ability to withstand heat sterilisation without damage and its ease of manipulation in terms of structural formation.[87] Crosslinked pHEMA hydrogels have been extensively studied in the biomedical and pharmaceutical fields for a range of applications including contact lenses and drug delivery devices.[88] The solute permeability of this and other hydrogels make them ideal materials for devices for the controlled release of drugs and other active agents, with the permeability and hydrophilicity of the matrix dependent on the monomers and crosslinking agent used.

1.2.5 Hydrogels: applications

As stated above, pHEMA-based hydrogels were first examined and prepared for biological use by Wichterle and Lím.[68] The non-toxicity and biocompatibility of pHEMA hydrogels are evident in their use as contact lenses.[89,90] In addition to their non-toxicity, non-antigenic properties and good biocompatibility, pHEMA hydrogels have also been developed as carriers for water soluble anticancer drugs, including 5-fluorouracil,[91] topical mitomycin-C,[92] and cytarabine.[93]

Hsiue and co-workers reported on the potential use of pHEMA hydrogel films as a drug carrier for a long acting delivery system for pilocarpine (**31**),[74] which has been widely used as a topical miotic for controlling elevated intraocular pressure associated with glaucoma. It has been demonstrated that its features remain unchanged once incorporated into pHEMA. The carbonyl group of **31** and the hydroxyl group of pHEMA form hydrogen bonds. Films with different concentrations of cross-linking agent were prepared, namely 0, 6, 10, 20, and 30 wt % of TMPTMA (trimethylolpropane trimethacrylate). It was found

that the pilocarpine diffusion release rate could be retarded by the increase of polymer cross-linking density and that the optimal swelling ratio occurred at a solution of 10 % TMPTMA. Therefore, the cross-linked film with 10 % TMPTMA has the optimal release effect. The results of *in vivo* experiments conducted on albino rabbits were consistent with the observed *in vitro* behaviour.

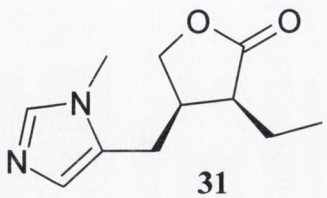

31

Maitra *et al.* developed a nonpolymeric aqueous gel which undergoes colour change when it is doped with a pH indicator.[94] A pH sensitive dye, the sodium salt of bromophenol blue (BPB), incorporated into the hydrogel of a tripodal cholic acid derivative (**32**) was green in colour and changed to yellow upon melting. Bromophenol blue changes colour from yellow at pH < 3 to blue at pH > 4.6.

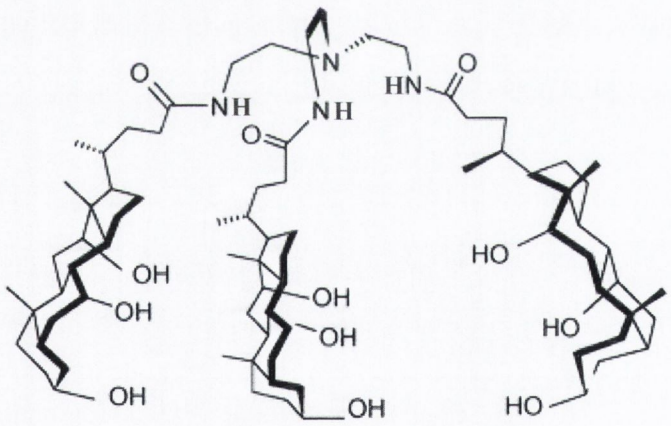

32

It has been hypothesised that the conversion of the sp^3 centre in the neutral form of yellow BPB (**33**) to an sp^2 centre in the ionised blue form (**34**) makes the species more planar (Scheme 1.2), and this form is more easily accommodated in the hydrophobic pockets present in the hydrogel. In the gel phase the hydrophobicity is enhanced due to the formation of networks having high hydrophobic cavities which can accommodate the blue form of the indicator. As the concentration of the blue form increased in the gel state, it appeared green.

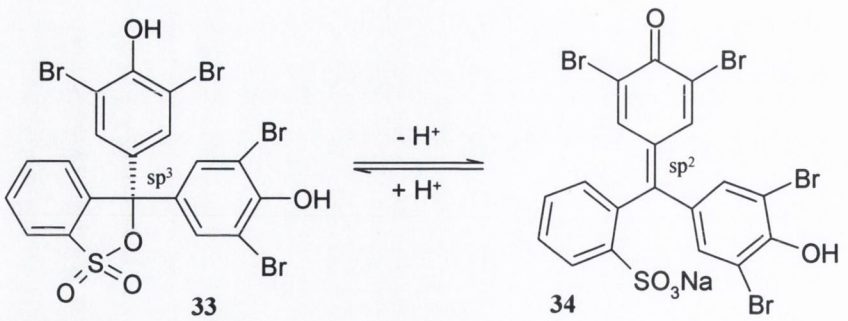

Yellow at pH 3
λ_{max} = 420 nm

Blue at pH 4.6
λ_{max} = 589 nm

Scheme 1.2 Proton-transfer equilibrium of bromophenol blue.

Hamachi and co-workers demonstrated that the molecular recognition features (binding selectivity and affinity) that artificial chemosensors display in solution, can be retained even when the chemosensor is immobilised in a gel matrix.[95] The gel matrix employed was a supramolecular hydrogel consisting of a glycosylated amino acid type of hydrogelator (**35**). A supramolecular hydrogel is formed through self- aggregation of the gelator molecules by means of non-covalent interactions, such as H-bonding, π–π stacking, donor-acceptor interactions, metal coordination, solvophobic forces (hydrophobic forces for gels in water) and van der Waals interactions.[96]

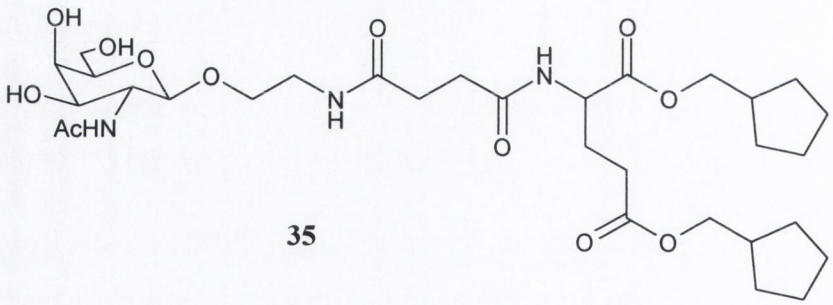

35

The hydrogel used in the experiment was so transparent that spectroscopic analysis of the events inside the gel matrix could be readily carried out. In order to perform a rapid and efficient sensing, the hydrogel was also miniaturised and arranged into an array on a glass support (Scheme 1.3).[95]

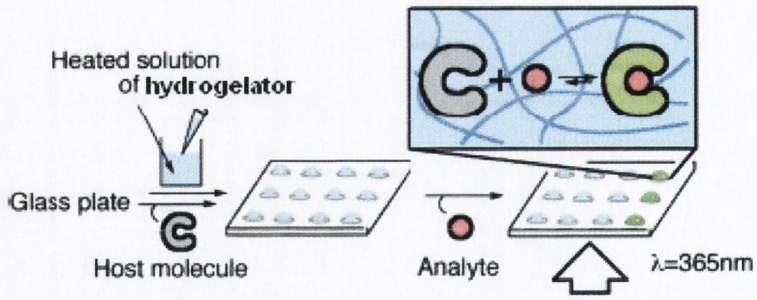

Scheme 1.3 Preparation scheme of a semi-wet sensor array.[95]

High-throughput analysis was carried out using a semi-wet molecular recognition chip involving a fluorescent Zn^{II} receptor (**36**). "Semi-wet" indicates an intermediate property of the hydrogel between aqueous solution and dry solid, which can entrap an artificial receptor non-covalently.

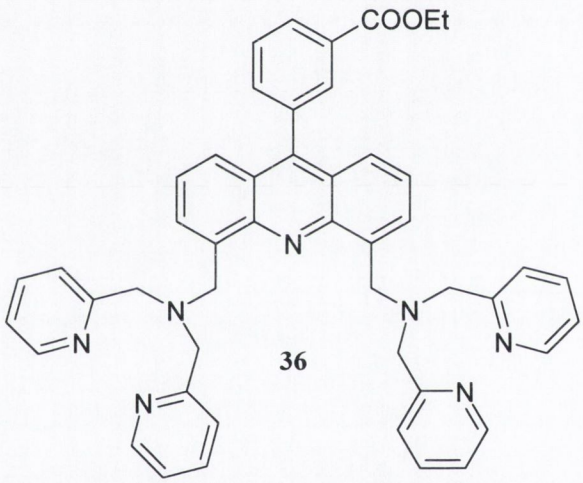

In Figure 1.17 a photo of the hydrogel chip is shown, after corresponding cations were put into each spot. Strong blue emission was observed only in two spots when Zn^{2+} and Cd^{2+} solutions were injected, whereas a very weak emission was observed in others containing Na^{+}, K^{+}, Mg^{2+}, Ca^{2+}, Cu^{2+}, Fe^{3+}, Co^{2+}, or Ni^{2+}.

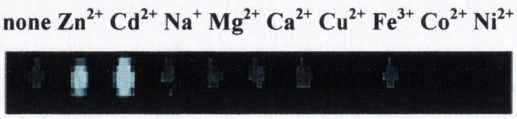

Figure 1.17 Photograph of a sensing pattern of a semi-wet chemosensor chip containing 36 (80 μl) in the presence of various metal cations.[95]

Bioresponsive hydrogel microlenses have been used to develop a novel protein assay method by Lyon *et al.*[97] Stimuli-responsive poly(*N*-isopropylacrylamide-*co*-acrylic acid) (pNIPAm-*co*-AAc) microgels were synthesised *via* free-radical precipitation polymerisation. These hydrogel microparticles were then functionalised with biotin by EDC coupling. The biotinylated microgels then interacted with multivalent proteins (avidin and anti-biotin), which formed additional cross-links between polymer chains in the network (Scheme 1.4). Such a cross-linking event resulted in a change in the equilibrium swelling volume of the microgel and, hence, in an increase in the local refractive index (RI) of the microgel.

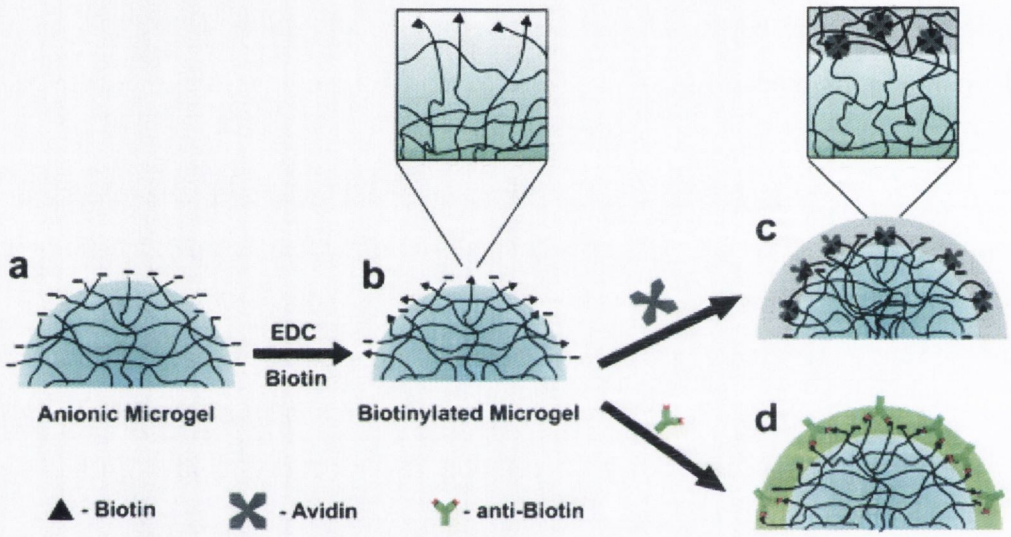

Scheme 1.4 Schematic representation of the hydrogel microlens assay: (a) pNIPAm-*co*-AAc hydrogel microparticles synthesised by aqueous free-radical precipitaton polymerisation method. (b) Biotinylation of pNIPAm-*co*-AAc *via* EDC coupling. (c) Formation of cross-links in the hydrogel by multivalent binding of avidin to biotin on the hydrogel microlenses. (d) Formation of cross-links in the hydrogel by multivalent binding of anti-biotin to biotin on the hydrogel microlenses.

1.3 Work described in this thesis

The versatility of the lanthanide ions has been shown to be of paramount importance in several examples of luminescent sensors and supramolecular assemblies. It has also been outlined how a photonic response can be obtained from a lanthanide luminescent system by way of a sensitising *antenna*. Particular emphasis has been placed on the construction of supramolecular architectures based on lanthanide ions and on the use of organic ligands, as predetermined structural building blocks. With this in mind, the main focus of this thesis will be the development of lanthanide luminescent sensors, in solution and incorporated into water-permeable hydrogels, as well as the design, synthesis and physical evaluation of lanthanide-based supramolecular self-assemblies.

In Chapter 2, the photophysical properties of the two fluorescent pH sensors based upon the amino-1,8-naphthalimide structure, **43** and **44**, will be investigated in solution prior to their incorporation into hydrogels. After assessing the suitability of such fluorescent sensors for incorporation into soft matter (*i.e.* hydrogels), the study of these "luminescent hydrogels" will be further extended to the field of lanthanide complexes. For this purpose, the synthesis and characterisation of ligand **51** and the corresponding Eu^{III} complex (**Eu.51**) will be conducted. Their behaviour in aqueous solution will be then investigated using potentiometric and spectroscopic techniques.

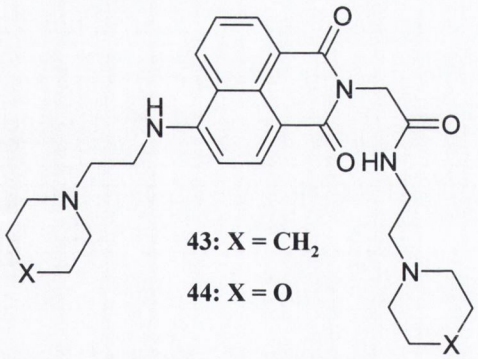

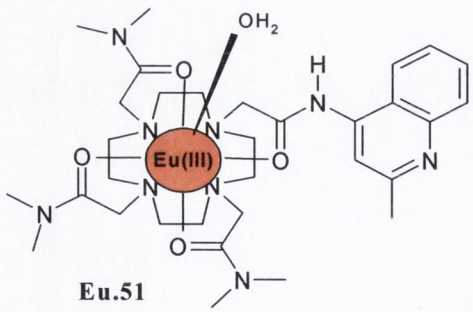

Eu.51

The incorporation of **Eu.51** into water-permeable hydrogels will be addressed using poly[methylmethacrylate-*co*-2-(hydroxyethyl)methacrylate]-based hydrogels and the luminescent properties of the novel sensor materials, using confocal laser-scanning microscopy and steady-state luminescence, will be evaluated.

In Chapters 3 and 4, the synthesis, characterisation, potentiometric and photophysical studies of two chiral bis-tridentate ligands **66** (***R,R***) and **67** (***S,S***) and their

corresponding Eu^{III} triple helical complexes, will be addressed in partially aqueous or organic media.

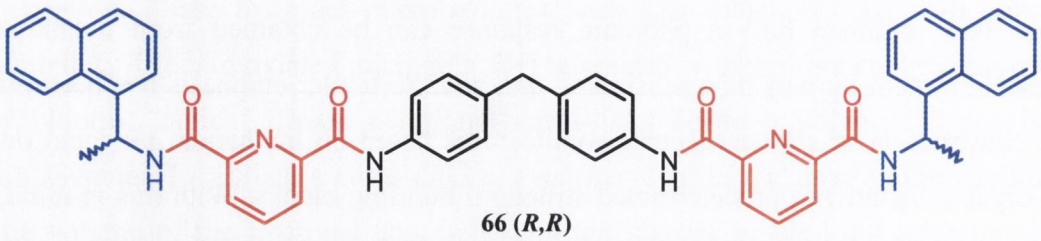

66 (***R,R***)

67 (***S,S***)

An insight into the formation of the desired dinuclear triple helical species, Eu_2L_3, in solution will be gained through the use of several spectroscopic techniques, ^{1}H-NMR, CD, CPL, UV-Vis and luminescence spectroscopy.

2 pH Luminescent Sensors in Solution and Soft-Matter

2.1 Introduction

In recent times great interest has been shown in developing miniaturized molecular devices within the field of supramolecular chemistry. Such molecules are designed to mimic the actions of macroscopic devices such as switches, motors and other machinery.[98,99] The interest in supramolecular devices is due to the fact that they show large changes in their so called "*off*" and "*on*" states, where these states refer to their luminescent, magnetic or electronic properties.[100] The changes in these properties can then be used to signal an interaction at the molecular level. By employing external sources or "inputs", such as ions, molecules, light, *etc.*, it becomes possible to modulate the "state" of a supramolecular device. At the forefront of this emerging field is the development of simple chemical sensors and switches.

2.2 Molecular sensors: from recognition to signalling

The term "sensor" indicates a device that generates a detectable signal in response to an external impulse. Typically a supramolecular sensor is made up of a receptor unit covalently linked to a signalling unit. The receptor needs defined chemical and structural features to be complementary to a specific substrate, such as ionic or molecular. The signalling unit is required to transduce information from the receptor, signalling the presence or absence of the target substrate at the receptor site. A classical example of a spaced luminescent sensor is shown in Figure 2.1.[99]

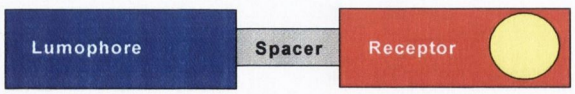

Figure 2.1 Representation of a spaced luminescent sensor.

In this case, the method of communication between the receptor and the lumophore occurs by means of electron transfer (eT)[101] or energy transfer (ET).[102] The spacer must be present to prevent any π-π or σ-π orbital interactions between the two components.[103] The efficiency of a sensor is related to:

- the selective interaction between the receptor and the substrate,
- the simple identification and easy monitoring of the signal.

The latter requirement depends mainly on the choice of the signalling unit. With this regard, optical sensors are highly desirable due to the ease in measuring their response; among all the mechanisms of signal transduction, optical properties, such as fluorescence and luminescence, are the most simply monitored. Moreover, fluorescence and luminescence do not require excessively expensive instruments to be measured and permit detection of the target analyte even at low concentrations (in the order of 10^{-7} M).

2.3 Fluorescent sensors

Fluorescence is the result of a three-stage light induced process that occurs in molecules called fluorophores (these are generally molecules that contain polyaromatics or heterocyclic rings). The process is illustrated by the Jablonski diagram shown in Figure 2.2.

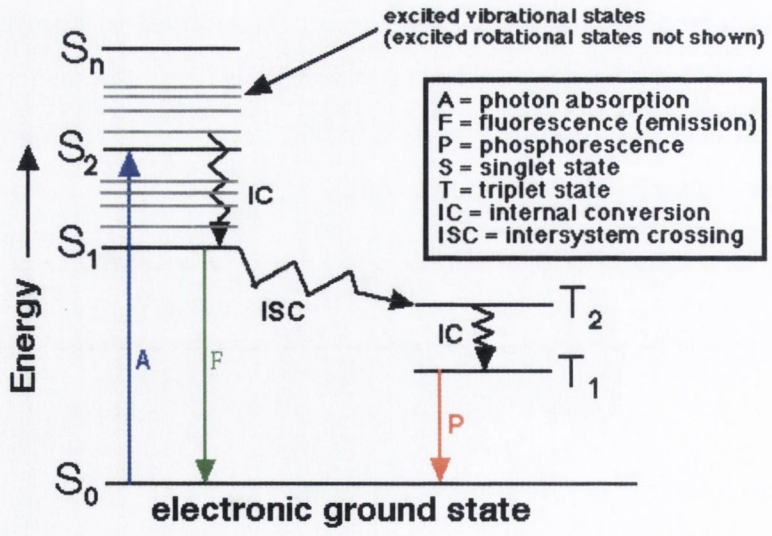

Figure 2.2 Jablonski diagram illustrating the process involved in the creation of an excited state and the subsequent quenching.[104]

The first stage involves the absorption of a photon of light, generated by an external source, by the fluorophore. This results in the excitation of an electron from the ground electronic state, S_0, to one of the several vibrational levels in the electronic state S_1^v (v = 0, 1,...n). The excited state exists for a finite time (1×10^{-5} to 10^{-8} seconds). During the second stage, vibrational energy is lost due to interactions of the fluorophore with its molecular environment. The energy dissipation from the excited vibrational levels S_1^v to S_1^0 yields a relaxed singlet state from which fluorescence emissions originate. Not all the molecules excited return to the ground state by fluorescence emission. Other processes such as collisional quenching, internal conversion (thermal), fluorescence energy transfer and intersystem crossing to a triplet state (T_1) can also cause depopulation of the S_1 state. The third stage involves the emission of light, as fluorescence, as the energy is dissipated from S_1 to S_0.[105] Such photophysics have been shown to be quite useful as a method of signalling for optically based sensors.[106] In the past years, several fluorescent sensors have been studied. Some of the earliest examples are sensors **37a** and **37b** designed by the group of de Silva,[106] who developed sensors for alkali metal ions using anthracene as a fluorescent fragment, pioneering the research in this field.

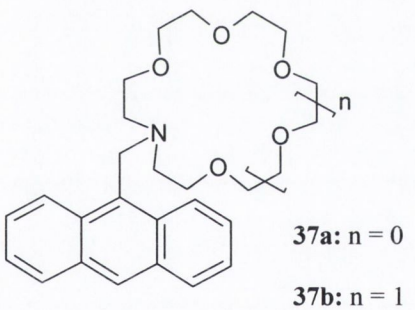

37a: n = 0

37b: n = 1

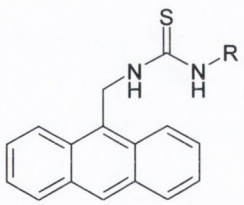

38

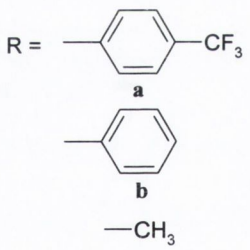

a

b

c

These are examples of the fluorophore-spacer-receptor system mentioned in Section 2.1. The anthracene molecule is the fluorophore, which is connected to the receptor *via* a methylene group. The receptor is the macrocycle 1-aza-15-crown-5 in **37a** and 1-aza-18-crown-6 in **37b**. The type of crown ether confers selectivity to the ligand, as the macrocycle in **37a** binds Na^+ selectively and the macrocycle in **37b** is complementary to K^+. In both cases, in the absence of any metal ions, the system is not fluorescent, as the anthracene fluorescence is switched *"off"* due to "*photoinduced electron transfer*" (PET) from the lone pair of the nitrogen of the macrocyclic ring to the excited state of the anthracene. Upon coordination of the metal ion (Na^+ for **37a** and K^+ for **37b**) the

fluorescence is switched on, as the nitrogen lone pair is now involved in coordination to the metal ion, thus increasing its oxidation potential – hence the *quenching* becomes thermodynamically unfavourable. The interaction between substrate and receptor is signalled by the emission spectrum of the anthracene. Illustration of the PET mechanism is shown in Figure 2.3.[107,108]

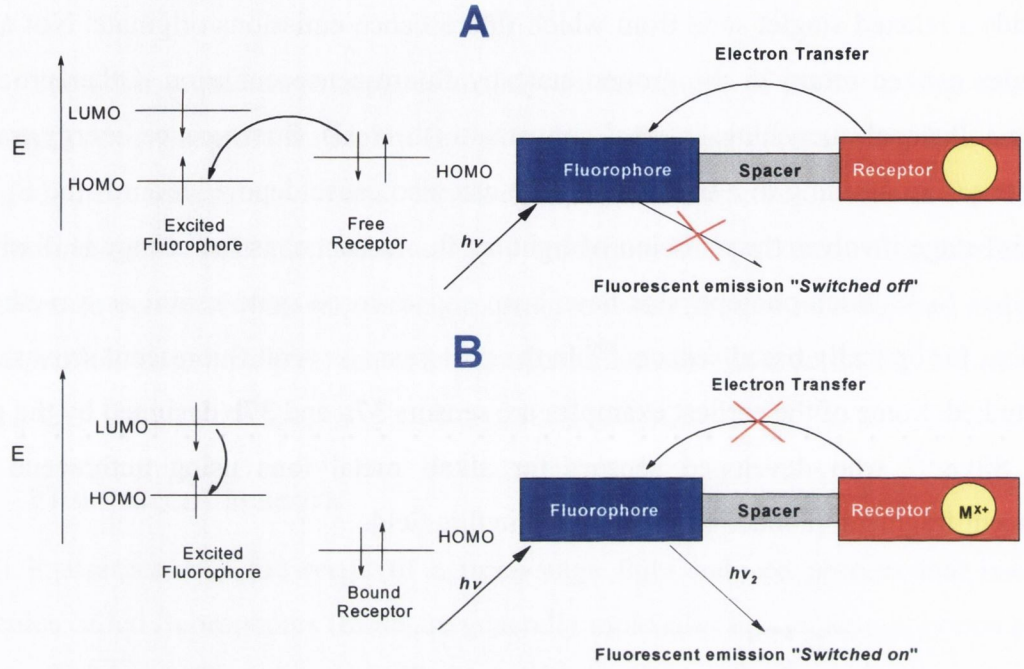

Figure 2.3 Illustration of the PET signalling mechanism present in 37a and 37b. A: when the receptor is in the unbound state, electron transfer from the receptor's HOMO can occur, preventing fluorescence. B: when the receptor is bound to a substrate, its oxidation potential increases and electron transfer from the receptor's HOMO becomes unfeasible, resulting in fluorescence.[109]

Both **37a** and **37b** are classical examples of "*off-on*" sensors: fluorescence is "*off*" in the absence of the substrate and it is switched "*on*" as recognition occurs. Other examples of fluorescent sensors are those in which the analyte recognition is signalled by quenching of the fluorescence. These are called "*on-off*" sensors and **38a-c** represent recent examples of this type.[110] The charge neutral chemosensors **38a-c** employ the criteria of PET for anion sensing. In such molecules, the anthracene moiety represents the fluorophore and the aromatic (**38a-b**) or aliphatic thiourea (**38c**) are the anion receptors. The anthracene fluorescence emission in DMSO is selectively quenched upon titration with anions, such as acetate, dihydrogenphosphate and fluoride over bromide and chloride.

Many sensors of this type have been designed and studied in detail, using different receptors and fluorophores depending on the target analyte.[101,110-113] With the aim of

achieving real-life applications, such sensors have also been incorporated into everyday-use devices. One of the most remarkable examples involves the implementation of fluorescent sensors in a 'critical care analyser' (OPTI CCA, Figure 2.4). De Silva and co-workers developed 4-amino-1,8-naphthalimide-based fluorescent sensors specific for sodium, potassium and calcium.[114] Such sensors were then incorporated into a portable diagnostic tool, *i.e.* a blood gas analyzer for hospital critical care units and ambulances, in collaboration with scientists at AVL Bioscience Corporation, Roswell, GA. The OPTI system measures eight analytes in whole blood with only six sensors, performing the measurement within two minutes using only 120 μl of blood sample. The six sensors (or optodes) are incorporated into a disposable cassette (see Figure 2.4) for detecting pH, pCO_2, pO_2, Na^+, K^+ and Ca^{2+}, all using fluorescence as the method for the signal transduction.

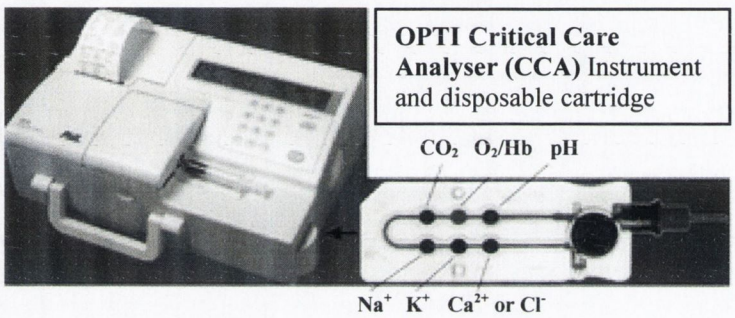

Figure 2.4 Picture of OPTI CCA instrument (left) and the disposable cartridge (right).[114]

The next sections of this chapter detail some examples of fluorescent and luminescent sensors incorporated into soft-matter, with potential applications in the interference-free analysis of biological media.

2.4 Naphthalimides

Among the many fluorophores used as signalling units in PET sensors, 4-amino-1,8-naphthalimides represent an important example. 1,8-Naphthalimide derivatives are well known due to their potency as anticancer compounds.[115] However, their use extends further as they find applications as fluorescent brighteners (**39**)[116] and dyes (**40**),[117] as fluorescent probes and labels (**41**),[118] as pH sensors (**42**),[119] as solar energy collectors[120] and as dye lasers.[121]

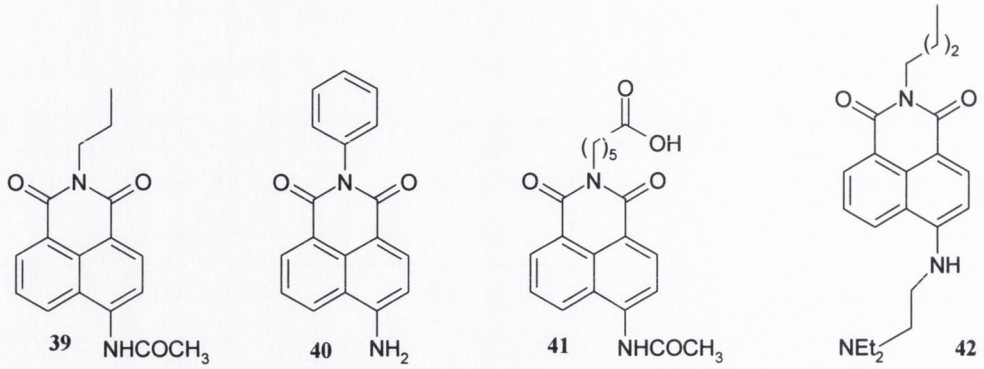

Some naphthalimides are also photonucleases/cleavage molecules as they possess the ability to kill cells when photoactivated.[122] They have also been used as fluorescent units in the design of PET anion sensors.[123] It is thus not difficult to understand why naphthalimides are of such importance in the scientific and medicinal world, but their contribution also lies in the fact that they are relatively easy to synthesise and produce on a large scale.

1,8-Naphthalimide derivatives functionalised with an amino group in the 3, and 4 positions show a high quantum yield of fluorescence. This is due to an internal charge transfer excited state, which creates a separated partial positive and negative charge upon excitation; here the amino group has a partial positive charge while the imide function is partially negatively charged. This results in a so-called push-pull excited state that deactivates itself through emission of light in the green part of the electromagnetic spectrum. This property becomes particularly attractive from a physiological point of view, since it avoids the problems of auto-fluorescence and light scattering present in most biological environments.[124]

With this regard, different 1,8-naphthalimide derivatives will be studied as pH-sensors either in solution or in soft-matter, *i.e.* hydrogels, as discussed in the following section.

2.4.1 Naphthalimide-based chemosensors

With the aim of achieving *in vivo* sensing, the design and photophysical studies of naphthalimide-based chemosensors were addressed. In biological environments, it is important to consider the photophysical features of the lumophore, in relation to its excitation and emission wavelengths, as well as its excited state lifetime. Specifically, 4- or 3-amino-1,8-naphthalimides are of particular interest in this respect as they absorb and

emit at long wavelengths,[32] with λ_{abs} max ~ 450 and λ_{em} max ~ 550 nm. Moreover, they are easily synthesised and suitable for incorporation into polymeric matrices and onto solid-surfaces. These properties are essential when employing such devices in real-time analysis. However, such immobilization often decreases the efficiency of the sensors. In particular, as they are often placed into organic phases or lipophilic membranes, which affect the uptake of the aqueous based analyte, the response time and the photophysical properties of the solid state device are also affected.[125]

With this in mind we set out to develop fluorescent chemosensors based upon the amino-1,8-napthalimide structure and incorporate these into water-permeable hydrogels. Such hydrogels are easily handled and, when the composition is chosen judiciously, do not require that the sensor be covalently bonded to the polymeric matrix.[125-128] Compounds **43** and **44** are examples of our general design. The following is an account of the synthesis and photophysical studies of **43** and **44** in solution and soft-matter.

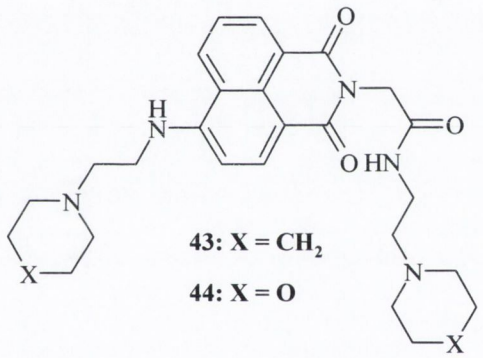

2.4.2 Design and synthesis of 43 and 44

The two chemosensors, **43** and **44**, were designed for determining pH changes within the physiological pH range. They are based on the above discussed "*fluorophore-spacer-receptor*" model,[106] where the 4-amino-1,8-naphthalimide moiety is the fluorophore and the piperidine (**43**) or morpholine (**44**) amines are the proton receptors. The ethylene spacer covalently separates the two units. In the "*off*" state, an electron transfer from the amine to the excited state of the fluorophore quenches the fluorescence emisson of the naphthalimide unit. Upon protonation of the piperidine (**43**) or morpholine (**44**) amino moieties, their oxidation potentials decrease, thus preventing electron transfer to the fluorophore and resulting in fluorescence emission ("*on*" state).

In both sensors, there are two tertiary amino moieties. However, as demonstrated by de Silva *et al.*,[129] only the receptor that is directly attached through the 4-amino moiety can quench the excited state of the fluorophore, *i.e.* the naphthalimide. As previously mentioned, this is due to an internal charge transfer excited state, creating a separated partial positive and negative charge upon excitation; the 4-amino group thus gains a partial positive charge while the imide function is partially negatively charged (see Figure 2.5). In other words, the amino group is acting as an electron donor, whereas the imide function is an electron acceptor. Consequently, a push-pull mechanism is in operation and due to charge repulsion, the electron transfer from the receptor linked to the imide moiety is unfavourable.

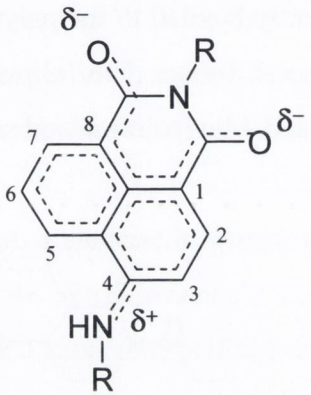

Figure 2.5 ICT within the naphthalimide molecule

The synthesis of **43** and **44** was achieved in two steps as shown in Scheme 2.1. The ester **46**, was recovered in a 77 % yield by reacting the 4-chloro-1,8-naphthalic anhydride with glycine methyl ester in refluxing anhydrous toluene in the presence of triethylamine. The desired product was isolated after treating it with aqueous acid and recrystallisation from methanol. The two chemosensors were subsequently formed by reacting **46** in a large excess with either 1-(2-aminoethyl)-piperidine (**a**) or 4-(2-aminoethyl)-morpholine (**b**) at 80 °C for 12 hours. The resulting solutions were then cooled to room temperature before pouring them onto an ice cold water solution with vigorous stirring. The products were then isolated by filtration and washed several times with 1 M HCl solution, affording the two products in 74 and 80 % yield, respectively. No further purification was necessary, as the product was confirmed to be pure using conventional techniques, such as elemental analysis, NMR, ES-MS and IR.

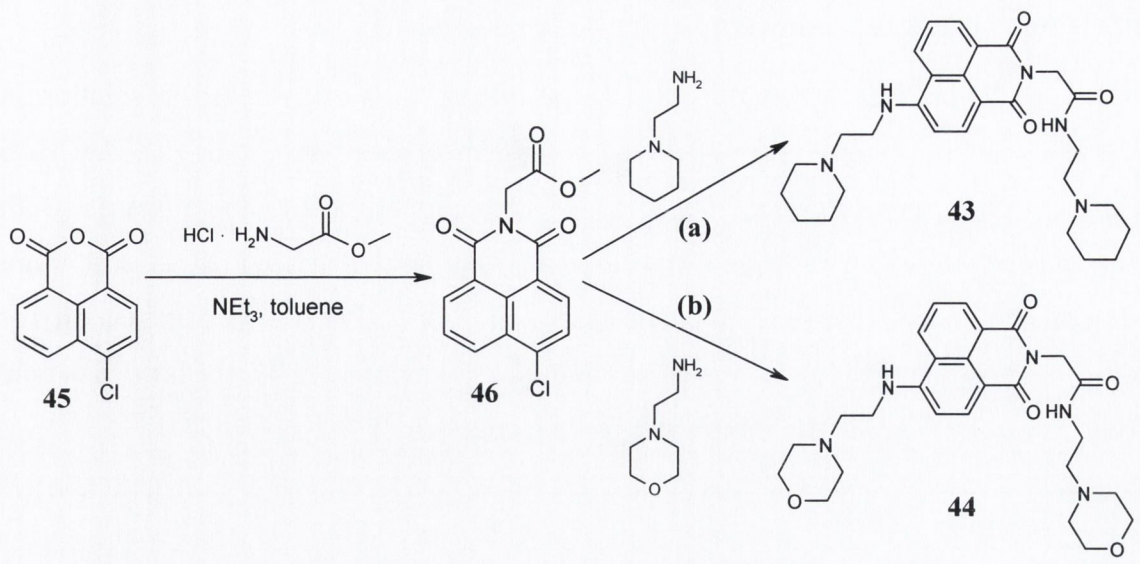

Scheme 2.1 Synthesis of 43 and 44.

The ^{1}H NMR (400 MHz, $CDCl_3$) spectra of **43** and **44** showed a signal at 6.78 and 6.56 ppm, respectively (*cf.* Figure 2.6 for ligand **44**). These resonances are characteristic of the proton in position 3 on the naphthalimide ring when adjacent to a 4-amino group, therefore providing evidence of the desired substitution at the 4-position (in the starting material, **46**, the H_3 signal appears at 8.09 ppm, whereas in both **43** and **44**, the resonances were shifted upfield). Furthermore, the correct integration, together with the absence of the CH_3 signal in the ^{1}H NMR and in the ^{13}C NMR spectra is further evidence of the reaction of the methyl ester. This, in addition to the chemical shift of H_3, confirmed that di-substitution had occurred. Moreover, the electro-spray mass spectrum contained the M^+ peaks at 492.3 (**43**) and 495.8 (**44**) mass units, respectively.

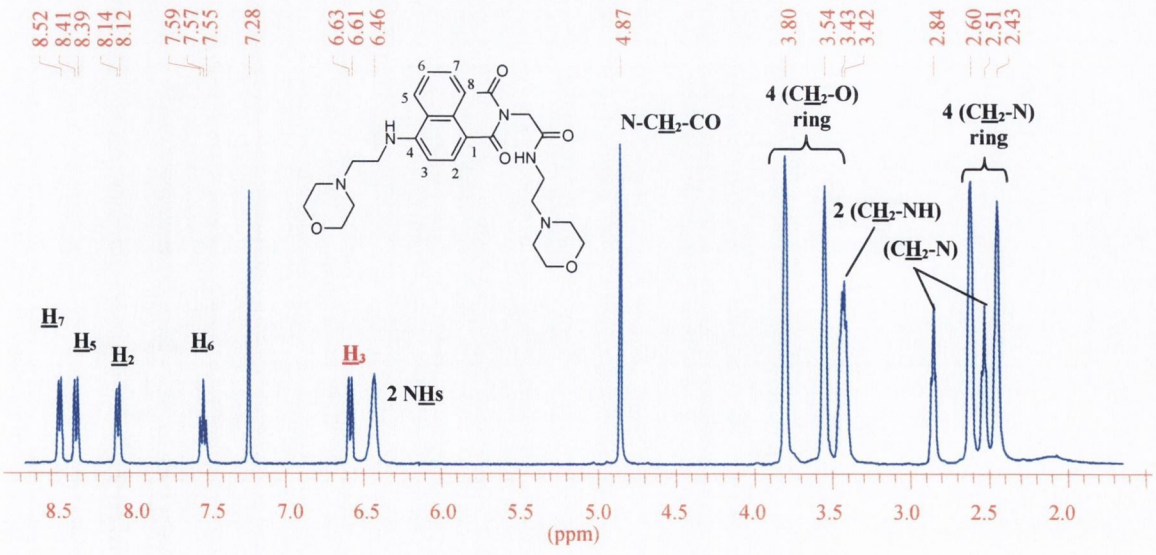

Figure 2.6 ^{1}H-NMR (400 MHz, $CDCl_3$) of compound 44.

2.4.3 Photophysical studies of 43 and 44 in solution

The photophysical properties of **43** and **44** were first investigated in solution in deionised water, in the presence of 0.1 M tetramethylammonium chloride (TMACl) to maintain constant ionic strength, prior to their incorporation into a hydrogel matrix. Both compounds are highly coloured and show a broad absorbance band centred at *ca.* 450 nm due to the previously discussed ICT excited state. The UV-visible spectra were recorded at acidic, neutral and basic pHs: as shown in Figure 2.7 for compound **43**, the band was blue shifted upon acidification with minor changes in intensity.

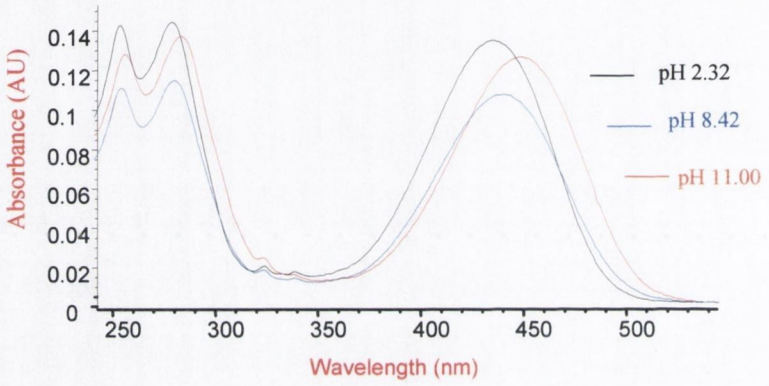

Figure 2.7 UV-Vis. spectra of 43 at three different pHs.

The fluorescence emission spectra of **43** and **44** were also recorded in water in the presence of 0.1 M TMACl. In alkaline solution, only a week emission was observed, with a λ_{max} at *ca.* 540 nm for both compounds. However, upon acidification the emission was gradually increased as demonstrated in Figure 2.8 (a) and (b).

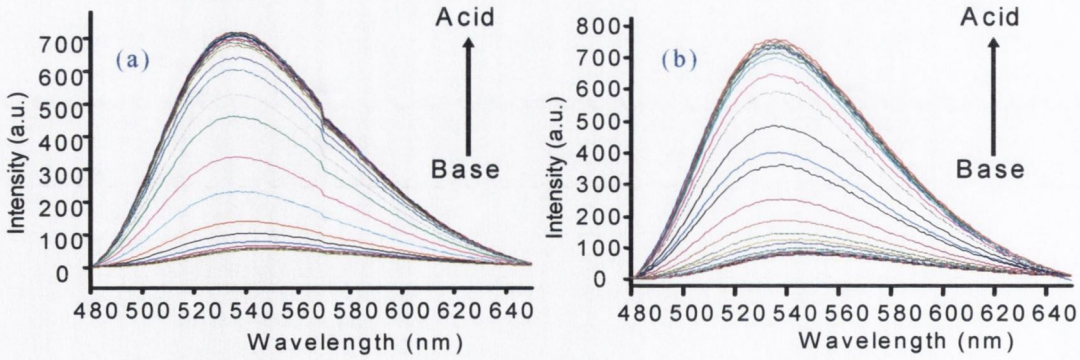

Figure 2.8 Fluorescence emission spectra of 43 (a) and 44 (b) upon acidification from pH 12 to pH 2.5.

A pH titration was carried out from pH 12 to 2.5 and an emission enhancement by over an order of magnitude was observed. It is therefore possible to say that the sensors are in their "*off*" state in alkaline solution, whereas they are in the "*on*" state in acidic solution. These changes are due to the protonation of the nitrogen directly attached to the 4-amino moiety in both **43** and **44**. In alkaline solution these moieties are engaged in the quenching of the naphthalimide excited state by a photoinduced electron transfer (PET), whereas upon protonation this quenching process becomes thermodynamically unfavourable.

As further evidence, the photophysical properties of compound **50** were also investigated. As expected, this derivative, which lacks the amino receptor, showed no changes in emission as a function of pH.

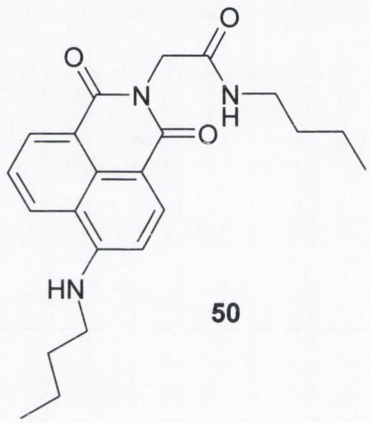

50

Compounds **43** and **44** are thus efficient "*off-on*" switches for pH in solution. From the changes in the fluorescence emission spectra as a function of pH, the pK_a's of the two sensors were determined, resulting in a pK_a=8.4(±0.1) for **43** and pK_a=6.3(±0.1) for **44**. As expected, the morpholine nitrogen is more acidic due to the electron withdrawing effect of the oxygen. The sigmoidal curves of I_f at 536 nm *vs* pH for both compounds are shown in Figure 2.9.

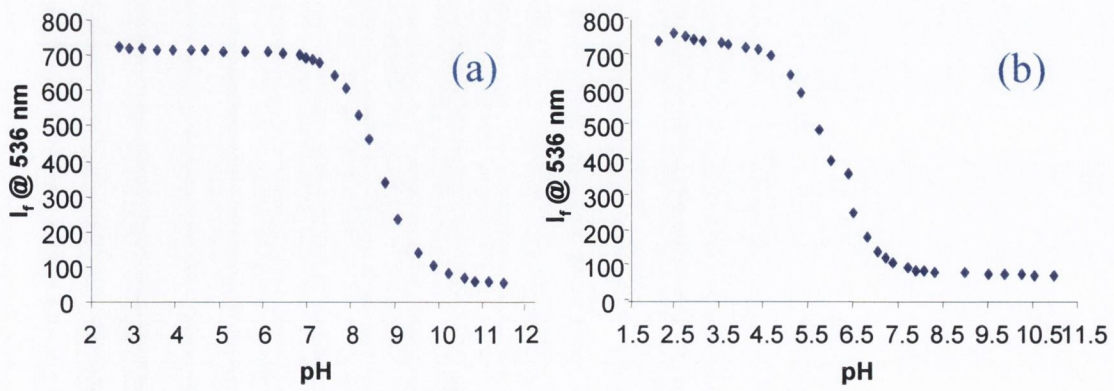

Figure 2.9 Fluorescence intensity at 536 nm of 43 (a) and 44 (b) as a function of pH.

2.4.4 Incorporation of 43 and 44 into hydrogel

Hydrogels are, by definition, soft, solid polymer structures, which contain a significant volume fraction of water (often over 90 %). The three-dimensional polymer structure in the hydrogel is usually held together by cross-linking, not only by physical interactions such as Van der Waals or hydrogen bonds but also by covalent bonds, formed by cross-linking reagents or γ-irradiation.[130] Amongst the most widely studied hydrogels are those based on poly[2(hydroxyethylmethacrylate)] (pHEMA) (**30**).[70] As detailed in Chapter 1 (*cf.* Table 1.2), HEMA (**47**) is a hydrophilic monomer and, as such, pHEMA hydrogels swell extensively in water, thus becoming highly permeable. Such permeability is not desirable for the current study since the immobilisation of **43** and **44** into the hydrogel matrix would not be permanent, as the sensors are non-covalently incorporated. To reduce the permeability, methylmethacrylate (MMA, **48**) was copolymerised with HEMA to give copolymers comprising of a MMA/HEMA ratio of 3:1 (w/w). Using MMA as a comonomer confers hydrophobic character on the resulting copolymer as homopolymeric pMMA (**49**) takes up significantly less water than pHEMA.

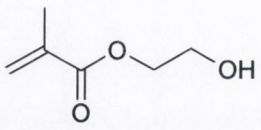

47 (HEMA)

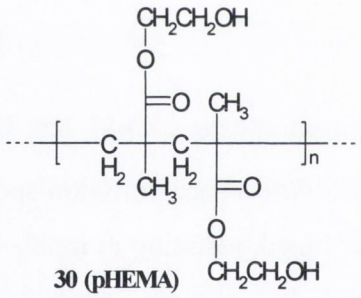

30 (pHEMA)

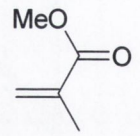

48 (MMA)

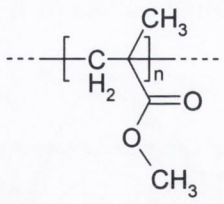

49 (pMMA)

In order to study the behaviour of these sensors in a hydrogel matrix, **43** and **44** were incorporated in a hydrogel comprised of poly[methylmethacrylate-*co*-2-(hydroxyethylmethacrylate)] in a monomer ratio 3:1 MMA to HEMA by weight, crosslinked with 1 % by weight ethyleneglycol dimethacrylate. A mixture of HEMA, MMA, ethyleneglycol dimethacrylate and radical initiator (azo-*bis*-isobutyronitrile) was stirred until solubilisation was complete (*cf.* Section 5.10.2). In order to achieve a homogeneous dispersion of **43** and **44** in the hydrogel, the appropriate sensor was dissolved in the monomer mixture prior to polymerisation. The mixture obtained was then injected into a 1 mm mould with release liner. The mould was heated at 90 °C for 6 hours and the resulting material swollen to equilibrium in water. The immobilisation of **43** and **44** was verified by allowing hydrogel segments to soak for one month in deionised water. This water was found to contain no trace of sensor as determined by UV-visible and fluorescence spectroscopy.

2.4.5 Photophysical studies of 43 and 44 in soft-matter

As the hydrogel contains water in its structure, the photophysical behaviour of **43** and **44** was expected to be very similar to that in solution. Fluorescence measurements were performed using confocal laser-scanning microscopy (CLSM) in Queen's University Belfast. CLSM allows direct, non invasive detection of fluorescence from the surface of a sample following excitation from an appropriate laser source.[77] To build up a single image, data are collected pixel by pixel with the laser rastering over the sample. The overall fluorescence intensity within a defined wavelength range is allocated a colour according to a look-up table (LUT). The LUT ranges from black (allocated to a low detected photomultiplier voltage) to bright green (allocated to a high detected photomultiplier voltage), with shades of green allocated on an increasing intensity scale to increasing intermediate PMT voltages. The intensity of colour of each pixel thus correlates with fluorescence intensity within the defined wavelength range of the sample at that point.[131] Using this technique, it is therefore possible to measure the fluorescence emission from any defined area within a collected series of images. This allowed us to characterise both the distribution of the sensors within the hydrogel matrix and their emission features on a macro (from square micron up to square millimetre) scale. Excitation was achieved using the 458 nm line from an Ar/ArKr laser. Monochromated xyλ data were collected as a series of scans every 2.5 nm with a bandwidth of 5 nm over the range 465-750 nm. A

typical image showing the emission integrated over the range 465-750 nm is shown in Figure 2.10, from which the homogeneity of the sensor within the hydrogel can be seen.

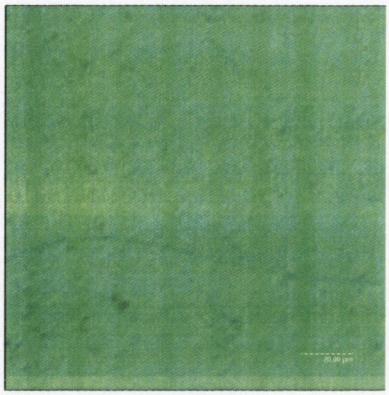

Figure 2.10 CLSM image of a section of the hydrogel incorporating 0.05% w/w 44 at pH 2.5 showing the homogeneity of the film.

The xyλ data collected allowed fluorescence emission spectra from the surface of the hydrogel to be obtained, in both acidic and basic media (Figure 2.11).

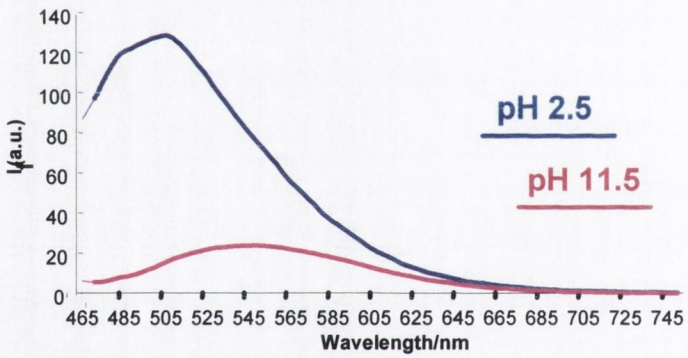

Figure 2.11 Fluorescence emission spectra of hydrogel incorporating 0.05% w/w 44 at pH 2.5 and 11.5 (λ_{exc} = 458 nm).

Although not shown, the results for compound **43** were similar. These studies demonstrated that the fluorescence properties of **43** and **44** are strongly pH dependent in both hydrogel matrices and in solution. The emission maximum at pH 11.5 occurred at 550 nm and shifted to 510 nm at pH 2.5, with an enhancement in intensity of approximately an order of magnitude. The blue shift can be explained by the destabilisation of the ICT state of the naphthalimide moiety, due to the proximity of the protonated amine to the partially positively charged end of the molecule. This was observed also in solution but to a lesser extent. The greater hypsochromic shift shown in soft-matter is possibly attributable to the

intermolecular forces between the sensors and the hydrophobic polymer chains, which further destabilise the polar excited state.

2.4.6 From fluorescent to lanthanide luminescent sensors

The purpose of the first project described in this thesis was to develop pH PET sensors suitable for water-permeable hydrogels, in order to preliminarily evaluate the adaptability and suitability of such sensors to medical and environmental fields. The determined pK_a values for the two chemosensors **43** and **44** indicated that they would be able to monitor pH changes in the physiological pH range. These sensors were then incorporated into hydrogels without having to covalently bind them to a polymeric support. The fluorescence properties of the resulting films were investigated using confocal laser-scanning microscopy. For both compounds, the emission was switched "*off*" or "*on*" as a function of pH, mirroring the behaviour in aqueous solution. Having assessed the functionality of these fluorescent sensors in water-permeable hydrogels, it was decided to further extend the use of such soft-materials to lanthanide chemistry. As extensively detailed in Chapter 1, the chemistry of lanthanides has been the centre of enormous interest in the last decades, due to their photophysical and magnetic features. In the next section, the behaviour of a lanthanide-based pH sensor will be investigated in both solution and soft-matter.

2.5 Lanthanide sensitised luminescent sensors

The development of luminescent signalling devices is a very active area in the field of supramolecular chemistry. Among the innumerable luminescent sensors, a considerable interest has been shown in the unusual spectroscopic properties of some lanthanide ions, especially when they are chelated with appropriate organic ligands.[132] The main advantages of lanthanide chelates in fluorescence spectrometry include large Stokes shifts (relative to biological substances), narrow emission bands and long excited state lifetimes, rendering separation of the luminescent signal from the background biological autofluorescence relatively easy. These have led to numerous applications in various fields[21]- from uses in optical amplifiers and lasers to clinical chemistry and molecular biology. Due to these properties, lanthanide ion complexes are of special interest with regard to *in vivo* measurements.

The main drawback of lanthanide ions is their low absorption coefficients, resulting in inefficient direct excitation.[21] One way to solve this problem is to use polyaromatics as

sensitisers or antennae, taking advantage of the generally high extinction coefficient of these molecules. The antenna absorbs the excitation energy efficiently passing into its singlet-excited state. Then the energy can pass into the antenna triplet state *via* inter system crossing (ISC) and can eventually be transferred to the lanthanide ion $(Ln^{3+})^*$ by means of an intramolecular energy tranfer (ET), thus resulting in lanthanide ion luminescence (Figure 2.12).[10]

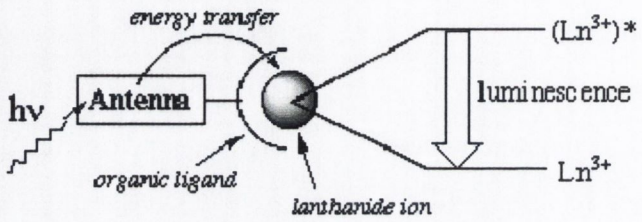

Figure 2.12 Schematic representation of the sensitisation process of a lanthanide ion.[10]

This process can be realised by either the direct coordination of sensitiser molecules to a lanthanide ion[27] or by the covalent attachment of sensitiser molecules to an organic ligand, which is able to complex a lanthanide ion.[26] By incorporating an appropriate recognition moiety into the antenna, it is possible to achieve sensing through selective modulation of the lanthanide luminescence. With this in mind, the synthesis, potentiometric and photophysical studies of **Eu.51** as a pH sensor have been addressed, its photophysical properties have been studied both in aqueous solution and in soft-matter, *i.e.* incorporated into hydrogels.

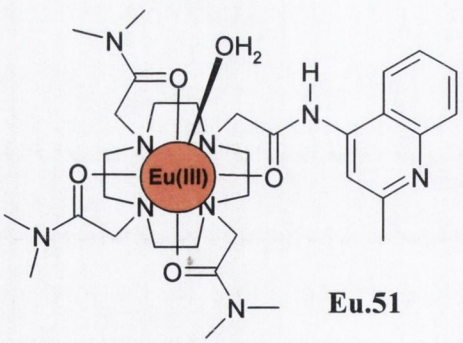

Eu.51

2.5.1 Design and synthesis of Eu.51

Ligand **51** is derived from 1,4,7,10-tetraazacyclododecane (cyclen). Cyclen derivatives are commonly used as they are known to form kinetically and thermodynamically stable complexes with lanthanide ions.[133-136] Due to their low extinction coefficients and large energy gaps between the emissive and the ground states,[137] lanthanide ions are in general photophysically inert. However, their emissive states can be populated indirectly by using a sensitising *antenna*, *i.e.* a chromophore able to transfer its own energy to the lanthanide ion. This energy transfer can be achieved if the triplet excited state of the antenna is sufficiently long-lived and its energy is close to the energy of the emissive state of the lanthanide ion. The *antenna* can either be covalently connected to cyclen or be directly coordinated to the lanthanide ion.

In order to develop a Eu^{III} pH sensor, the choice of a suitable sensitiser was crucial. The quinoline derivative (**54**) was chosen as an *antenna* for the system due to the fact that its photophysical properties are such that efficient Eu^{III} sensitisation can occur.[26] In our case, the *antenna* was covalently attached to the ligand. The synthesis of the ligand **51** is shown in Scheme 2.2. The α-chloroacetamide **54** was made in one step by reacting 4-aminoquinaldine (**52**) with chloroacetyl chloride (**53**) at –10 °C in dry CH_2Cl_2 and 1 equivalent of NEt_3, followed by acid-base extraction to yield an off-white solid (40%) which required no further purification. The tri-arm cyclen **57** was synthesised by reacting cyclen with the α-chloroamide of *N*,*N*-dimethyl acetamide in dry CH_3CN (in a 3:1 molar ratio of acetamide: cyclen) at 65 °C for 72 hours in the presence of $NaHCO_3$. The product was then purified by column chromatography on alumina (gradient elution from 100% CH_2Cl_2 to 60:40 v/v, $MeOH.NH_3$:CH_2Cl_2) and obtained in 34.5% yield. The coupling of **54** and **57** was finally carried out in DMF in the presence of Cs_2CO_3 and KI for three days at 85 °C. The ligand **51** was purified by precipitation from dry diethyl ether (53% yield) and characterised using conventional analytical techniques.

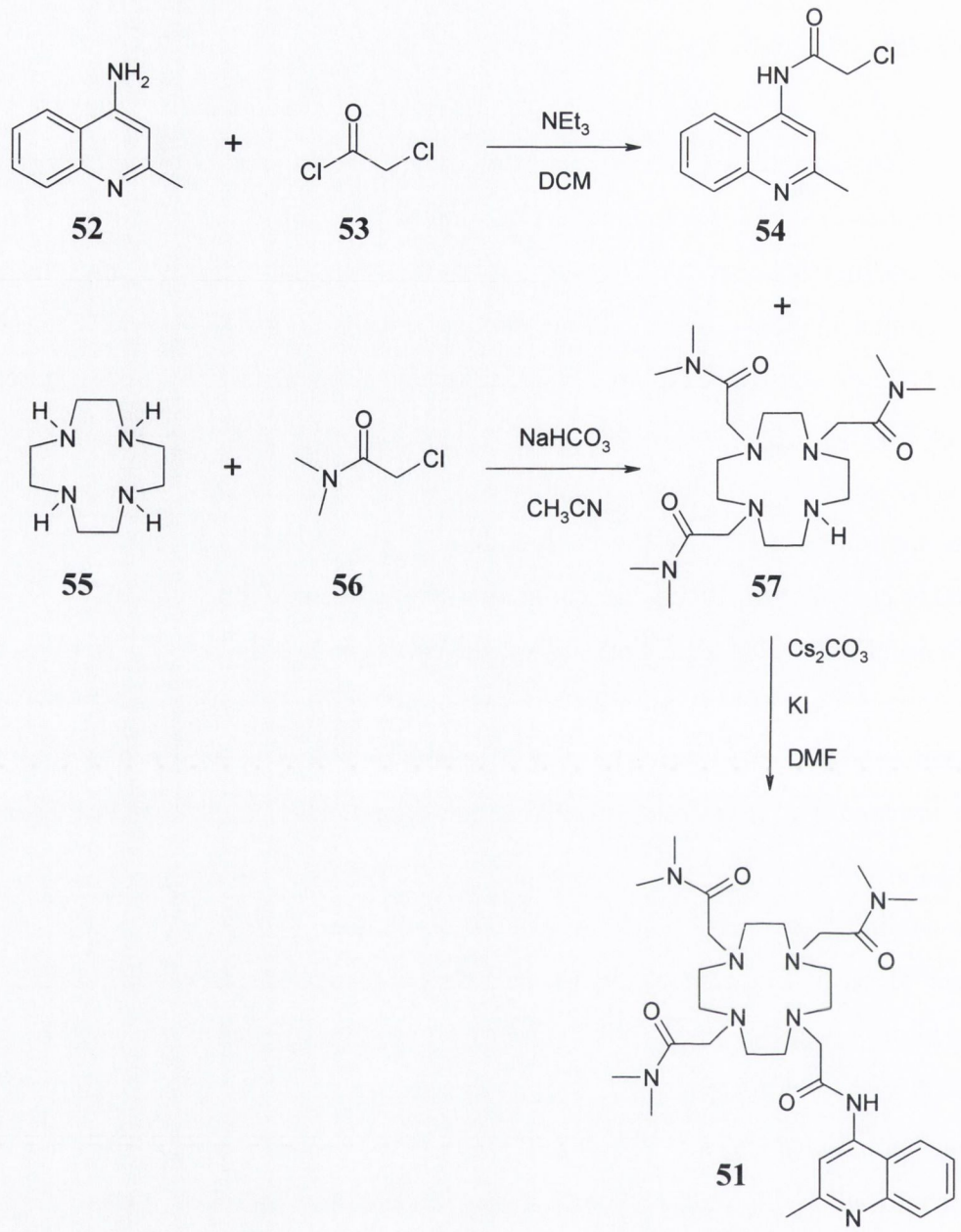

Scheme 2.2 Synthesis of the antenna α-chloroamide 54, the tri-substituted cyclen 57 and Ligand 51.

In the ^{1}H NMR (400 MHz, $CDCl_3$) of **51**, the loss of the cyclen NH proton at 10.00 ppm is evidence of the forth substitution occurring on the cyclen ring. Furthermore, the CH_2 singlet of the quinoline arm has been shifted upfield (Δ ppm = -0.51). This indicates substitution of the α-Cl with a tertiary amine. High resolution mass spectrometry ($C_{32}H_{51}N_9O_4$, *m/z* = 626.4163) also confirmed the identity of the compound.

Finally, the Eu(III) complex of **51** was made by heating equivalent amounts of **51** and $Eu(CF_3SO_3)_3$ in dry CH_3CN under reflux in an inert atmosphere for 24 hours. Upon

cooling to room temperature the solution was poured into a stirring solution of dry diethyl ether, which resulted in the formation of a brown solid. This precipitation method was repeated several times yielding a pale green solid in 83.6% yield.

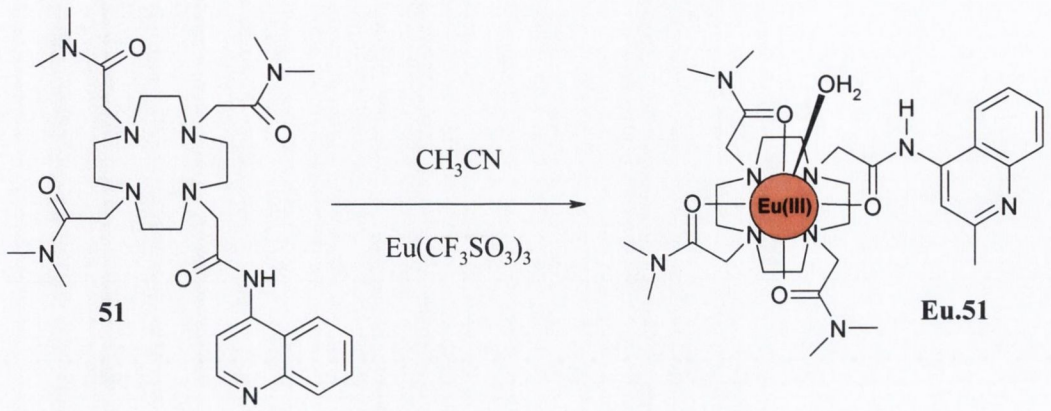

Scheme 2.3 Eu(III) complex formation.

The ^{1}H-NMR of this solid in acetone-d_6 (Figure 2.13) showed the characteristic europium shifted axial and equatorial cyclen hydrogens, in the range of -10 to 13 ppm. This shift/line broadening is characteristic of lanthanide complex formation and confirms that in solution the complex adopts a square prismatic geometry.[138] The shift in the IR carbonyl signal from 1645 cm^{-1} (**51**) to 1624 cm $^{-1}$ (**Eu.51**) provides further evidence of complexation; the carbonyl groups are in fact involved in the coordination of the metal cation, thus weakening the C=O stretching resulting in a peak at a lower wavenumber.

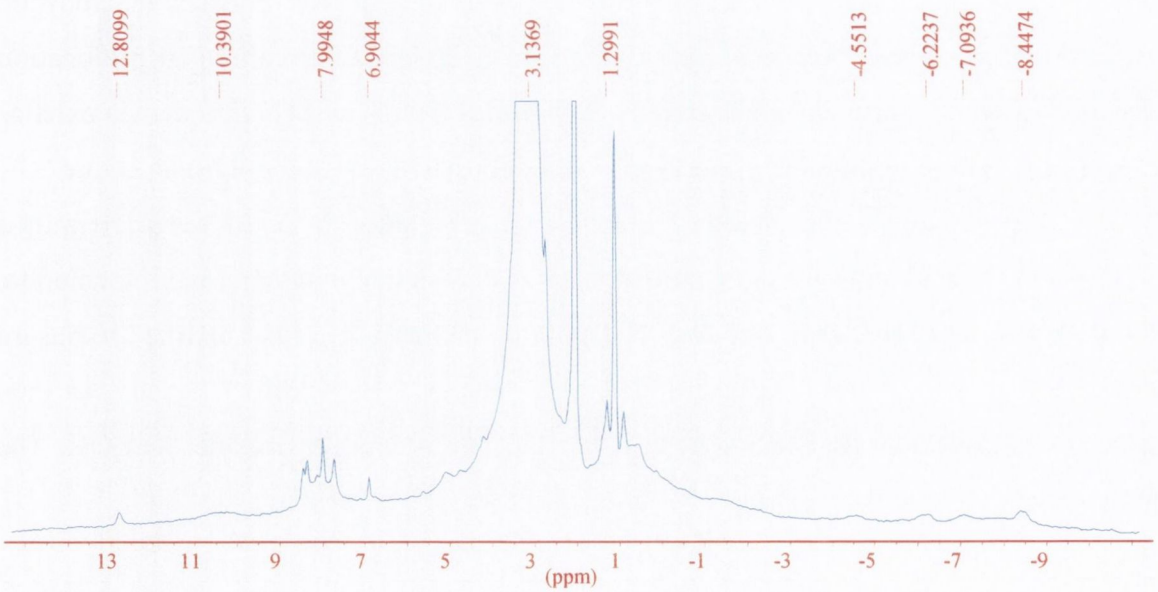

Figure 2.13 ^{1}H-NMR (400 MHz, acetone-d_6) of Eu.51.

The ESMS also showed that complexation had occurred as a characteristic europium isotopic distribution pattern was observed as shown in Figure 2.14.

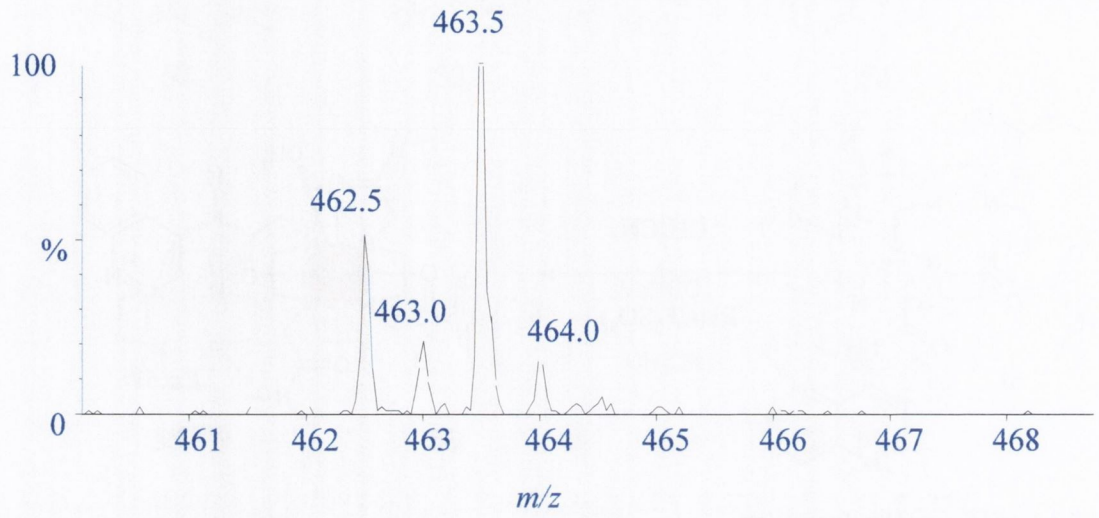

Figure 2.14 ESMS of Eu.51 in CH_3OH showing the correct isotopic distribution pattern.

Based on the above information and according to TLC, it was presumed complex formation had occurred and that the complex was isolated in its pure state.

2.5.2 Potentiometric measurements of ligand 51

2.5.2.1 Protonation constants (pK_as)

In order to fully investigate the metal ion binding affinities of ligand **51**, preliminary studies on its acid-base properties were conducted. Polyaza macrocyclic ligands, such as cyclen, behave as bases in aqueous solutions; therefore, their protonation may compete with complexation reactions. In aqueous solution, such compounds exist as an equilibrium mixture of their free and protonated forms due to their polybasic nature.[139]

The protonation constants (pK_a values) of the protonated ligand **51** were determined in 100 % H_2O, with constant ionic strength, I = 0.1 M (tetraethylammonium perchlorate, NEt_4ClO_4), by potentiometric titration. The solution of the ligand was acidified to ensure complete protonation of all basic nitrogen donor atoms. The acidified ligand was then gradually deprotonated by titration against tetraethylammonium hydroxide, NEt_4OH. The stepwise acid-base equations for a tetra-basic system can be expressed as follows:

$$[LH]^{+} \xrightleftharpoons{K_{a1}} H^{+} + L \qquad K_{a1} = \frac{[H^{+}]\,[L]}{[LH]^{+}} \qquad \textbf{(2.1)}$$

$$[LH_2]^{2+} \xrightleftharpoons{K_{a2}} H^{+} + [LH]^{+} \qquad K_{a2} = \frac{[H^{+}]\,[LH^{+}]}{[LH_2^{2+}]} \qquad \textbf{(2.2)}$$

$$[LH_3]^{3+} \xrightleftharpoons{K_{a3}} H^{+} + [LH_2]^{2+} \qquad K_{a3} = \frac{[H^{+}]\,[LH_2^{2+}]}{[LH_3^{3+}]} \qquad \textbf{(2.3)}$$

$$[LH_4]^{4+} \xrightleftharpoons{K_{a4}} H^{+} + [LH_3]^{3+} \qquad K_{a4} = \frac{[H^{+}]\,[LH_3^{3+}]}{[LH_4^{4+}]} \qquad \textbf{(2.4)}$$

In these equations K_{a1}, K_{a2}, K_{a3} and K_{a4} are the stepwise equilibrium constants (or acid dissociation constants) and L is the ligand under study. The negative logarithm of the equilibrium constant, K_a, can be used to obtain the pK_a value of each nitrogen donor atom as expressed below in Equations 2.5 - 2.8. The pK_a of an acid corresponds to the stepwise protonation constant of its conjugate base.

$$pK_{a1} = - \log K_{a1} \qquad \textbf{(2.5)}$$

$$pK_{a2} = - \log K_{a2} \qquad \textbf{(2.6)}$$

$$pK_{a3} = - \log K_{a3} \qquad \textbf{(2.7)}$$

$$pK_{a4} = - \log K_{a4} \qquad \textbf{(2.8)}$$

Ligand **51** was subjected to potentiometric titrations to determine the pK_a values associated with its nitrogen donor atoms. These protonation constants were measured by a pH-metric method using a glass electrode. A linear calibration curve of experimental emf readings versus logarithms of the corresponding calculated H^+ concentrations was obtained by means of strong acid ($HClO_4$) - strong base (NEt_4OH) titration. By using such a calibration method, there is a reduced range of free H^+ concentrations suitable for calibration, corresponding to *ca.* 2.5 < observed pH < 10.5, because of liquid junction potentials in more acidic solutions and increasing electrode sensitivity to alkali metal cations at higher pH.[139] Further limitations to measurements carried out under extreme pH conditions are related to the fact that at high pH the concentration of free ligand is

insensitive to pH change. At low pH the free ligand concentration becomes negligible owing to virtually complete protonation.[140] Therefore, not all the pK_a values were measurable due to the detection limit for the method used, as pK_a values ≤ 2 and ≥ 11 cannot be accurately measured using glass electrodes and, as such, must be evaluated very critically.[139]

2.5.2.2 Protonation constants for the cyclen derived ligand 51

The pK_a values for ligand **51** were determined according to the procedure described above. A typical titration curve obtained by potentiometric measurements is shown in Figure 2.15.

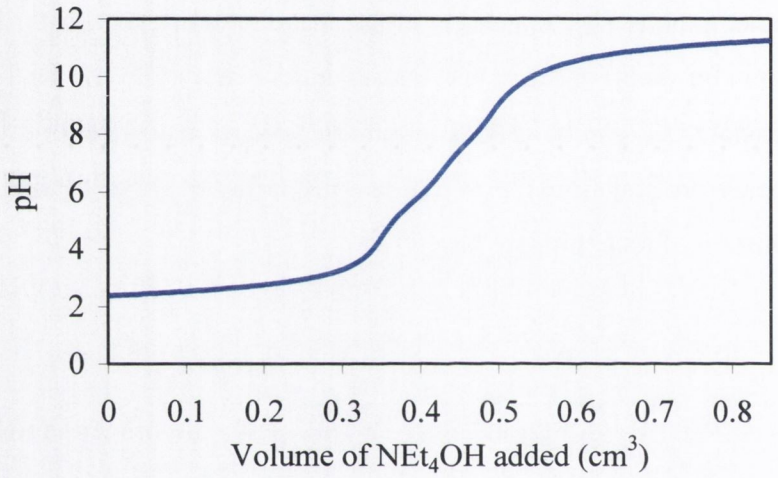

Figure 2.15 Typical titration curve of the protonated ligand 51 against NEt_4OH at 298.2 K. [51] = 6.4 × 10^{-4} M, [H^+] = 6.5 × 10^{-3} M, [NEt_4OH] = 0.103 M, I = 0.10 M (NEt_4ClO_4)

The presence of different inflection points on this curve indicates the presence of several pK_as, which were calculated using the program HYPERQUAD.[141] This program uses a non-linear least squares regression method to minimise the differences between the experimental data and the theoretical values calculated for the proposed model. The logarithm of the stepwise protonation constants for the studied ligand, obtained by mathematical treatment of the potentiometric titration data are displayed in Table 2.1. The pK_a values given in Table 2.1 decrease from pK_{a1} to the lowest measurable pK_a value. In systems of multiple pK_as, the value of each sequential pK_a will decrease for two reasons; increasing charge and a statistical effect. Protonation of one amino group results in a ligand with an overall +1 charge, which coincides with a large pK_a value. The addition of a second proton causes repulsion between the two protons, which lowers the value for the second

protonation constant, pK_{a2}. With ligands having more than two protonation sites, the increase of the electrostatic repulsion between the ammonium groups affects the stability of the protonated forms even further, thus causing a large decrease to the pK_a value.[139] The second reason for the decrease is the statistical effect. For a ligand such as **51**, there are five protonation sites. The initial addition of a proton will leave four sites to which a proton can coordinate. As a consequence, the probability with which the next proton will coordinate is decreased, resulting in a decrease of the pK_a value, and so on for the remaining sites.

Acidity can also be affected by hydrogen bond formation between protonated and non-protonated amino groups. A proton involved in a hydrogen bond is more difficult to abstract, thus contributing to the difference in the measurable pK_a values. Moreover, solvation of the ligand can have a large effect on the ability of the ligand to form hydrogen bonds; a decrease in solvation can lead to weak coordination of the donor atom to the bound proton, hence lower pK_a values may be observed.

Table 2.1 pK_a values of the protonated ligand 51 obtained at 298.2 K and I = 0.1 M (NEt_4ClO_4) in H_2O[a]

equilibrium quotient	pK_a	*designation*
[**51**][H^+]/[H**51**$^+$]	10.65 ± 0.02	pK_{a1}
[H**51**$^+$][H^+]/[H_2**51**$^{2+}$]	8.96 ± 0.04	pK_{a2}
[H_2**51**$^{2+}$][H^+]/[H_3**51**$^{3+}$]	6.84 ± 0.05	pK_{a3}
[H_3**51**$^{3+}$][H^+]/[H_4**51**$^{4+}$]	4.95 ± 0.07	pK_{a4}
[H_4**51**$^{4+}$][H^+]/[H_5**51**$^{5+}$]	low	pK_{a5}

[a] [**51**] = 6.4 × 10^{-4} M, [H^+] = 6.5 × 10^{-3} M, [NEt_4OH] = 0.103 M

In the case of ligand **51**, the two larger pK_a values, pK_{a1} and pK_{a2}, and the smallest determined pK_a, pK_{a4}, are assigned to the protonation of the macrocyclic ring amines. The protonation constant of the remaining ring amine is below the range of accurate potentiometric measurements. The remaining pK_a value of 6.84 ± 0.05 (pK_{a3}) is assigned to the protonation of the quinoline aryl nitrogen moiety. For similar systems, large pK_a values for protonated quinoline nitrogens have also been observed.[26]

2.5.3 Determination of metal complex stability constants by potentiometric titrations

Numerous methods are employable for the determination of metal complex ion stability constants, *e.g.* UV-vis, fluorescence and luminescence spectroscopy, NMR titrations *etc*. One method often used is that of potentiometric titrations. When a ligand complexes a metal ion in solution, an equilibrium is established between the ligand (L), the solvated metal ion (M^{n+}) and the metal complex ion (ML^{n+}), as shown below in Equation 2.9, where K represents the stability constant for metal ion complexation.

$$M^{n+} + L \underset{}{\overset{K}{\rightleftharpoons}} M^{n+}L \qquad K = \frac{[ML^{n+}]}{[M^{n+}]\,[L]} \qquad \textbf{(2.9)}$$

In solution, the metal ion competes with the protons in the acidic media for the ligand coordination sites, altering the pH of the solution. Therefore, a change in the titration curve upon addition of a metal ion to the solution indicates the formation of a metal complex ion; the larger the change, the higher the metal complex ion stability constant. Determination of metal ion stability constants was achieved by adding one or two equivalents of the metal ion to the acidic solution prior to titration with the relevant base. As for the protonation constants (see Section 2.5.2), the calculation of the metal complex ion stability constant was achieved by means of the computer program HYPERQUAD.[141]

The factors that affect metal complex ion stability include the relative sizes of the metal ion and the ligand cavity, the solvation energy of the metal ion, the structure and flexibility of the macrocycle, and the number of donor atoms in the macrocycle.[142,143] The coordination of the metal ion by the ligand involves the substitution of solvent molecules from the first coordination sphere of the metal ion. Consequently, the nature of the solvent affects the stability of the metal complex ion. In general terms, the formation of the metal complex ion by the pendent arm ligand **51** involves complexation by the amine nitrogens of the macrocyclic ring, as well as the amide oxygens of the pendent donor arms. Upon complexation of the metal ion, the ligand effectively forms a cavity, at the centre of which the metal ion is sited. The overall stability of the complex is thus affected by the number of coordination sites and by the 'fit' of the metal ion to the cavity formed by the coordinated pendent arm macrocycle.

The metal complex ion stability constants for ligand **51** were determined in an analogous manner to the protonation constants; in 100 % H_2O with constant ionic strength I = 0.1 M (NEt_4ClO_4). The only difference was that an equimolar quantity of $Eu(CF_3SO_3)_3$ was also present in solution, as shown in the titration curve in Figure 2.16. The derived complexation constants and pK_as for the protonated ligand complexes were determined using the program HYPERQUAD,[141] and are listed in Table 2.2.

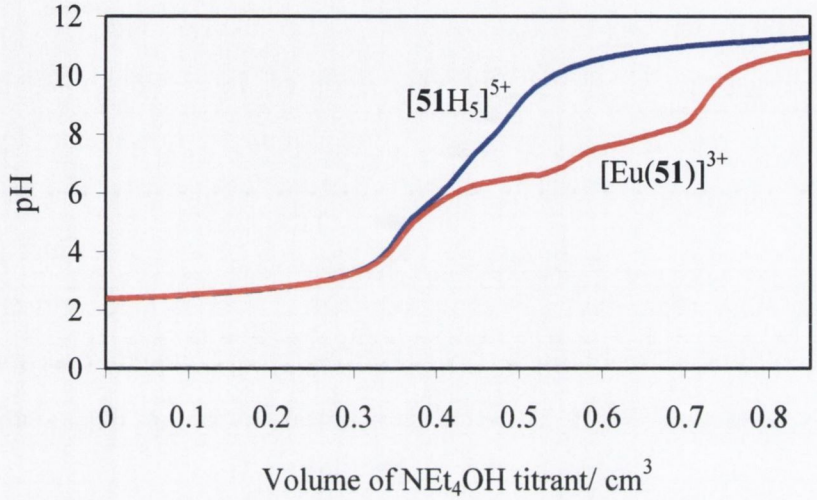

Figure 2.16 Titration curves for the protonated ligand $[51H_5]^{5+}$ at 298.2 K. [51] = 6.4 × 10^{-4} M, $[H^+]$ = 6.5 × 10^{-3} M, I = 0.10 M (NEt_4ClO_4) in the absence (blue curve) and presence of $[Eu^{3+}]$ = 6.4 × 10^{-4} M (red curve). Titrant [NEt_4OH] = 0.103 M

Table 2.2 Complexation constants, log(K/dm^3 mol^{-1}) and pK_a values for the complexation of $Eu(CF_3SO_3)_3$ with ligand 51 at 298.2 K and I = 0.1 M (NEt_4ClO_4).

equilibrium quotient	*log(K/dm^3 mol^{-1})*
$[Eu(\mathbf{51})^{3+}]/[Eu^{3+}][\mathbf{51}]$	9.59 ± 0.02
	pK_a
$[Eu\mathbf{51}^{3+}][H^+]/[Eu(H\mathbf{51})^{4+}]$	6.13 ± 0.09
$[Eu\mathbf{51}H_{-1}^{2+}][H^+]/[Eu\mathbf{51}^{3+}]$	7.47 ± 0.05
$[Eu\mathbf{51}H_{-2}^{+}][H^+]/[Eu\mathbf{51}\ H_{-1}^{2+}]$	8.77 ± 0.09

The pK_a of the monoprotonated complex (MLH), 6.13 ± 0.09, can be assigned to the deprotonation of the quinoline nitrogen. This value is similar to the pK_{a3} value of the free ligand **51**. It was anticipated that the two pK_a values would be similar because the quinoline nitrogen is not expected to be directly involved in the metal ion coordination. It

has been previously observed that the pK_a of a metal bound water in a Eu^{III} complex with a sensitising chromophore present, is significantly reduced and generally occurs between pH 7-8.[144] Therefore, the pK_a values of 7.47 ± 0.05 can be assigned to deprotonation of the metal bound water molecule. The presence of this metal bound water molecule was expected as ligand **51** has only eight coordination sites and europium is capable of forming nine-coordinate complexes. It has also been observed that in the presence of a strong Lewis acid, such as Eu^{III}, the pK_a of a carboxylic amide is also reduced.[26] As such, the pK_a of 8.77 ± 0.09 can be assigned to deprotonation of the quinoline carboxylic amide.

In order to assess the effect that the counterion of the europium salt has on the stability constant of the metal ion complex **Eu.51**, potentiometric titrations of ligand **51** in the presence of an equimolar quantity of $Eu(ClO_4)_3$ were conducted in 100 % H_2O with constant ionic strength I = 0.1 M (NEt_4ClO_4), following the same procedure previously described. The titration curve obtained is compared with the corresponding titration curve using triflate as the counterion in Figure 2.17. The derived complexation constants and pK_as for the protonated ligand complexes, determined using the program HYPERQUAD,[141] are listed in Table 2.3.

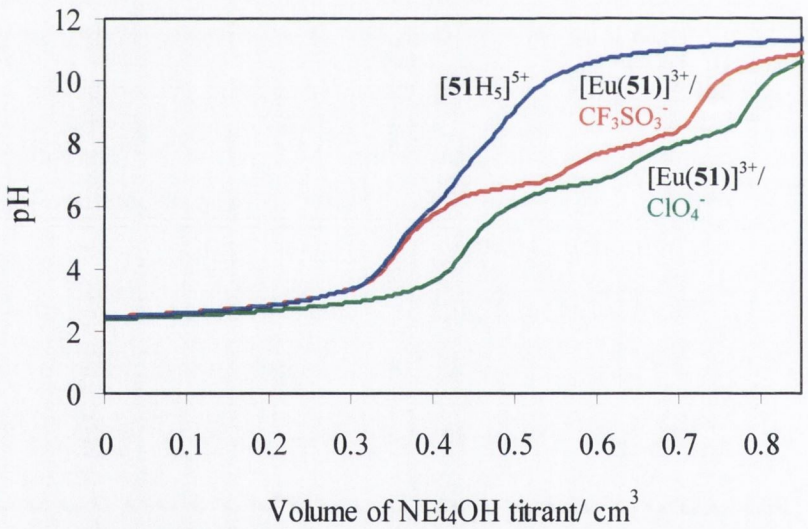

Figure 2.17 Titration curves for the protonated ligand $[51H_5]^{5+}$ at 298.2 K (blue curve). [51] = 6.4 × 10^{-4} M, $[H^+]$ = 6.5 × 10^{-3} M, I = 0.10 M (NEt_4ClO_4) in the absence and presence of $Eu(CF_3SO_3)_3$ (red curve) and $Eu(ClO_4)_3$ (green curve). $[Eu^{3+}]$ = 6.4 × 10^{-4} M, titrant [NEt_4OH] = 0.103 M

As expected, the stability constant of the europium complex **Eu.51** is higher by more than eight orders of magnitude when perchlorate is used as the counterion instead of triflate. Hence, the counterion has a big influence on the stability constants of the metal ion complexes formed. Perchlorate is a less coordinating anion than triflate and therefore does

not compete with the ligand and the water for metal ion binding sites. As a result of the higher stability constant, the metal ion titration curve is shifted further away from the ligand curve (*cf.* Figure 2.17). This demonstrates that the metal ion complex starts forming when the ligand is still in its protonated form.

Table 2.3 Complexation constants, log(K/dm^3 mol^{-1}) and pK_a values for the complexation of $Eu(ClO_4)_3$ with ligand 51 at 298.2 K and I = 0.1 M (NEt_4ClO_4).

equilibrium quotient	*log(K/dm^3 mol^{-1})*
[Eu(**51**)$^{3+}$]/[Eu^{3+}][**51**]	17.89 ± 0.08
	pK_a
[Eu**51**$^{3+}$][H$^+$]/[Eu(H**51**)$^{4+}$	6.66 ± 0.06
[Eu(H**51**)$^{4+}$][H$^+$]/[Eu(H_2**51**)$^{5+}$	6.47 ± 0.04
[Eu(H_2**51**)$^{5+}$][H$^+$]/[Eu(H_3**51**)$^{6+}$	3.69 ± 0.05
[Eu**51**H_{-1}^{2+}][H$^+$]/[Eu**51**$^{3+}$]	6.91 ± 0.03
[Eu**51**H_{-2}^{+}][H$^+$]/[Eu**51** H_{-1}^{2+}]	7.91 ± 0.07

The presence of the pK_a values corresponding to the deprotonation of MLH_2 and MLH_3 complexes is further evidence, as they were not detected when triflate was the counterion. As expected, these values are much lower than the corresponding pK_a values of ligand **51** (*cf.* Table 2.1), due to the coordination of the ring nitrogens to a strong Lewis acid, *i.e.* Eu^{III}, upon complexation. The two pK_a values of 6.47 ± 0.04 and 6.66 ± 0.06 are too close to be assigned with accuracy to either the deprotonation of the quinoline nitrogen or the deprotonation of a cyclen amine. In either case, the deprotonation of the quinoline nitrogen is not significantly affected by the change of the counterion, as it is not directly involved in the coordination of the lanthanide centre. Finally, the pK_as corresponding to the deprotonation of the metal bound water molecule and the quinoline carboxylic amide both decrease to 6.91 ± 0.03 and 7.91 ± 0.07, respectively. This can be attributed to a stronger coordination of the water molecule and the amide moiety to the Eu^{III} centre in the presence of the non-coordinating perchlorate ion.

2.5.4 Speciation

The pK_a values of a ligand, in conjunction with metal complex ion stability constants, can be used to calculate the concentration of all species present in solution at any pH. The concentration of the species is expressed as a percentage relative to the total amount present in solution. The speciation diagrams for the deprotonation of ligand **51** and the corresponding $Eu(CF_3SO_3)_3$ and $Eu(ClO_4)_3$ complexes are shown Figures 2.18 – 2.20.

The speciation diagram of ligand **51** (Figure 2.18) shows the consecutive deprotonation of the ligand, starting from its tetra-protonated form (LH_4^{4+}), which is predominantly present below *ca.* pH 5 according to the pK_a values (pK_{a4} = 4.95 ± 0.07). The species LH_3^{3+} is mainly present between pH 5 and 6.9 and LH_2^{2+} in the pH range 6.9 - 8.7. The mono-protonated form is present until pH 10.65; above this pH the ligand in its unprotonated form is the predominant species in solution.

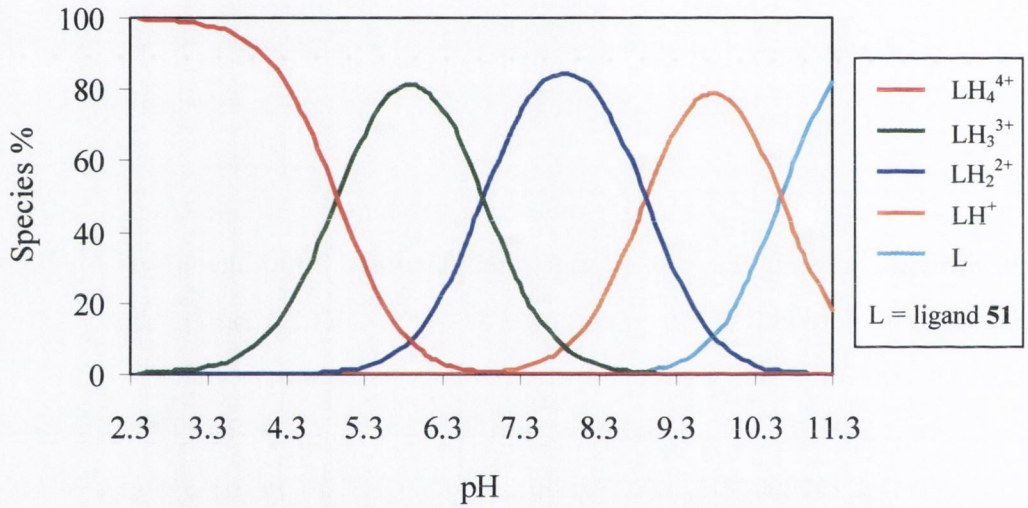

Figure 2.18 Speciation variation of ligand 51, showing the species present in H_2O at various pH in which [51] = 6.4 × 10^{-4} M with constant ionic strength *I* = 0.10 M (NEt_4ClO_4) at 298.2 K. Speciation is shown relative to the total concentration of ligand 51.

The speciation diagram for the coordination of ligand **51** with $Eu(CF_3SO_3)_3$ is more complicated, due to the number of species present in solution (Figure 2.19). The ligand coordinates the lanthanide metal ion as both the mono-protonated species $EuLH^{4+}$ and the unprotonated species EuL^{3+}. The latter species, EuL^{3+}, is mainly present in the pH range 6.5 – 8. Deprotonation of the metal bound water molecule and of the amide moiety above pH 7, yield the dicationic $EuLH_{-1}^{2+}$and the monocationic species $EuLH_{-2}^{+}$, which predominate in the basic pH region.

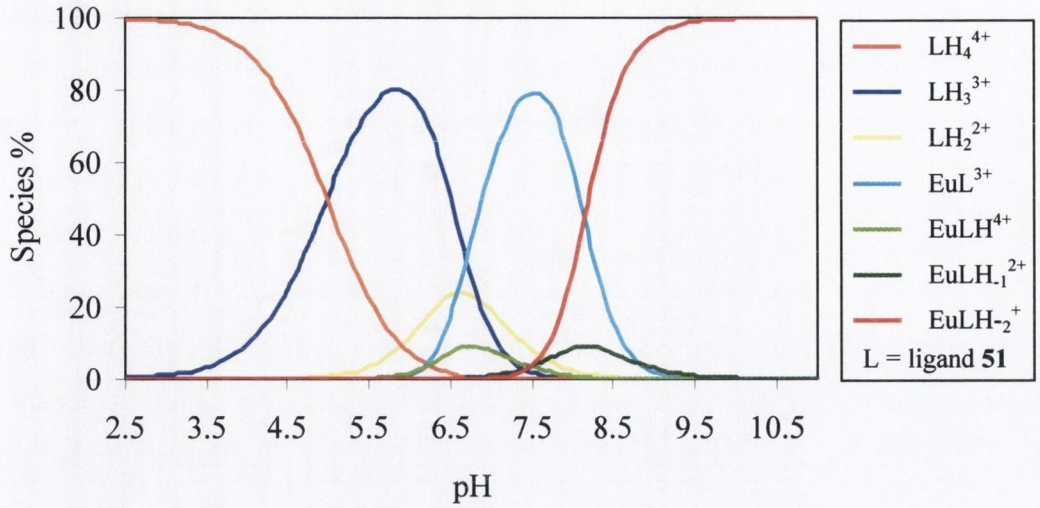

Figure 2.19 Speciation variation of ligand 51, showing the species present in H_2O at various pH in which [51] = 6.4 × 10^{-4} M, [$Eu(CF_3SO_3)_3$] = 6.4 × 10^{-4} M with constant ionic strength I = 0.10 M (NEt_4ClO_4) at 298.2 K. Speciation is shown relative to the total concentration of ligand 51.

The speciation diagram for the coordination of ligand **51** with Eu^{III} as a perchlorate salt $Eu(ClO_4)_3$, shows that the complex forms instantly, even at very acidic pH. This reflects the high metal complex ion stability constant measured for ligand **51** with $Eu(ClO_4)_3$ (*cf.* Table 2.3). The ligand coordinates the europium ion in its tri-protonated form ($EuLH_3^{6+}$). After subsequent deprotonations, the complex in the unprotonated form EuL^{3+} is predominantly present in a very narrow pH window (*ca.* 6.5-7). At this pH, deprotonation of the metal bound water and of the amide moiety occur, yielding the species $EuLH_{-1}^{2+}$ and $EuLH_{-2}^{+}$. The latter is observed predominantly above pH 8. Above this pH, the formation of the metal hydroxide species $Eu(OH)^{2+}$ is also observed.

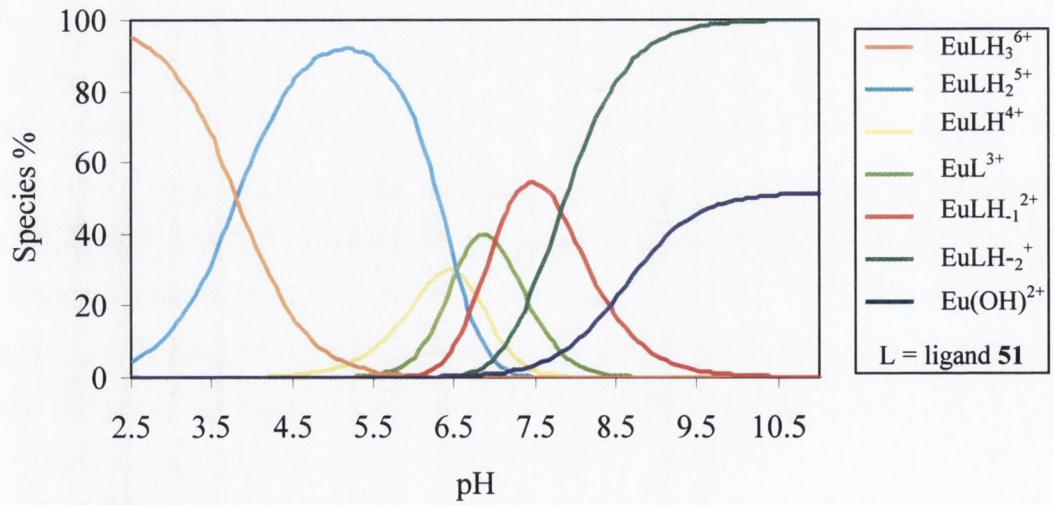

Figure 2.20 Speciation variation of ligand 51, showing the species present in H_2O at various pH in which [51] = 6.4 × 10^{-4} M, [$Eu(ClO_4)_3$] = 6.4 × 10^{-4} M with constant ionic strength I = 0.10 M (NEt_4ClO_4) at 298.2 K. Speciation is shown relative to the total concentration of ligand 51.

In summary, the pK_a values of ligand **51** were determined by potentiometric titration. As expected, three pK_as (pK_{a1}, pK_{a2} and pK_{a4}) were assigned to the protonation of the macrocyclic ring amines. A fourth protonation occurred at very acidic pH and, therefore, could not be measured by this method. The remaining pK_a value of 6.84 ± 0.05 (pK_{a3}) was assigned to the protonation of the quinoline aryl nitrogen moiety. The Eu^{III} complex ion stability constants were also determined for ligand **51**. It was found that changing the counterion of the Eu^{III} salt used in the potentiometric titrations had a large effect on the corresponding metal complex ion stability constant. The stability constant of **Eu.51** in the presence of perchlorate (log K = 17.89 ± 0.08) was significantly higher than that with triflate (log K = 9.59 ± 0.02). This was ascribed to the fact that perchlorate is a non-coordinating anion and therefore it does not compete with the ligand and the water for metal ion binding. The pK_a values for the protonation of the quinoline aryl nitrogen moiety, derived from the potentiometric titrations of ligand **51** in the presence of either 1 equiv. of $Eu(CF_3SO_3)_3$ or $Eu(ClO_4)_3$ were found to be similar to the value calculated for the free ligand. The quinoline nitrogen does not participate directly in the coordination of the lanthanide centre; therefore its deprotonation is not considerably affected by the presence of the metal centre or by the change of the counterion.

In the following sections, the photophysical properties of ligand **51** and the corresponding Eu^{III} complex **Eu.51** will be investigated as a function of pH. The resulting pK_a values will be then compared to those obtained by potentiometric studies.

2.5.5 Determination of the coordination number of Eu.51

Ligand **51** can provide eight coordination sites suitable for lanthanide ion complexation: four from the nitrogens of the cyclen structure, and four from the oxygens of the carboxylic amides. Europium generally has a coordination number of nine in such tetrasubstituted cyclen complexes, with the axial ninth site being occupied by a solvent molecule or an anion, as demonstrated by studies in solution and in the solid state.[27,48] As mentioned in Chapter 1, the presence of OH oscillators in the first coordination sphere of the metal ion provides an efficient pathway for radiationless de-excitation *via* energy transfer to OH vibrational overtones.[145] This pathway is virtually eliminated upon replacement of OH by OD oscillators. Vibrational quenching in D_2O is much less efficient than in H_2O, therefore a difference in the radiative rate constants is observed.[146] Horrocks and Sudnick were the first to determine the number of water molecules coordinated to the

metal ion, by means of decay constant measurements in both H_2O and D_2O solutions.[145] Subsequently, Parker *et al.* revised this method by evaluating the relative contributions of OH, NH (both amide and amine) and CH oscillators.[29] In the case of **Eu.51**, the hydration number (q) was determined by measuring the lifetimes of the Eu^{III} emission in H_2O and D_2O, respectively, using the following equation developed by Parker *et al.*:[29]

$$q^{Eu(III)} = 1.2\ [(1/\tau_{H2O} - 1/\tau_{D2O}) - 0.25 - 0.075x]\ (\pm 0.3) \qquad (2.10)$$

These values are obtained by direct excitation of the lanthanide ion complex. The prefix 1.2 is a proportionality constant that mirrors the sensitivity of Eu^{III} to quenching by metal bound water molecules. The correction term -0.25 represents quenching by second sphere water molecules and $-0.075x$ represents the quenching by NH oscillators, where x is the number of bound amide NH groups. Luminescence lifetime measurements of **Eu.51** were carried out in H_2O and D_2O at neutral pH, on a Varian Carey Eclipse Fluorimeter; the excitation wavelength employed was 395 nm. Figure 2.21 shows the single exponential decay profiles obtained for **Eu.51** in D_2O and H_2O.

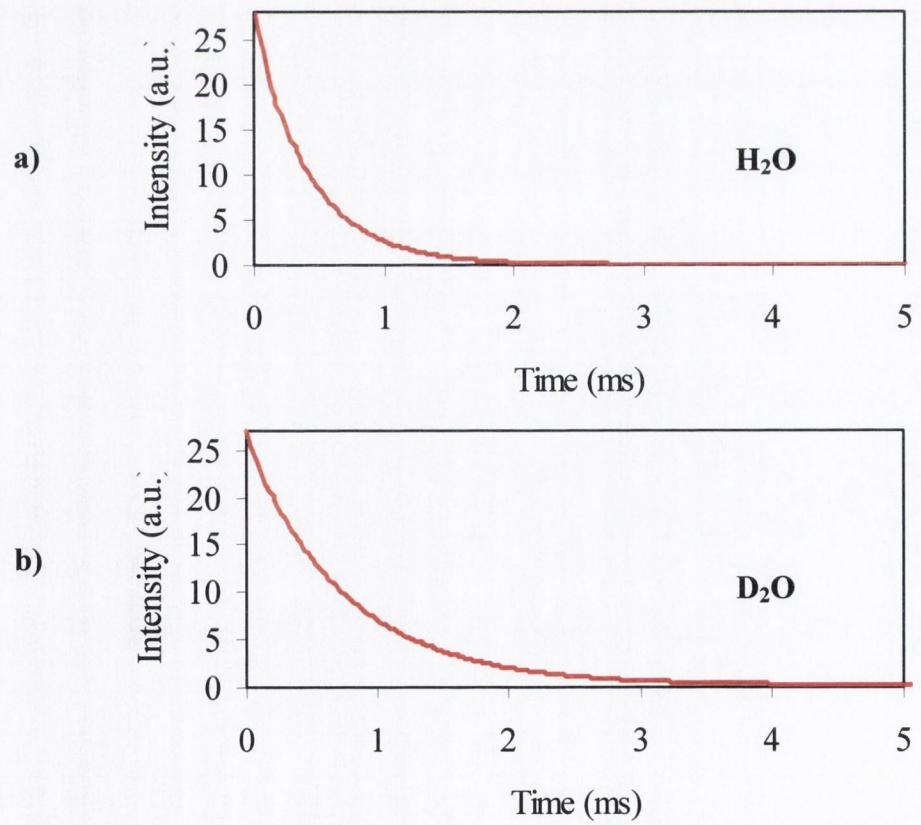

Figure 2.21 a) Decay profiles for Eu.51 in H_2O. b) Decay profile for Eu.51 in D_2O.

The lifetime in H_2O (τ_{H2O}) and D_2O (τ_{D2O}) was measured to be 0.429 ± 0.01 ms and 0.758 ± 0.01 ms, respectively. Using Equation 2.8 a q value of 0.91 was determined, which was relative to the inner and outer coordination sphere, after correcting for the amide NH oscillators. This indicates that the complex has a single metal bound water molecule, hence the complex is nine coordinate. This result is in agreement with the potentiometric titrations.

2.5.6 Photophysical studies of ligand 51 in solution

The UV-visible and fluorescence properties of ligand 51 have been investigated as a function of pH. The results of these measurements will be discussed in the next two sections.

2.5.6.1 Ground state investigations

The changes in the absorption spectra of ligand **51** as a function of pH were evaluated in water, in the presence of tetraethylammonium perchlorate (I = 0.1 M) to maintain a constant ionic strength. In acidic conditions, the ligand displays a maximum band at 315 nm (ε = 10600 M^{-1} cm^{-1} at pH 2.38) due to $\pi \rightarrow \pi^*$ transition, with a shoulder at about 330 nm. Upon basification a significant hypsochromic and hypochromic shift was observed with formation of a band centred at 300 nm (ε = 6500 M^{-1} cm^{-1} at pH 11.19), with a shoulder at 318 nm (Figure 2.22).

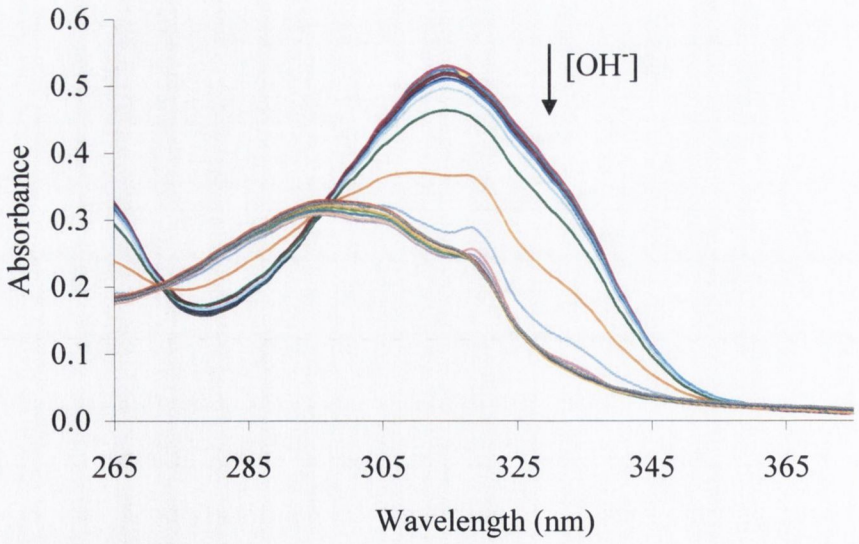

Figure 2.22 Overlaid UV-vis spectra for the pH titration of ligand 51 [5.0 × 10^{-5} M] against NEt_4OH in H_2O (I = 0.1 M, NEt_4ClO_4) at 298.2 K. The arrow indicates the spectral trend with increasing pH between pH 2.4 – 11.2.

As shown in Figure 2.22, not all spectra pass through the isosbestic point at 296 nm indicating the presence of more than two species in equilibrium in solution.[147] This was anticipated since the ligand undergoes four deprotonation steps in the pH range titrated. The changes in absorbance at 330 nm were plotted as a function of pH, as shown in Figure 2.23. A significant decrease in the absorbance was observed between pH 4.2 – 7.2.

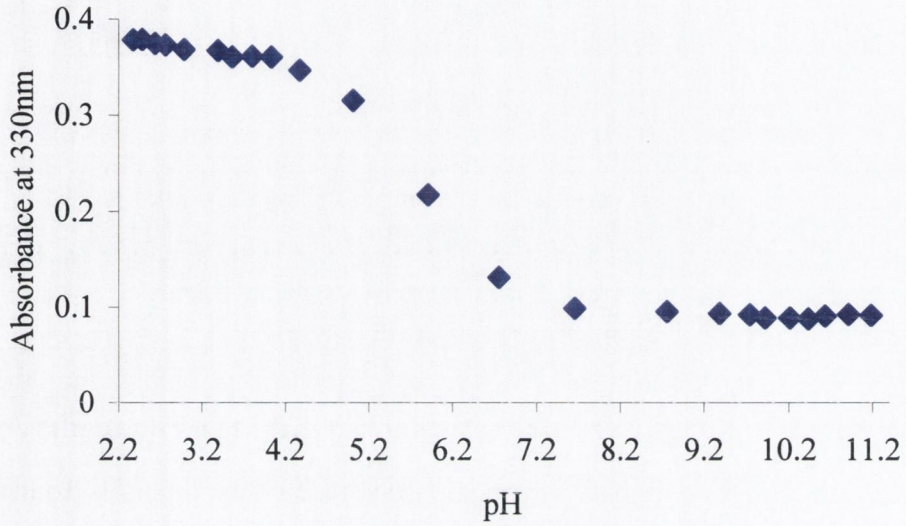

Figure 2.23 Changes in absorbance at 330 nm as a function of pH for the titration of ligand 51 [5.0 × 10^{-5} M] against NEt_4OH in H_2O (I = 0.1 M, NEt_4ClO_4) at 298.2 K.

A pK_a of 5.71 ± 0.1 was determined from these data using the standard formula for the calculation of ground state pK_as (S_0):[148]

$$pK_a(S_o) = pH - \log \frac{(Abs_{AH} - Abs_A)}{(Abs_A - Abs_{A^-})} \qquad \textbf{(2.11)}$$

where Abs_{AH}, Abs_A, and Abs_{A^-} are the absorbances of the protonated species, the absorbance of each solution, and the absorbance of the deprotonated species, respectively. This pK_a value is lower than the pK_a associated to the deprotonation of the quinoline nitrogen (pK_{a3} = 6.84 ± 0.05) but higher than the pK_a corresponding to deprotonation of the ring nitrogen (pK_{a4} = 4.95 ± 0.07), as obtained by potentiometric titration (*cf.* Table 2.1). The difference may be attributed to the combination of the two deprotonation steps in the same pH interval. As illustrated in Figure 2.24, in the pH range within which the absorbance markedly changes, two deprotonation steps occur: $LH_4^{4+} \rightarrow LH_3^{3+}$ and $LH_3^{3+} \rightarrow LH_2^{2+}$.

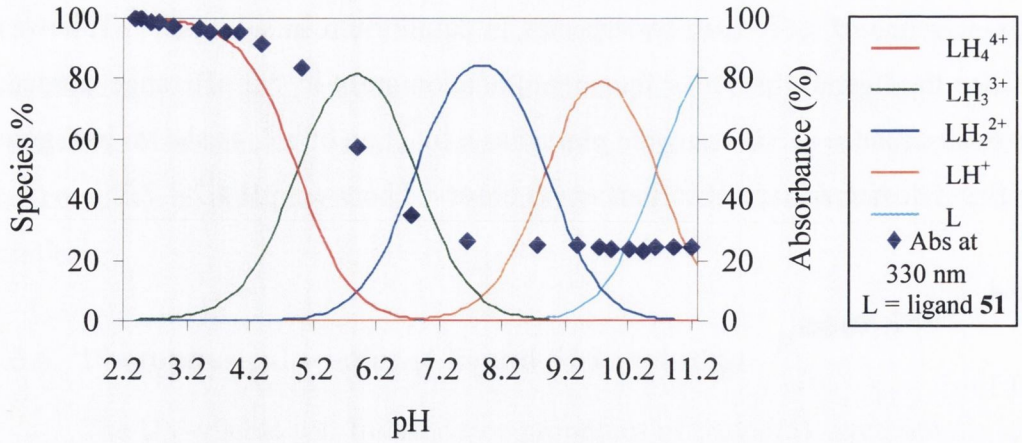

Figure 2.24 Left vertical axis: speciation variation of ligand 51, showing the species present in H_2O at various pH in which [51] = 6.4 × 10^{-4} M with constant ionic strength I = 0.10 M (NEt_4ClO_4) at 298.2 K. Right vertical axis: dependence of the absorbance (%) at 330 nm of the solution as a function of pH (blue diamonds ♦). Speciation is shown relative to the total concentration of ligand 51.

After pH 7.5, the absorbance reaches a plateau, thus indicating that the deprotonation of the remaining nitrogens on the cyclen ring (pK_{a2} and pK_{a1} in Table 2.1) do not have any detectable effect on the spectroscopic properties of the ligand's ground state. The same behaviour was observed by plotting the changes in absorbance at different wavelengths.

In the next section, the spectroscopic properties of the singlet excited state of ligand **51** will be examined as a function of pH.

2.5.6.2 Singlet excited state investigations

The changes in the fluorescence emission spectra of ligand **51** were also investigated as a function of pH in water in the presence of tetraethylammonium perchlorate (I = 0.1 M). The changes were monitored following excitation at 330 nm, where the difference in the magnitude of the extinction coefficient, between the alkaline and acidic solution, was at its maximum (*cf.* Figure 2.22). In acidic solution, up to pH 4.2, there was a structural band centred at 356 nm with two shoulders at 342 and 374 nm. Between pH 4.2 - 7.5, the emission intensity of the bands at 356 and 342 nm increased, while a decrease of the shoulder at 374 nm was observed. Upon further basification beyond pH 7.5, a significant hypochromic and bathochromic shift was observed with the formation of a band centred at 374 nm and concomitant loss of the hyperfine structure (Figure 2.25).

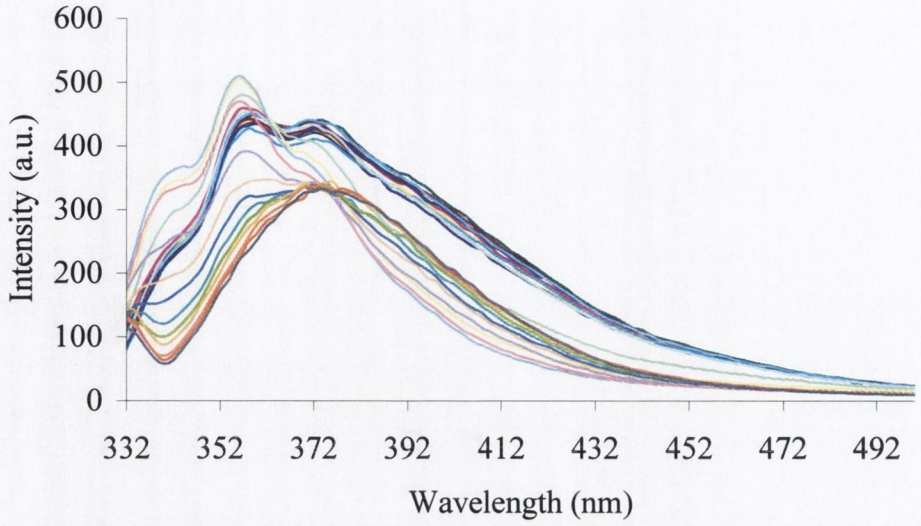

Figure 2.25 Overlaid fluorescence emission spectra for the pH titration of ligand 51 [5.0 × 10^{-5} M] against NEt_4OH in H_2O (I = 0.1 M, NEt_4ClO_4) at 298.2 K.

When the changes at 356 nm were plotted against the pH, a sigmoidal curve was observed, as shown in Figure 2.26. A slight increase in emission intensity was observed up to pH 7.5, as mentioned above. However, the major changes occurred in the alkaline region, between pH 7.5 – 11. The reduced emission intensity observed at high pH is in keeping with the intramolecular amine quenching mechanism. [107,149-152] Gunnlaugsson *et al.* reported that the low emission intensity in alkaline media of a similar macrocyclic system can be partly explained by photoinduced electron transfer (PET) quenching from one of the amino groups of the cyclen ring.[26]

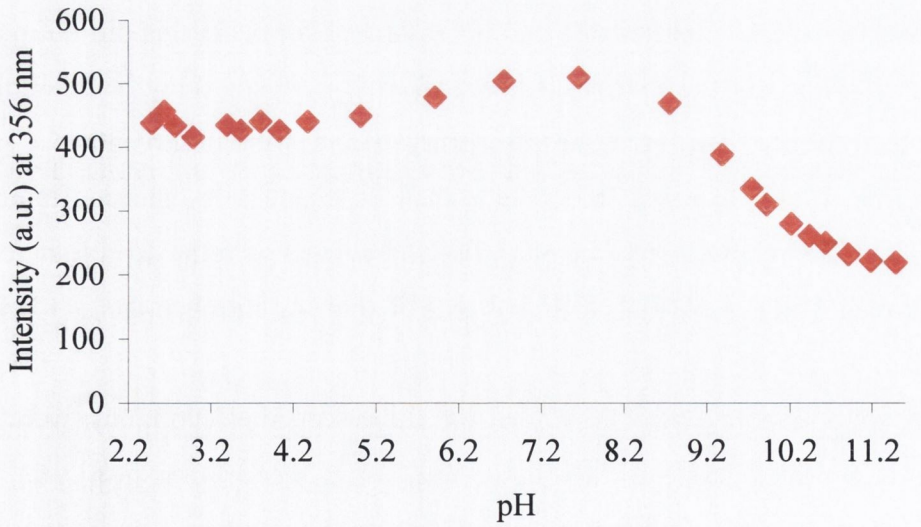

Figure 2.26 Changes in emission intensity at 356 nm as a function of pH for the titration of ligand 51 [5.0 × 10^{-5} M] against NEt_4OH in H_2O (I = 0.1 M, NEt_4ClO_4) at 298.2 K.

It has been documented in the literature that the acid-base properties of aromatic chromophores in the lowest excited state may differ substantially from the corresponding ground state properties, owing to the redistribution of electronic charge density on excitation.[153,154] The theoretical methods to study these excited state acid-base equilibria involve the calculation of the negative logarithm of the excited state acid dissociation constant ($pK_a(S_1)$).[155] The singlet excited state $pK_a(S_1)$ may be calculated either by the change in charge distribution due to the electronic excitation by means of molecular orbital theory, or from the Förster cycle,[156] which is the method of choice herein. From the changes above pH 7.5, using the Förster equation (Equation 2.12),[156] a pK_a of 8.55 ± 0.1 was calculated for the singlet excited state;

$$pK_a(S_1) = pK_a(S_0) + \frac{0.625}{T} \Delta\nu \qquad \textbf{(2.12)}$$

where $\Delta\upsilon$ is the difference between the energy of the protonated and deprotonated form in reciprocal centimetres and T is the absolute temperature. This value is marginally lower than the pK_{a2} value calculated by potentiometric titration (pK_{a2} = 8.96 ± 0.04; *cf.* Table 2.1). This may suggest that the cyclen amino group responsible for the quenching of the fluorescence emission of the ligand is slightly more acidic in the singlet excited state compared to the ground state.

As for the changes in intensity below pH 7.5, the calculation of an excited state pK_a using the Förster equation (Equation 2.12) requires a change in the wavelength of the maximum intensity between the protonated and unprotonated form. As this did not occur, the excited state pK_a value for the changes between pH 4.2 – 7.5 could not be determined using this method. However, changes in the absorbance spectra were observed in the same pH range. Therefore, it is reasonable to conclude that the changes in emission intensity between pH 4.2 – 7.5 are attributable to the pK_a values associated with the deprotonation of the quinoline nitrogen (pK_{a3} = 6.84 ± 0.05) and that of the ring nitrogen (pK_{a4} = 4.95 ± 0.07), as calculated for the ground state.

The same set of experiments, UV-visible and fluorescence pH titrations, were also carried out on complex **Eu.51**. In this case, the luminescence emission was also investigated as a function of pH. The results will be illustrated hereafter.

2.5.7 Photophysical studies of Eu.51 in solution

2.5.7.1 Ground state investigations

The UV-vis absorption spectra of **Eu.51** were recorded in water, in the presence of tetraethylammonium perchlorate (I = 0.1 M) to maintain a constant ionic strength, at different pHs, from 3 to 11.5. As can be seen from Figure 2.27, the absorbance of the complex is highly pH dependent. In acidic solution, the complex displays an intense absorption band at 318 nm (ε = 7300 M^{-1} cm^{-1} at pH 2.36), with a shoulder at 330 nm. Upon basification, a significant hypsochromic and hypochromic shift to a broad absorption band centred at 305 nm (ε = 6300 M^{-1} cm^{-1} at pH 11.01), was observed. This band was assigned to the π - π^* transition of the ligand. The isosbestic points observed in the spectra at *ca.* 263 and 303 nm, suggest the presence of more than two species in equilibrium.[147] This is reasonable as three deprotonation steps occur across the range titrated; deprotonation of the quinoline nitrogen (pK_a = 6.13 ± 0.09), deprotonation of the metal bound water molecule (pK_a = 7.47 ± 0.05) and that of the quinoline carboxylic amide (pK_a = 8.77 ± 0.09).

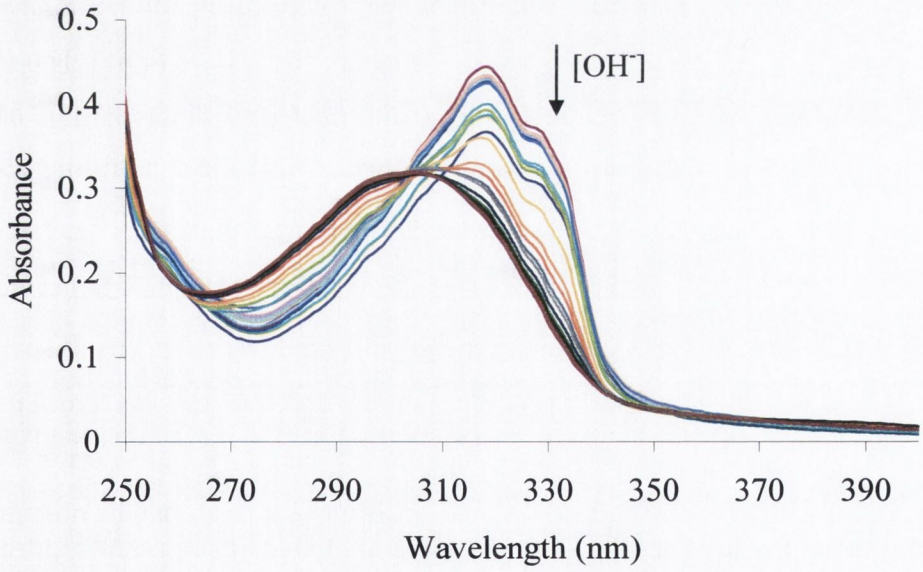

Figure 2.27 Overlaid UV-vis spectra for the pH titration of Eu.51 [5.0 × 10^{-5} M] against NEt_4OH in H_2O (I = 0.1 M, NEt_4ClO_4) at 298.2 K. The arrow indicates the spectral trend with increasing pH between pH 3 – 11.5.

The changes in the absorption spectra at 330 nm were plotted as a function of pH, as shown in Figure 2.28. This clearly shows that there is a significant decrease in the absorbance of the complex above pH 8.

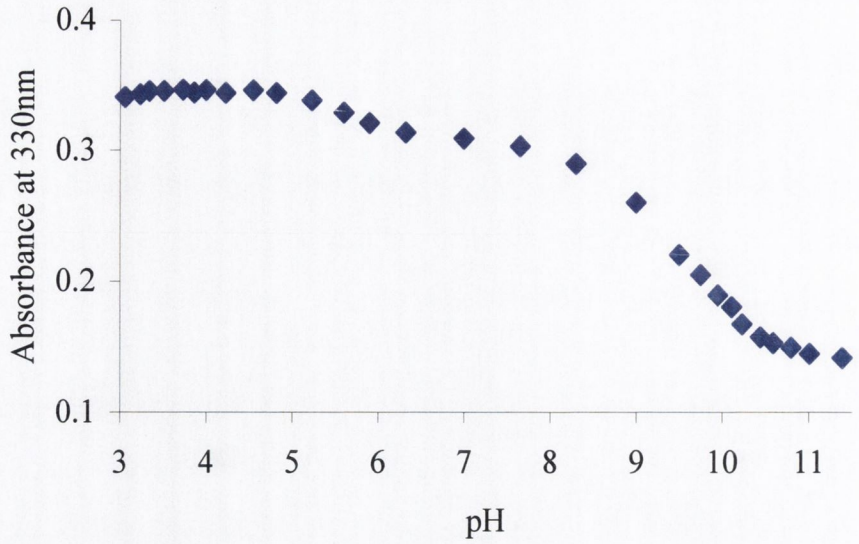

Figure 2.28 Changes in absorbance at 330 nm as a function of pH for the titration of Eu.51 [5.0×10^{-5} M] against NEt_4OH in H_2O (I = 0.1 M, NEt_4ClO_4) at 298.2 K.

A pK_a of 8.82 ± 0.1 was determined from these changes using the standard formula for the calculation of ground state pK_as (S_0) (Equation 2.11). This pK_a coincides with the pK_a of 8.77 ± 0.09 determined by potentiometric titrations, and it is most likely due to the deprotonation of the quinoline carboxylic amide. A slight decrease in absorbance is also noted above pH 5. A pK_a of 5.93 ± 0.1 was calculated according to Equation 2.11. This change is therefore most likely due to the deprotonation of the quinoline nitrogen (6.13 ± 0.09). As expected, deprotonation of the metal bound water molecule did not have an observable effect on the absorption spectra of the complex. The same conclusions could be drawn by looking at the changes in absorbance at a variety of wavelengths.

2.5.7.2 Single excited state investigations

The fluorescence emission of **Eu.51** was also investigated as a function of pH in water in the presence of tetraethylammonium perchlorate (I = 0.1 M). The changes were monitored following excitation at 330 nm, where the difference between the absorbance of the complex in acidic (high ε) and basic media (low ε) is at its maximum (Figure 2.27). The changes in the emission spectra of **Eu.51** when excited at 330 nm mirrored those seen in the absorption spectra. In acidic solution, a band with a maximum at 357 nm and two shoulders at 345 and 375 nm, was observed. Upon basification, there was a distinctive bathochromic shift in the emission spectra, with the formation of a structural band centred at 375 nm, with concomitant decrease of the emission intensity (Figure 2.29).

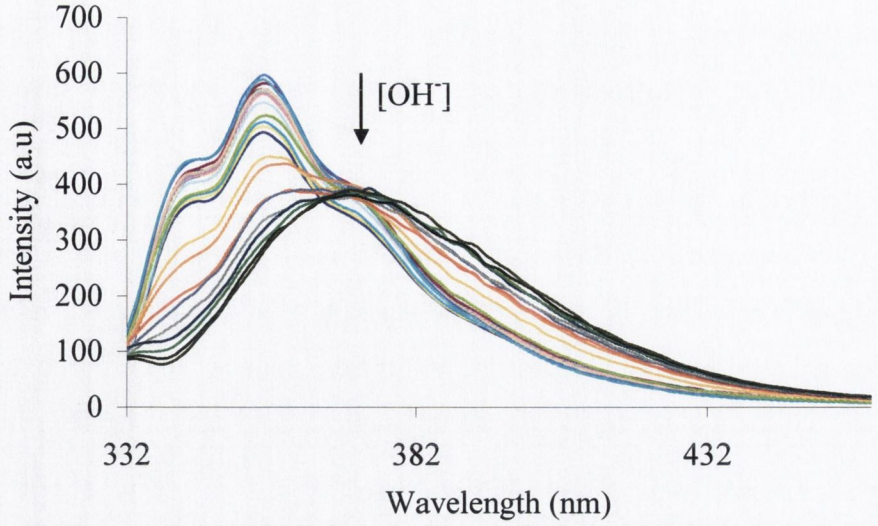

Figure 2.29 Overlaid fluorescence emission spectra for the pH titration of Eu.51 [5.0 × 10^{-5} M] against NEt_4OH in H_2O (I = 0.1 M, NEt_4ClO_4) at 298.2 K. The arrow indicates the spectral trend with increasing pH between pH 3 – 11.5.

When the changes at 356 nm were plotted as a function of pH, a sigmoidal curve was observed, as shown in Figure 2.30. The changes observed show that the singlet excited state is only slightly affected below pH 8 and that the emission is switched "*off*" in alkaline solution by 55%. It is well known that the acid-base behaviour of many organic molecules can be strongly affected by electronic excitation.[157]

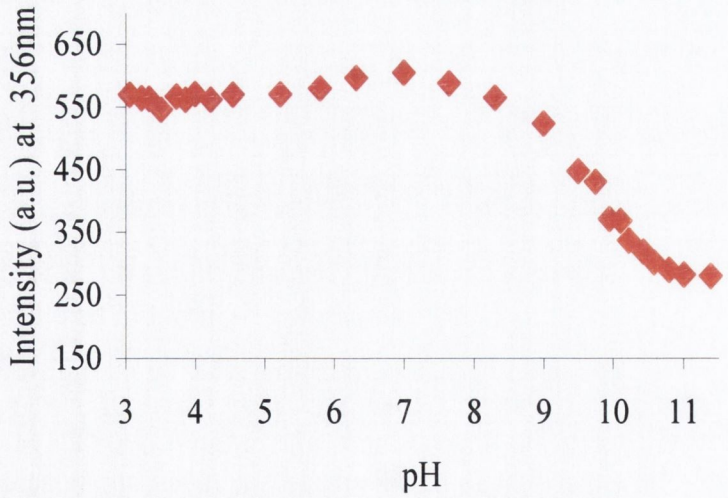

Figure 2.30 Changes in emission intensity at 356 nm as a function of pH for the titration of Eu.51 [5.0 × 10^{-5} M] against NEt_4OH in H_2O (I = 0.1 M, NEt_4ClO_4) at 298.2 K.

From the changes above pH 8, using the Förster equation (Equation 2.12),[156] a pK_a of 9.47 ± 0.1 was calculated for the singlet excited state. This indicates that the basicity of the amide moiety in **Eu.51** is increased upon excitation to the first singlet state. There is also a slight increase in the fluorescence intensity above pH 5; at this pH value, small changes in the absorption spectra were also noted. The calculation of an excited state pK_a value using the Förster equation (Equation 2.12) requires a change in wavelength of the maximum in emission intensity. As this did not occur, the excited state pK_a value for the changes between pH 5 – 8 cannot be determined in this manner. Therefore, excited state pK_a values and hence the assignment of the deprotonation steps cannot be determined with the same degree of accuracy as those for the ground state.[158] However, it is expected that the changes between pH 5 – 8 are caused by the deprotonation of the quinoline nitrogen, while the changes above pH 8 are associated with the deprotonation of the quinoline carboxylic amide. The changes in intensity monitored at different wavelengths occurred within the same pH intervals as those shown in Figure 2.30 for the changes in emission intensity at 356 nm.

In summary, the photophysical pH studies on complex **Eu.51** discussed above showed that the UV-visible and fluorescence properties of the complex are affected by the deprotonation of the quinoline nitrogen and that of the quinoline carboxylic amide, with the latter being responsible for the major changes. Calculation of the singlet excited state pK_a using the Förster equation revealed that the quinoline carboxylic amide becomes a weaker acid upon excitation.

2.5.7.3 Eu(III) excited state investigations

The pH dependence of the delayed Eu^{III} luminescence emission spectra of **Eu.51** was investigated in water in the presence of tetraethylammonium perchlorate (I = 0.1 M) under ambient conditions; room temperature and aerated solution. In acidic solution, when excited at 330 nm, the Eu^{III} emission of **Eu.51** was found to be of high intensity in the range of 550-750 nm, proving the ability of the *antenna* to efficiently populate the lanthanide excited state. The emission can be said to be "*switched on*" in acidic conditions, appearing as well-separated emission bands at 580, 593, 615, 624, 654, 683 and 701 nm, representing the deactivation of the $^5D_0 \rightarrow {}^7F_J$ ground states (J = 0 (580 nm), J = 1 (593 nm), J = 2 (split; 615 and 624 nm), J = 3 (654 nm), and J = 4 (split; 683 and 701 nm)).[159] However, the Eu^{III} emission intensity was gradually quenched, with increasing pH, as shown in Figure 2.31.

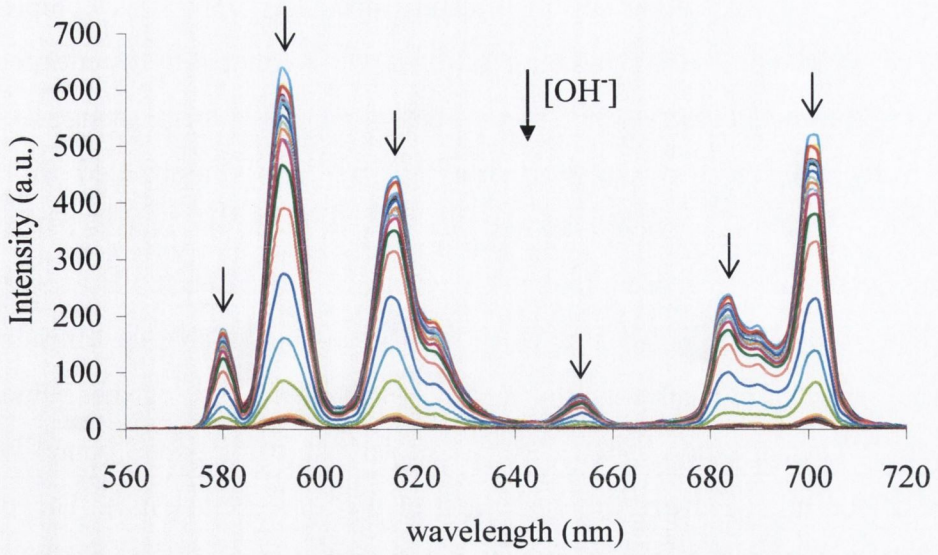

Figure 2.31 Overlaid luminescence emission spectra for the pH titration of Eu.51 [5.0 × 10^{-5} M] against NEt_4OH in H_2O (I = 0.1 M, NEt_4ClO_4) at 298.2 K, showing the deactivation of the $^5D_0 \rightarrow {}^7F_J$ ground states (J = 0, 1, 2 (split), 3 and 4(split)). The arrows indicate the spectral trend with increasing pH between pH 3 – 11.5. These changes are fully reversible.

The luminescence enhancement in acidic media highlights the ability of the antenna to populate the lanthanide excited state by sensitisation, and that this process is highly pH-dependent. Moreover, the luminescence switching is fully reversible, since addition of strong base (pH ~10) quenches the emission, which can be subsequently "*switched on*" again by the addition of acid (pH = 1.6). The changes in the Eu^{III} emission when plotted as a function of pH at 580, 593, 615, 654, 683 and 701 nm gave rise to a sigmoidal curve. The intensity *vs* pH profile obtained for the luminescence intensity of the J = 1 band (593 nm) is shown in Figure 2.32.

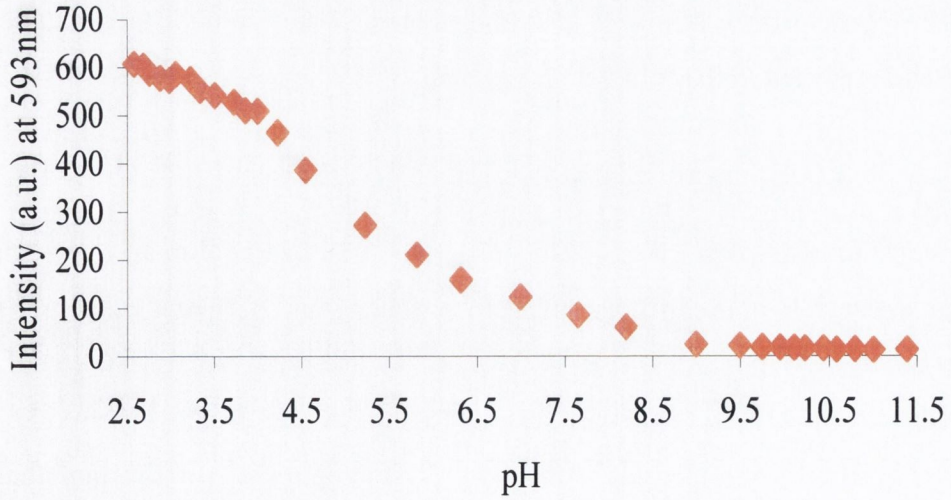

Figure 2.32 Changes in the Eu^{III} emission intensity at 593 nm as a function of pH for the titration of Eu.51 [5.0 × 10^{-5} M] against NEt_4OH in H_2O (I = 0.1 M, NEt_4ClO_4) at 298.2 K.

Above pH 4.5 the Eu^{III} emission significantly decreases until it is completely quenched above pH 9. The pK_a of the quinoline nitrogen as determined by potentiometric titration (6.13), absorption and fluorescence spectroscopy (5.93) is in the pH range of 4-8. Therefore, the decrease in the Eu^{III} emission above pH 4.5 can be associated with the deprotonation of the quinoline nitrogen. Above *ca* pH 8, it would be expected that the effect due to the quinoline nitrogen deprotonation would be insignificant. However the Eu^{III} emission is not fully quenched at this pH. It may be anticipated that the emission is affected by either the deprotonation of the metal bound water, that of the quinoline carboxylic amide or a combination of the two. Deprotonation of the metal bound water molecule would affect the O-H harmonic quenching of the Eu^{III} excited state. The small change in Eu^{III} emission that occurs between pH 2.5-4 cannot be readily explained only through ligand or complex deprotonation. Potentiometric titration, absorption and fluorescence spectroscopy of the complex had shown no evidence of deprotonation in this pH range. The anion effect has also been discounted as a plausible explanation for the observed quenching between pH 2.5-4, as the luminescence titrations were repeated using a variety of counterions, *i.e.* ClO_4^-, $CF_3SO_3^-$ and Cl^-. The effect is therefore associated with the metal ion.

From these results, it is evident that the Eu^{III} emission in **Eu.51**, is sensitive to changes in pH, and that the changes shown in Figure 2.31 occur over a large pH range. Hence, **Eu.51** can be used as a pH sensor to monitor pH changes from *ca.* 2.5 to 8.

With the aim of developing such luminescent sensors with medical and pharmaceutical monitoring applications, the non-covalent incorporation of **Eu.51** into water permeable hydrogels was undertaken. The physical and photophysical properties of the resulting responsive materials were also investigated. The results of these studies will be discussed and analysed in the following sections.

2.5.8 Incorporation of Eu.51 into hydrogel

The europium complex **Eu.51** was incorporated in a hydrogel matrix comprised of poly[methylmethacrylate-co-2-(hydroxyethylmethacrilate)] in 3 different monomer ratios: 1:1 (MMA:HEMA, w/w), 1:3 (MMA: HEMA, w/w) and 100 % HEMA. In all cases ethyleneglycol dimethacrylate was used as a crosslinker and benzoyl peroxide as an initiator, both in 1% by weight. In contrast to the incorporation of the naphthalimide derivatives discussed in the previous section, with **Eu.51** a more hydrophilic, *i.e.* more

permeable, hydrogel matrix was tested, using higher percentages of HEMA. Since **Eu.51** is a positively charged complex, a hydrophilic matrix would be a more suitable media for its dispersion. In order to achieve a homogeneous distribution of **Eu.51** in the hydrogel, the complex (0.05 % w/w and 0.1% w/w) was dissolved in the appropriate monomer mixture prior to polymerisation. Due to the different permeability grades of the films, an unquantifiable amount of **Eu.51** was found in the water when the hydrogel films were left soaking for longer than a month, as detected by fluorescence spectroscopy. The immobilisation of the complex into the hydrogel was therefore not "permanent". Due to time constraints, no further investigations were conducted to determine the exact amount of **Eu.51** released into solution, or the kinetics of the process.

2.5.9 Characterisation of Eu.51-incorporated water-permeable polymers

After proving that the europium complex **Eu.51** worked as a pH switch in aqueous solution, its photophysical properties were studied when incorporated into water-permeable polymers (hydrogel). As already mentioned, three different hydrogel matrices comprised of poly[methylmethacrylate-co-2-(hydroxyethylmethacrilate)] were tested, in order of increasing hydrophilicity: MMA/HEMA 1:1, MMA/HEMA 1:3 and 100 % HEMA. The sensor was homogeneously incorporated at a concentration of 0.05 % and 0.1 % w/w.

2.5.9.1 Equilibrium water content

The water uptake kinetics and content of sensor-incorporated films was investigated using dehydrated samples of the materials (xerogels). When immersed into a hydrating medium, water enters and equilibrium is eventually established between solvation of the copolymer and the forces holding the chains together. The degree of water uptake at equilibrium is a function of both the nature of the copolymer and the degree of crosslinking within that copolymer. Once this equilibrium is reached the equilibrium water content (EWC) can be determined. The EWC of a material is an important parameter that has an influence on the physical properties of the hydrogels; the more hydrophilic the hydrogel the higher its EWC value.

Complex-incorporated hydrogel films prepared with different ratios of HEMA and MMA were cut into squares of 1cm × 1cm in their water-swollen state. The samples were dehydrated at 60 °C to constant weight. The samples were then immersed in deionised water and reweighed, following gentle removal of excess surface water with a tissue, at intervals until a constant weight was achieved. All measurements were made in triplicate

and values are quoted as the mean ± 1 standard deviation. The equilibrium water content (EWC), defined as the ratio of the mass of water taken up to the mass of dry sample, was calculated using the following equation:

$$\textbf{EWC (\%)} = \frac{\text{mass of hydrated sample} - \text{mass of dehydrated sample}}{\text{mass of dehydrated sample}} \times 100 \quad \textbf{(2.13)}$$

The EWC results for the complex-incorporated films using the three different ratios of HEMA and MMA clearly demonstrate that increasing the HEMA content of the film significantly increased the equilibrium water content, as shown in Figure 2.33.

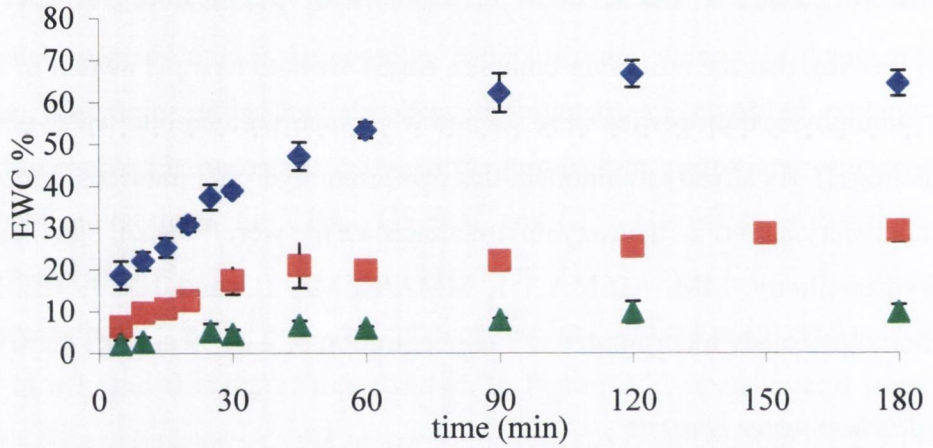

Figure 2.33. EWC (%) of the three different compositions of hydrogel with 0.1% (w/w) of Eu.51 during uptake from xerogels. ♦ 100% HEMA; ■ (3 : 1) HEMA : MMA; ▲(1 : 1) HEMA : MMA. Results are shown as the mean of three replicates ± one standard deviation.

The EWCs for 1:1 MMA:HEMA, 1:3 MMA:HEMA and 100% HEMA copolymers containing 0.1 % (w/w) **Eu.51** were determined to be 10.3 ± 1.9 %, 27.6 ± 3.3 % and 63.2 ± 1.9 %, respectively. All materials are fully equilibrated within 90 minutes of immersion. As previously mentioned, polymeric structures are termed hydrogels when the amount of water retained is between 20-100% of the total weight;[69] therefore the copolymer comprised of 1:1 MMA:HEMA is not a hydrogel by definition. The results of the EWC % were then confirmed by weighing triplicates of the hydrated samples and by reweighing them after being in the oven at 60 °C overnight, in order to establish the water content. The results are shown in Table 2.4.

An increase in EWC as the relative proportion of HEMA in the copolymers increases is expected due to the high hydrophilicity of HEMA compared to MMA. This results from the pendant hydroxyl moiety of HEMA, which can participate in hydrogen bonding with water. The ability to control the EWC of the copolymer within which the complex resides is of considerable importance.

Table 2.4 Water content of the three different types of film in the absence and presence of Eu.51

TYPE OF POLYMERIC FILM		*AVERAGE WATER CONTENT (%)*	*ST. DEV.*
100% HEMA	Blank	59.24	0.86
	+ 0.05% (w/w) Eu.51	58.94	1.01
	+ 0.1% (w/w) Eu.51	50.39	4.47
(3 : 1) HEMA : MMA	Blank	29.9	5.23
	+ 0.1% (w/w) Eu.51	39.6	1.39
(1 : 1) HEMA : MMA	Blank	17.52	1.21
	+ 0.1% (w/w) Eu.51	22.94	1.67

High EWC hydrogels with immobilised sensors are expected to show enhanced response times, compared to low EWC hydrogels, due to their relatively high permeability to water. However, very high EWC gels, with resulting highly-expanded polymer network structure, will facilitate the release of non-covalently incorporated sensors such as those employed here. Importantly, it was observed that all the hydrogels retained the **Eu.51** complex entirely within the matrix for $\leq$ 1 month, as both absorbance and luminescence measurements of the solution in which the hydrogels were soaked showed no detectable levels of complex. The ability of all the matrices to physically retain the **Eu.51** complex is ascribed to the hydrogen bonding interactions between the polymer chains and the complex. This interaction is proposed to take place through the free, ninth coordination site, which may be occupied by either a water solvent molecule (as demonstrated in solution) or a complex-polymer hydrogen bond. The retention of the complex in all the matrices examined, within one month of immersion in deionised water, is attributable to the latter interaction.

2.5.9.2 Density of the Eu.51-incorporated polymers

In order to gain insight into the physical properties of the three polymers under study, a method developed in our laboratory was used to measure the density of such polymers. The method used refers to the definition of density in its most basic acceptation.

Density is a measure of mass per unit of volume. The average density of an object equals its total mass divided by its total volume. In order to measure the volume of a piece of polymeric film of known mass, such a piece was immerged in a known volume of deionised water. The volume of the water displaced by the film was then measured, and it was assumed to be the volume of the film, according to Archimedes's principle.[160,161] With this method, the weight density of 1:1 MMA:HEMA, 1:3 MMA:HEMA and 100% HEMA copolymers containing 0.05 % (w/w) **Eu.51** was measured. The results are listed in Table 2.5.

Table 2.5 Density (g/cm^3) of the three different compositions of hydrogel with 0.05% (w/w) of Eu.51

TYPE OF POLYMERIC FILM	DENSITY (g/cm^3)
100% HEMA	0.672
(3 : 1) HEMA : MMA	0.832
(1 : 1) HEMA : MMA	1.322

As expected, the least dense polymer is the polymer comprised of 100 % HEMA, which is the most hydrophilic. The density of the hydrogel increases with increasing hydrophobicity of the polymer network.

2.5.10 Luminescence measurements of Eu.51 in hydrogels

After assessing the physical properties of the three hydrogel compositions, photophysical investigations of the properties of the Eu^{III} complex incorporated in the hydrogel films were also carried out.

Hydrogel films were investigated using confocal laser-scanning microscopy (CLSM) and steady-state luminescence (see section 2.3.5 for details). For all films the Eu^{III} emission was modulated by changing from an alkaline to an acidic medium. After soaking the strips in acidic or alkaline solution for 1 hour, the changes in the Eu^{III} emission were recorded using CLSM.

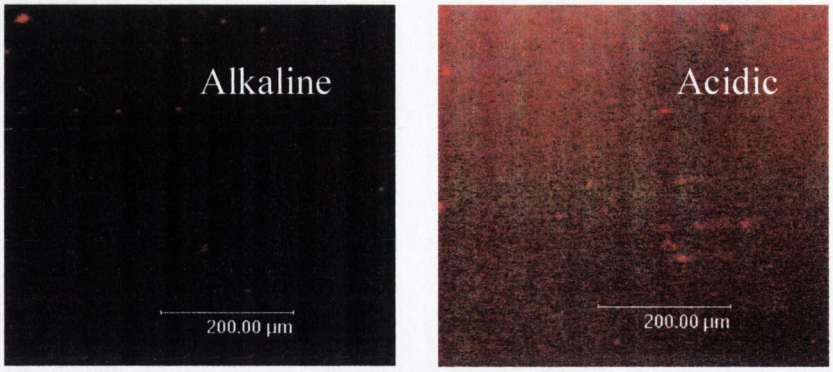

Figure 2.34 Confocal laser-scanning microscopy (CLSM) images of a section of hydrogel (MMA/HEMA, 1:3) incorporating 0.05 % w/w Eu.51 in acidic and basic media.

The reflectance images in Figure 2.34 show that the complex is not homogeneously dispersed within the medium. However, it is possible to observe the difference in emission between the films after soaking in acidic or basic solution. As clearly shown in the luminescence emission micrographs in Figure 2.34, at pH 2 the hydrogel (1:3 MMA : HEMA) incorporating 0.05 % w/w of **Eu.51** shows the typical red emission of Eu^{III}, whereas at pH 11 the red emission is almost entirely quenched. Hence, the luminescence of **Eu.51** in the films is as highly sensitive to pH, as in solution.

Luminescence studies of the films were also carried out using a Varian Cary Eclipse Fluorescence Spectrophotometer using a modified cuvette. A quartz glass slide was fixed to a cuvette lid. The glass slide was then coated with 2 cm × 1 cm sections of the chosen hydrogel film and placed diagonally (45°) inside the cuvette. The luminescence spectrum was then measured.

After 1 hour soaking in acidic or basic solution, both the most hydrophilic (100 % HEMA, **A**) of the three polymers, and the most hydrophobic (1:1, MMA/HEMA, **B**), showed an appreciable difference in the Eu^{III} emission intensity (Figure 2.35). This mirrored the behaviour in aqueous solution. On the other hand, the emission intensities in **B** are higher than those observed in **A**. This may suggest a higher retention of **Eu.51** in **B**, due to the lower permeability of the matrix containing MMA. The hydrogel with composition **C** (1:3 MMA : HEMA) was also switched "*on*" and "*off*" after 1 hour soaking in acidic and basic solution, with an emission intensity at 616 nm of 104.7 and 54.9 a.u., respectively. This gives further evidence that the emission intensity of the hydrogel films depends on the permeability of the matrix, which is related to the retention of the Eu^{III} complex within the film.

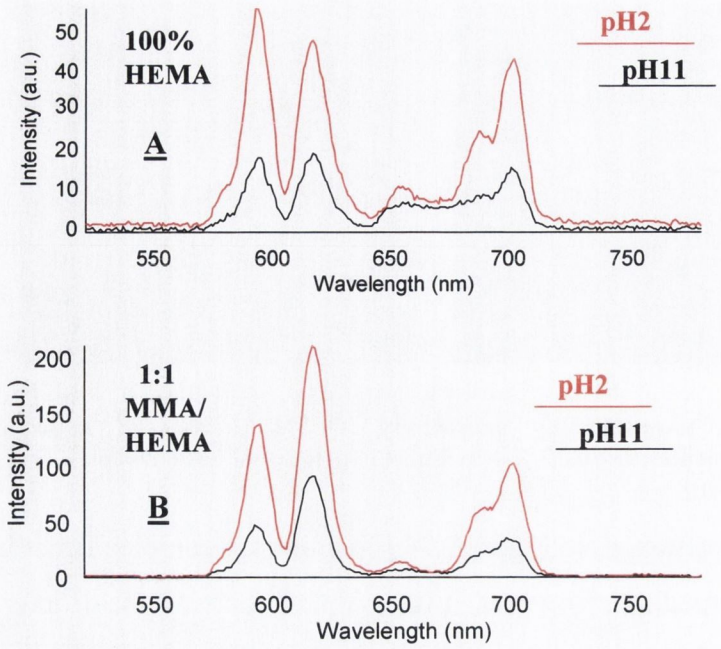

Figure 2.35 Luminescence emission spectra of Eu.51 incorporated into 100 % HEMA and MMA/HEMA (1:1) hydrogel at two different pHs after soaking for 1 hour.

Further luminescence measurements were performed on the hydrogels, after a soaking time of 24 hours. In this case, the most efficient quenching of the Eu^{III} emission occurred with the 1:3, MMA/HEMA hydrogel (**C**) (Figure 2.36).

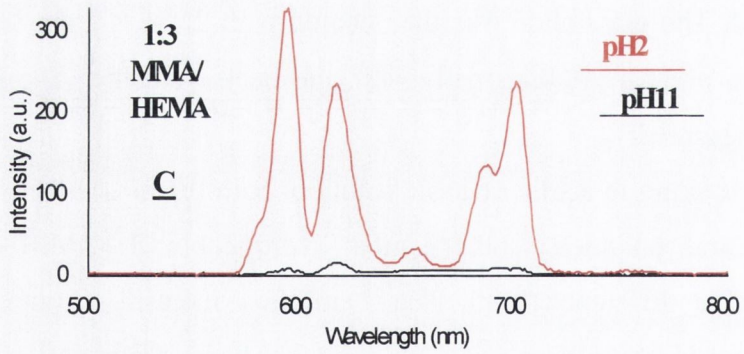

Figure 2.36 Luminescence emission spectra of Eu.51 incorporated into MMA/HEMA (1:3) hydrogel at two different pHs after soaking for 24 hours.

With this mind, it is possible to hypothesise that **C** represents the compromise between an appropriate retention of the complex within the hydrogel matrix and an efficient diffusion process, between film and solution, in order to allow a reasonably fast acid-base equilibrium. The three hydrogel compositions, **A**, **B**, and **C**, all showed a significant (>1 order of magnitude) difference in their Eu^{III} emission intensities as a

function of pH, however not to the same extent. These results mirror those seen in aqueous solution; *e.g.* the emission was switched *"on"* in acid whereas in a basic environment the emission was switched *"off"*. The maximum switching factor (luminescent enhancement), observed for the MMA/HEMA, 1:3 w/w material (**C**), is 53, which is greater than the factor of 30 observed in solution and is a clear "*on-off*" signal. By comparison with the luminescence spectra obtained from the studies in solution (Figure 2.31), the relative intensities of each luminescence band (ΔJ = 0, 1, 2, 3, and 4) are in agreement within experimental error. This indicates the close similarity of the europium environment in solution and within the hydrogel matrix. Due to the experimental method, the resolution of the spectra obtained from the hydrogels is lower than in solution, with the ΔJ = 0 band (580 nm) observed as a shoulder on the ΔJ = 1 band (593 nm).

These results clearly demonstrate that such "*on-off*" pH dependent switching is possible both in hydrogels and in solution. However, the time taken to achieve the fully switched *"on"* equilibrium was significantly different in the films to that observed in solution. In solution, the response is instantaneous, whereas the hydrogel media responded more slowly, as the aqueous medium to be analysed must diffuse into the hydrogel matrix. Nevertheless, the materials studied all give a measurable *"on-off"* switching on the minute timescale. However, due to such time dependence in the response, difficulties were encountered in obtaining reproducible results from the studies of the hydrogel matrices. Hence, it is crucial to ensure all conditions (*i.e.* soaking time, homogeneity and position of the films in the cuvette) are kept constant.

2.6 Conclusions

This Chapter was divided into two parts; the first part dealt with the synthesis and characterisation of the fluorescent naphthalimide-based pH sensors **43** and **44** in solution and incorporated in soft-matter. The second part presented the synthesis and photophysical studies, in solution and in soft-matter, of the luminescent pH sensor **Eu.51**.

The pK_a values of the naphthalimide-based sensors **43** and **44** were determined by means of fluorescence pH titrations in water. The pK_a values obtained indicated that both sensors are suitable for monitoring the pH changes in the physiological pH range. The fluorescent sensors were incorporated into a hydrogel matrix without having to covalently bind them to the polymeric network. The emission properties of the resulting films were investigated using confocal laser-scanning microscopy. These studies proved that both

sensors are switched "*on*" or "*off*" as a function of pH, mirroring the behaviour in aqueous solution.

After assessing the suitability of such fluorescent sensors for incorporation into soft matter (*i.e.* hydrogels), the study of these "luminescent hydrogels" was further extended to the field of lanthanide complexes. Eu^{III} was the lanthanide of choice, as it emits at long wavelengths, with characteristic line-like emission bands and long-lived excited states. These are all highly desirable features for *in vivo* sensing as they can overcome short-lived background emission from the active biological environment (autofluorescence) and light scattering. The synthesis and characterisation of ligand **51** and the corresponding Eu^{III} complex (**Eu.51**) were conducted. Their behaviour in aqueous solution was investigated using potentiometric and spectroscopic techniques. The protonation constants of both ligand and Eu^{III} complex were determined using triflate or perchlorate as the Eu^{III} conteranion. Following the determination of the pK_a values, the metal complex ion stability constants and pK_a values of the metal bound water molecule were also measured. The Eu^{III} emission of the complex was shown to be highly pH sensitive and the emission could be reversibly switched '*off-on*' as a function of pH in solution. The incorporation of **Eu.51** in a non-covalent manner into three hydrogels of composition 1:1 (MMA:HEMA, w/w), 1:3 (MMA:HEMA, w/w) and 100 % HEMA, was successfully achieved. Of significant importance, the emission of these water-permeable materials was on all occasions found to be highly pH sensitive and reversible. These materials thus represent matrices which can be switched *"on"* or *"off"*, with potential application in the interference-free analysis of biological media.

In summary, the Eu^{III} based chemosensor **Eu.51** works as a pH switch both in aqueous solution and in soft-matter, *i.e.* incorporated into hydrogels. Different compositions of the hydrogel matrix have been investigated in order to achieve the optimum conditions for the sensor's response. The photophysical properties of the hydrogels have been analysed using confocal laser-scanning microscopy and standard techniques for luminescence studies.

2.7 Future work

The demonstration of retention of behaviour in non-solution environments is important for the development of soft-matter real-time sensors, which can be used in clinical monitoring environments. The choice of soft matter immobilisation allows the

development of materials which are responsive to complex liquid analytes, such as blood, but can be employed reversibly, as the material is permeable to water but not to complex biomolecules or cells, and can be returned to its initial state of switching by flushing with water.

Future work should involve a systematic study of the hydrogels' properties, with particular interest in the kinetic evaluation of the diffusion process. This will allow for the fine-tuning of the polymer composition with respect to its intended application. Further investigations should also focus on the incorporation of a variety of chemosensors into the hydrogel matrices, in order to improve their capability and adaptability as sensors in medical and environmental fields. In addition, a synthetic method to covalently attach the desired sensors to the hydrogel network should also be explored, with the aim to attain the permanent incorporation of the sensor within the hydrogel matrix and to improve the homogeneity of the hydrogel films.

3 LANTHANIDE-ION INDUCED SUPRAMOLECULAR ASSEMBLIES

3.1 Introduction

Supramolecular chemistry refers to the spontaneous self-assembly of molecular architectures from smaller components. Such structures are held together by relatively weak intermolecular forces which include hydrogen-bonding, Van der Waals and hydrophobic-hydrophilic interactions, ionic forces and metal-ligand coordination interactions. Metal-ligand interactions are generally labile and are mainly of electrostatic nature, where the structures formed are usually the thermodynamically most stable products.[162] Supramolecular chemistry involves either the formation of discrete oligomeric species from the intermolecular association of a few components, such as receptor/substrate interactions, metal-ion binding, or the formation of polymolecular assemblies by spontaneous association of a large number of components into a specific phase (films, layers, membranes, vesicles, micelles, *etc.*).[163] Examples of supramolecular systems include monolayer assembly, membrane formation, molecular recognition (*i.e.* substrate binding to proteins, DNA/protein interactions, antibody/antigen interactions), and metal ion coordination.[164,165]

Self-assembly and self-organisation have been implemented in a variety of novel supramolecular species such as helicates, [162,60] catenanes,[166,167] threaded entities (rotaxanes),[168,169] cage compounds[170] and so forth. In order to control the evolution of supramolecular species as they are built up from their components, implementing molecular information and recognition becomes of primary importance.[163] Hence the need for self-organised systems, such as systems capable of spontaneously generating well-defined supramolecular entities by self-assembly from their components.

The focus of the current and the following chapter is the self-assembly of helicates induced by lanthanide ions. The term helicate was introduced for the first time in 1987 by Lehn and co-workers[171] to indicate a polynuclear helical complex composed of either two or three organic strands (ligands) coordinated to a series of metal ions defining the helical axis.[162,172] The ligands, which present two or more metal ion binding sites, organise themselves around the metal ions (self-assembly), forming the "classical" intertwining structures of double and triple helices. Interest in the self-assembly of helicates and other metal-based supramolecular structures has largely arisen due to to the potential for the self-

assembly of molecular devices and nanostructures.[162] The importance of helicates is also related to the development and understanding of self-assemblies in supramolecular chemistry.[172] Many examples of helicates in the literature have involved double and triple helical structures based on transition metal ions, as well as anions, with bipyridine and terpyridine derived ligands.[173-175] Our research focuses on lanthanide based helicates and self-assemblies. Lanthanide-based supramolecular systems have been investigated as light-converting molecular devices[165,176,177] and their potentials may ultimately be extended to sensing and diagnostic applications. Characterisation of theses complexes has depended largely upon electrospray mass spectrometry, NMR techniques and X-ray crystallography to establish speciation and structural information.[172] Optical techniques, such as UV-Vis and luminescence spectroscopy, have also been used to characterise and follow the formation of helicates in solution.[162,172] The next section shall detail some examples of such lanthanide-based supramolecular systems and their characterisation.

3.1.1 Getting inspired by lanthanide ion based helicates

In 1998, Bünzli and co-workers developed the first lanthanide-contaning helicates which self-assemble in water.[60,178] As already detailed in Chapter 1, ligand **22** yields neutral triple-stranded dimetallic helicates with the entire series of lanthanide ions [Ln_2(**22**-$2H)_3$]; such complexes are stable in water in the pH range 4-13, with stability comparable to that of DOTA-derived complexes (pLn ≈ 21-22; where pLn = -log[$Ln^{III}(aq)]^{3+}$ when $[Ln^{III}]_t = 10^{-6}$ M and [dota] = 10^{-5} M, at pH = 7.4).[4] This indicates that the large hydration energy of the trivalent lanthanide ions is adequately compensated by the favourable thermodynamic contribution of the self-assembly process. The three ligand strands are wrapped around the two nine-coordinate Ln^{III} ions in a helicate shaped structure with pseudo-D_3 symmetry around the metal. These results were confirmed by ^{1}H-NMR studies in D_2O, as further evidence that the complexes adopt a helical structure in solution as well as in the solid state. Moreover, the q value of the Eu^{III} complex was found to be zero, which proves that the Eu^{III} ions are completely protected from direct water interaction, thus providing a good Eu^{III}-containing luminescent probe. A thorough investigation of the metal-centred luminescence spectra of the Eu^{III} and Tb^{III} complexes, both in solution and in the solid state, were also in perfect agreement with the D_3 symmetry reflected in the NMR spectra.

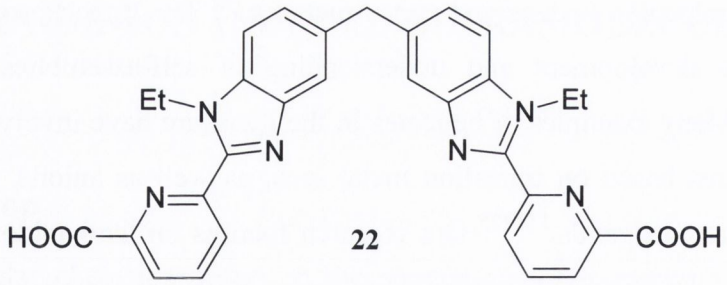

22

In 2000, Horrocks and Lessmann reported the second example of neutral helicates in aqueous solution.[162] The ligands used (**58** and **59**) consist of two tridentate chelating units linked by an organic diamine (1,2-diaminocyclohexane in **58**, 4,4'-diaminodiphenylmethane in **59**). Thus, each ligand coordinates to two different metal ions and the complexes formed are dinuclear with two 9-coordinate lanthanide ions and a stoichiometry of $[Ln_2L_3]$.

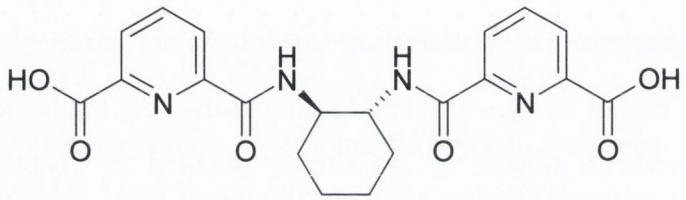

58

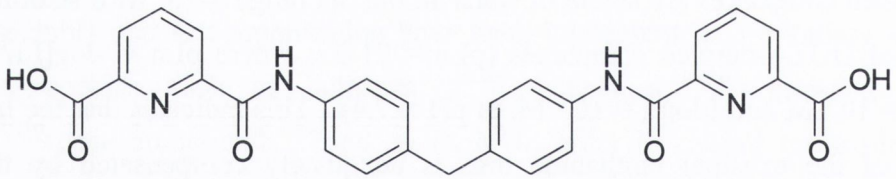

59

The coordinating units chosen by Horrocks are based on the well-known **dpa** ligand (**dpa** = 2,6-pyridinedicarboxylic acid). This ligand forms the well-studied, propeller-shaped complex $[Ln(\mathbf{dpa})_3]^{3-}$,[179,180] which is 9-coordinate with trigonal prismatic, D_3 geometry and either Δ or Λ chirality at the metal centre. The diamines link the coordinating moieties *via* amide bonds. In **58**, both *R,R* and *S,S* enantiomers of the diamine linker have been used in order to impose a handedness to the helicate and to produce a complex which retains its metal-centred (ΔΔ or ΛΛ) optical activity in solution. $[Ln(\mathbf{dpa})_3]^{3-}$ and other chiral lanthanide complexes of this type all racemize rapidly in solution, resulting in racemic mixtures.[162]

The formation and speciation of the lanthanide complex assemblies derived from **58** and **59** have been studied by laser-induced lanthanide luminescence spectroscopy in aqueous solution. Molecular mechanic modelling calculations have also been used to predict the likely structures of dinuclear helicates with a 3 : 2 ligand : metal (L : M) stoichiometry and D_3 symmetry. The models for the triple helical complexes for the two ligands are shown in Figure 3.1.

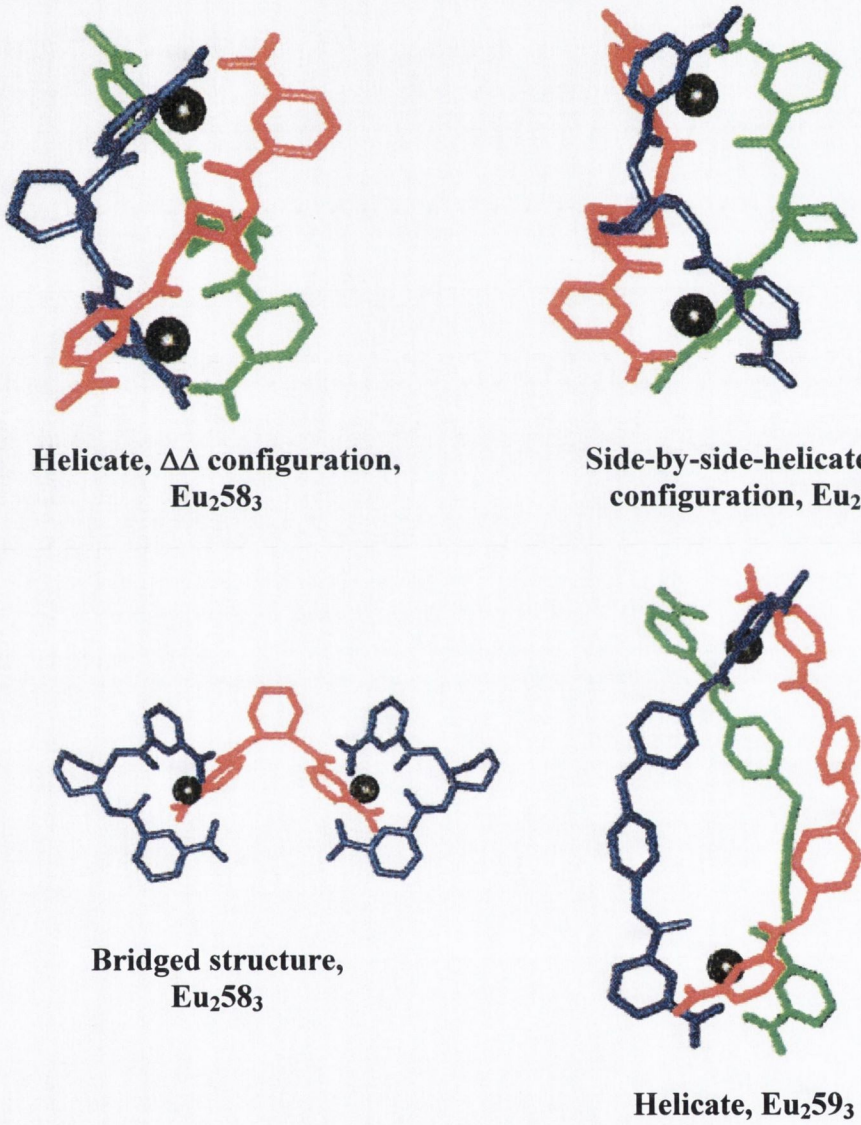

Helicate, ΔΔ configuration, $Eu_2$58$_3$

Side-by-side-helicate, ΔΛ configuration, $Eu_2$58$_3$

Bridged structure, $Eu_2$58$_3$

Helicate, $Eu_2$59$_3$

Figure 3.1 Possible structures for Eu^{III} complexes of dpa-L ligands 58 and 59.[162]

Besides the true helix form (ΔΔ or ΛΛ configuration at the metal ion centres) and the side-by-side helicate (ΔΛ configuration), ligand **58** is able to form a bridged structure, where one ligand chelates one metal ion through both binding sites; two such coordinated metal ions are then bridged by a third ligand. Although unable to obtain X-ray crystal

structures of the complexes, the authors collected sufficient spectroscopic evidence to conclude that both ligands, **58** and **59**, form triple helicates in the presence of Ln^{III} ions.

Recently, the disassembly of bimetallic triple-stranded lanthanide helicates has been thoroughly investigated in the presence of an excess of metals, revealing the competitive formation of standard linear bimetallic complexes and circular trimetallic single-stranded helicates.[181] Except for ligand **62**, which quantitatively forms the triple-stranded helicate $[Ln_2(\mathbf{62})_3]^{6+}$ for a 2:3 Ln:**62** ratio, all other ligands (**60**, **61**, **63**) slowly interconvert into a mixture of complexes, as detected by ^1H NMR in $CH_3CN/CHCl_3$ (1:1) and ESI-MS titrations.

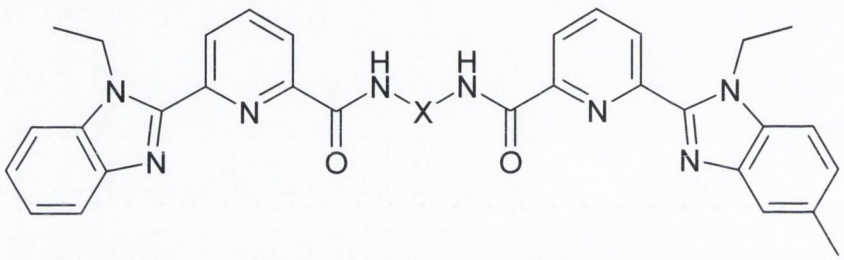

X =  **60**

X = 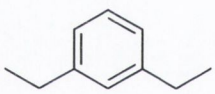 **61**

X = 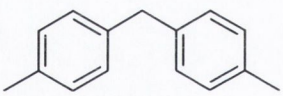 **62**

X = $-(CH_2)_6-$ **63**

For these complexes, the assembly of the bimetallic triple-stranded helicates (2:3, Ln:Ligand) competes with the formation of complexes with a 1:1 stoichiometry. The crystal structure of the Eu^{III} assembly with ligand **60** with a 1:1 stoichiometry is shown in Figure 3.2 and represents the first circular single-stranded lanthanide helicate.

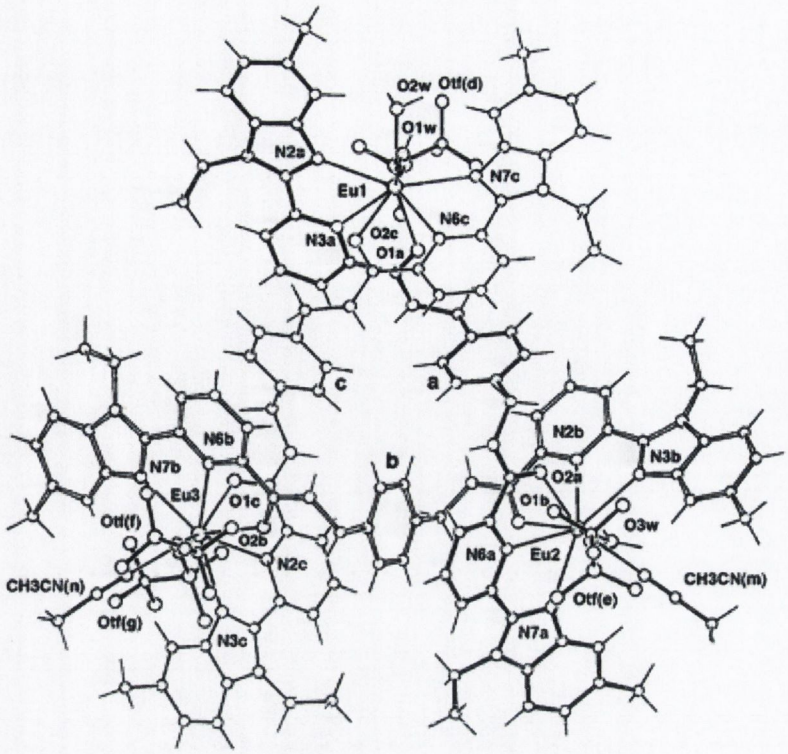

Fibure 3.2 Perspective view along the pseudo-threefold axis, and partial numbering scheme for the cation $[Eu_3(60)_3(CF_3SO_3)_4(CH_3CN)_2(H_2O)_3]^{5+}$.[181]

3.1.2 Lanthanide ion - induced assemblies by Gunnlaugsson *et al.*

Inspired by the work of Horrocks's and Bünzli's research groups, the Gunnlaugsson group have investigated the formation of lanthanide self-assemblies in organic and partially aqueous solution. A series of chiral luminescence lanthanide complexes have been prepared by Dr. Joseph Leonard from the two chiral 2,6-pyridine diamide based ligands **64** (*S,S*) and **65** (*R,R*).

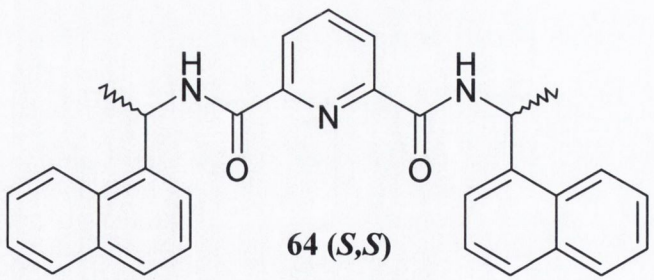

64 (*S,S*)

65 (*R,R*)

The Sm^{III}, Eu^{III}, Tb^{III}, Dy^{III} and Yb^{III} complexes were studied. They all gave rise to sensitised lanthanide luminescence in methanol. Such complexes were shown to adopt

chiral "bundle-like" conformation in the solid state, where the stereochemistry around the metal centre was either Δ or Λ. The crystal structure of **[Tb(64)$_3$]** is shown in Figure 3.3. The enantiomerically pure nature of these complexes was further confirmed by circular dichroism (CD) and circularly polarised luminescence (CPL) spectroscopy.

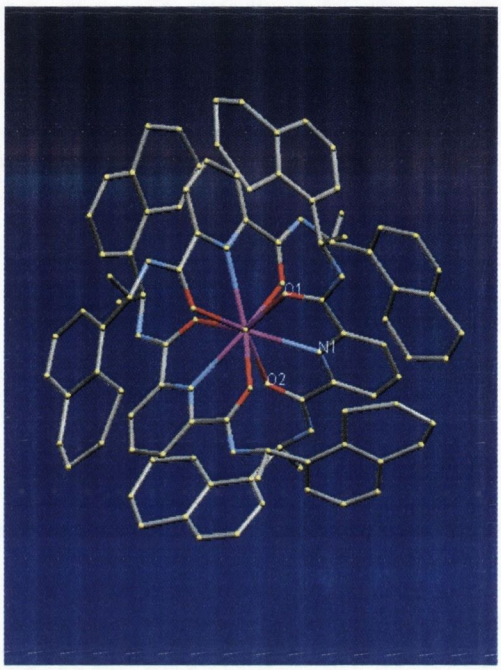

Figure 3.3 Crystal structure of [Tb(64)$_3$].

Based on the results of this family of chiral ligands, we set out to develop novel chiral lanthanide-based helicates by extending this family. The following sections shall detail the design, synthesis and characterisation in partially aqueous solution of these new systems.

3.2 Lanthanide ion-induced supramolecular assemblies

The aim of this project was to develop lanthanide-based helicates with specific photophysical properties. The design principle for such supramolecular structures was mainly based on the aforementioned work carried out within our research group by Dr. Joseph Leonard. In **64** and **65**, the coordinating unit is the diamide derivative of **dpa** (2,6-pyridinedicarboxylic acid), which is known to form the propeller-shaped complex [Ln(**dpa**)$_3$]$^{3-}$,[179,180] as previously discussed. In these ligands, both enantiomers of the 1-(1-naphthyl)-ethylamine (the *S*-isomer in **64**, the *R*-isomer in **65**) act as sensitisers of the lanthanide ion luminescence in the corresponding complex. Moreover, such sensitisers also

provide chirality to both ligands and complexes. With this in mind, we designed ligands **66** and **67**. In such ligands, the two tridentate chelating units are the diamides derived from **dpa**, which are linked by the diamine 4,4'-diaminodiphenylmethane. The *antennae* of the system, the (*R*) and the (*S*) isomers of 1-(1-Naphthyl)-ethylamine, confer the chirality upon the ligands.

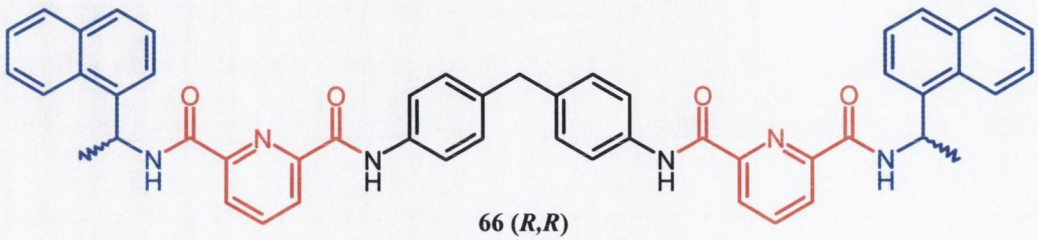

66 (*R,R*)

67 (*S,S*)

3.2.1 Synthesis of ligands 66 and 67

The synthesis of ligands **66** and **67** involved two peptide bond formations *via* coupling reactions with EDCI·HCl. The first step of this pathway was the monoprotection of the 2,6-pyridinedicarboxylic acid **68**, illustrated in Scheme 3.1.[182] A mixture of 2,6-pyridinedicarboxylic acid, water, benzyl alcohol and concentrated sulphuric acid was refluxed for 2 hours and then allowed to stir at room temperature overnight. The mixture was neutralised with saturated aqueous $NaHCO_3$ and extracted with $CHCl_3$ to remove the diester side product. The aqueous layer was acidified to pH 3.8, at which point the monoester **69** crystallised as white needles in 22 % yield. The purity of the compound was assessed by ^1H and ^{13}C-NMR, which were found to be in agreement with the literature values.[183]

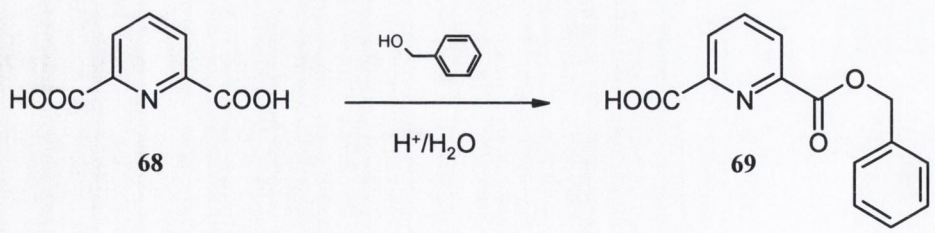

68 **69**

Scheme 3.1 Monoprotection of 2,6- pyridinedicarboxylic acid with benzyl alcohol.

The appropriate 1-(1-naphthyl)-ethylamine, either the *R* or *S* isomer, was then added to a solution of HOBt, monobenzyl ester **69** and triethylamine. This solution was stirred for 20-30 minutes at -10 °C in anhydrous THF, before the coupling reagent EDCI·HCl was added. The resulting mixture was stirred for further 12 hours at room temperature and under argon. The solution was filtered and the solvent evaporated under reduced pressure. The resulting residue was dissolved in CH_2Cl_2, washed with 1.0 M HCl, then with saturated aqueous $NaHCO_3$ and finally with water. The organic phase was dried over $MgSO_4$ and the solvent removed under reduced pressure to yield a pale yellow oil in 81 % yield. The product was characterised by ^1H and ^{13}C-NMR and high resolution mass spectrometry (HRMS).

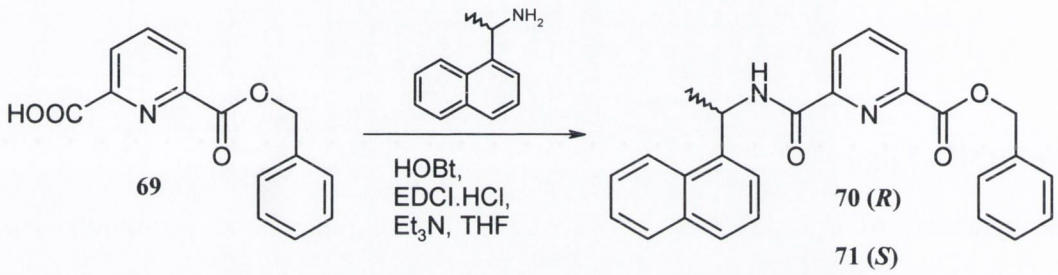

Scheme 3.2 EDCI·HCl coupling of 2,6- pyridinedicarboxylic acid, monobenzyl ester with 1-(1-naphthyl)-ethylamine (*R* and *S*).

The reduction of both isomers (**70** and **71**) was carried out in CH_3OH, using a Parr hydrogen shaker apparatus with a 10 % Pd/C catalyst under 3 atm of $H_{2(g)}$ (Scheme 3.3). The reaction yielded the two carboxylic acids derivatives **72** and **73** in quantitative yields. The removal of the benzylic group was confirmed by the ^1H-NMR spectrum. The identity of the two products, **72** and **73**, was also confirmed by elemental analysis and ESMS.

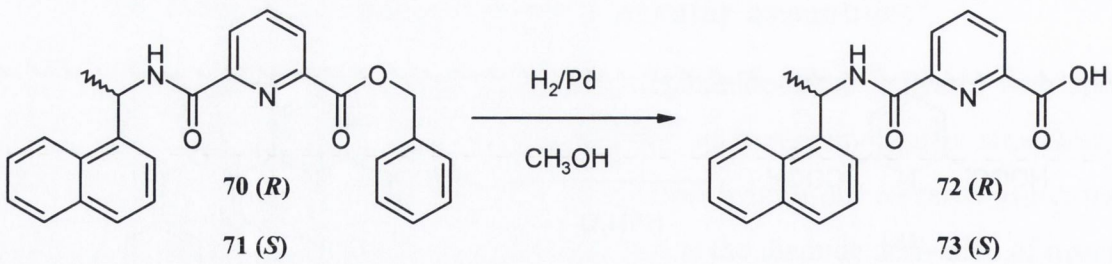

Scheme 3.3 Deprotection of the benzyl ester *via* Pd-catalysed hydrogenation.

Finally, both *R* (**72**) and *S* (**73**) isomers were reacted with 4,4'-diaminodiphenylmethane *via* a peptide coupling reaction using EDCI·HCl, following the same procedure described above and illustrated in Scheme 3.4. The two desired ligands were isolated in 80 % yields and characterised with ^{1}H-NMR, ^{13}C-NMR, IR and elemental analysis.

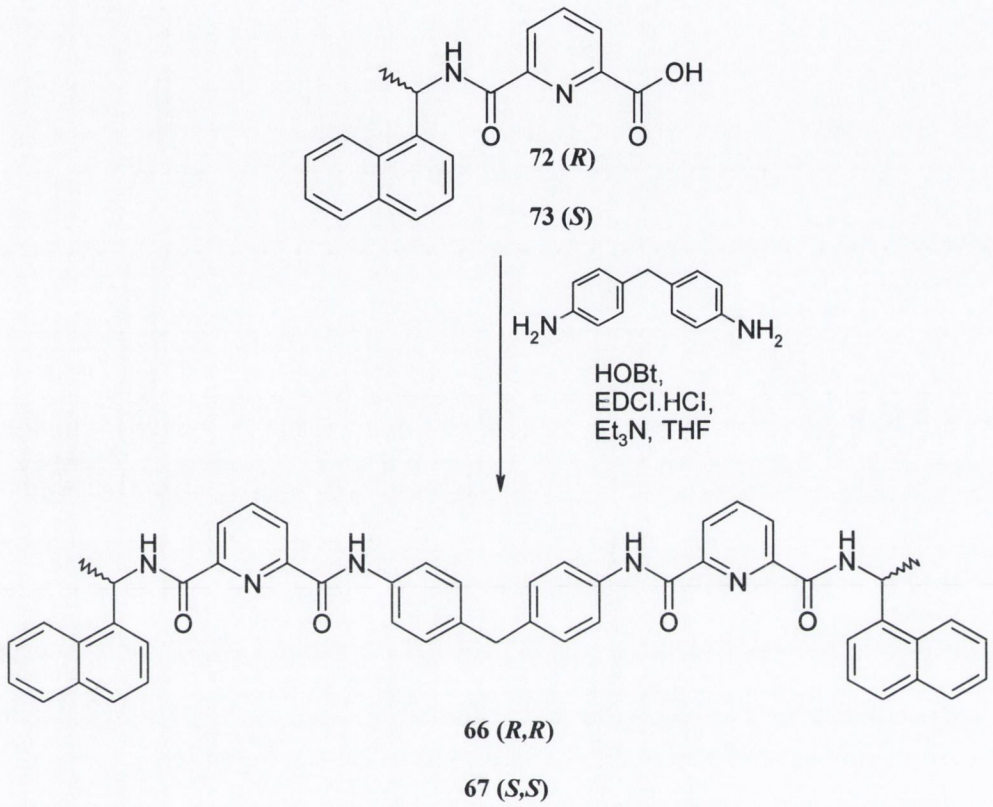

Scheme 3.4 EDCI·HCl coupling of 72 and 73 with 4,4'-diaminodiphenylmethane.

The ^{1}H-NMR spectrum shown in Figure 3.4 clearly indicates the C_2 symmetry of the molecule. The methyl group appeared as a doublet at 1.83 ppm and the central methylene group as a singlet at 3.94 ppm. The proton on the chiral centre appeared as a multiplet at 6.10 ppm. The resonances of the two amide protons were found at 9.32 and 8.06 ppm, the latter appearing as an unresolved doublet due to the coupling with the adjacent CH. The identity of the ligands was also confirmed by elemental analysis and IR. Neither of the ligands **66** and **67** were detectable by ESMS nor was there evidence of unreacted starting materials. Variation of the solvent (methanol, acetonitrile) had no effect on the ESMS experiments.

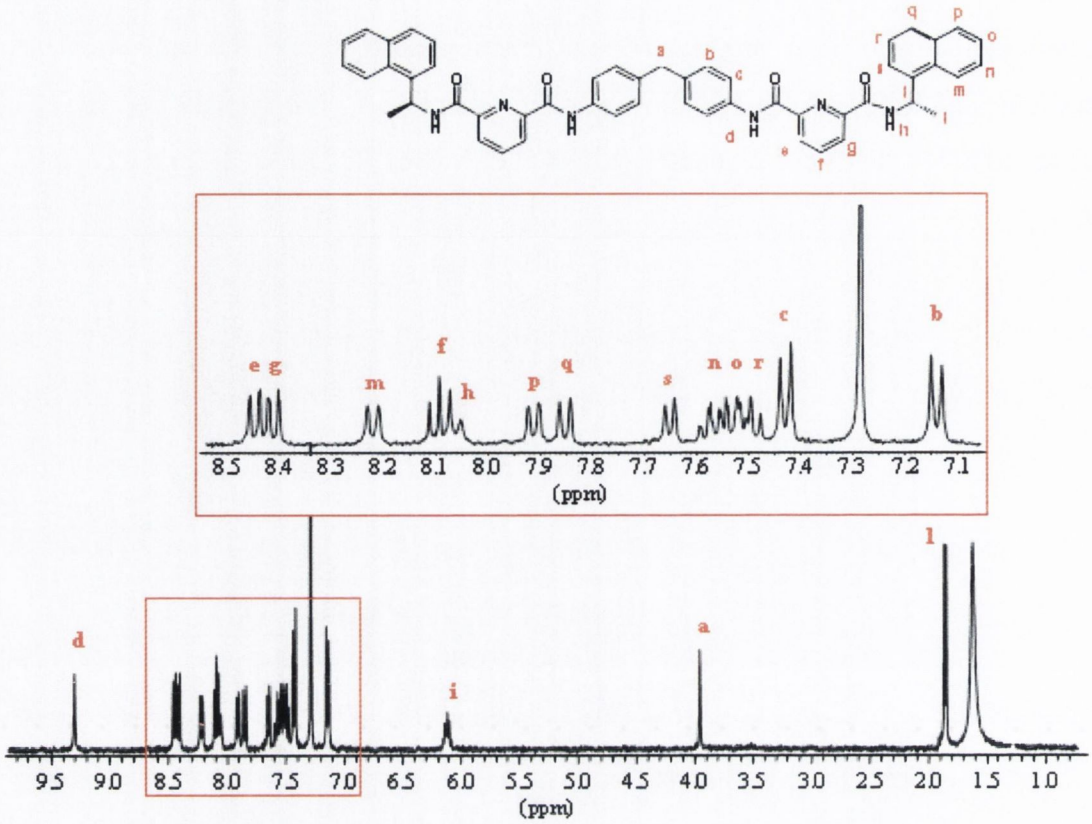

Figure 3.4 ^{1}**H-NMR (400 MHz, $CDCl_3$) of *(R,R)* Ligand 66.**

The two target bis-tridentate ligands, **66** ***(R,R)*** and **67** ***(S,S)***, were successfully prepared and isolated. The synthesis and characterisation of the corresponding Eu^{III} complexes were subsequently carried out and will be discussed hereafter.

3.2.2 Formation of Eu^{III} assemblies with ligands 66 and 67

The final step in the synthesis of the supramolecular assemblies $\mathbf{Eu_2(66)_3}$, (**74**), and $\mathbf{Eu_2(67)_3}$, (**75**), required the preparation of the desired europium complexes of ligands **66** and **67** (Scheme 3.5). The appropriate ligand was dissolved in $CH_3CN/CHCl_3$ (**66**) or MeOH (**67**) and $Eu(CF_3SO_3)_3$ was added in a 2:3 metal:ligand ratio. The mixture was then refluxed overnight followed by dropwise addition to a stirred solution of diethyl ether. A brown solid was collected by filtration in 48.5% (**74**) and 90% (**75**) yield and identified as the desired $[Eu_2L_3]$ complex by ^{1}H-NMR and elemental analysis.

The presence of three species is to be anticipated for $[Eu_2L_3]$ complexes in solution: the *rac*-isomers, ΛΛ and ΔΔ, in which both complex units posses the same configuration and give rise to triple helical structures; or the corresponding *meso*-form, ΛΔ, where each complex unit has opposite configuration (*meso*-cate).[175]

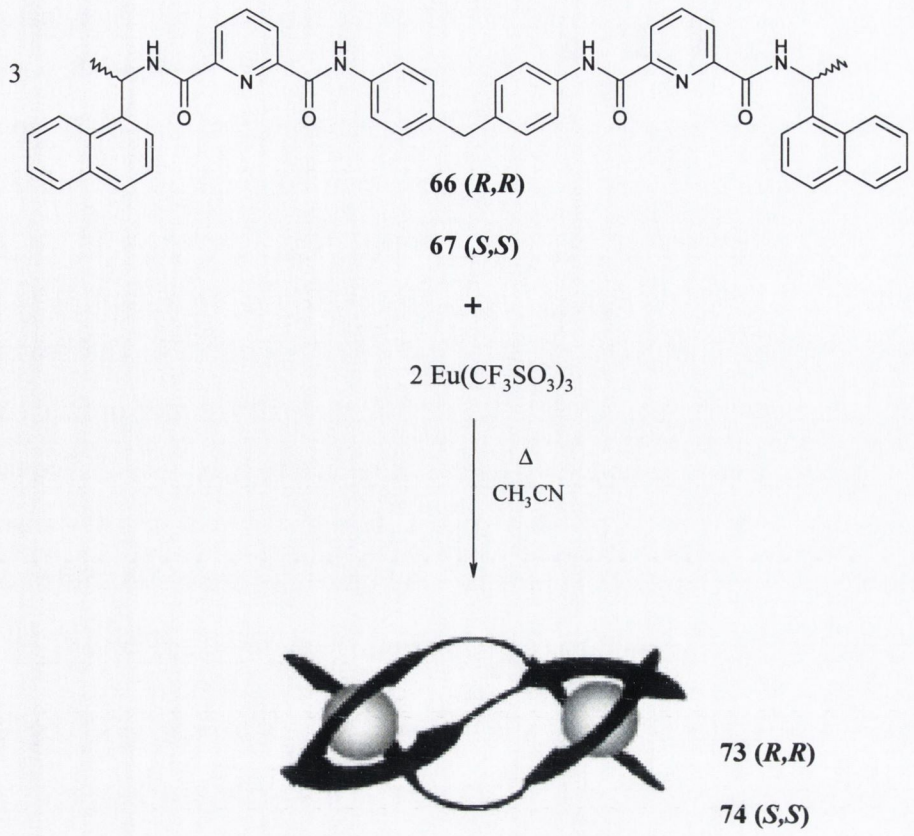

Scheme 3.5 Preparation of the Eu^{III} helicates from ligands 66 and 67.

The ^{1}H-NMR spectra of both Eu^{III} complexes, **74** and **75**, were particularly informative, as the CH_2 protons of the spacer permit easier assignment of the resonances to either of the *rac*-(helical) or *meso*-(non-helical) isomers. In the *rac*-form these protons are equivalent and a single resonance is observed, whereas in the *meso*-form they are diastereotopic and give rise to two doublets. From the ^{1}H-NMR spectrum (400 MHz, CD_3CN) of **74 (R,R)** in Figure 3.5, it appears evident that the complex posses high symmetry and that only the *rac*-form of the complex was present in solution, as the CH_2 protons resonated as a singlet at 4.37 ppm. The ^{1}H-NMR spectrum also showed that the symmetry of the ligands was "maintained" upon complexation, *i.e.* the number of resonances in the complex was the same as in the ligand. This denotes that the coordination environments of both metal ions in the complex molecule are exactly the same. It is well known that paramagnetic lanthanide ions induce proton shifts in the ^{1}H-NMR within a wide ppm range.[184] Protons in close proximity to the paramagnetic lanthanide ion are influenced by the presence of the unpaired *f* electrons, leading to paramagnetic relaxation and broadening of resonances, as well as a shift to a different NMR frequency.

However, the europium centre did not induce the expected large chemical shifts. As can be seen from the ^{1}H-NMR spectrum (400 MHz, CD_3CN) of **74 (*R,R*)** shown in Figure 3.5, the chemical shifts of the complex all appeared within the 0-10 ppm range. Nevertheless, the resonances of the protons closely involved in the Eu^{III} coordination were signifcantly shifted, when compared to the corresponding resonances of the ligand in CD_3CN (Figure 3.5). Both NH signals were shifted upfield from 9.93 to 6.68 ppm and from 8.81 to 3.95 ppm, with Δppm of -3.25 and -4.86, respectively. The protons in the pyridine ring (indicated with an asterisk in Figure 3.5) were also shifted upfield (Δppm (H_4 pyridine) = -1.72). Conversely, the proton on the chiral centre (CH) was shifted downfield, to a resonance at 8.18 ppm. The CH_2 and CH_3 signals and the 4,4'-disubstituted diphenylmethane protons (shown in the red box in Figure 3.6) were also shifted downfield upon complexation, however not to the same extent as they are not directly involved in the coordination of the Eu^{III} centre.

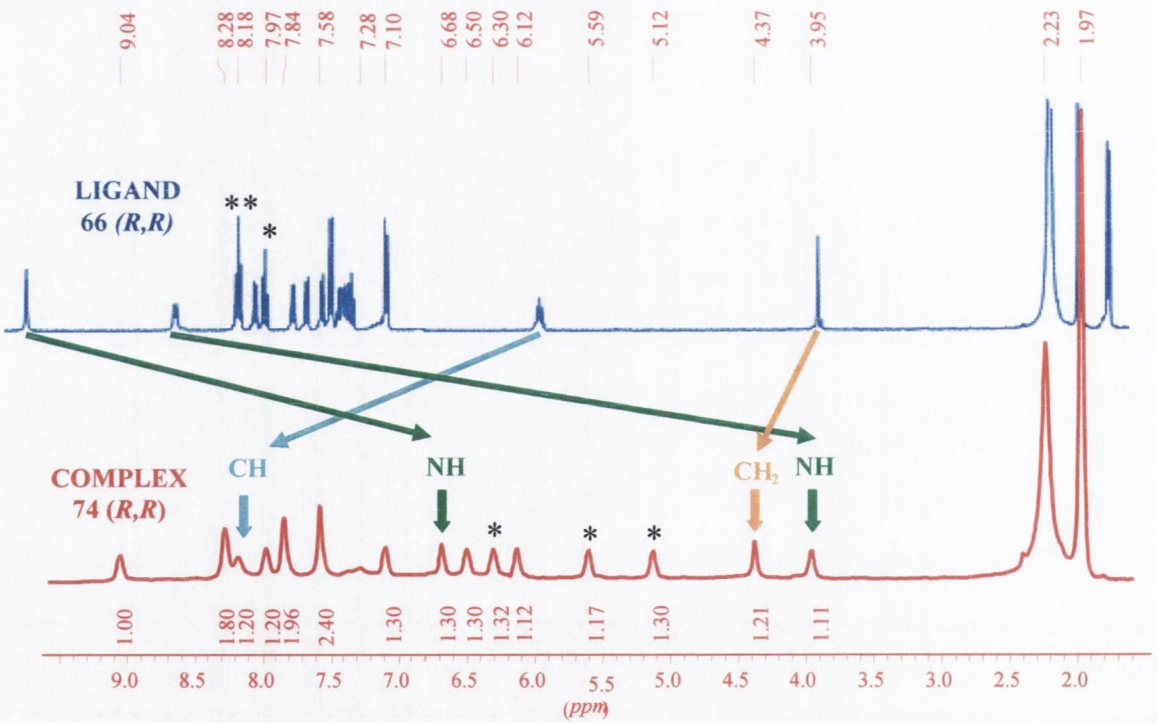

Figure 3.5 Bottom: ^{1}H-NMR (400 MHz, CD_3CN) of 74 (*R,R*). The NH protons are indicated by the green arrows. The protons in the pyridine ring are indicated by a black asterisk (*). Top: ^{1}H-NMR (400 MHz, CD_3CN) of *(R,R)* Ligand 66.

The signal at 7.28 ppm in the ^{1}H-NMR spectrum indicates traces of chloroform present in the molecular structure of the complex, which will be addressed in Section 3.2.4. This was confirmed by the elemental analysis (*cf.* experimental section). The assignation of

the NH, the pyridine and the alkyl protons was carried out through the H-H and N-H cosy experiments. The spectra are shown in Figure 3.6 and 3.7, respectively.

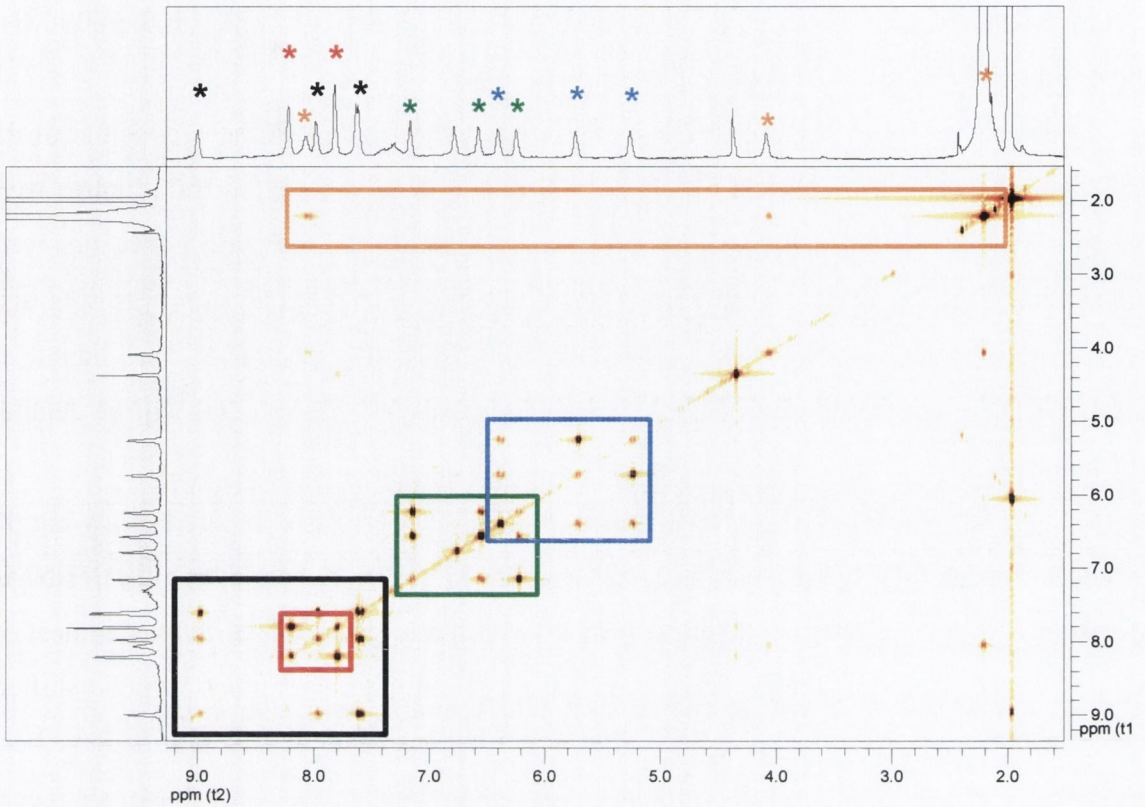

Figure 3.6 HSQC ($^{1}H - ^{13}C$) spectrum (600 MHz, CD_3CN) of 74 (*R,R*). The coloured rectangles and corresponding asterisks indicate the spin systems in the molecule.

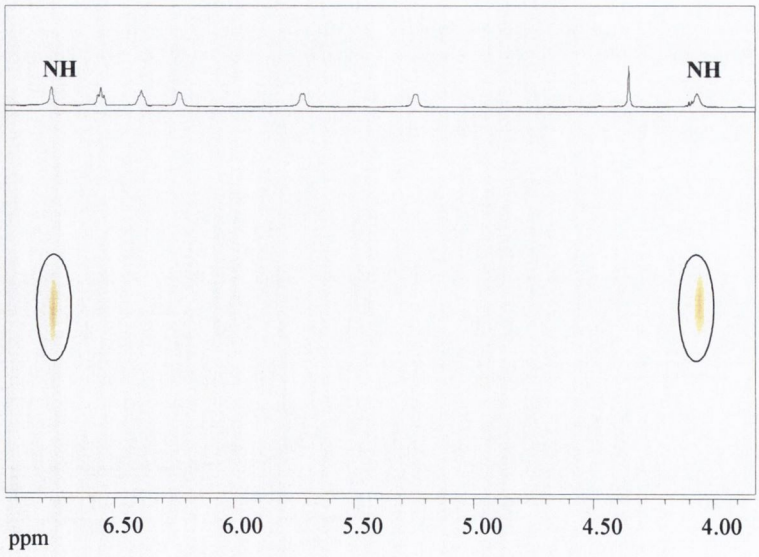

Figure 3.7 HSQC ($^{1}H - ^{15}N$) spectrum (600 MHz, CD_3CN) of 74 (*R,R*). (δ ^{15}N = 79.5 and 79.2 ppm).

The resonances at 9.04, 7.97 and 7.58 ppm (black box in Figure 3.6) correspond to the 4-spin system of the 1-naphthyl moiety, the first belonging to the proton in position 8. The signals at 7.10, 6.50 and 6.12 ppm (green box in Figure 3.6) correspond to the 3-spin system of the 1-naphthyl group; the resonance at 6.50 appears as a triplet in the 600 MHz spectrum and belongs to the proton in position 3.

From the ^{1}H-NMR data, it was also possible to conclude that the *rac*-isomer of the Eu^{III} complex **74**, $[Eu_2(\mathbf{66})_3]$ had indeed been formed. As predicted, the Eu^{III} centres were bound to the ligands through the **dpa** moieties, as the amide and the pyridine protons were substantially shifted upfield. The formation of the 2:3, Eu^{III}:Ligand, complex was also investigated by monitoring the changes in the ^{1}H-NMR spectra of the ligand in $CD_3CN/CDCl_3$ upon addition of $Eu(CF_3SO_3)_3$. The results of these studies will be detailed in Chapter 4.

The Tb^{III} and Sm^{III} complexes of ligand **66** ***(R,R)*** were also prepared following the procedure previously described for **74** ***(R,R)*** and **75** ***(S,S)***. As expected, the ^{1}H-NMR spectrum of the Tb^{III} complex (Figure 3.8) showed large chemical shifts over almost 50 ppm. Conversely, the proton signals of the Sm^{III} complex were not largely shifted, appearing between 0 and 10 ppm. Such differences in paramagnetic NMR shifts have been previously reported in axially symmetric lanthanide chelates;[180] they have also been observed within the Gunnlaugsson group, in the lanthanide complexes derived from ligands **64** ***(S)*** and **65** ***(R)***.

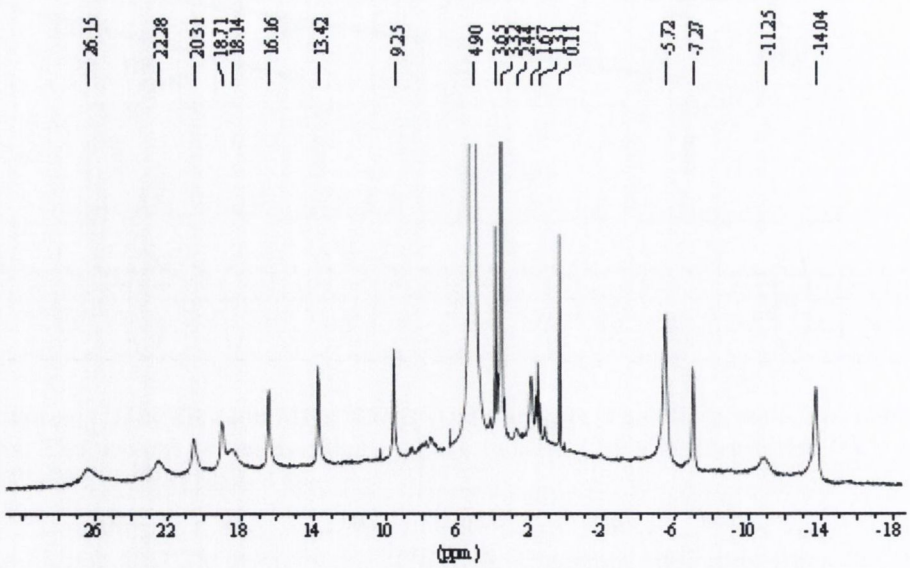

Figure 3.8 ^{1}H-NMR (400 MHz, CD_3OD) of $Tb_2[66(R,R)]_3$.

3.2.3 Attempted crystal growth for X-ray studies

Several attempts to grow crystals suitable for X-ray structure determination of both ligands **66 (*R,R*)** and **67 (*S,S*)** and their corresponding complexes were undertaken. At this purpose, numerous crystallisation techniques were used and they will be outlined in this section. All the compounds under study are moisture sensitive; therefore special care was to be taken in this regard.

- *Slow Evaporation.* Saturated or nearly saturated solutions of the compounds were prepared in a suitable solvent. The solutions were then transferred to a crystal growing dish and covered. The container was left undisturbed and the solvent was allowed to evaporate. Different solvents and solvent mixtures were used; *e.g.* DCM, chloroform, CH_3CN, MeOH, ethyl acetate, EtOH.
- *Vapour Diffusion.* A solution of the chosen compound was prepared using solvent S_1 and placed in test tube T. A second solvent, S_2, was placed in a closed beaker, B. S_2 was chosen such that when mixed with S_1 the solute will become less soluble. The test tube containing S_1 was then placed in the beaker and the beaker was sealed. Slow diffusion of S_2 into T and S_1 out of T should cause crystals to form. Several solvents were used as S_1 and S_2; namely S1: CH_3Cl, CH_3CN, MeOH, ethyl acetate, DMF. S_2: diethyl ether, DCM, water (when suitable), THF, EtOH, toluene.
- *Solvent Diffusion (Layering Technique).* The solute was dissolved in S_1 and placed in a test tube. S_2 was slowly added into the tube so that S_1 and S_2 form discreet layers. In order for this to occur the density of S_2 has to be less than S_1. The solvent combinations used were: DCM/diethyl ether, chloroform/diethyl ether, DCM/water, chloroform/water, MeOH/pentane, CH_3CN/hexane, DMF/cyclohexane.
- *Effect of counterions*. Metathesis reactions were performed in order to change the counterion of the Eu^{III} complexes **74 (*R,R*)** and **75 (*S,S*)**. These complexes were synthesised as triflate salts; therefore other anions, such as perchlorate, nitrate, acetate, camphorate, were used to perform the metathesis reaction in different solvents, i.e. MeOH, CH_3CN and DMF.

In each case the crystals obtained were not of X-ray quality. Therefore, in order to probe the feasibility of the helical structure of the Eu^{III} complexes, molecular mechanics studies were pursued.

3.2.4 Molecular mechanics modelling studies

Molecular mechanics calculations have been successfully used in the past to model the structures of lanthanide chelates in solution.[185-187] Such calculations are used as a guide in ligand design and to test the feasibility of various helical structures.[162] Molecular modelling followed by geometry optimisation of complex **75** ***(S,S)***, undertaken by Dr. P. E. Kruger, School of Chemistry, Trinity College Dublin, gave the structure as shown in Figure 3.9, which is consistent with the ^{1}H-NMR findings.

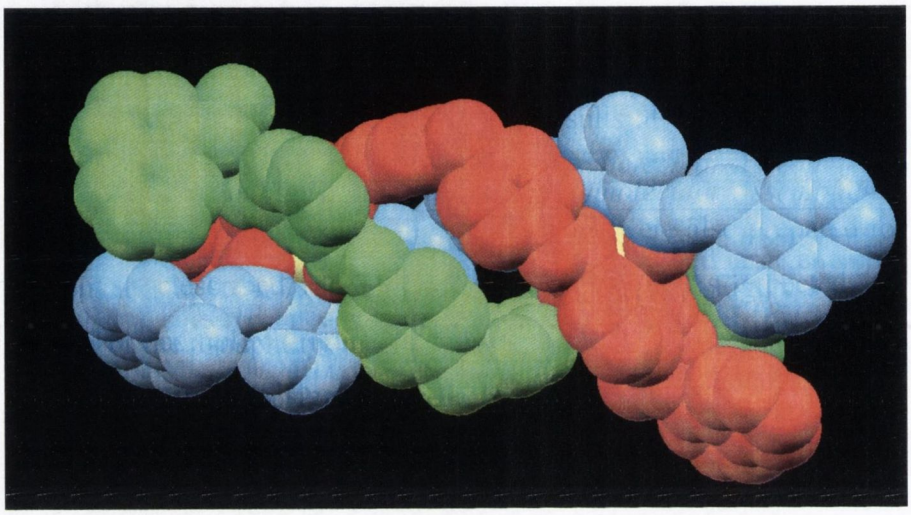

Figure 3.9 Molecular model of a prospective 75 (S,S); $[Eu_2(67)_3]^{6+}$ (P-helix), shown in space-filling mode.

From the molecular model, it is clear that, upon coordination of the two metal ions, the ligands arrange themselves in a helical structure generating an inter-strand cavity. Such a cavity may enable the inclusion of solvent molecules, as proven by the presence of traces of chloroform in the ^{1}H-NMR spectrum and in the elemental analysis of complex **74 (*R,R*)**, as discussed in Section 3.2.2. Each of the two metal ions is coordinated by the three **dpa** moieties. Based on the model, it is also possible to observe that the naphthalene groups (the *antennae* of the system) do not interact with each other, *i.e.* no π–π stacking is involved. Molecular mechanics calculations on **74 (*R,R*)** and **75 *(S,S)*** were undertaken with Hyperchem version 7.52 (*cf.* Chapter 5 for details). Molecular dynamics was also used (simulating heating to 1000 K) to ensure that the true energy minima had been reached. Guided by ^{1}H-NMR spectroscopic data and elemental analysis, the modelling studies were limited to dinuclear species of general formula $[Eu_2L_3]^{6+}$ of *rac*-(helical) and *meso*-(non-helical) configuration. The lowest energy structures were found to be the *rac*-**74 (*R,R*)** and *rac*-**75 (S,S)**; the latter is shown in Figure 3.9.

3.2.5 Potentiometric measurements of ligands 66 and 67

Ligands **66** ***(R,R)*** and **67** ***(S,S)*** were subjected to potentiometric titrations to determine the pK_a values associated with their donor atoms (*cf.* Chapter 2 for details). The protonation constants of the protonated ligands were determined in an CH_3CN/H_2O solvent system (80:20; v/v), with constant ionic strength, I = 0.1 M (NEt_4ClO_4). The solvent system was chosen to ensure complete dissolution of the ligands whilst maintaining an adequate percentage of water to allow the pH electrode to function correctly. The titration curve obtained by the potentiometric titration of ligand **67** is shown in Figure 3.10.

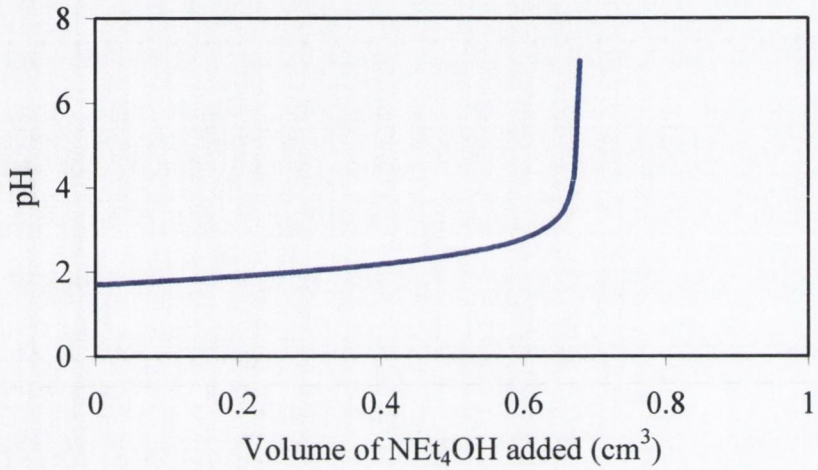

Figure 3.10 Titration curve of the protonated ligand 67 *(S,S)* against NEt_4OH at 298.2 K. [67] = 1.18 × 10^{-3} M, $[H^+]$ = 6.5 × 10^{-3} M, $[NEt_4OH]$ = 0.096 M, I = 0.10 M (NEt_4ClO_4)

The pK_a values were calculated using the program HYPERQUAD.[141] The logarithms of the protonation constants for the studied ligands, obtained by mathematical treatment of the potentiometric titration data, are displayed in Table 3.1.

Table 3.1 pK_a values of the protonated ligands 66 and 67 obtained at 298.2 K and I = 0.1 M (NEt_4ClO_4) in CH_3CN/H_2O (80:20; v/v)

ligand	*equilibrium quotient*	pK_a
66 *(R,R)* [a]	$[66][H^+]/[H66^+]$	3.45 ± 0.03
67 *(S,S)* [b]	$[67][H^+]/[H67^+]$	3.45 ± 0.05

[a] [66] = 1.00 × 10^{-3} M, $[H^+]$ = 7.91 × 10^{-3} M, $[NEt_4OH]$ = 0.188 M

[b] [67] = 1.18 × 10^{-3} M, $[H^+]$ = 6.50 × 10^{-3} M, $[NEt_4OH]$ = 0.096 M

Both ligands **66** ***(R,R)*** and **67** ***(S,S)*** precipitated out of solution above pH 7, therefore only pK_a values below this pH could be determined. Within this pH range, only one pK_a was calculated for each ligand. This pK_a corresponds to the protonation of the pyridine nitrogen and is the same for both ligands, as expected for pK_a values corresponding to two enantiomers. The presence of only one protonation constant relative to the pyridine moiety is further evidence of the C_2 symmetry of the ligands, which implies the equivalence of the two pyridine nitrogens. This denotes that the two protonation equilibria occur simultaneously, without reciprocal influence. The pK_a values obtained are lower than those reported in the literature for the pyridine pK_a in water;[188,189] this may be attributed to a combination of effects from the organic-enriched solvent effect, which reduces the solvation of the ligand, and the presence of electron withdrawing groups *ortho* to the protonation site. The formation of a precipitate above pH 7 may indicate the presence of other pK_as in this pH region, which could not be determined potentiometrically.

In order to compare the results, the pK_a values of the analogue monodentate ligands, **64 (*S*)** and **65 (*R*)**, were determined with the same technique. As found for ligands **66** ***(R,R)*** and **67** ***(S,S)***, it was not possible to determine any pK_a values above pH 7, due to precipitate formation. The pK_a values, obtained using the program HYPERQUAD, are shown in Table 3.2.

Table 3.2 pK_a values of the protonated ligands 64 and 65 obtained at 298.2 K and I = 0.1 M (NEt_4ClO_4) in CH_3CN/H_2O (80:20; v/v)

ligand	*equilibrium quotient*	pK_a
64 (*S*)[a]	[**64**][H^+]/[H**64**$^+$]	3.04 ± 0.02
65 (*R*)[b]	[**65**][H^+]/[H**65**$^+$]	3.03 ± 0.01

[a] [**64**] = 8.91×10^{-4} M, [H^+] = 3.49×10^{-3} M, [NEt_4OH] = 0.096 M

[b] [**65**] = 7.00×10^{-4} M, [H^+] = 3.48×10^{-3} M, [NEt_4OH] = 0.096 M

As expected, the protonation constants of the analogue monodentate ligands **64** and **65** are of the same order of magnitude as those found for ligands **66** and **67**, due to the same nature of the protonation site and the close similarity between the structures.

Potentiometric titrations were also undertaken in order to calculate the stability constants of the metal complex ions present in an CH_3CN/H_2O (80:20; v/v) solution. The results of these titrations will be shown in the next section.

3.2.6 Determination of metal complex ion stability constants by potentiometric titrations

In order to determine the metal complex ion stability constants relative to the formation of the Eu^{III} complexes with both ligands **66** ***(R,R)*** and **67** ***(S,S)***, potentiometric titrations were carried out in an CH_3CN/H_2O solvent system (80:20; v/v), with constant ionic strength, I = 0.1 M (NEt_4ClO_4). As previously detailed in Chapter 2 (Section 2.5.3), the metal ion competes with the protons in acidic media for the ligand coordination sites, altering the pH of the solution. Therefore, a change in the titration curve upon addition of a metal ion to the solution indicates the formation of a metal complex ion; the larger the change, the higher the metal complex ion stability constant. Determination of metal ion stability constants was achieved by adding one or half an equivalent of the metal ion to the acidic solution prior to titration with the relevant base. As for the protonation constants (see Section 3.2.5), the calculation of the metal complex ion stability constant was attempted by means of the computer program HYPERQUAD.[141]

The coordination of the metal ion by the ligand involves the substitution of solvent molecules from the first coordination sphere of the metal ion. Consequently, the nature of the solvent affects the stability of the metal complex ion. In ligands **66** ***(R,R)*** and **67** ***(S,S)*** the two tridentate coordinating units present three coordination sites: one from the pyridine nitrogen and two from the amide oxygens. In order to fulfil the coordination requirements of the Eu^{III} ion, three ligands are therefore necessary, such that each ligand will coordinate to two different metal ions. The complex formed will be dinuclear with two 9-coordinate Eu^{III} ions and a stoichiometry of $[Eu_2L_3]$. The overall stability of the complexes is thus affected by the number of coordination sites, the solvation energy of the metal ion and the structure and flexibility of the ligands.

It may be anticipated that the formation mechanism of the helicate Eu_2L_3 will involve at least four equilibrium steps, described in Equations 3.1 - 3.4:

$$Eu^{3+} + L \overset{K_{11}}{\rightleftharpoons} [EuL]^{3+} \quad \textbf{(3.1)}$$

$$[EuL]^{3+} + L \overset{K_{12}}{\rightleftharpoons} [EuL_2]^{3+} \quad \textbf{(3.2)}$$

$$[EuL_2]^{3+} + Eu^{3+} \overset{K_{22}}{\rightleftharpoons} [Eu_2L_2]^{3+} \quad \textbf{(3.3)}$$

$$[Eu_2L_2]^{3+} + L \overset{K_{23}}{\rightleftharpoons} [Eu_2L_3]^{6+} \quad \textbf{(3.4)}$$

It is worth noting that, in addition to Equation 3.2, when the metal ion is present in excess, the formation of the Eu_2L species must be taken into consideration. The potentiometric measurements for the determination of the metal complex ion stability constants for ligands **66** ***(R,R)*** and **67** ***(S,S)*** were performed in an analogous manner to that described above for the protonation constants (*cf.* Section 3.2.5); in an acetonitrile/water solvent system (80:20; v/v), with constant ionic strength, I = 0.1 M (NEt_4ClO_4). The only difference was that either 0.5 or 1 equivalent of $Eu(ClO_4)_3$ was also present in solution, as shown in the titration curves in Figure 3.11 for ligand **66** ***(R,R)***. The two Eu^{III} concentrations were used to ensure a more accurate determination of the species in solution and to confirm the reproducibility of the stability constants calculated.

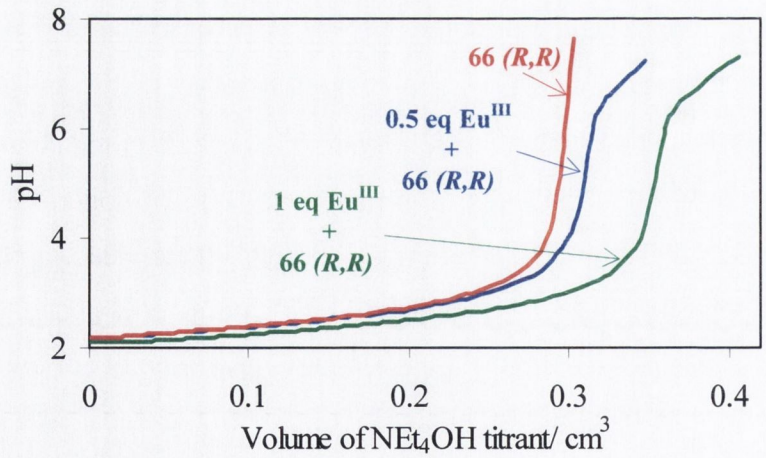

Figure 3.11 Titration curves of the protonated ligand 66 *(R,R)* against NEt_4OH at 298.2 K. [66] = 1.0 × 10^{-3} M, $[H^+]$ = 7.91 × 10^{-3} M, $[NEt_4OH]$ = 0.188 M, I = 0.10 M (NEt_4ClO_4) (red curve) and of the same solution except that $[Eu^{3+}]$ = 1.0 × 10^{-3} M (green curve) and $[Eu^{3+}]$ = 5.0 × 10^{-4} M (blue curve) were also present.

As can be clearly seen from Figure 3.11, the titration curves in the presence of Eu^{III} are remarkably different from that of the ligand. The concentration of Eu^{III} has a significant

effect on the formation of the various species present in solution; this accounts for the large difference between the titration curves corresponding to 0.5 (blue curve) and 1 equivalent (green curve) of $Eu(ClO_4)_3$. Early precipitate formation (observed visually above pH 6.5) hindered the determination of the log *K* values for the species in solution through refinement of the potentiometric data with HYPERQUAD (*i.e.* insufficient data points). However, it may be anticipated that both the deprotonation of the Eu^{III} hydroxide species and that of the amide moieties of the ligands may account for the observed precipitation above pH 7. Lanthanide ions form hydroxide species in aqueous solution due to their borderline hard acid behaviour. In the case of the equilibrium processes involved in the potentiometric titrations illustrated in Figure 3.11 for ligand **66** ***(R,R)***, the europium ions are coordinatively unsaturated in all the intermediate species except the final $[Eu_2L_3]^{6+}$ species (*cf.* Equations 3.1 - 3.4). Metal bound water molecules can occupy the remaining coordination sites. Deprotonation of these metal bound water molecules can then lead to the formation of the corresponding hydroxide (*i.e.* MLOH). The pH range of the titrations is therefore limited by the formation of these insoluble hydroxide species. In order to investigate the pH range within which such hydroxide species would form in the solvent system under study, the protonation constants of $Eu(OH)_2^+$ were determined potentiometrically. The results from these measurements are listed in Table 3.3.

Table 3.3 pK_a values of $Eu(OH)_2^+$ obtained at 298.2 K and I = 0.1 M (NEt_4ClO_4) in CH_3CN/H_2O (80:20; v/v)

species	*equilibrium quotient*	pK_a
$Eu(OH)^{2+}$ [a]	$[Eu(OH)^{2+}][H^+]/[H_2O][Eu^{3+}]$	6.26 ± 0.04
$Eu(OH)_2^+$	$[Eu(OH)_2^+][H^+]/[Eu(OH)^{2+}][H_2O]$	6.96 ± 0.03

[a] $[Eu(ClO_4)_3] = 1.0 \times 10^{-3}$ M, $[H^+] = 4.1 \times 10^{-3}$ M, $[NEt_4OH] = 0.105$ M

From these values, it can be anticipated that the Eu^{III} monohydroxide species starts forming at pH ~ 5. Therefore, it is plausible to assume that, at this pH, the MLOH species will also form. Consequently, only the potentiometric data obtained below pH 5, when less than 10% of the hydroxide species has been formed, can be used to determine the species present in solution. Unfortunately, this limits the number of points which can be used to accurately derive the stability constants (*e.g.* not enough meaningful data is available for a *chi squared*/log *K* to be determined) using the HYPERQUAD program. This, in addition to

the large number of possible species present in solution, precluded an accurate determination of the metal ion stability constants for the systems under study.

In order to gain a better insight of the equilibria and the species present in solution, photophysical studies of the two ligands and corresponding Eu^{III} complexes were undertaken. The details of these measurements are discussed in the following sections.

3.2.7 Photophysical studies of ligands 66 and 67 in partially aqueous solution

All photophysical measurements were determined in a mixture of CH_3CN/H_2O (80:20; v/v), with constant ionic strength, I = 0.1 M (NEt_4ClO_4). The choice of solvent was governed by the solubility of the two ligands **66** ***(R,R)*** and **67** ***(S,S)*** and allows for direct comparison with the data obtained from potentiometric titrations. The concentrations used for photophysical measurements, however, differ from those used in the potentiometric titrations (*cf.* Section 3.2.3). Concentrations of the order of 10^{-5} and 10^{-6} M are compatible with UV-Visible absorption and luminescence measurements. Furthermore, by working within this range of concentrations, it is also possible to overcome any potential precipitate formation. The same solutions were used for both UV-Visible absorption and luminescence measurements.

3.2.7.1 Ground state investigations

To observe the influence of pH on the UV-Visible absorption of ligands **66** ***(R,R)*** and **67** ***(S,S)***, a solution of the protonated ligand in the CH_3CN/H_2O solvent system (80:20; v/v), with constant ionic strength, I = 0.1 M (NEt_4ClO_4), was titrated against a solution of tetraethylammonium hydroxide (NEt_4OH). The absorption spectra obtained from the titration of the protonated ligand **66** ***(R,R)*** are shown in Figure 3.12. An absorption band centred at 281 nm (ε = 35900 M^{-1} cm^{-1}) was observed, which presented hyperfine structure with two shoulders at 271 and 293 nm, characteristic of a 1-substituted naphthalene derivative.[190,191] Upon titration with NEt_4OH, the absorbance of ligand **66** ***(R,R)*** at 281 nm increased by 42%, preserving the hyperfine structure. However, the relative increase in absorbance of the shoulder at 271 nm was greater than that at 293 nm. The changes in absorbance at 281 nm were plotted as a function of pH, as shown in Figure 3.13. The main changes in the absorbance occurred between pH 2.5 and 4.5. A pK_a of 3.48 ± 0.1 was calculated from these data using the standard formula for the calculation of ground state

pK_as (S_0),[148] reported in Chapter 2 (Equation 2.11). The formula is shown again here for clarity:

$$pK_a(S_o) = pH - \log \frac{(Abs_{AH} - Abs_A)}{(Abs_A - Abs_{A^-})} \qquad \textbf{(2.11)}$$

This pK_a value is consistent with the pK_a obtained by potentiometric titration (pK_a = 3.45 ± 0.03) and corresponds to the deprotonation of the pyridine nitrogen.

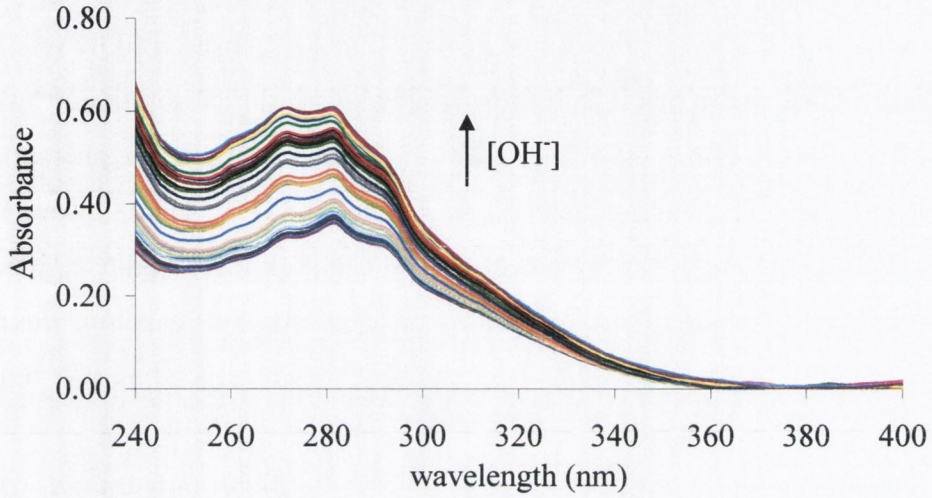

Figure 3.12 Overlaid UV-Vis spectra for the pH titration of ligand 66 *(R,R)* [1.0 × 10^{-5} M] against NEt_4OH in CH_3CN/H_2O (80:20; v/v) (*I* = 0.1 M, NEt_4ClO_4) at 298.2 K. The arrow indicates the spectral trend with increasing pH from 1.5 to 10.

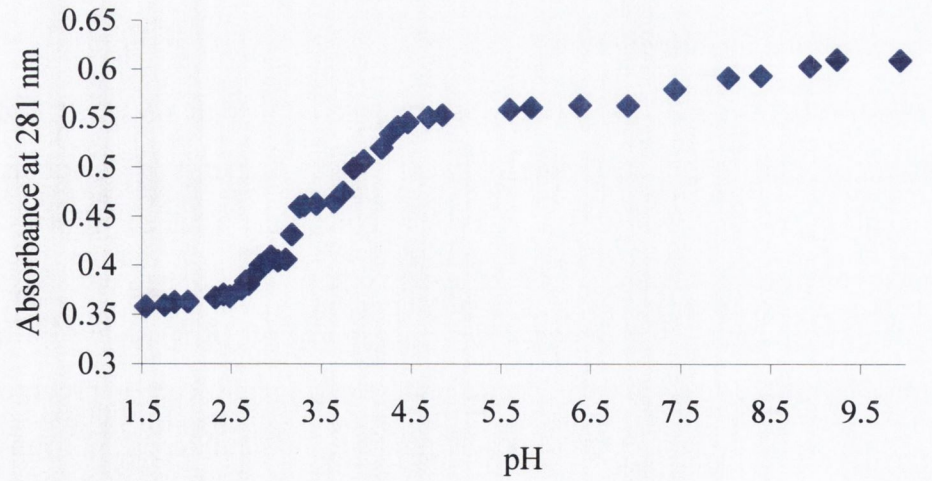

Figure 3.13 Changes in absorbance at 281 nm as a function of pH for the titration of ligand 66 *(R,R)* [1.0 × 10^{-5} M] against NEt_4OH in CH_3CN/H_2O (80:20; v/v) (*I* = 0.1 M, NEt_4ClO_4) at 298.2 K.

A slight increase in the absorbance was also observed in the alkaline region, starting from pH 7. This is in keeping with the formation of a precipitate detected during potentiometric titrations above this pH (see Section 3.2.5). No precipitate was detected during spectrophotometric titrations as they were performed at much lower concentrations (10^{-5} M rather than 10^{-3} M). However, the data collected did not allow an accurate determination of the pK_a value (or values) in the alkaline range, as the changes in absorbance were too small. Nonetheless, it is reasonable to assume that the changes in this pH region may be caused by the deprotonation of the amide moieties present in the molecule.

A UV-Visible absorption pH titration of ligand **67** ***(S,S)*** against NEt_4OH was also carried out under the same conditions. The results obtained were similar to those shown in Figure 3.12 and 3.13 for the isomer **66** ***(R,R)***. From the titration data (absorbance at 281 nm *vs* pH), a pK_a of 3.64 ± 0.1 was determined using Equation 2.11. This pK_a value is in good agreement with the pK_a obtained by potentiometric titration (pK_a = 3.45 ± 0.05, *cf.* Table 3.1). An increase in the absorbance, similar to that observed for ligand **66**, was also observed above pH 7, but again an accurate calculation of the corresponding pK_a proved not to be feasible.

Consistently with the results from the potentiometric titrations, only the pK_a of the pyridine nitrogen could be accurately determined from the UV-Vis absorption titrations of the two ligands. In order to investigate the changes in the excited state energies of the ligands upon pH titrations, fluorescence measurements were also carried out.

3.2.7.2 Singlet excited state investigations

To observe the influence of pH on the fluorescence of ligands **66** ***(R,R)*** and **67** ***(S,S)***, a solution of the protonated ligand was titrated against a solution of tetraethylammonium hydroxide (NEt_4OH), under the conditions detailed above. The fluorescence spectra obtained for ligand **66** ***(R,R)*** upon excitation at 281 nm are shown in Figure 3.14. In acidic conditions, the fluorescence emission of **66** ***(R,R)*** showed a band centred at 360 nm. Upon basification, the spectra underwent a significant hypsochromic shift with the formation of a band centred at 338 nm, with a shoulder at 312 nm and concomitant increase in the emission intensity. The emission band shift indicates a decrease in the electron delocalisation within the pyridine ring, upon deprotonation. When the changes at 360 nm were plotted against the pH, a sigmoidal curve was observed, as shown in Figure 3.15. The fluorescence changes match those observed in the UV-Vis

absorption titration, where the major changes occurred in the pH range between 2.5 and 4.5. Therefore, it can be anticipated that such changes reflect the ground state deprotonation equilibria only, with a pK_a value consistent with that determined for the ground state (3.48 ± 0.1).

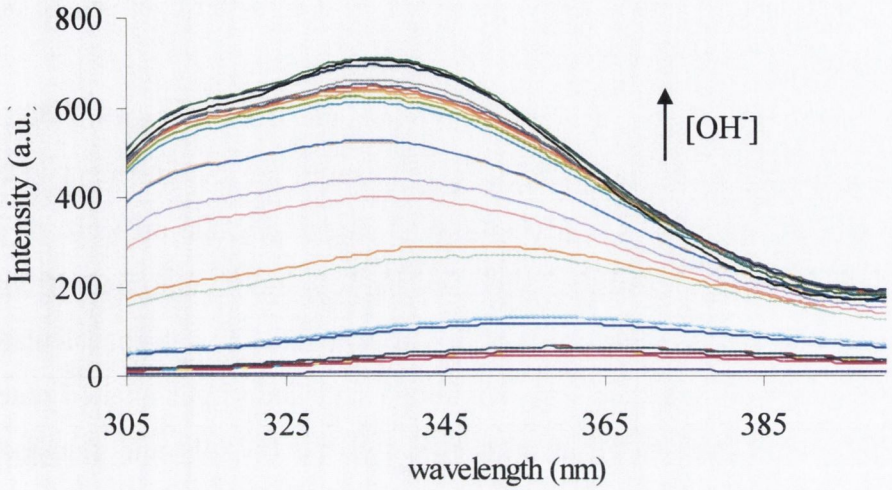

Figure 3.14 Overlaid fluorescence emission spectra for the pH titration of ligand 66 *(R,R)* [1.0 × 10^{-5} M] against NEt_4OH in CH_3CN/H_2O (80:20; v/v) (*I* = 0.1 M, NEt_4ClO_4) at 298.2 K. The arrow indicates the spectral trend with increasing pH from 1.5 to 10.

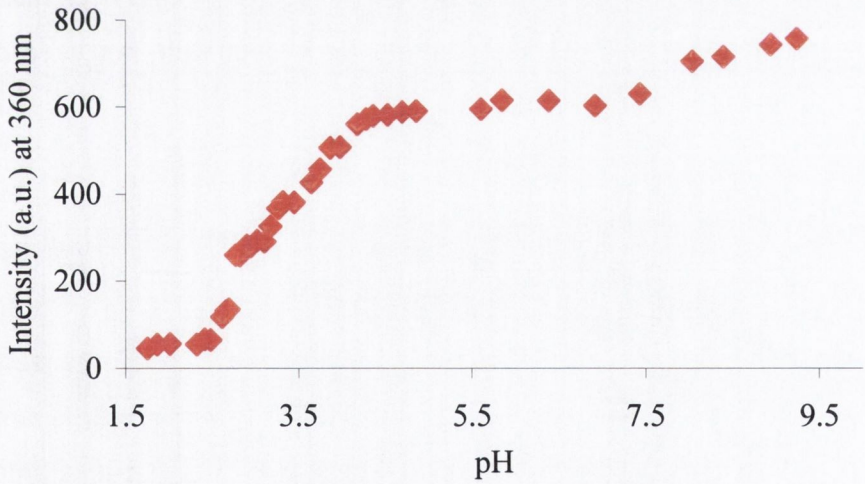

Figure 3.15 Changes in emission intensity at 360 nm as a function of pH for the titration of ligand 66 *(R,R)* [1.0 × 10^{-5} M] against NEt_4OH in CH_3CN/H_2O (80:20; v/v) (*I* = 0.1 M, NEt_4ClO_4) at 298.2 K.

However, the theoretical pK_a value for the singlet excited state obtained with the Förster equation[156] (*cf.* Equation 2.12, Chapter 2), did not correspond to the observed process.

$$pK_a(S_1) = pK_a(S_0) + \frac{0.625}{T} \Delta\nu \qquad \textbf{(2.12)}$$

It has been reported previously that Förster's cycle calculations may not describe the actual behaviour of the excited species if equilibrium is not established during their lifetimes.[155,192,193] The Förster cycle refers, in fact, to an equilibrium, which is attained physically only if the rate of the acid-base reactions is comparable with or greater than the rate of deactivation of the excited state species. Otherwise, the calculated pK_a values are purely theoretical constructs.[155] Thus, the pK_a predicted by the Förster cycle could not be experimentally verified.

As detected in the UV-Visible pH titration of ligand **66** ***(R,R)***, a minor increase was also observed in the fluorescence above pH 7. These changes are in agreement with the formation of a precipitate upon potentiometric titration, suggesting the presence of other possible pK_as. However, such pK_a values could not be accurately determined from the fluorescence experimental data, as the corresponding ground state pK_a was not calculated.

As further evidence of the match between ground state and singlet excited state pK_a values with the pK_a value calculated potentiometrically, the UV-Vis and fluorescence titration profiles are illustrated in Figure 3.16 with the speciation diagram of ligand **66** ***(R,R)***. From this figure, it is clear that the main changes occurring in both the absorbance and the fluorescence emission upon pH titration are due to the deprotonation of the two pyridine nitrogens in the ligand. The pH range illustrated in Figure 3.16 has been limited to below pH 7 for clarity, as above this pH, the potentiometric data were not valid due to precipitation of the ligand.

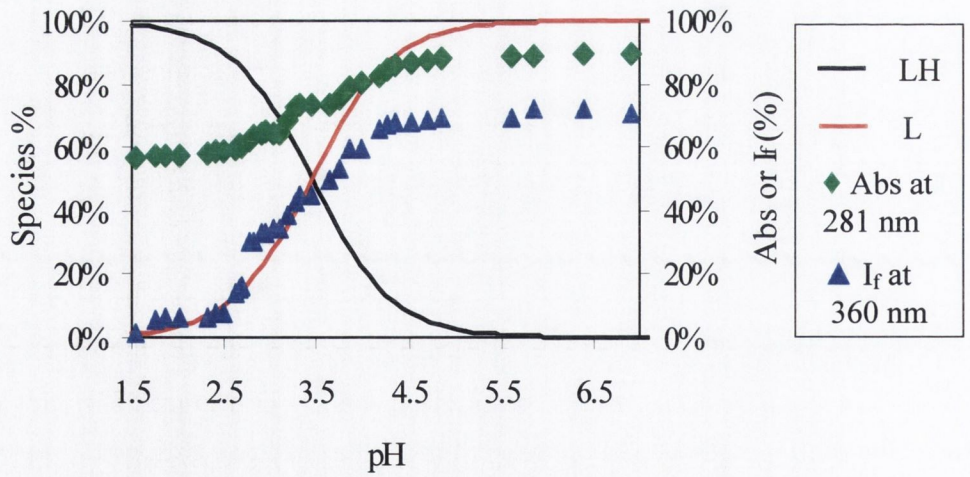

Figure 3.16 Left vertical axis: Speciation variation of ligand 66 *(R,R)*, showing the species present in CH_3CN/H_2O at various pH in which [66] = 1.0 × 10^{-3} M with constant ionic strength *I* = 0.10 M (NEt_4ClO_4) at 298.2 K. Right vertical axis: dependence of the absorbance (%) at 330 nm (green diamonds ♦) and emission intensity (%) at 360 nm (blue triangles ▲) of the solution as a function of pH. Speciation is shown relative to the total concentration of ligand 66 *(R,R)*.

The change in the fluorescence emission of ligand **67** ***(S,S)*** as a function of pH was also evaluated. The titration profile obtained was very similar to that shown in Figure 3.15 for ligand **66** ***(R,R)***. The pK_a value of the singlet excited state determined by Equation 2.12 did not correspond to the experimental data. The emission intensity increased mainly between pH 2.8 and 4.8 and to a lesser extent above pH 7, as for ligand **66** ***(R,R)***, in keeping with the ground state investigations.

For both ligands **66** and **67**, the fluorescence titration profiles were consistent with those obtained by the UV-Vis absorption titrations. This suggests that, in the singlet excited state, the pyridine nitrogens maintain the same degree of acidity as in the ground state. This conclusion, however, was not supported by the pK_a value calculated by the Förster equation. Such a discrepancy between the experimental data and the pK_a value derived from the Förster cycle has been reported previously.[155,192,193]

The UV-Vis and fluorescence measurements above described for the two ligands were also carried out for the corresponding Eu^{III} complexes, as discussed below.

3.2.8 Photophysical studies of 74 and 75 in partially aqueous solution

3.2.8.1 Ground and singlet excited state investigations

The changes in UV-Visible absorption and fluorescence spectra of both Eu^{III} complexes **74** and **75** were investigated as a function of pH in an CH_3CN/H_2O solvent system (80:20; v/v), with constant ionic strength, I = 0.1 M (NEt_4ClO_4). The absorption spectra of complex **74** are shown in Figure 3.17. The complex displayed a band centred at 281 nm ($\varepsilon = 1.33 \times 10^5$ M^{-1} cm^{-1}) with two shoulders at 271 nm and 292 nm. A smaller "shoulder" was also visible at 313 nm. Upon titration with NEt_4OH, the absorbance of complex **74** increased slightly, but the hyperfine structure was preserved. When the absorbance at 281 nm was plotted as a function of pH, the profile shown in Figure 3.18 was obtained. A slight increase in the absorbance was visible above pH 5.5. However, the changes were too small to allow for an accurate determination of the pK_a/pK_as. Moreover, as clearly visible from Figure 3.18, the absorbance *vs* pH profile is not consistent with a sigmoidal isotherm, thus precluding the determination of the actual inflection points.

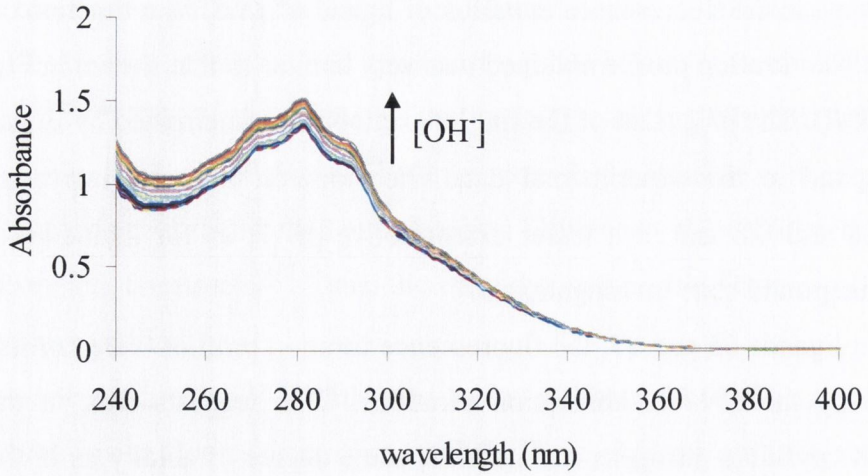

Figure 3.17 Overlaid UV-Vis spectra for the pH titration of complex 74 (*R,R*) [1.0 × 10^{-5} M] against NEt_4OH in CH_3CN/H_2O (80:20; v/v) (*I* = 0.1 M, NEt_4ClO_4) at 298.2 K. The arrow indicates the spectral trend with increasing pH from 2.5 to 9.

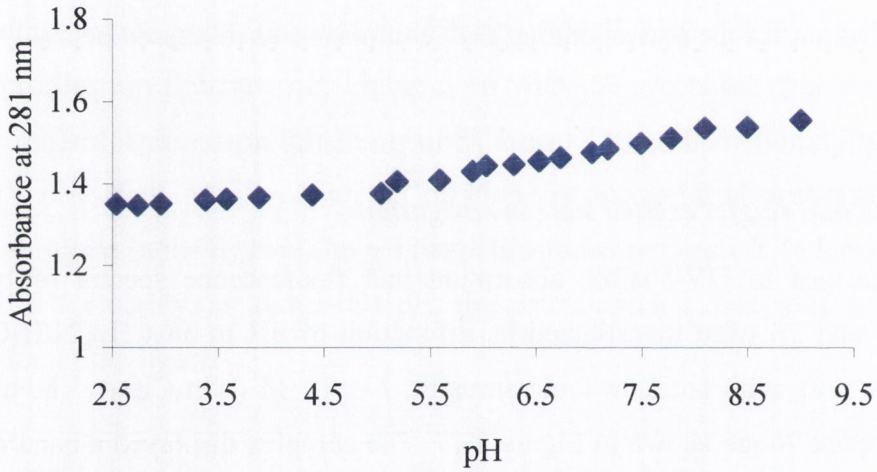

Figure 3.18 Changes in absorbance at 281 nm as a function of pH for the titration of complex 74 (R,R) [1.0 × 10^{-5} M] against NEt_4OH in CH_3CN/H_2O (80:20; v/v) (*I* = 0.1 M, NEt_4ClO_4) at 298.2 K.

In the acidic pH region, below pH 4, no significant change in absorbance was observed, indicating that the deprotonation of the pyridine nitrogen had no effect on the ground state of the complex. This was expected since, in the complex, the pyridine nitrogens are coordinated to the Eu^{III} ions. The changes in absorbance above pH 5.5 may be associated with the deprotonation of the amide moieties. Although the exact pH at which such deprotonation occurs could not be determined with any accuracy, the titration profile indicates a shift towards more acidic pH, if compared to the corresponding changes in absorbance above pH 7 for ligand **66** ***(R,R)*** (*cf.* Figure 3.11). The shift towards more acidic pH in **74** can be ascribed to the effect of the strong Lewis acidity of the Eu^{III} centre,

which renders the protonation sites closely involved in the metal ion coordination more acidic (lower pK_a). Complex **75** showed similar behaviour upon pH titration.

The fluorescence emission spectra obtained for complex **74** are shown in Figure 3.19. Single emission maxima bands centred at 342 nm were observed. The emission intensity increased significantly between pH 5 – 6, and also above pH 7, although to a lesser extent. As there were no significant changes in the acidic region below pH 4, the influence of the deprotonation of the pyridine nitrogen can be discarded. As stated above, this was anticipated due to the coordination of the pyridine nitrogens to the Eu^{III} ions. As no pK_a values were measured above pH 5 by potentiometric titrations, based on the information obtained to date, the fluorescence changes between pH 5-6 could not be assigned to any protonation equilibrium. However, changes in the fluorescence of the complexes may be related to changes in the structures of the *antennae* (*i.e.* the naphthalene moieties). It is therefore reasonable to assume that the changes above pH 7 are attributable to deprotonation of the amide moieties, as deprotonation of the metal bound water molecules in the coordination sphere of the metal ion would have no effect on the singlet excited state of the complex.

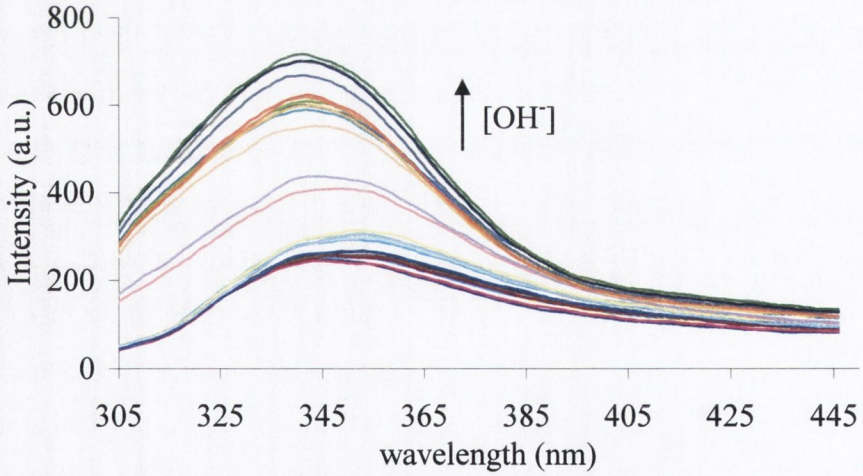

Figure 3.19 Overlaid fluorescence emission spectra for the pH titration of complex 74 (*R,R*) [1.0×10^{-5} M] against NEt_4OH in CH_3CN/H_2O (80:20; v/v) (I = 0.1 M, NEt_4ClO_4) at 298.2 K. The arrow indicates the spectral trend with increasing pH from 2.5 to 9.

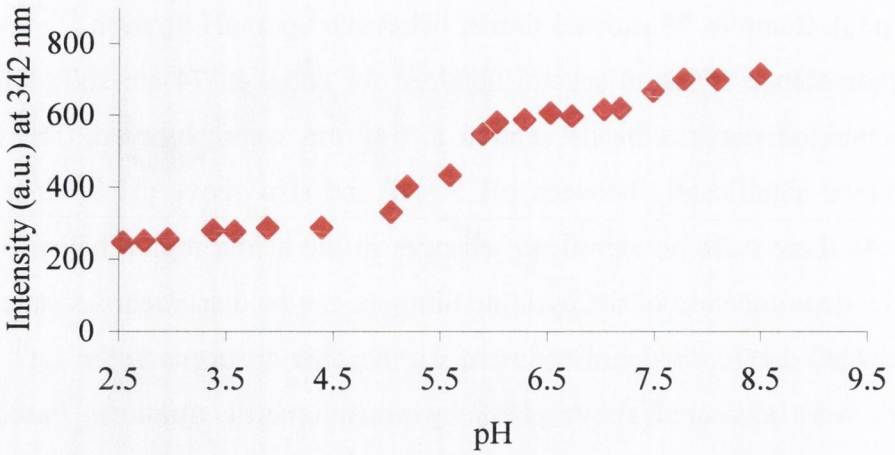

Figure 3.20 Changes in emission intensity at 342 nm as a function of pH for the titration of complex 74 (*R,R*) [1.0 × 10^{-5} M] against NEt_4OH in CH_3CN/H_2O (80:20; v/v) (*I* = 0.1 M, NEt_4ClO_4) at 298.2 K.

3.2.8.2 Eu(III) excited state investigations

The pH dependence of the delayed Eu^{III} luminescence emission of both complexes **74 (*R,R*)** and **75 (*S,S*)** was also investigated under the same conditions as described above. In acidic solution, when excited at 281 nm (λ_{max} of the *antenna*), the Eu^{III} emission of both complexes was found to be of low intensity in the range of 560-720 nm. However, a gradual enhancement of the Eu^{III} emission intensity was observed upon basification of the solution, between pH 5.5-7. This implies an efficient energy transfer from the antenna to the Eu^{III} ions up to pH 7. The luminescence spectra and the corresponding titration profile for the Eu^{III} complex **74 (*R,R*)** are shown in Figures 3.21 and 3.22, respectively.

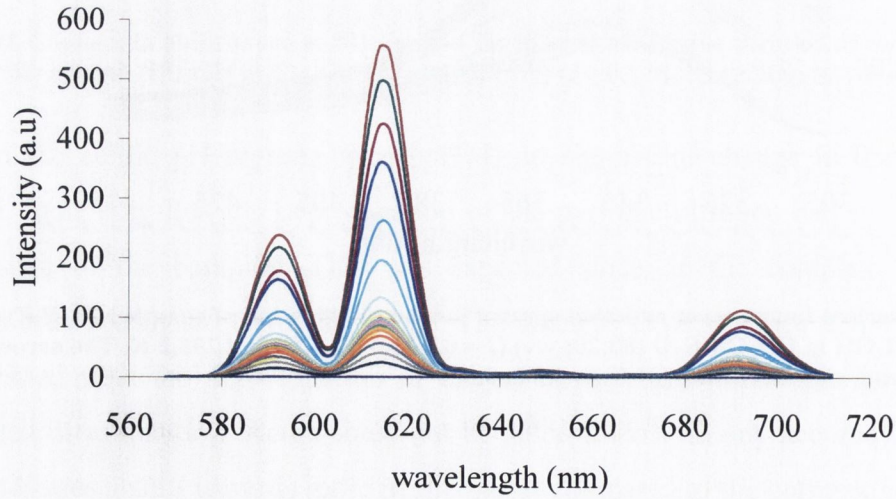

Figure 3.21 Overlaid luminescence emission spectra for the pH titration of complex 74 (*R,R*) [1.0 × 10^{-5} M] against NEt_4OH in CH_3CN/H_2O (80:20; v/v) (*I* = 0.1 M, NEt_4ClO_4) at 298.2 K, showing the deactivation of the $^5D_0 \rightarrow {}^7F_J$ ground states (J = 1-4). The J = 0 band was not observed.

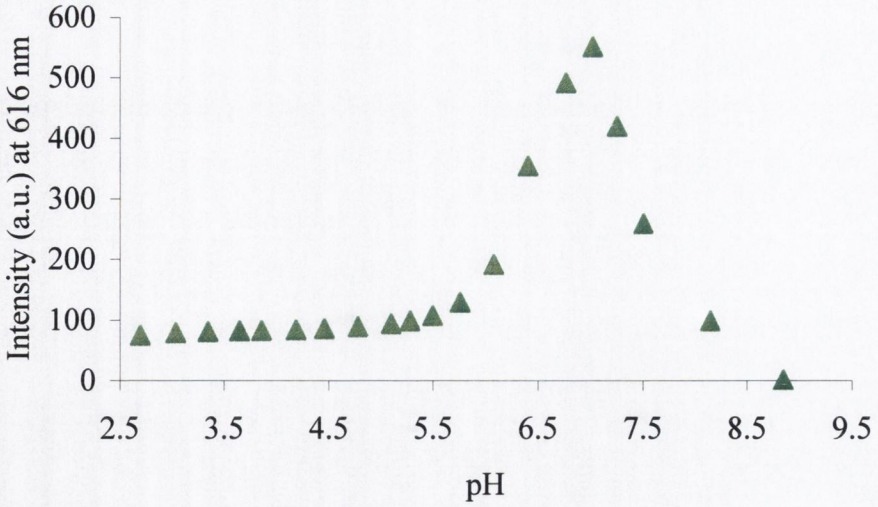

Figure 3.22 Changes in the Eu^{III} emission intensity at 616 nm as a function of pH for the titration of complex 74 (*R*,*R*) [1.0×10^{-5} M] against NEt_4OH in CH_3CN/H_2O (80:20; v/v), I = 0.1 M, NEt_4ClO_4 at 298.2 K.

The Eu^{III} luminescence presented a maximum at pH 7.03 and pH 6.99 for complex **74** and **75**, respectively, and proved to be completely reversible upon acidification of the solution. Under neutral conditions, the Eu^{III} emission appeared as well-separated emission bands at 593, 616, 651, 695 nm, exhibiting no fine structure. These bands represent the deactivation of the $^5D_0$ excited state to the ^7F_J ground states (J = 1 (593 nm), J = 2, (616 nm), J = 3 (651 nm), and J = 4 (695 nm)).[159] It is noteworthy that the band corresponding to J = 0 is not visible. Examples of luminescent complexes, with no $^5D_0 \rightarrow {}^7F_0$ band (or a very weak one), have been reported previously in the literature.[194] Above pH 7, the Eu^{III} emission intensity was gradually quenched, reaching zero at *ca.* pH 9 for both complexes. Therefore, the luminescence *vs* pH profile exhibits two inflection points, which indicate at least two possible pK_as. The same profile shown in Figure 3.22 was obtained by plotting the luminescence intensity at the maximum wavelength for each emission band. The changes between pH 5.5-7 do not match the changes in fluorescence emission which occurred within pH 5-6. Changes in the luminescence emission as a function of pH must be related to protonation processes involving the Eu^{III} ion and its coordination environment. As previously determined through potentiometric titrations, the pK_as of the Eu^{III} hydroxides are in the same pH region (*cf.* Table 3.3). Therefore, it is reasonable to hypothesise that deprotonation of the metal bound water molecules is affecting the Eu^{III} excited states below pH 7. Above pH 7, the quenching of the Eu^{III} luminescence coincides with an increase in the fluorescence emission of the complex (*cf.* Figure 3.20). These

changes must therefore be related to the *antennae* (*i.e.* naphthalene moieties) and may be associated with the amide deprotonation.[26,195]

To summarise, both Eu^{III} complexes **74** and **75** exhibit a characteristic and fully reversible luminescence profile as a function of pH, with a maximum at pH 7. In the pH region below pH 7 it is reasonable to assume that deprotonation of the metal bound water molecules is affecting the Eu^{III} excited states. Above pH 7, the quenching of the luminescence is most likely due to the amide moieties deprotonation, as supported by the fluorescence emission changes in the same pH region.

3.2.9 Lifetimes of 74 and 75

In an attempt to gain insight into the nature of the species present in solution at various pHs, the lifetimes of the Eu^{III} complexes **74** and **75** were measured in CH_3CN/H_2O (80:20; v/v) solution and in the analogous deuterated solvent system (CD_3CN/D_2O, 80:20; v/v) at varying pH/pD values. The pH, or pD, was adjusted using HCl and NaOH in the case of the CH_3CN/H_2O (80:20; v/v) solution, and DCl and NaOD in the case of the CD_3CN/D_2O (80:20; v/v) solution. The pD was obtained by measuring the pH and applying the formula; $pD = pH_{measured} + 0.4$.[196] The luminescence decays were found to be bi-exponential at all pH values. The bi-exponential luminescence decays were fitted to Equation 3.5:[197]

$$I(t) = A_1\exp(-k_1t) + A_2\exp(-k_2t) + B, \text{ where } 1/k = \tau \qquad \textbf{(3.5)}$$

where $I(t)$ is the luminescence intensity *versus* time, A_1 and A_2 are pre-exponential parameters, k_1 and k_2 are the de-activation rate constants, and τ is the lifetime of the excited state. The resulting lifetimes for complex **74** are reported in Table 3.4.

Table 3.4 Lifetimes of complex 74 (R,R) (ms ± 5%) upon direct excitation of Eu^{III} at 395 nm.

pH		2.5	5.0	7.0	9.5
CH_3CN/H_2O	τ_1 (ms)	0.66	0.64	0.80	0.46
	τ_2 (ms)	0.15	0.17	0.14	0.10
CD_3CN/D_2O	τ_1 (ms)	1.65	1.84	1.74	1.02
	τ_2 (ms)	0.65	0.45	0.32	0.17

It can be observed that the lifetimes (τ_1) in CH_3CN/H_2O (80:20; v/v) did not change significantly between pH 2.5 and 5. This was to be expected as no change in the luminescence emission was observed in the same pH range (*cf.* Figure 3.22). This points to a similarity in the inner-sphere arrangement of the species present in solution in the acidic pH region. The lifetimes (τ_1) became longer at pH 7, indicating a less efficient deactivation process, *i.e.* less number of water molecules in the coordination sphere of the Eu^{III} ions. This coincides with the luminescence enhancement between pH 5.5-7 observed in Figure 3.22 and associated with the deprotonation of the metal bound water molecules in the complex (*i.e.* formation of the metal hydroxide species MLOH). Finally, the changes in the lifetime (τ_1) above pH 7 are consistent with the quenching of the Eu^{III} luminescence emission, which corresponds to the deprotonation of the amide moieties. This is an indication of more efficient quenching pathways of the Eu^{III} excited states and/or a change in the energy of the antenna upon deprotonation of the amide moieties. The second lifetimes (τ_2) did not undergo significant change until pH 7. Above this pH, τ_2 decreased in keeping with τ_1. The changes in lifetime are illustrated in Figure 3.23 for both complexes **74** and **75**.

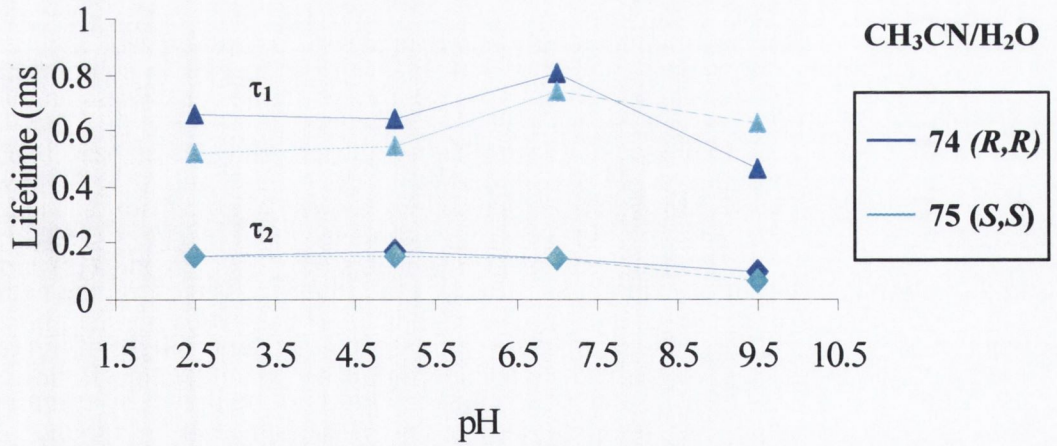

Figure 3.23 Lifetimes of the Eu^{III} complexes 74 and 75 in CH_3CN/H_2O (80:20; v/v) at different pHs.

From the τ_1 profile, a similarity with the luminescence changes of the complexes upon pH titration can be drawn. By comparison between the profiles in Figure 3.22 and 3.23, it can be observed that the longest-lived and most luminescent species is predominantly present in solution at pH 7. Hence the complex is luminescent only in a narrow pH window (pH 6.5 - 7.5), upon deprotonation of the metal bound water molecules

(*i.e.* when the Eu^{III} hydroxide species are present in solution) but prior to complete deprotonation of the amide moieties.

From the lifetimes (τ_1 and τ_2) in CH_3CN/H_2O (80:20; v/v) solution and in the analogous deuterated solvent system CD_3CN/D_2O (80:20; v/v), the hydration state (q values) of the complexes were calculated using the equation by Parker *et al.*,[29] introduced in Chapter 2 and reported here again for clarity:

$$q^{Eu(III)} = A\,[(1/\tau_{H_2O} - 1/\tau_{D_2O}) - 0.25 - 0.075x]\ (\pm 0.3) \qquad (2.10)$$

where A = 1.2 for measurements conducted in 100% water and x is the number of bound amide NH groups. The resulting q values for complex **75 (*S,S*)** at different pHs are reported in Table 3.5.

Table 3.5 q values (± 0.3) for complex 75 (*S,S*) in CH_3CN/H_2O (80:20; v/v) at different pHs

pH	2.5	5.0	7.0	9.5
q_1 (± 0.3)	5.51	4.06	4.01	4.87
q_2 (± 0.3)	0.61	0.74	0.02	0.93

Interpretation of these results proved quite difficult. The two q values determined for each pH were rather dissimilar, indicating that the multiple species in solution have a different effect on the two rate constants. It is also important to observe that the Parker equation applies to determination of the hydration state of systems in 100% water. However, in order to calculate the q values for the complexes in CH_3CN/H_2O (80:20; v/v) solution, Equation 2.10 was used without any further modification. Therefore, the nature of the solvent in use (only partially aqueous) must be taken into account in light of the results obtained (Table 3.5). Consequently, a clear conclusion could not be drawn by examination of the q values obtained; further investigations on the kinetics of the process are therefore necessary in order to comprehensively interpret the results.

3.3 Conclusions

This chapter has discussed the synthesis, characterisation, potentiometric and photophysical studies of the two new chiral bis-tridentate ligands **66** and **67** and their corresponding Eu^{III} complexes **74** and **75** in a partially aqueous solution of CH_3CN/H_2O (80:20; v/v).

Much of the preparation of both isomers **66** (***R,R***) and **67** (***S,S***) was based on simple peptide coupling reactions between a 2,6-pyridinedicarboxylic acid (**dpa**) derivative and a chosen amine. The **dpa** moieties represent the two tridentate coordinating units in each ligand. The corresponding Eu^{III} complexes **74** and **75** were also successfully synthesised and fully characterised. Several attempts to crystallise both complexes and ligands were carried out, but proved unsuccessful on all occasions. Molecular mechanics calculations followed by geometry optimisation were consistent with the proposed dinuclear triple helicate model for the two complexes, **74** and **75**. ^{1}H-NMR spectroscopy also confirmed that the target complexes exist in solution in their *rac*-form (helical).

Potentiometric titrations of ligands **66** and **67** in CH_3CN/H_2O (80:20; v/v) yielded the pK_a value for the pyridine nitrogen moieties. Determination of the metal complex ion stability constants, however, proved unsuccessful despite several attempts. This may be attributed to the presence of numerous species in solution and, most importantly, to the formation of the europium hydroxide species.

UV-Vis and fluorescence studies of the ligands as a function of pH confirmed the pK_a value for the pyridine nitrogen obtained by potentiometric titrations. As expected, the deprotonation of the pyridine nitrogens did not have any effect on the ground state, singlet excited state nor on the Eu^{III} excited states of the complexes, as proven by UV-Vis, fluorescence and lanthanide luminescence pH titrations. In contrast, deprotonation of the metal bound water molecules and that of the amides moieties played a major role in the photophysical properties of these complexes.

In order to gain some insight into the metal complex species present in solution and to be able to prove the formation of the desired dinuclear triple helicate Eu_2L_3, an investigation into the spectroscopic (NMR, UV-Vis, Luminescence) properties of the complexes in less competitive media was set out. Titrations in non-aqueous solution were therefore undertaken and the results will be presented in the next chapter.

4 ^{1}H-NMR AND PHOTOPHYSICAL STUDIES OF Eu^{III} HELICATES IN ORGANIC MEDIA

4.1 Introduction

As discussed in Chapter 3, the Eu^{III} dinuclear complexes **74** ***(R,R)*** and **75** ***(S,S)*** have been studied in partially aqueous solution, by means of potentiometric and photophysical measurements. Their design was inspired by the work on dinuclear lanthanide helicates carried out by Bünzli's and Horrocks' research groups.[60,162] The study of these novel compounds was an extension of the work already carried out by Dr. Leonard within the Gunnlaugsson group (*cf.* Section 3.1.2). The study of **74** ***(R,R)*** and **75** ***(S,S)*** in partially aqueous solution proved very difficult due to the presence of intricate mixtures of interconverting complexes in solution. It was therefore decided to analyse the formation of the Eu^{III} complexes in less competitive media. In this chapter, the ^{1}H-NMR and photophysical studies of the Eu^{III} complexes **74** ***(R,R)*** and **75** ***(S,S)*** in organic media are discussed. The CPL (Circularly Polarised Luminescence) studies were carried out in collaboration with Dr. R. D. Peacock, Department of Chemistry, Joseph Black Building, University of Glasgow. The data collected from the UV-Vis and luminescence titrations have been used to determine the metal complex ion stability constants using the non-linear least squares regression program SPECFIT.[198] The results of these studies will also be discussed in this chapter.

4.2 ^{1}H-NMR titrations

The formation of the Eu^{III} complexes of ligands **66** ***(R,R)*** and **67** ***(S,S)*** was firstly investigated by monitoring the changes in the ^{1}H-NMR (400 MHz) spectra of $CD_3CN/CDCl_3$ (50:50, v/v) solutions of each ligand upon addition of Eu^{III} (as its triflate salt). The choice of the solvent system was dictated by the low solubility of the ligands in CH_3CN. The addition of $Eu(CF_3SO_3)_3$ to each of the ligand afforded gradual changes in the chemical shifts of the protons until addition of 0.6 equivalents of Eu^{III}, as shown in Figure 4.1 for the titration of ligand **66** ***(R,R)***. Thereafter, the changes in the ^{1}H-NMR spectra were only minor. All proton resonances were observed to broaden on addition of Eu^{III}. This was to be expected due to the more efficient relaxation of the nuclear spins in the presence of a paramagnetic centre (*i.e.* Eu^{III}).

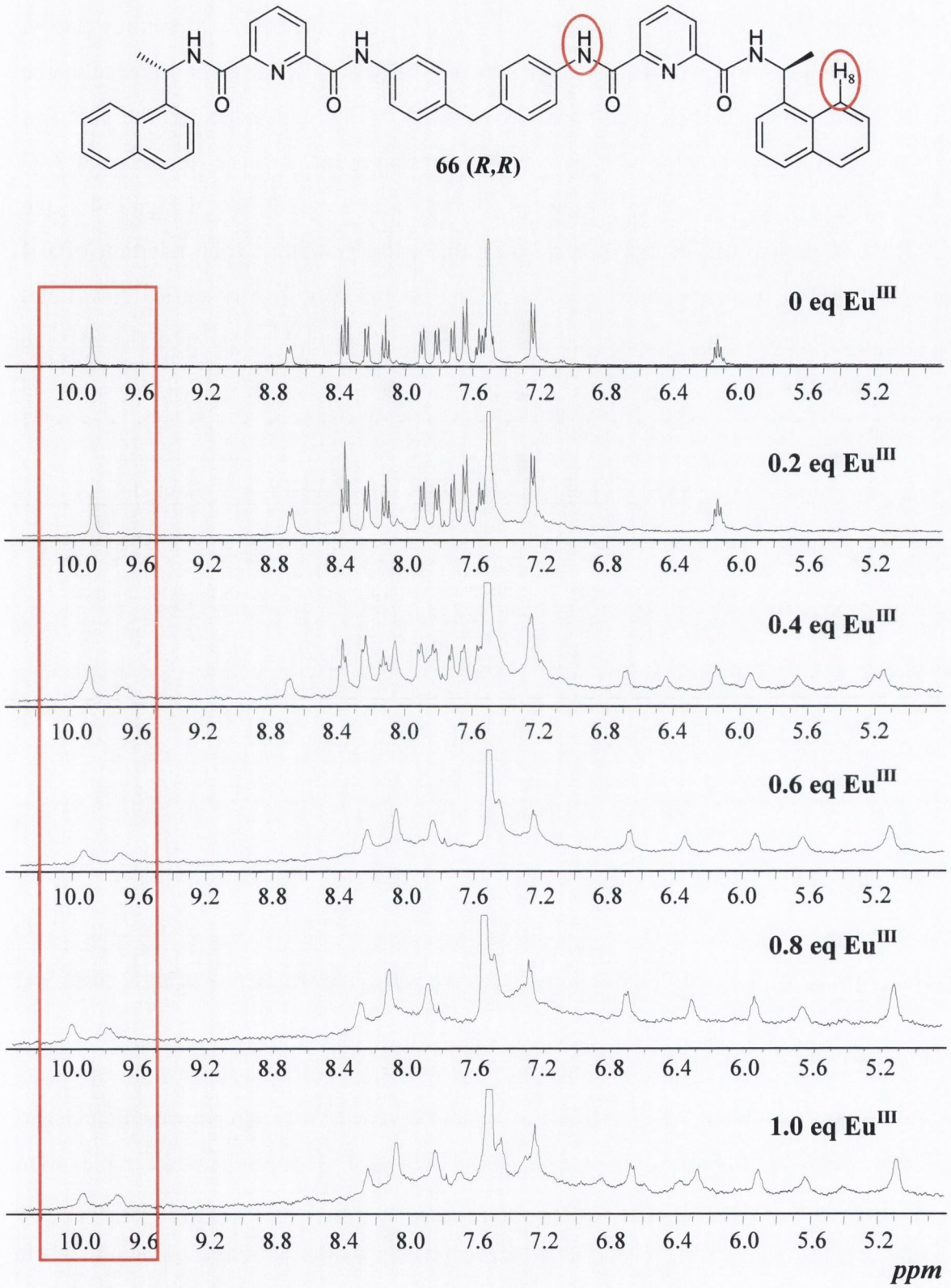

Figure 4.1 ^{1}H-NMR spectra (400 MHz, $CD_3CN/CDCl_3$, 50:50, v/v) of ligand 66 *(R,R)* upon titration of $Eu(CF_3SO_3)_3$, [66 *(R,R)*] = 1.24 x 10^{-3} M, [Eu^{III}] = 2 x 10^{-2} M, (0-1 eq); the red box highlights the formation of the H_8 resonance and simultaneous disappearance of the NH signal. The appearance of the resonance at 9.69 ppm is also highlighted. Top: structure of ligand 66 *(R,R)* indicating the two protons: NH and H_8.

The signal at 9.88 ppm has been used to describe the changes upon titration of the ligand with Eu^{III}, in order to follow the binding events. This signal was chosen for clarity, as it is remote from the majority of the signals (see Figure 4.1). The disappearance of the ligand amide proton at 9.88 ppm was accompanied by the appearance of the complex naphthalene H_8 signal at 9.94 ppm and simultaneous appearance of the resonance at 9.69 ppm, which may be assigned to the proton on the chiral centre (CH). In Figure 4.2, the peak at 9.88 ppm (NH) in the second spectrum (corresponding to the addition of 0.4 equivalents of Eu^{III}) clearly shows the formation of a shoulder slightly shifted downfield. This shoulder becomes the resonance of the H_8 proton of the naphthalene after the addition of 0.6 equivalents of Eu^{III}.

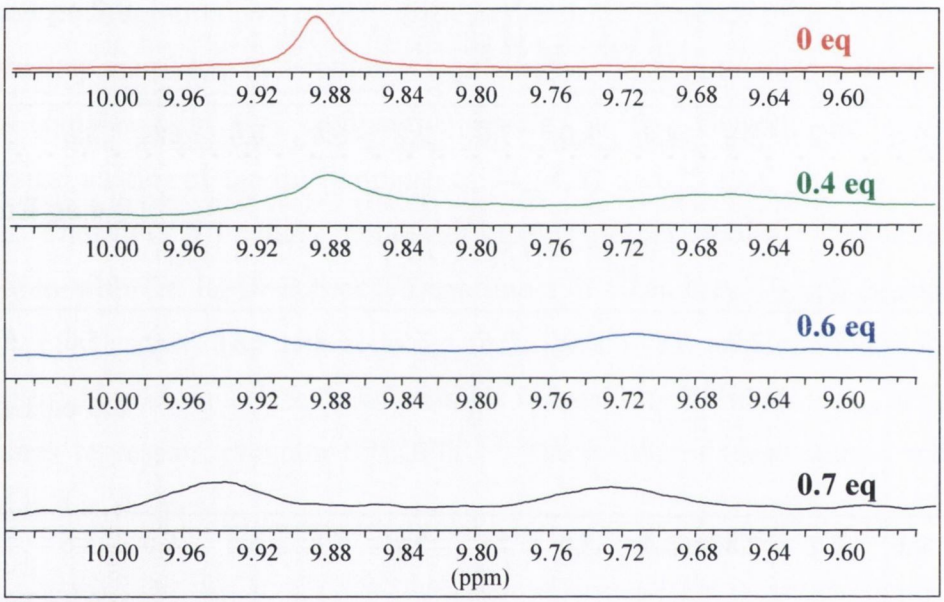

Figure 4.2 Expanded NH and H_8 region of the ^{1}H-NMR spectra (400 MHz, $CD_3CN/CDCl_3$, 50:50, v/v) of ligand 66 *(R,R)* upon titration of $Eu(CF_3SO_3)_3$ (0-0.7 eq).

The integration of the signal at 9.88 ppm (NH) was plotted against the equivalents of Eu^{III} added; the resulting profile is shown in Figure 4.3. As already mentioned and clearly illustrated in Figure 4.2, the signal at 9.88 ppm (NH) disappears upon complexation of the ligand and a new one (H_8) appears just underneath it at 9.94 ppm. In order to follow the changes by integration, it has been necessary to work out the integration of the disappearing signal as the difference between the peak at 9.88 ppm and the peak at 9.69 ppm (CH), which appears upon complexation at the same rate as the one at 9.94 ppm. The integration for all signals has been referenced against the signal at 3.30 ppm; this signal is due to traces of methanol in the sample and hence is impervious to the Eu^{III} binding events.

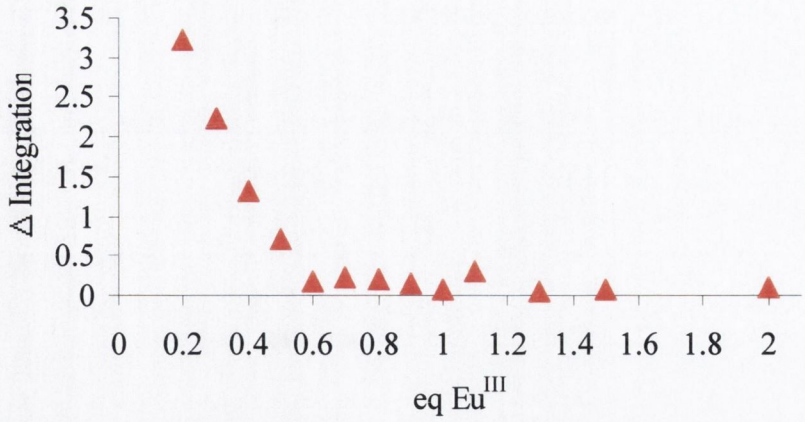

Figure 4.3 Integration of the appearing signal at 9.88 ppm as a function of the equivalent of Eu^{III} added in the ^{1}H-NMR (400 MHz, $CD_3CN/CDCl_3$, 50:50, v/v) titration of ligand 66 *(R,R)*.

As evidenced from the profile in Figure 4.3, the integration of the NH signal at 9.88 ppm decreases upon addition of 0.6 equivalents of Eu^{III} and then reaches a plateau. This is indicative of a 2:3, Eu:**66** stoichiometry and provides further support to the proposed triple stranded dimetallic helical structure of the complex in solution. It is also worth noting that the ^{1}H-NMR spectrum of the ligand on addition of 0.6 equiv. of Eu^{III} indicates the presence of only one species in solution or a fast P $\rightleftharpoons$ M interconversion on the NMR time scale. This will be addressed in section 4.4.

4.3 CD studies

To help determine the structure of the chiral Eu^{III}-ligand complexes, a number of studies were carried out using other spectroscopic techniques, such as Circular Dichroism (CD) and Circularly Polarised Luminescence spectroscopy (CPL).

Circular dichroism is the difference in absorption of left and right circularly polarised light.[199] A beam of circularly polarised light has an electric field vector that retains constant magnitude in time but traces out a helix about the direction of propagation. A chiral molecule has no reflection in any plane and therefore its electrons will not have one either. Electrons move following a helical pattern. In circularly polarised light the electric field vectors also trace out helices and so the interaction between a chiral molecule and left- and right- handed photons of light will be different. Every molecule will have both positive and negative CD signals, as different electronic transitions involve electron distributions of different handedness. However, the overall effect would be that chiral molecules absorb left and right polarised light to different extents. Measuring the

difference over the UV-Vis spectrum yields a plot characteristic of the chiral nature of the molecule (Figure 4.4).

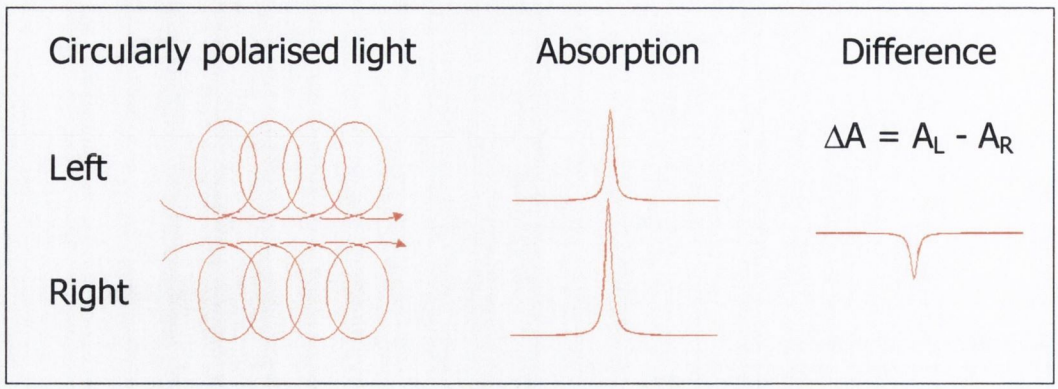

Figure 4.4 Schematic representation of the absorption of right and left circularly polarised light by a chiral molecule.

Circular dichroism spectra of both *R,R* and *S,S* enantiomers of the ligand (**66** and **67**, respectively) and their corresponding Eu^{III} complexes were recorded in methanol to determine if it would be possible to establish the overall chirality of the helicate.[162] Studies on other helicate-forming ligands in non-aqueous solution suggest that chiral ligands produce only one enantiomer of a helicate.[200,201] The CD spectra of the free ligands **66** ***(R,R)*** and **67** ***(S,S)*** illustrated in Figure 4.5, are almost mirror images of each other, clearly showing their chirality. Ligand **66** ***(R,R)*** exhibited two negative bands centred at 234 and 298 nm. For ligand **67** ***(S,S)*** two positive bands were observed at 230 and 298.5 nm. The discrepancy in the intensity of the two signals arises from the difference in the concentration of the two samples (*i.e.* [**66**] > [**67**]).

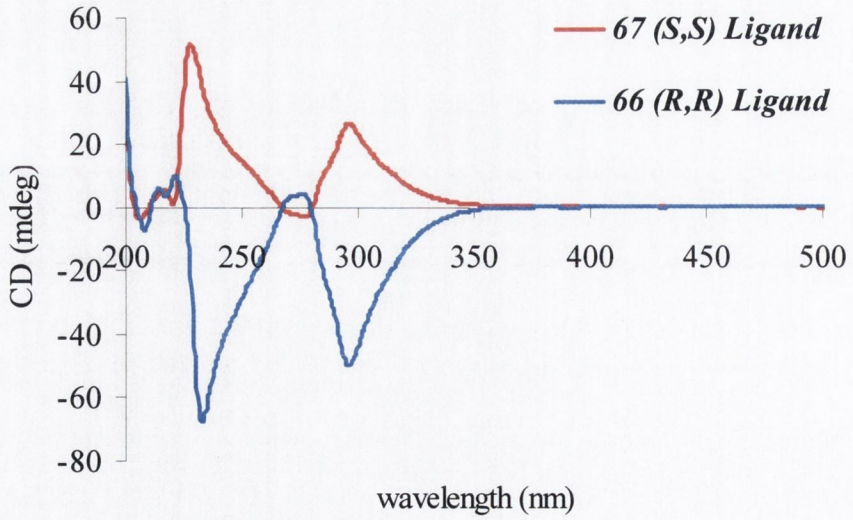

Figure 4.5 CD spectra of ligands 66 *(R,R)* (Abs at 281 nm = 2.088) and 67 *(S,S)* (Abs at 281 nm = 1.624) in MeOH.

The CD spectra of the two Eu^{III} complexes **74** ***(R,R)*** and **75** ***(S,S)*** were also recorded in methanol. As shown in Figure 4.6, two negative bands centred at 232 and 298 nm were detected for complex **74** ***(R,R)***. The CD spectrum of complex **75** ***(S,S)*** presented two positive bands with maxima at 231 and 299.5 nm. Due to the close similarity of the CD spectra of the ligands and the corresponding Eu^{III} complexes, it is plausible to assume that the ligands do not undergo major conformational changes upon complexation. However, the CD results pertaining to the complexes do not imply the chirality of the metal binding sites, nor do they establish the handedness (ΔΔ or ΛΛ) at the metal centres.[162] In order to gain a better insight into the metal ion binding environment in the complexes, CPL studies were carried out and their results will be discussed in the next section.

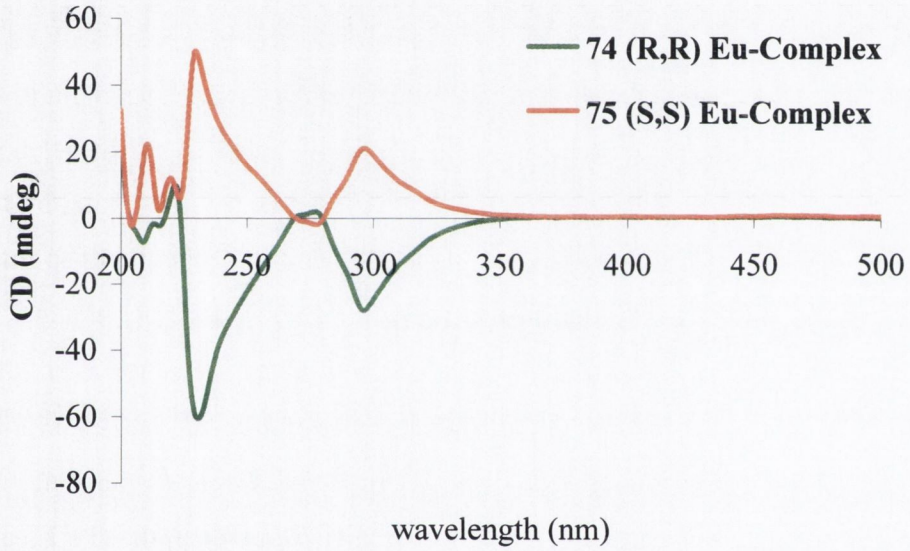

Figure 4.6 CD spectra of the Eu^{III} complexes 74 *(R,R)* (Abs at 281 nm 1.374) and 75 *(S,S)* (Abs at 281 nm = 1.104) in MeOH.

4.4 CPL studies

Circularly polarised luminescence (CPL) is the differential emission of right-circularly polarised light versus left-circularly polarised light by chiral molecular systems.[202] The primary observable in CPL spectroscopy is the "emission circular intensity differential" (ECID):

$$\Delta I(\lambda) = I_L(\lambda) - I_R(\lambda) \qquad \textbf{(4.1)}$$

where $I(\lambda) = I_L(\lambda) + I_R(\lambda)$ and I_L and I_R denote the intensity of the left (L) and right (R) circularly polarised components of the emitted radiation. Electronic CPL spectroscopy is the emission analogue of electronic circular dichroism (CD) spectroscopy. CPL and CD depend on the same general aspects of molecular structures. The only difference is that CD reflects the structural properties of the ground electronic state of a system, whereas CPL reflects the structural properties of the luminescent excited states.[202]

CPL spectra of the Eu^{III} complexes **74** ***(R,R)*** and **75** ***(S,S)*** were recorded in methanol at the Department of Chemistry, University of Glasgow, in collaboration with Dr. R. D. Peacock. The resulting spectra are illustrated in Figure 4.7 and 4.8, respectively.

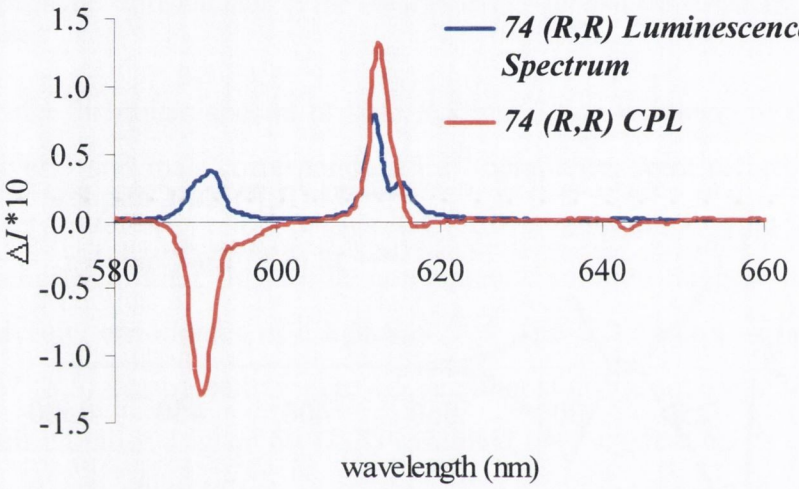

Figure 4.7 CPL spectra of 74 *(R,R)* 3×10^{-5} M in methanol at 298.2 K, upon excitation at 360 nm.

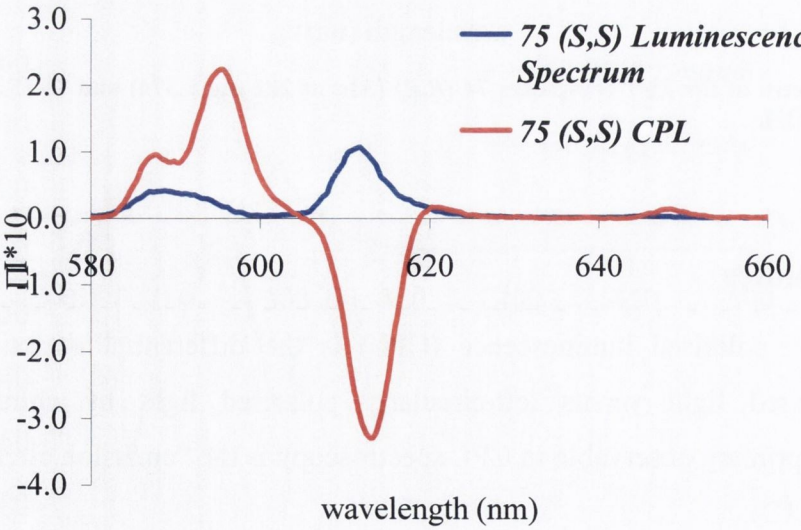

Figure 4.8 CPL spectra of 75 *(S,S)* 3×10^{-6} M in methanol at 298.2 K, upon excitation at 281 nm.

The CPL spectrum of the Eu^{III} complex **74** ***(R,R)*** displays a negative ΔI band at 591 nm corresponding to the $^5D_0 \rightarrow {}^7F_1$ transition, with a shoulder at 598 nm, and a positive band at 613 nm for the $^5D_0 \rightarrow {}^7F_2$ transition. Conversely, the Eu^{III} complex **75** ***(S,S)*** exhibits positive ΔI values for the $^5D_0 \rightarrow {}^7F_1$ at 595 nm with a shoulder at 587 nm, and negative ΔI values which correspond to the $^5D_0 \rightarrow {}^7F_2$ electronic transition. The discrepancy between the CPL spectra of the two isomers is mainly related to the different excitation wavelengths (360 nm for **74** *vs* 281 nm for **75**) and different concentrations (3×10^{-5} M *vs* 3×10^{-6} M) of the two samples. Nonetheless, from the CPL data collected it is possible to assess the opposite chirality of the two Eu^{III} complexes. A helix may be right-handed (plus, *P*) or left-handed (minus, *M*); helicity is, in fact, a special case of chirality.[200] It is worth noting that the CPL properties observed for the two complexes **74** ***(R,R)*** and **75** ***(S,S)*** may result from a combination of two contributions: the chirality of the ligands and the structural contribution of the helical arrangement of the ligands. Small ΔI values have been reported when the CPL properties result solely from the effect due to the chirality of the ligands.[203] Therefore, the relatively large ΔI values may suggest the predominance of one helical diastereoisomer (either *P* or *M*) in solution (diastereomeric excess). This also supports the presence of a single species in solution in the ^{1}H-NMR spectrum of the two complexes (*cf.* Section 3.2.2).

In summary, the CPL data indicate that the helicity of **74** ***(R,R)*** and **75** ***(S,S)*** is driven by asymmetric induction from the ligands: the chiral centres present in the backbone of the ligand strands induce the preferential formation of a right-handed or left-handed helicate. Further investigations are needed in order to assess whether the induced helicity from a given configuration of the ligand (either *R,R* or *S,S*) is right-handed or left-handed.

4.4.1 Job's method for determination of stoichiometry

In order to define and evaluate the metal complex ion stability constants for the two ligands **66** ***(R,R)*** and **67** ***(S,S)***, the stoichiometry coefficients *m* and *n* in $\mathbf{M}_m\mathbf{L}_n$ must be known. The *method of continuous variations*, often called Job's method,[204] is one of the methods used to determine the stoichiometric coefficients *m* and *n* in a complex $\mathbf{M}_m\mathbf{L}_n$. The experimental procedure consists of preparing a series of solutions of metal ion (*i.e.* Eu^{III}, in this case) and ligand according to the condition that the sum of the total metal ion and ligand concentrations is constant.[147] By measuring a property (*i.e.* absorbance or

luminescence), which varies in solution when the ligand forms a complex with the metal, it is possible to obtain the *n/m* ratio from the maximum/minimum of such a property, such as:

$$\frac{n}{m} = \frac{\chi_{max}}{1 - \chi_{max}} \quad \textbf{(4.2)}$$

where χ = L/ L + M is the molar fraction of the ligand ($0 \leq \chi \leq 1$).

Most applications of the method have used absorption spectroscopy as the experimental tool, choosing a wavelength at which a large absorbance change is observed on complexation; this absorbance is then plotted against χ to find χ_{max} (or χ_{min}).[147] This was also the method of choice herein. In order to determine the stoichiometric ratios of the Eu^{III} complexes with ligands **66** ***(R,R)*** and **67** ***(S,S)*** the absorbance of 11 samples, each containing the same total number of moles of ligand and Eu^{III} but in a different ratio, was measured. The absorbance of each sample was then plotted against the molar fraction of the ligand (χ_L). As an example, the Job's method plot obtained from the absorbance data at 350 nm relative to the Eu^{III} complex of ligand **67** ***(S,S)*** in $CH_3CN/CHCl_3$ (50:50, v/v) is shown in Figure 4.9.

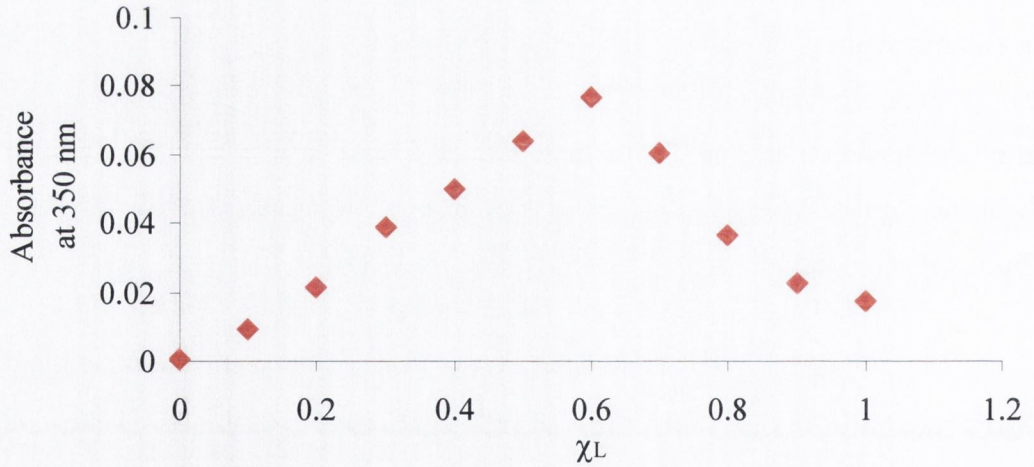

Figure 4.9 Job's plot for the determination of the stoichiometry of the Eu^{III} complex of ligand 67 *(S,S)*; absorbance at 350 nm measured in $CH_3CN/CHCl_3$ (50:50, v/v) *vs* χ_L ($0 \leq \chi \leq 1$); $[Eu^{III} + 67]_{tot} = 1 \times 10^{-5}$ M

From the plot in Figure 4.9, $\chi_{max} = 0.6$ was determined, which corresponds to a stoichiometric ratio of 3/2:

$$\frac{n}{m} = \frac{\chi_{max}}{1 - \chi_{max}} = \frac{0.6}{1 - 0.6} = \frac{0.6}{0.4} = \frac{3}{2}$$

Therefore, the stoichiometric coefficients of the Eu^{III} complex are $m = 2$, $n = 3$: Eu_2L_3, which is consistent with the formation of a dimetallic triple-stranded helicate. The Job's method was also applied to the luminescence data, resulting in the graph shown in Figure 4.10. From these data, a $\chi_{max} = 0.6$ was also obtained, supporting the values of the stoichiometric coefficients determined by the UV-Visible data: $m = 2$, $n = 3$ (Eu_2L_3).

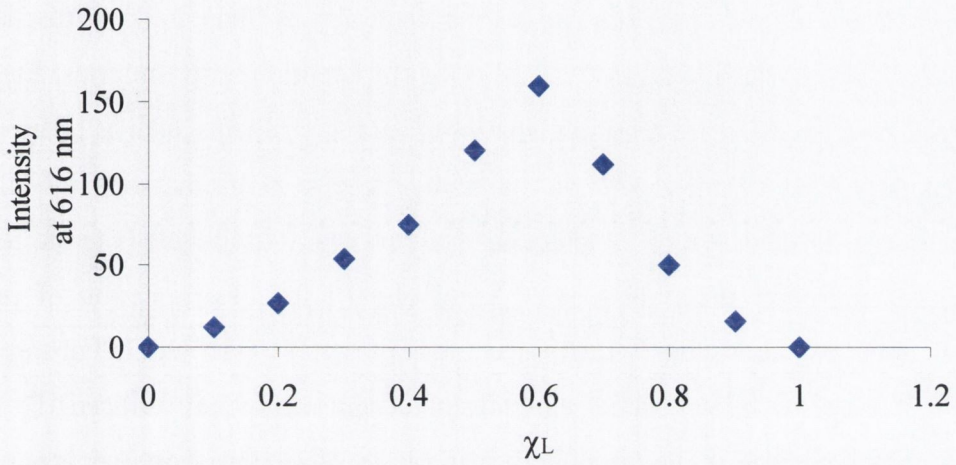

Figure 4.10 Job's method plot for the determination of the stoichiometry of the Eu^{III} complex of ligand 67 *(S,S)*; luminescence emission at 616 nm measured in $CH_3CN/CHCl_3$ (50:50, v/v) *vs* χ_L ($0 \leq \chi \leq 1$); $[Eu^{III} + 67]_{tot} = 1 \times 10^{-5}$ M

UV-Visible and luminescence measurements to determine the stoichiometry of the Eu^{III} complex of ligand **67** ***(S,S)*** using Job's method, were also carried out in CH_3CN, resulting in the same complex stoichiometry: Eu_2L_3. The same results were obtained for the (*R,R*) isomer **66** in both CH_3CN and in $CH_3CN/CHCl_3$ (50:50, v/v) solutions.

It is important to note that one of the limitations of the method of continuous variations is the requirement that only one equilibrium of metal complex ion formation be present in a solution of M and L. That is, it will give non-integral values of *n* if in addition to M, L, and ML_n another complex, ML_{n+1}, is also present. This is true if the stepwise stability constants for the system are greatly different. In order to verify the reliability of the Job's method, the comparison between the stability constants involved in the formation of metal complex ions from ligand **66** ***(R,R)*** and **67** ***(S,S)*** will be addressed in the next section. Consequently, the results obtained from this method can only be considered as an indication that the predominant species in solution is the desired dimetallic triple helicate Eu_2L_3, for both ligands **66** and **67**, and in both CH_3CN and in $CH_3CN/CHCl_3$ (50:50, v/v) solutions, in the presence of $Eu(CF_3SO_3)_3$.

4.5 Determination of metal complex ion stability constants by UV-Visible and luminescence spectroscopy

The determination of stability constants is often used to gain a better understanding of the factors controlling metal ion complexation. As already stated in Chapter 2, a variety of techniques can be used in the determination of metal complex ion stability constants. Potentiometric titrations have already been used in the study of the Eu^{III} ion complexation of ligands **66** ***(R,R)*** and **67** ***(S,S)*** in partially aqueous solution (see Chapter 3). As discussed in Chapter 3, there are some limitations associated with potentiometric titrations. Firstly, large concentrations ($\geq 10^{-3}$ M) are required which can lead to problems such as precipitate formation. Secondly, the technique is best suited to those systems that display higher stability constants ($K \geq 100$ dm^3 mol^{-1}), which can lead to sensitivity issues. Potentiometric titrations are, however, not the only method available for the determination of metal complex ion stability constants; NMR spectroscopy,[205,206] UV-Visible absorption spectroscopy[207,65] and luminescence spectroscopy can also be utilised.[208] The determination of metal complex ion stability constants by NMR spectroscopy was not a viable option for this study, due to the complicated ^{1}H-NMR spectra obtained for ligands **66** ***(R,R)*** and **67** ***(S,S)*** upon addition of Eu^{III} (*cf.* Figure 4.1). In contrast to potentiometric titrations, luminescence and UV-Visible absorption measurements require only relatively small concentrations and are more sensitive to small changes. Therefore, the metal complex ion stability constants in CH_3CN and $CH_3CN/CHCl_3$ (50:50, v/v) were determined using these two spectroscopic techniques.

The complexation of ligands **66** ***(R,R)*** and **67** ***(S,S)*** with Eu^{III} can be expressed as the equilibria shown in Equations 3.1 - 3.4, which were discussed in Chapter 3 and are reported here for convenience:

$$Eu^{3+} + L \overset{K_{11}}{\rightleftharpoons} [EuL]^{3+} \qquad \textbf{(3.1)}$$

$$[EuL]^{3+} + L \overset{K_{12}}{\rightleftharpoons} [EuL_2]^{3+} \qquad \textbf{(3.2)}$$

$$[EuL_2]^{3+} + Eu^{3+} \overset{K_{22}}{\rightleftharpoons} [Eu_2L_2]^{3+} \qquad \textbf{(3.3)}$$

$$[Eu_2L_2]^{3+} + L \overset{K_{23}}{\rightleftharpoons} [Eu_2L_3]^{6+} \qquad \textbf{(3.4)}$$

In addition to Equation 3.2, when the metal ion is present in an excess, the formation of the Eu_2L species must also be accounted for, according to Equation 3.2-a:

$$[EuL]^{3+} + Eu^{3+} \overset{K_{21}}{\rightleftharpoons} [Eu_2L]^{6+} \qquad \textbf{(3.2-a)}$$

An overall stability constant, β_{23}, can also be derived, which is the product of the stepwise formation constants (K_{mn}), as illustrated in Equation 4.3 and 4.4:

$$2\ Eu^{3+} + 3\ L \overset{\beta_{23}}{\rightleftharpoons} [Eu_2L_3]^{6+} \qquad \textbf{(4.3)}$$

$$\beta_{23} = \frac{[Eu_2L_3{}^{6+}]}{[Eu^{3+}]^2\,[L]^3} = K_{11} \times K_{12} \times K_{22} \times K_{23} \qquad \textbf{(4.4)}$$

Two methods were used in the determination of the metal complex ion stability constants by UV-Visible and luminescence spectroscopy. The mole ratio method (**method A**) involved varying the metal ion concentration relative to a constant ligand concentration; the resulting solutions were then allowed to equilibrate overnight. The second method (**method B**), the so called dilution method, involved the addition of small aliquots of a known concentration of the metal to a solution of the ligand; the measurements were then taken at controlled intervals. In both cases, measurements at different metal ion concentrations were performed incrementally until no further spectral changes were observed, since this was assumed to coincide with completion of ligand-metal ion complexation. The data obtained was fitted with the non-linear least-squares regression programme, SPECFIT.[198] Different stoichiometries can be tested by this method, as exemplified by the complexation of the metal complex ions to form 1:1 (EuL), 1:2 (EuL_2) or 2:1 (Eu_2L), 2:2 (Eu_2L_2) and 2:3 (Eu_2L_3) species (*cf.* Equations 3.1 – 3.4 and 3.2-a). The program also takes into account the ability of the theoretical data to fit well with the experimental data, in the form of the sum of the squared standard deviation (SSD). This is determined along with the metal complex ion stability constants for each complexation model. However, SPECFIT cannot accurately fit data when $K \geq 10^7$ dm^3 mol^{-1}, because, at equilibrium, the ratio of the product metal complex ion concentration to those of its precursors, becomes very large. Therefore, the minor error in the stability of the former induces a very large error in the latter; hence the overall error in the determined K becomes

significant. Moreover, for species to be accurately fitted with SPECFIT, they need to be present in a concentration >10% and <90% of formation. Outside this range of concentrations, large errors are associated with the calculated log *K* values.

4.6 UV-Vis and luminescence studies

As discussed in Chapter 3, the results obtained from the potentiometric and photophysical studies of the two ligands (**66** and **67**) and the corresponding Eu^{III} complexes (**74** and **75**) conducted in partially aqueous solution, did not allow a definite interpretation of the various species present in solution. This was due to the complexity of the system under study and to the numerous equilibria which derive from it. Therefore, with the objective to gain insight into the stoichiometry of these supramolecular systems, a simplification was needed in order to lessen the variables of the system. With this in mind, UV-Visible and luminescence studies of the two ligands upon addition of Eu^{III} were carried out in less competitive media, by using aprotic organic solvents. The solvents of choice were CH_3CN and a mixture of $CH_3CN/CHCl_3$ (50:50, v/v). Such a choice was primarily governed by solubility reasons; that is, the ligand was not as soluble in CH_3CN as it was in $CHCl_3$, but the concentrations used in the spectroscopic titrations (10^{-5} M) allowed the use of pure CH_3CN. In the next sections, the results from the UV-Visible and luminescence titrations of ligands **66** ***(R,R)*** and **67** ***(S,S)*** against Eu^{III} in these two solvent systems will be detailed. All the measurements reported were fully reproducible.

4.6.1 Experimental details

All photophysical measurements were determined in either CH_3CN or $CH_3CN/CHCl_3$ (50:50, v/v). UV-Visible and luminescence measurements of a 1×10^{-5} M solution of ligand **66** ***(R,R)*** or **67** ***(S,S)*** were carried out using $Eu(CF_3SO_3)_3$. The same solutions were used for both the UV-Visible and the luminescence measurements. Two different methods were used in performing the experiment, which will be discussed individually below.

4.6.1.1 Method A (mole ratio method)

Seventeen samples (5 ml each) of ligand **66** ***(R,R)*** and **67** ***(S,S)*** (1×10^{-5} M) were prepared with varying amounts of Eu^{III} (from 0 to 3 equivalents) and left standing overnight in the dark. The spectra were then recorded the following day.

4.6.1.2 Method B (dilution method)

A 10 ml sample of 1 × 10^{-5} M solution of ligands **66** ***(R,R)*** or **67** ***(S,S)*** were prepared. A known volume of 2.5 x 10^{-4} M solution of $Eu(CF_3SO_3)_3$ was added to either of the two solutions and the absorbance and luminescence spectra were recorded 3 min. after each addition.

4.6.2 UV-Visible titrations in CH_3CN

4.6.2.1 (S,S) isomer

The UV-Visible absorption spectra and corresponding profiles for the titrations of ligand **67** ***(S,S)***, carried out in CH_3CN using these methods, are shown below.

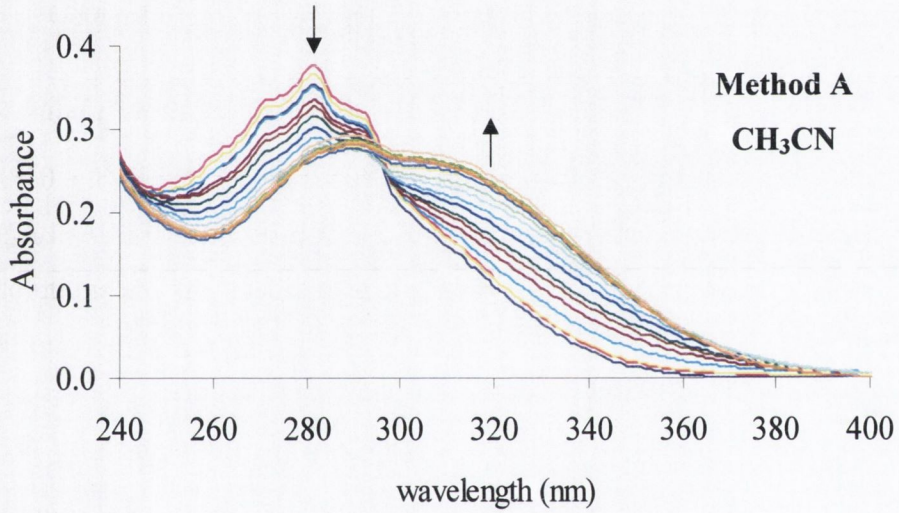

Figure 4.11 Method A: Overlaid UV-Vis spectra for the titration of ligand 67 *(S,S)* [1× 10^{-5} M] with $Eu(CF_3SO_3)_3$ in CH_3CN.

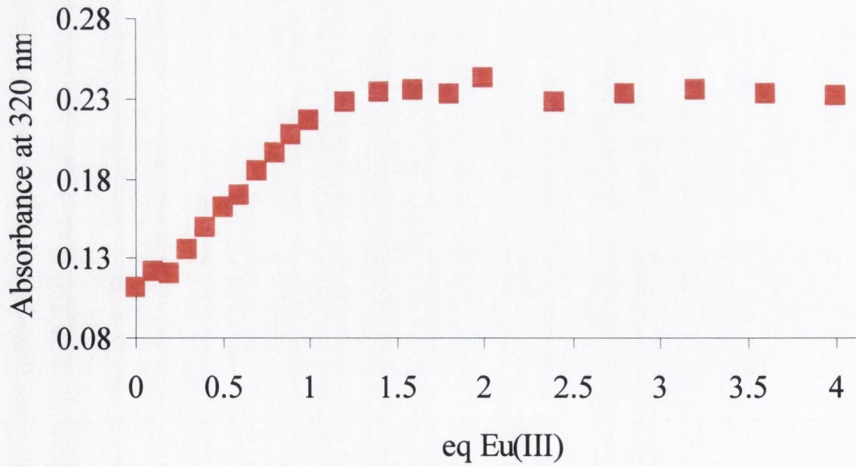

Figure 4.12 Method A: Absorbance at 320 nm as a function of Eu^{III} equivalents in the titration of ligand 67 *(S,S)* [1× 10^{-5} M] with $Eu(CF_3SO_3)_3$ in CH_3CN.

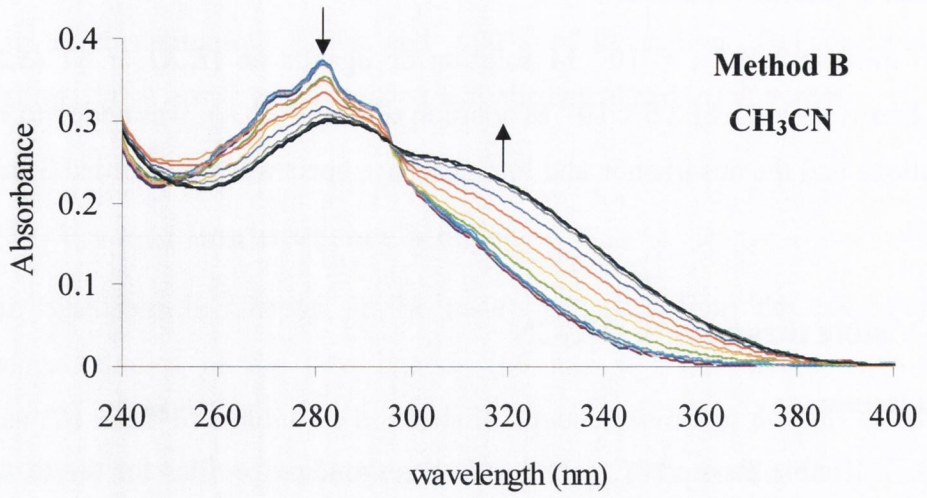

Figure 4.13 Method B: Overlaid UV-Vis spectra for the titration of ligand 67 *(S,S)* [1× 10^{-5} M] with $Eu(CF_3SO_3)_3$ in CH_3CN.

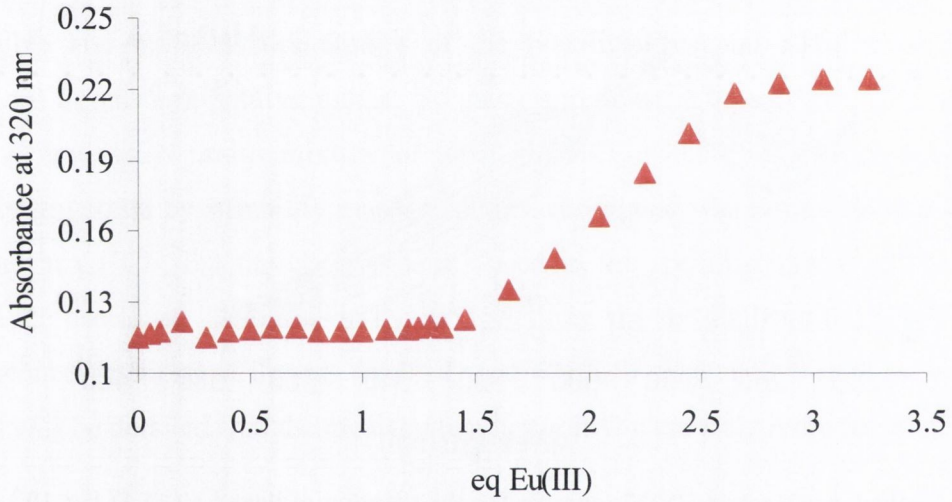

Figure 4.14 Method B: Absorbance at 320 nm as a function of Eu^{III} equivalents in the titration of ligand 67 *(S,S)* [1× 10^{-5} M] with $Eu(CF_3SO_3)_3$ in CH_3CN.

In both cases (*i.e.* **methods A** and **B**), the initial absorption spectrum of the ligand showed a band centred at 281 nm (ε = 35400 M^{-1} cm^{-1}) with two shoulders at 271 and 292 nm, characteristic of a 1-substituted naphthalene derivative[190,191] (*cf.* Figures 4.11 and 4.13). Upon addition of Eu^{III}, for both methods, the absorption bands at 281 nm underwent bathochromic and hypochromic shifts with concomitant loss of hyperfine structures. The formation of a new band centred at 320 nm (ε = 22400 M^{-1} cm^{-1}) was also observed with an isosbestic point at 296 nm, which was clearer with **method A**. However, the similarities between the two methods in terms of absorption spectra were not found in terms of titration profiles. In both cases, the changes in absorbance at 320 nm were plotted against the added equivalents of Eu^{III}, as shown in Figures 4.12 and 4.14. At this wavelength, the

changes in absorbance monitor the formation of a new absorption band, hence the formation of new species in solution. With **method A**, the change in absorbance at 320 nm reached a plateau after the addition of *ca.* 1 equivalent of Eu^{III}, whereas *ca.* 2.5 equivalents were needed to reach the end point using **method B**. This suggests that time is required to reach an equilibrium between the species involved. With **method B**, the species do not equilibrate instantaneously after each addition of Eu^{III}, therefore an excess of Eu^{III} is needed to drive the equilibrium towards the formation of the final species. However, from the profile obtained in Figure 4.12 (**method A**) it is not possible to draw any conclusions about the stoichiometry of the complex/complexes formed. The data obtained from these UV-Visible measurements have been used to determine the metal complex ions stability constants using the non-linear least squares regression program SPECFIT. These results will be discussed at the end of the next section.

4.6.2.2 (R,R) isomer

As detailed above for ligand **67** ***(S,S)***, the same set of measurements was carried out for the ***(R,R)*** isomer **66**. The UV-Visible titrations afforded appreciably different profiles with **method B** when compared with **method A**. This difference will be discussed later in Section 4.6. In order to appreciate the difference between the two isomers and not the methods, the spectra and corresponding profiles obtained from the titration of ligand **66** ***(R,R)*** with $Eu(CF_3SO_3)_3$ in CH_3CN using **method B** are shown below.

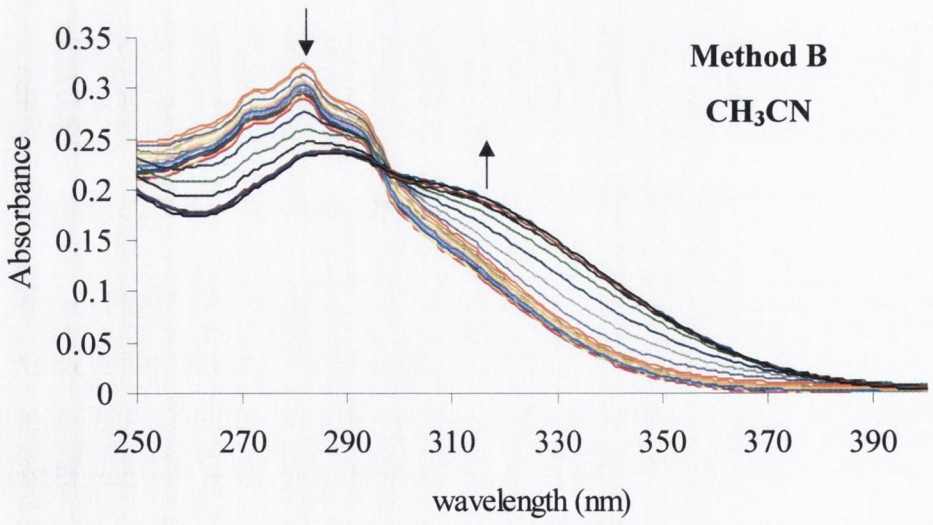

Figure 4.15 Method B: Overlaid UV-Vis spectra for the titration of ligand 66 *(R,R)* [1× 10^{-5} M] with $Eu(CF_3SO_3)_3$ in CH_3CN.

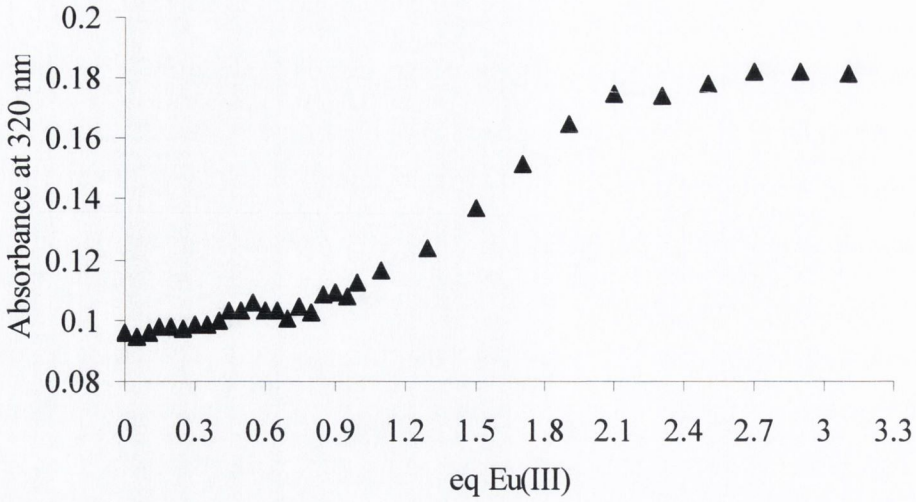

Figure 4.16 Method B: Absorbance at 320 nm as a function of Eu^{III} equivalents in the titration of ligand 66 *(R,R)* [1× 10^{-5} M] with $Eu(CF_3SO_3)_3$ in CH_3CN.

As shown in Figure 4.15, the absorption spectra of ligand **66** ***(R,R)*** are very similar to those obtained for ligand **67** ***(S,S)*** (*cf.* Figure 4.13); *e.g.* they both display the same band centred at 281 nm (ε = 32200 M^{-1} cm^{-1}), which undergoes a bathochromic and hypochromic shift upon addition of Eu^{III}, with concomitant loss of hyperfine structure. The formation of a new band centred at 320 nm (ε = 21100 M^{-1} cm^{-1}) was also observed with an isosbestic point at 296 nm. The noticeable difference between the two isomers, however, lies in the titration profiles, as the ***(R,R)*** isomer evidently needs less equivalents of Eu^{III} to reach saturation, *i.e.* 2 equiv. for the **(*R,R*)** isomer *vs* 2.5 equiv. for the **(*S,S*)** isomer. As the solutions were allowed the same equilibration time for both isomers, this difference must mirror a difference in their stability constants. The data collected from the UV-Visible titrations have been used to determine the metal complex ions stability constants using the non-linear least squares regression program SPECFIT. The results for both **(*R,R*)** and **(*S,S*)** isomer obtained with **method B** are listed in Table 4.1.

As expected from the difference between the two binding isotherms, the formation of the metal complex ions involving the **(*R,R*)** isomer presents higher stability constants than the corresponding equilibria with the **(*S,S*)** isomer. This dissimilarity also accounts for the different species present in solution; with the **(*S,S*)** isomer the Eu_2L_3 species does not form in appreciable quantity. The speciation diagrams will be shown and discussed in Section 4.8.

Table 4.1 Complexation constants, log (K/dm^3 mol^{-1}) values for the complexation of $Eu(CF_3SO_3)_3$ with ligand 66 *(R,R)* and 67 *(S,S)* in CH_3CN at 298.2 K calculated from the UV-Visible titration data (method B).

ABSORBANCE DATA – **METHOD B**: CH_3CN		
Species	**log K - 66 *(R,R)***	**log K - 67 *(S,S)***
EuL	6.49 ± 0.20	4.61 ± 0.84
EuL_2	> 7 (7.51)	> 7 (7.28)
Eu_2L	> 7 (8.22)	6.88 ± 0.14
Eu_2L_2	> 7 (8.04)	5.62 ± 0.36
Eu_2L_3	6.48 ± 0.36	—

The data obtained from **method A** for both isomers, was fitted to the following complexation model; 1:1 (EuL), 1:2 (EuL_2), 2:1 (Eu_2L), 2:2 (Eu_2L_2), 2:3 (Eu_2L_3). Except for the EuL species, which barely formed, all the other species were present in solution and exhibited very high stability constants. The log K values, relative to the formation of such species, were in fact ≥ 7 (*i.e.* $K \geq 10^7$); these values are therefore greater than the detection limit of the method in use and, for this reason, could not be reported.

4.6.3 Luminescence titrations in CH_3CN

4.6.3.1 (S,S) isomer

The luminescence spectra, upon excitation at 281 nm, and the corresponding profiles for the titrations of ligand **67** ***(S,S)***, carried out in CH_3CN using **method A** and **B**, are shown below. The addition of $Eu(CF_3SO_3)_3$ to ligand **67** ***(S,S)*** gave rise to the luminescence emission spectra typical of Eu^{III} complexes. The Eu^{III} emission appeared as well-separated emission bands at 593, 616, 652, 696 nm. These bands represent the deactivation of the $^5D_0 \rightarrow {}^7F_J$ ground states (J = 1 (593 nm), J = 2, (616 nm), J = 3 (652 nm), and J = 4 (696 nm)).[159] As for the Eu^{III} complex **75** ***(S,S)*** discussed in Section 3.2.7.2, the band corresponding at J = 0 is not visible. The luminescence measurements were also recorded upon excitation at 320 nm, resulting in similar spectra and titration profiles to those carried out upon excitation at 281 nm. Therefore, it is possible to conclude that both excitation energies allow an efficient sensitisation of the Eu^{III} excited states through the *antennae*.

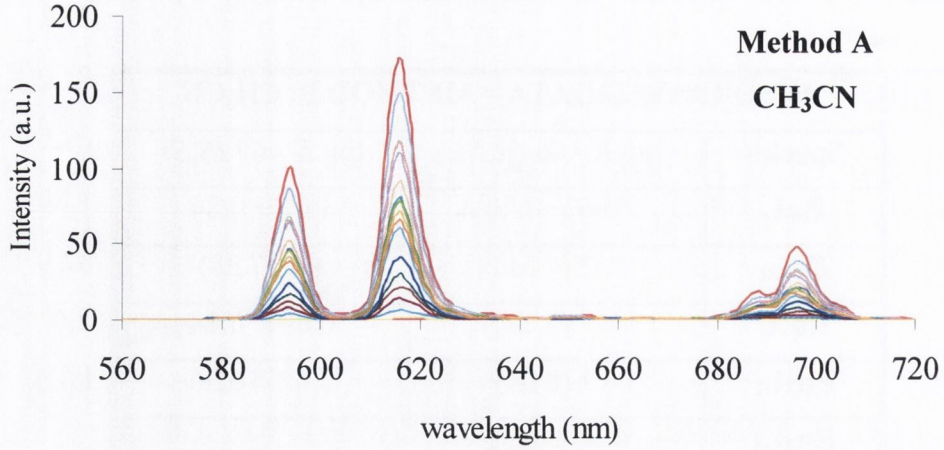

Figure 4.17 Method A: Overlaid luminescence spectra for the titration of ligand 67 *(S,S)* [1× 10^{-5} M] with $Eu(CF_3SO_3)_3$ in CH_3CN, upon excitation at 281 nm.

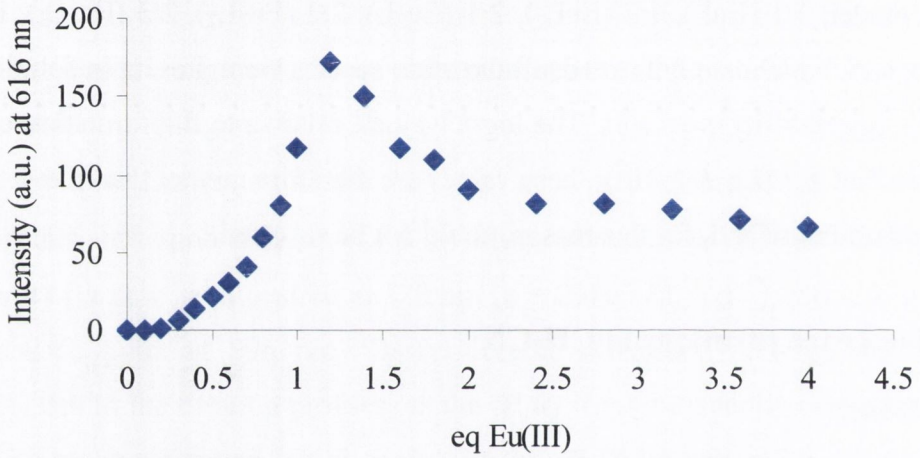

Figure 4.18 Method A: Luminescence emission intensity at 616 nm as a function of Eu^{III} equivalents in the titration of ligand 67 *(S,S)* [1× 10^{-5} M] with $Eu(CF_3SO_3)_3$ in CH_3CN.

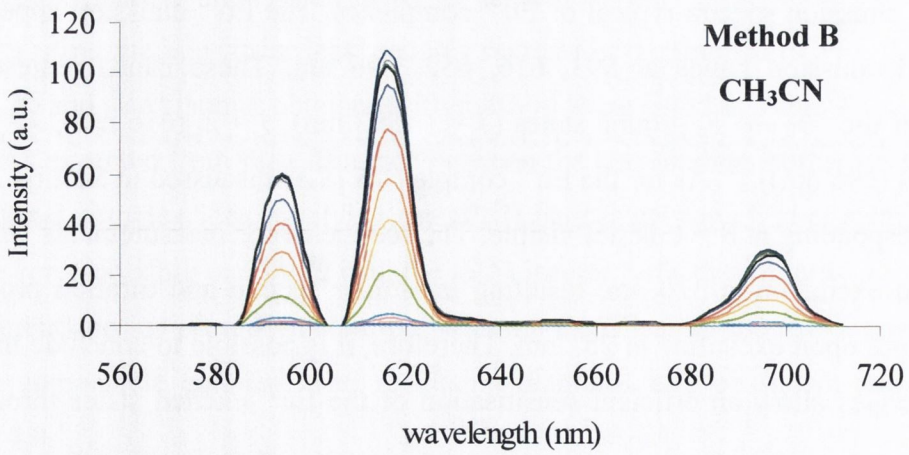

Figure 4.19 Method B: Overlaid luminescence emission spectra for the titration of ligand 67 *(S,S)* [1× 10^{-5} M] with $Eu(CF_3SO_3)_3$ in CH_3CN upon excitation at 281 nm.

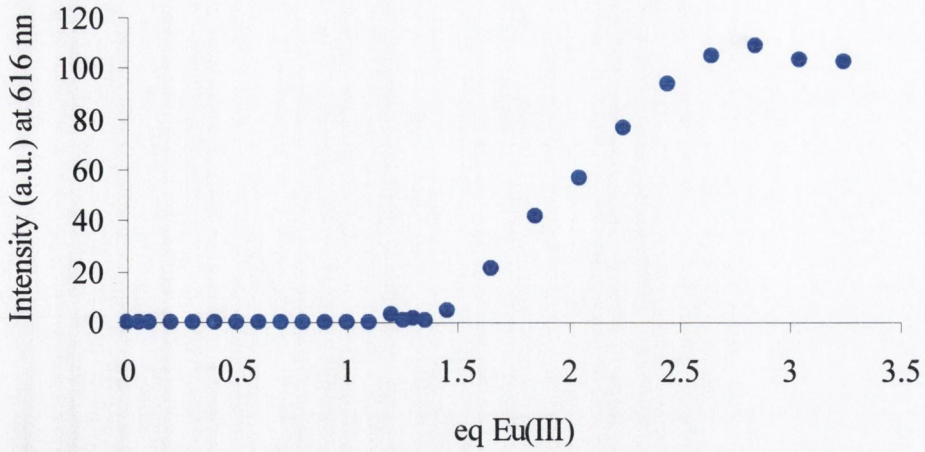

Figure 4.20 Method B: Luminescence emission at 616 nm as a function of Eu^{III} equivalents in the titration of ligand 67 *(S,S)* [1× 10^{-5} M] with $Eu(CF_3SO_3)_3$ in CH_3CN.

The difference between the two methods is evident from the profiles of luminescence *vs* equivalents of Eu^{III}. The intensity of each emission band was plotted against the equivalents of Eu^{III} added, affording the binding isotherms shown in Figure 4.18 and 4.20. With **method A**, the maximum luminescence intensity was reached upon addition of 1.2 equivalents of Eu^{III}; after that the luminescence was gradually quenched until the addition of two equivalents of Eu^{III}, when it reached the end point. This suggests that the species forming in excess of Eu^{III} are less luminescent than those forming within the addition of 1 equivalent of metal ion. The profile obtained using **method B** presents significant differences: luminescent species start forming only after the addition of 1.5 equivalent of Eu^{III}; the emission reaches a maximum at *ca.* 2.5 equivalents, undergoes a slight decrease then plateaus around 3 equivalents. These results suggest that the kinetics of the process play a major role in the formation of the metal ion complexes in solution.

4.6.3.2 (R,R) isomer

The luminescence titration in CH_3CN was repeated for ligand **66** ***(R,R)*** using both methods. The titration profile obtained with **method B** was remarkably different from the corresponding profile of the **(S,S)** isomer. This is in agreement with what has already been discussed for the absorbance data in Section 4.6.2. The luminescence emission spectra and the changes observed at 616 nm are shown in Figure 4.21 and 4.22, respectively.

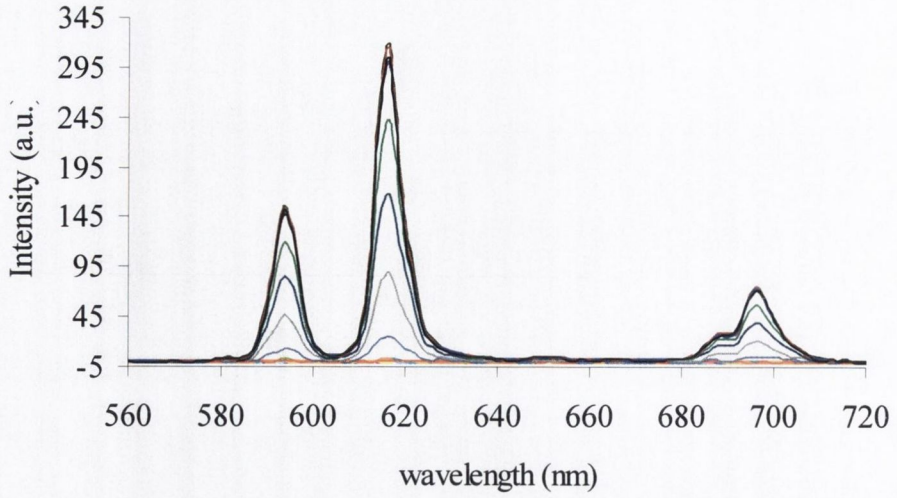

Figure 4.21 Method B: Overlaid luminescence emission spectra for the titration of ligand 66 *(R,R)* [1× 10^{-5} M] with $Eu(CF_3SO_3)_3$ in CH_3CN upon excitation at 281 nm.

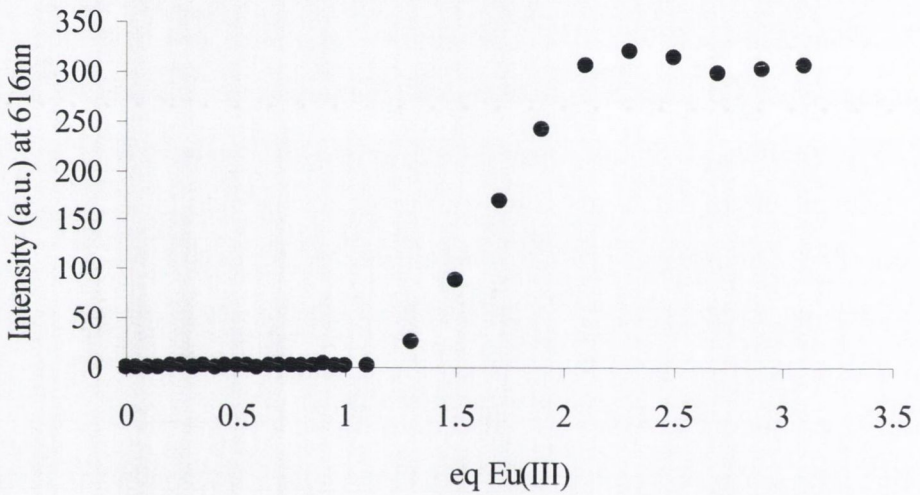

Figure 4.22 Method B: Luminescence emission at 616 nm as a function of Eu^{III} equivalents in the titration of ligand 66 *(R,R)* [1× 10^{-5} M] with $Eu(CF_3SO_3)_3$ in CH_3CN.

As clearly shown in Figure 4.21, the ***(R,R)*** isomer presents the same characteristic emission bands as the ***(S,S)*** isomer (*cf.* Figure 4.19). However, the luminescence only starts increasing after adding 1.1 equivalents of Eu^{III} compared to the 1.5 equivalents seen earlier for the ***(S,S)*** isomer. Consistent with the absorbance data, the luminescence titration also suggests that the binding constants for the two isomers are different. This was verified by calculating the stability constants using the non-linear least squares regression program SPECFIT. The log *K* values obtained by using **method B** for both ligands are shown in Table 4.2.

Table 4.2 Complexation constants, log (K/dm^3 mol^{-1}) values for the complexation of Eu(CF_3SO_3)$_3$ with ligand 66 *(R,R)* and 67 *(S,S)* in CH_3CN at 298.2 K calculated from the luminescence titration data (method B).

LUMINESCENCE DATA – **METHOD B**: CH_3CN		
Species	**log K - 66 *(R,R)***	**log K - 67 *(S,S)***
EuL	6.49 ± 0.20	4.61 ± 0.84
EuL_2	> 7 (7.51)	> 7 (7.28)
Eu_2L	> 7 (8.49)	> 7 (7.15)
Eu_2L_2	> 7 (7.02)	5.19 ± 0.25
Eu_2L_3	> 7 (7.63)	—

In keeping with the results obtained from the UV-Visible absorption titrations, the two isomers exhibited different stability constants, with the (*R,R*) isomer forming appreciably more stable species in solution. In a similar manner to the absorbance data, the (*S,S*) ligand fitted for the following complexation model: 1:1 (EuL), 1:2 (EuL_2), 2:1 (Eu_2L), 2:2 (Eu_2L_2), with the Eu_2L_3 being barely present in solution.

The analysis of the data obtained from **method A** with both isomers afforded similar results as those discussed for the absorbance data: the data fitted to the following complexation model; 1:1 (EuL), 1:2 (EuL_2), 2:1 (Eu_2L), 2:2 (Eu_2L_2), 2:3 (Eu_2L_3). Except for the EuL species, which exhibited very low stability constant and was scarcely present, all the other species were present in solution. The log K values, relative to the formation of such species, were ≥ 7 (*i.e.* $K \geq 10^7$); for this reason, these values could not be reported. Due to the different UV-Visible and luminescence properties of the species in solution, it was expected to observe different titration profiles for the data sets obtained from the absorbance and luminescence titrations.

4.6.4 UV-Visible titrations in $CH_3CN/CHCl_3$ (50:50, v/v)

4.6.4.1 (S,S) isomer

The UV-Visible absorption spectra and the corresponding profiles for the titrations of ligand **67** ***(S,S)***, carried out in $CH_3CN/CHCl_3$ (50:50, v/v) solution using **methods A** and **B**, are shown below. As for the UV-Visible absorption spectra carried out in CH_3CN, the ligand in $CH_3CN/CHCl_3$ (50:50, v/v) solution exhibits a band centred at 281 nm (ε = 33000 M^{-1} cm^{-1}) with two shoulders at 271 and 292 nm. Upon addition of Eu^{III}, the

absorption band at 281 nm underwent a bathochromic and hypochromic shift similar to that seen before with concomitant loss of the hyperfine structure. The formation of a new band centred at 320 nm (ε = 21800 M^{-1} cm^{-1}) was also observed. A clear isosbestic point at 297 nm was detected in the case of the titration carried out using **method B** (*cf.* Figure 4.25). In contrast, **method A** did not result in such a defined isosbestic point, possibly due to different concentrations of the metal complex species in solution.

Based on the binding isotherms derived from the absorbance data, it is clear that the absorbance at 320 nm reaches a plateau within 1 equivalent of Eu^{III} added using **method A**, whereas 2 equivalents are needed in the case of **method B** (see Figure 4.26 and 4.28).

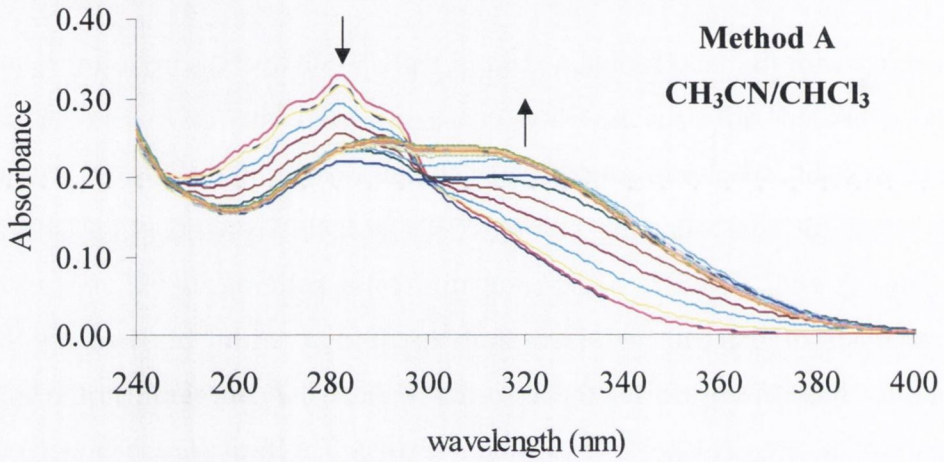

Figure 4.23 Method A: Overlaid UV-Vis spectra for the titration of ligand 67 *(S,S)* [1× 10^{-5} M] with $Eu(CF_3SO_3)_3$ in $CH_3CN/CHCl_3$ (50:50, v/v).

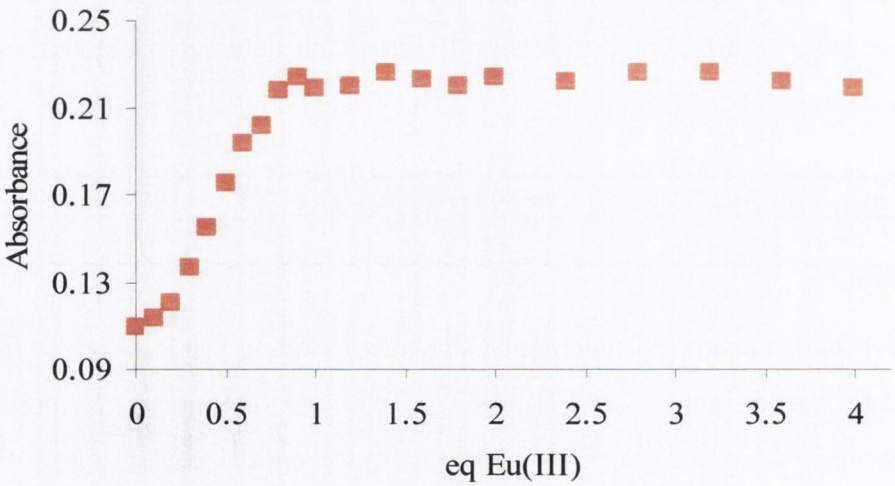

Figure 4.24 Method A: Absorbance at 320 nm as a function of Eu^{III} equivalents in the titration of ligand 67 *(S,S)* [1× 10^{-5} M] with $Eu(CF_3SO_3)_3$ in $CH_3CN/CHCl_3$ (50:50, v/v).

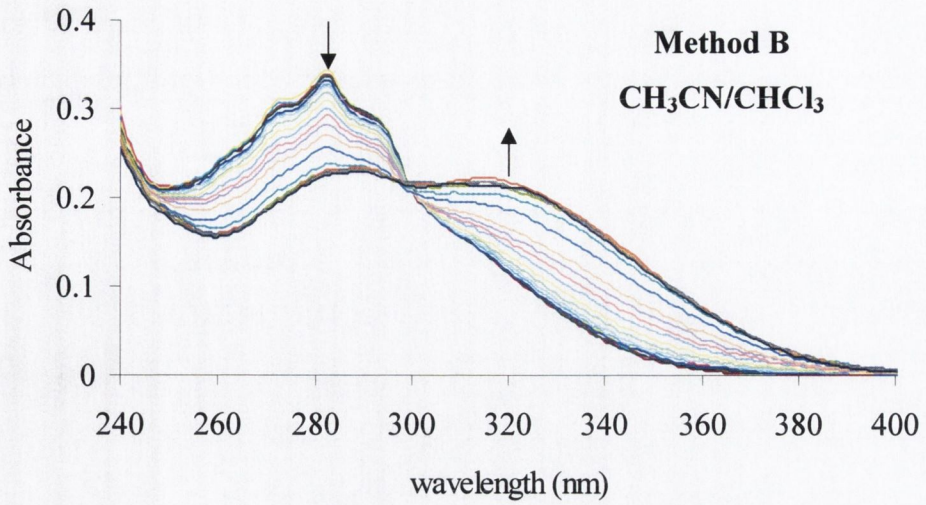

Figure 4.25 Method B: Overlaid UV-Vis spectra for the titration of ligand 67 *(S,S)* [1× 10^{-5} M] with $Eu(CF_3SO_3)_3$ in $CH_3CN/CHCl_3$ (50:50, v/v).

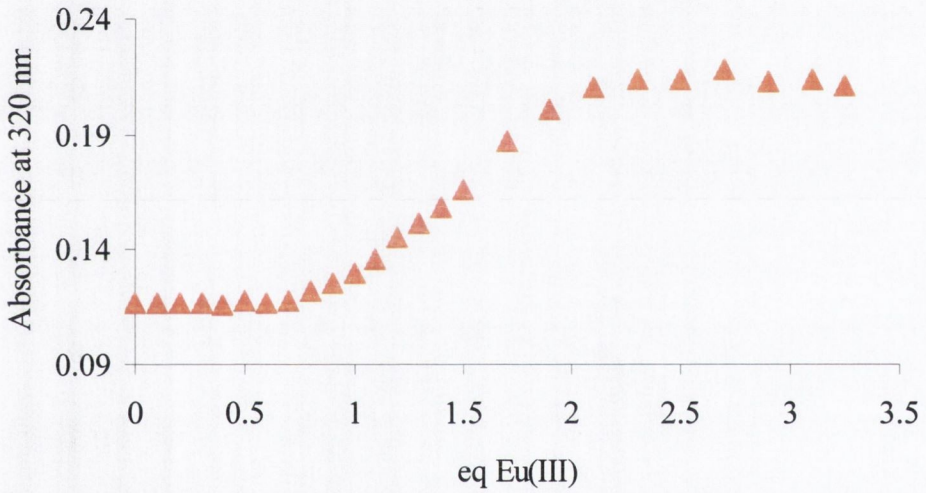

Figure 4.26 Method B: Absorbance at 320 nm as a function of Eu^{III} equivalents in the titration of ligand 67 *(S,S)* [1× 10^{-5} M] with $Eu(CF_3SO_3)_3$ in $CH_3CN/CHCl_3$ (50:50, v/v).

Therefore, it is reasonable to conclude that the kinetic parameters of the complexation process, in $CH_3CN/CHCl_3$ (50:50, v/v) as well as in CH_3CN, are of fundamental importance. It can also be observed that, for both methods, the equivalent of Eu^{III} required for the absorbance to plateau is less in $CH_3CN/CHCl_3$ (50:50, v/v) than it is in 100% CH_3CN, indicating that the polarity of the solvent has an influence on the formation of the Eu^{III} ion complexes in solution.

4.6.4.2 (R,R) isomer

The UV-Visible absorption titrations in $CH_3CN/CHCl_3$ (50:50, v/v) were also carried out using the **(*R,R*)** isomer with the two **methods A** and **B**. The same spectroscopic

features observed for the **(*S,S*)** isomer were observed with the **(*R,R*)** isomer **66**, where both methods showed a difference in the number of equivalents of Eu^{III} required to reach saturation. As an example, the spectra and corresponding titration profile obtained with **method B** are shown in Figure 4.27 and 4.28.

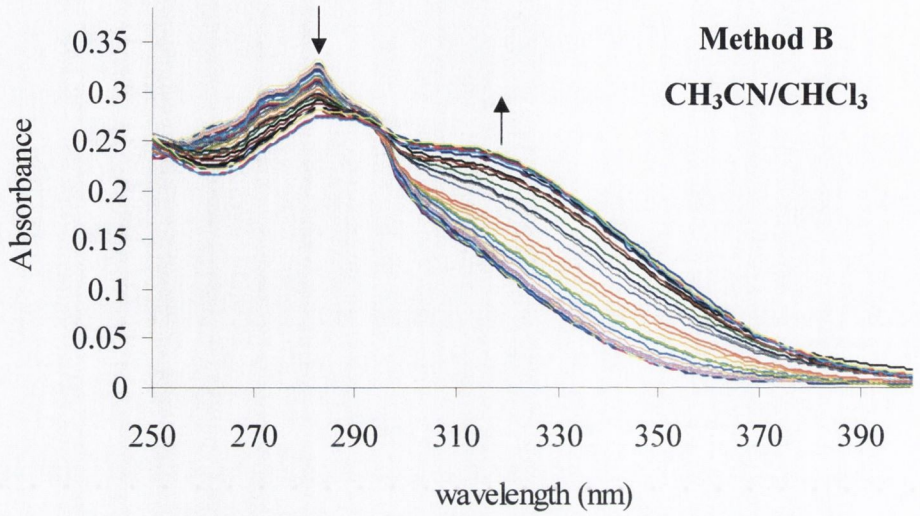

Figure 4.27 Method B: Overlaid UV-Vis spectra for the titration of ligand 66 *(R,R)* [1× 10^{-5} M] with $Eu(CF_3SO_3)_3$ in $CH_3CN/CHCl_3$ (50:50, v/v).

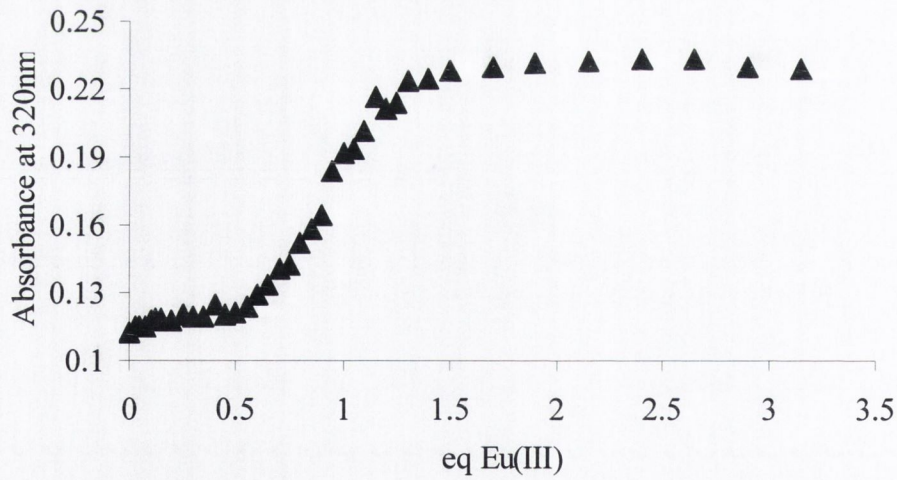

Figure 4.28 Method B: Absorbance at 320 nm as a function of Eu^{III} equivalents in the titration of ligand 66 *(R,R)* [1× 10^{-5} M] with $Eu(CF_3SO_3)_3$ in $CH_3CN/CHCl_3$ (50:50, v/v).

The UV-Visible absorption spectra of ligand **66** ***(R,R)*** exhibited similar spectroscopic features to ligand **67** ***(S,S)*** upon titration with Eu^{III}. The difference between the two isomers is clearly visible from the binding isotherms obtained from the absorbance data and shown in Figures 4.26 and 4.28. As evidenced from this profile in Figure 4.28, ligand **66** ***(R,R)*** reaches a plateau after the addition of 1.3 equivalents of Eu^{III}, rather than 2

equivalents as observed for ligand **67** ***(S,S)***. In a similar manner to the measurements in CH_3CN, a difference between the stability constants of the two systems can be anticipated. When fitted with SPECFIT, the absorbance variation of both ligands **66** ***(R,R)*** and **67** ***(S,S)*** fitted the same complexation model; 1:1 (EuL), 2:1 (Eu_2L), 2:2 (Eu_2L_2), 2:3 (Eu_2L_3). This resulted in the determination of the log *K* values listed in Table 4.3.

Table 4.3 Complexation constants, log (K/dm^3 mol^{-1}) values for the complexation of $Eu(CF_3SO_3)_3$ with ligand 66 *(R,R)* and 67 *(S,S)* in $CH_3CN/CHCl_3$ (50:50, v/v) at 298.2 K, calculated from the UV-Visible titration data (method B).

ABSORBANCE DATA – **METHOD B**: $CH_3CN/CHCl_3$		
Species	**log *K* - 66 *(R,R)***	**log *K* - 67 *(S,S)***
EuL	> 7 (8.10)	6.99 ± 0.24
Eu_2L	6.21 ± 0.54	6.97 ± 0.29
Eu_2L_2	5.19 ± 0.43	5.23 ± 0.92
Eu_2L_3	6.42 ± 0.53	> 7 (7.21)

The ***(R,R)*** isomer exhibited a higher stability constant than the ***(S,S)*** isomer for the formation of the EuL species. However, the log *K* value associated with this constant is >7, therefore it is greater than the upper limit for this method. Nonetheless, it is reasonable to attribute the difference between the titration profiles obtained with the two ligands (*cf.* Figure 4.26 and 4.28), to the difference in the corresponding EuL stability constants. By comparing the results obtained in CH_3CN to those in $CH_3CN/CHCl_3$ (50:50, v/v), an overall trend can be outlined (*cf.* Table 4.1 *vs* Table 4.3): the diminished polarity of the solvent system contributes to an increase in the stability constants for both isomers. Moreover, the overall difference between the two isomers is reduced in the less polar solvent system, *i.e.* $CH_3CN/CHCl_3$ (50:50, v/v); besides presenting similar log *K* values, both isomers form the desired Eu_2L_3 species in solution. This can be attributed to the lesser coordinating effect of $CHCl_3$ compared to CH_3CN.

The determination of the metal complex ion stability constants for both isomers from the data collected with **method A** in $CH_3CN/CHCl_3$ (50:50, v/v), resulted in log *K* values > 7 for all the species present in solution (EuL_2, Eu_2L, Eu_2L_2, Eu_2L_3), confirming a kinetic contribution to the formation of these species in solution.

4.6.5 Luminescence titrations in $CH_3CN/CHCl_3$ (50:50, v/v)

4.6.5.1 (S,S) isomer

The luminescence spectra of ligand **67** ***(S,S)*** upon titration with $Eu(CF_3SO_3)_3$ were carried out in $CH_3CN/CHCl_3$ (50:50, v/v) using both **methods A** and **B**. As for the studies in CH_3CN, the addition of $Eu(CF_3SO_3)_3$ to ligand **67** ***(S,S)*** gave rise to enhanced luminescence emission spectra, which showed the typical Eu^{III} transitions. The Eu^{III} emission appeared as well-separated emission bands centred at 593, 616, 652, and 696 nm upon excitation at 281 nm. Luminescence measurements were also carried out upon excitation at 320 nm, resulting in similar spectra and titration profiles to those outlined below.

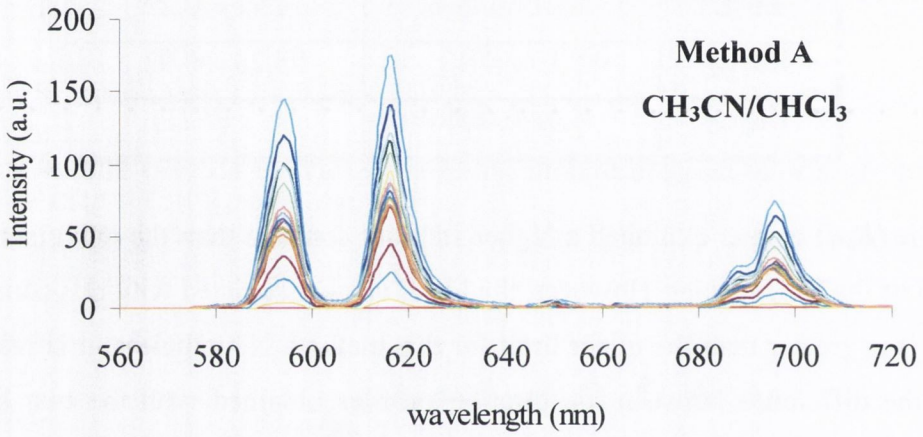

Figure 4.29 Method A: Overlaid luminescence emission spectra for the titration of ligand 67 *(S,S)* [1× 10^{-5} M] with $Eu(CF_3SO_3)_3$ in $CH_3CN/CHCl_3$ (50:50, v/v) upon excitation at 281 nm.

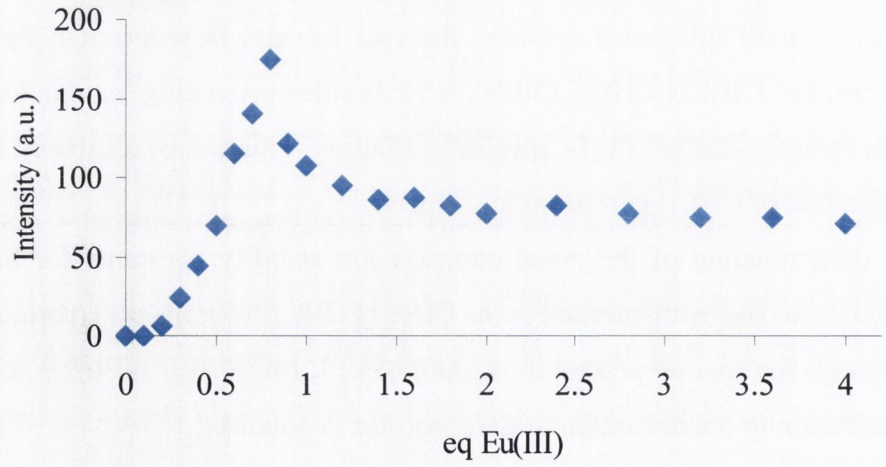

Figure 4.30 Method A: Luminescence emission intensity at 616 nm as a function of Eu^{III} equivalents in the titration of ligand 67 *(S,S)* [1× 10^{-5} M] with $Eu(CF_3SO_3)_3$ in $CH_3CN/CHCl_3$ (50:50, v/v)

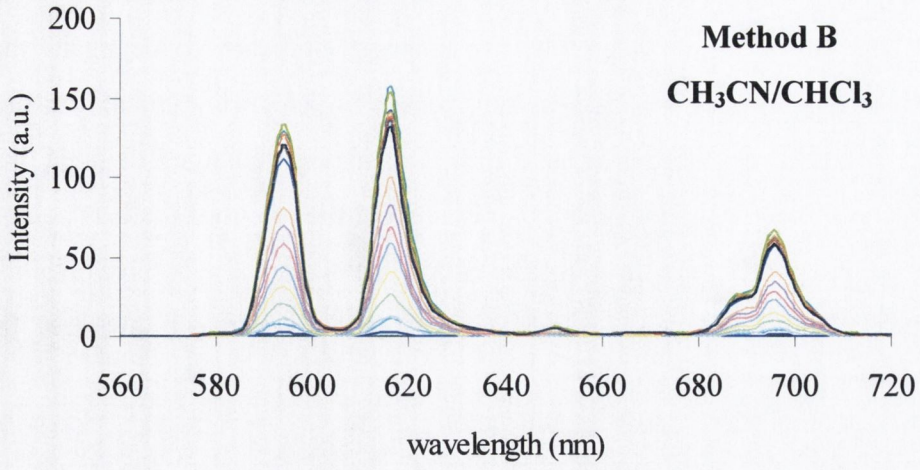

Figure 4.31 Method B: Overlaid luminescence emission spectra for the titration of ligand 67 *(S,S)* [1× 10^{-5} M] with $Eu(CF_3SO_3)_3$ in $CH_3CN/CHCl_3$ (50:50, v/v) upon excitation at 281 nm.

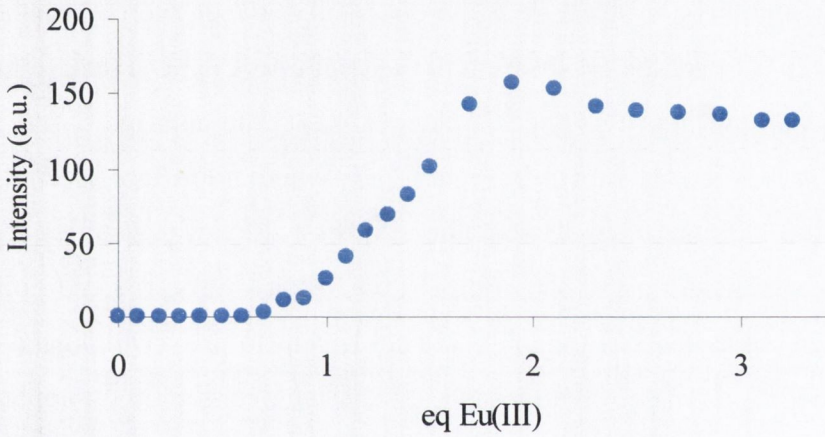

Figure 4.32 Method B: Luminescence emission intensity at 616 nm as a function of Eu^{III} equivalents in the titration of ligand 67 *(S,S)* [1× 10^{-5} M] with $Eu(CF_3SO_3)_3$ in $CH_3CN/CHCl_3$ (50:50, v/v).

The intensity of each emission band was plotted against the equivalents of Eu^{III} added, resulting in the profiles shown in Figure 4.30 and 4.32. The difference between the two methods is manifest from the profiles of luminescence *vs* equivalent of Eu^{III}. With **method A**, the maximum luminescence intensity was reached upon addition of 0.8 equivalents of Eu^{III}, after which the luminescence was gradually quenched until 1.5 equivalents of Eu^{III}; thereafter, no further changes were observed. This suggests that the species forming in excess of Eu^{III} are less luminescent than those forming within the addition of 1 equivalent of metal ion, as previously observed for the luminescence titrations in CH_3CN (*cf.* Section 4.6.3.1). The profile obtained using **method B** presents significant differences with that obtained with **method A**: luminescent species start forming only after addition of *ca.* 0.7 equivalent of Eu^{III}; the emission reaches a maximum

at *ca.* 1.8 equivalents then undergoes a slight decrease until it plateaus at around 2.5 equivalents. The difference between the two methods indicates once again that it is necessary to account for the kinetics of the process in the formation of the metal ion complexes in solution. Furthermore, as for the absorbance changes detailed before in Section 4.6.4, the same conclusions can be drawn about the effect of the less polar solvent on the equilibria involved in the titrations described above. In $CH_3CN/CHCl_3$ (50:50, v/v), the equivalents of Eu^{III} required to reach the maximum intensity are less than the corresponding method in CH_3CN.

4.6.5.2 (R,R) isomer

The experiments described in the previous section were also carried out for ligand **66** ***(R,R)***, affording the same emission bands as ligand **67** ***(S,S)*** and similar spectra. However, different titration profiles were again observed between the two methods. The luminescence spectra of ligand **66** ***(R,R)*** when titrated with $Eu(CF_3SO_3)_3$ using **method B**, upon excitation at 281 nm, are illustrated in Figures 4.33. The changes observed in the emission intensity at 616 nm are shown in Figure 4.34, where no further spectral changes are observed after the addition of *ca.* 1.3 equivalents of Eu^{III}. This was assumed to coincide with the completion of ligand metal ion complexation. Conversely, the end point of the titration was reached only after addition of *ca.* 1.8 equivalents of Eu^{III} with ligand **67** ***(S,S)***. It is therefore reasonable to assume that the stability constants for the Eu^{III} complex species formed by the two isomers are potentially different.

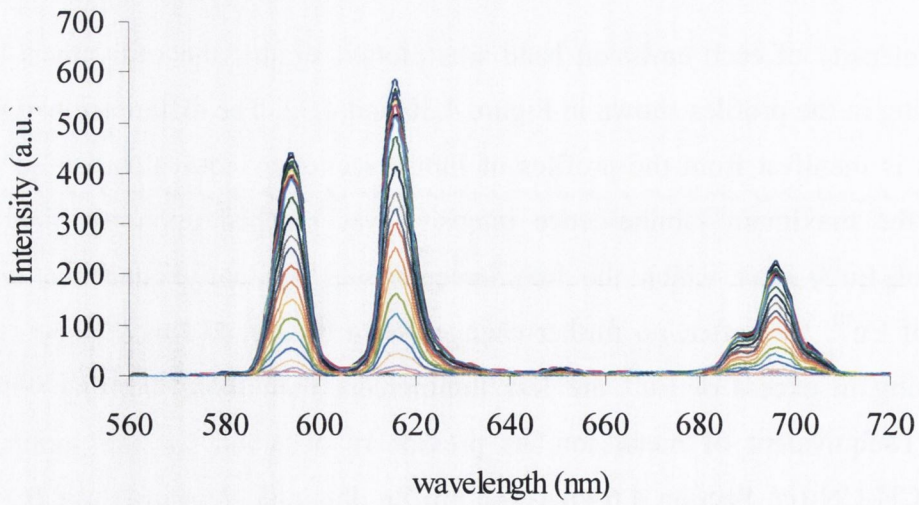

Figure 4.33 Method B: Overlaid luminescence emission spectra for the titration of ligand 66 *(R,R)* [1× 10^{-5} M] with $Eu(CF_3SO_3)_3$ in $CH_3CN/CHCl_3$ (50:50, v/v) upon excitation at 281 nm.

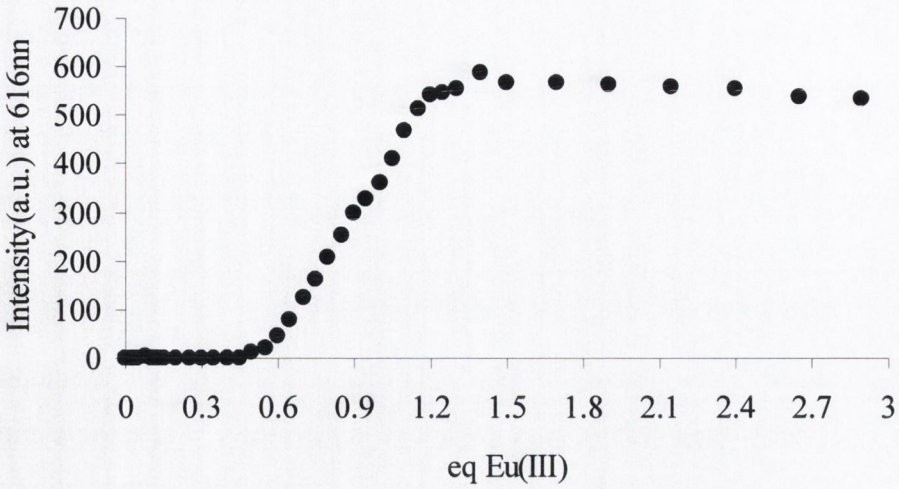

Figure 4.34 Method B: Luminescence emission intensity at 616 nm as a function of Eu^{III} equivalents in the titration of ligand 66 *(R,R)* [1× 10^{-5} M] with $Eu(CF_3SO_3)_3$ in $CH_3CN/CHCl_3$ (50:50, v/v).

The metal complex ion stability constants were determined from these changes with SPECFIT and the corresponding log *K* values are listed in Table 4.4.

Table 4.4 Complexation constants, log (K/dm^3 mol^{-1}) values for the complexation of $Eu(CF_3SO_3)_3$ with ligand 66 *(R,R)* and 67 *(S,S)* in $CH_3CN/CHCl_3$ (50:50, v/v) at 298.2 K, calculated from the luminescence titration data (method B).

LUMINESCENCE DATA – **METHOD B**: $CH_3CN/CHCl_3$		
Species	**log *K* - 66 *(R,R)***	**log *K* - 67 *(S,S)***
EuL	> 7 (7.57)	> 7 (8.12)
Eu_2L	> 7 (8.80)	> 7 (7.43)
Eu_2L_2	5.43 ± 0.63	6.56 ± 0.41
Eu_2L_3	> 7 (7.57)	6.52 ± 0.32

The log *K* values calculated are mostly greater than 7 and as such cannot be considered as accurate values. Nonetheless, the luminescence titration data for both isomers were in agreement with the absorbance data as they fitted for the same complexation model (EuL, Eu_2L, Eu_2L_2, Eu_2L_3). Also, the two isomers exhibited higher stability constants than in CH_3CN, as further evidence of the effect of the less polar solvent system on the formation of the species. In keeping with the results from the UV-Vis titration data, the difference between the stability constants of the two isomers obtained from the luminescence data was also reduced.

The log *K* values calculated for **method A** were, on all occasions, greater than 7 (for all of the metal complex ions derived from both isomers). This was expected due to the high linearity of the titration profiles (see Figure 4.30). The data from the luminescence titration were fitted to the following complexation model; 1:1 (EuL), 1:2 (EuL_2), 2:1 (Eu_2L), 2:2 (Eu_2L_2), 2:3 (Eu_2L_3), with the EuL species only present in small concentration.

4.6.6 A comparison between method A and method B

As already stated, a comparison of the data obtained from the two methods shows that the kinetics of the complexation process plays a major role. When the samples are prepared in advance, the species have reached the equilibrium in the complexation process by the time the measurements are carried out (16 h). The same cannot be said about the measurements conducted with **method B**. For clarity's sake, the profiles obtained from the luminescence titrations of **67** ***(S,S)*** in $CH_3CN/CHCl_3$ (50:50, v/v) with the two different methods are shown in Figure 4.35.

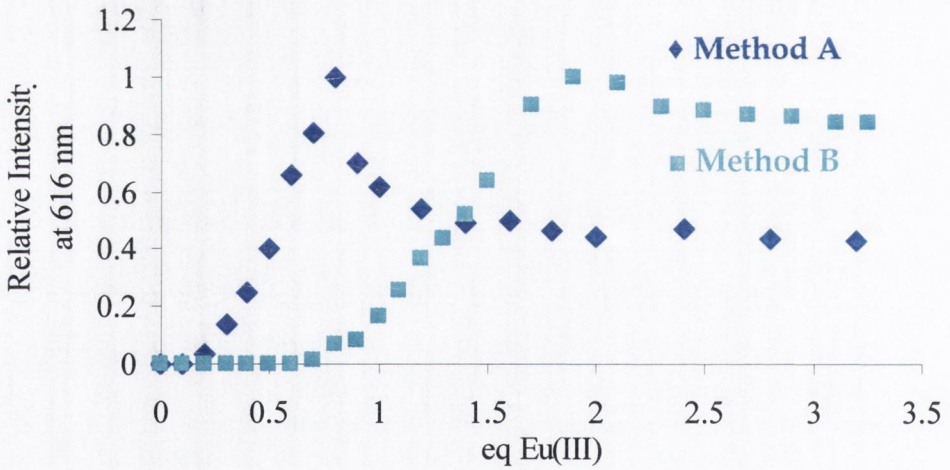

Figure 4.35 Luminescence changes for ligand 67 *(S,S)* with $Eu(CF_3SO_3)_3$ using method A (♦) and method B (■) in $CH_3CN/CHCl_3$ (50:50, v/v).

Moreover, in all the experiments conducted with **method A**, it was found that the monometallic species EuL was barely present in solution. This may be considered as an indication that, when allowed to equilibrate, only the most stable species are detected in solution. Most importantly, the desired dimetallic triple helicate species, Eu_2L_3, was crucial in the fitting of the data with SPECFIT, supporting its presence in solution. Therefore, the kinetic effect on the equilibria among the metal complex ion species must be accounted for.

In order to further investigate the kinetic aspects of the complexation process, kinetics experiment were carried out. The change in luminescence of a sample containing a given ligand (either **66** or **67**) and different equivalents of Eu^{III} was monitored as a function of time. Contrary to expectation, the obtained luminescence profile as a function of time did not afford suitable data for the calculation of the rate constant. To date, the reason behind this unexpected response could not be determined. This may be an area which warrants further investigation in future studies.

4.7 The effect of the counterion on the stability constants

In order to investigate the effect of the counterion on the metal complex ion stability constants, UV-Visible and luminescence measurements were undertaken with both ligands **66** ***(R,R)*** and **67** ***(S,S)*** in CH_3CN. The counterion employed in all of the titrations reported in the previous sections of this chapter was trifluoromethane sulfonate (triflate, $CF_3SO_3^-$). In this section the stability constants of the metal complex ions in the presence of Eu^{III} as either perchlorate or nitrate salt will be examined. These Eu^{III} salts were chosen for the titration studies as perchlorate is a less coordinating anion than triflate, whereas nitrate is more coordinating than either. The UV-Visible and luminescence experiments were carried out in CH_3CN using **method B** (dilution method, see Section 4.6.1). A comparison between the luminescence titration profiles for the ***(R,R)*** and ***(S,S)*** isomers with $Eu(ClO_4)_3$ and $Eu(NO_3)_3$ is shown in Figures 4.36 and 4.37, respectively.

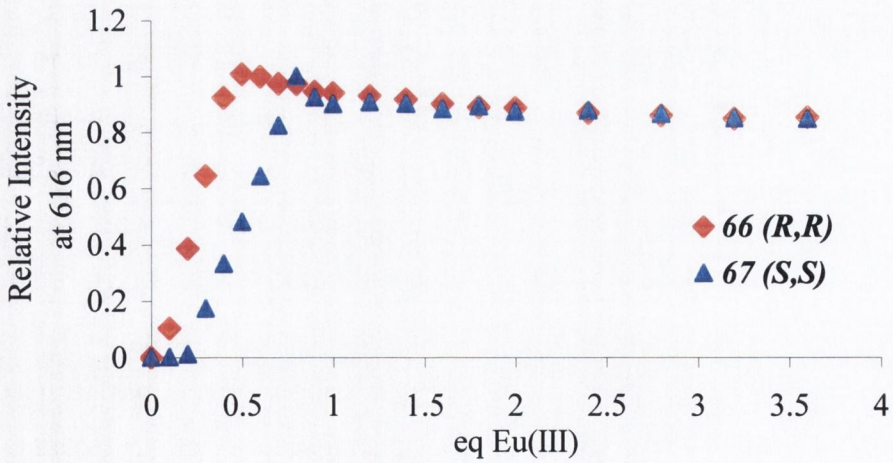

Figure 4.36 Luminescence changes at 616 nm for ligand 66 *(R,R)* (♦) and ligand 67 *(S,S)* (▲) with $Eu(ClO_4)_3$ using method B in CH_3CN.

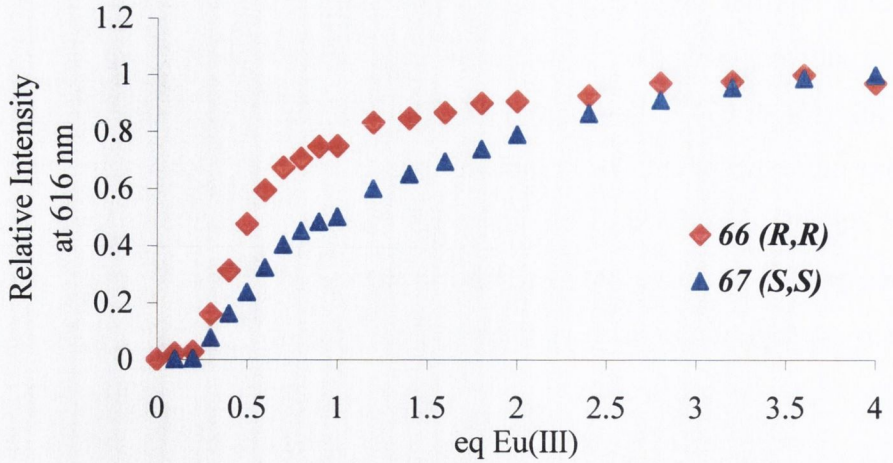

Figure 4.37 Luminescence changes at 616 nm for ligand 66 (*R,R*) (♦) and ligand 67 (*S,S*) (▲) with $Eu(NO_3)_3$ using method B in CH_3CN.

The UV-Visible and luminescence data for both ligands and Eu^{III} salts (perchlorate and nitrate) were fitted with a non-linear least-squares regression programme, SPECFIT. The log *K* values obtained are presented in Table 4.5 and 4.6.

Table 4.5 Complexation constants, log (K/dm^3 mol^{-1}) values for the complexation of $Eu(ClO_4)_3$ with ligand 66 *(R,R)* and 67 *(S,S)* in CH_3CN at 298.2 K, calculated from the absorbance and luminescence titration data (method B).

PERCHLORATE		
Absorbance data		
Species	**log *K* - *(R,R)* isomer**	**log *K* - *(S,S)* isomer**
EuL	> 7 (8.16)	6.66 ± 0.11
EuL_2	> 7 (7.66)	5.57 ± 0.23
Eu_2L	–	–
Eu_2L_2	–	5.23 ± 0.29
Eu_2L_3	–	–
Luminescence data		
EuL	> 7 (8.76)	> 7 (7.27)
EuL_2	> 7 (7.58)	5.58 ± 0.26
Eu_2L	–	–
Eu_2L_2	–	5.87 ± 0.35
Eu_2L_3	–	–

Table 4.6 Complexation constants, log (K/dm^3 mol^{-1}) values for the complexation of $Eu(NO_3)_3$ with ligand 66 *(R,R)* and 67 *(S,S)* in CH_3CN at 298.2 K, calculated from the absorbance and luminescence titration data (method B).

NITRATE		
Absorbance data		
Species	**log K - *(R,R)* isomer**	**log K - *(S,S)* isomer**
EuL	6.68 ± 0.21	6.38 ± 0.55
EuL_2	4.94 ± 0.21	5.67 ± 0.48
Eu_2L	3.85 ± 0.22	5.26 ± 0.49
Eu_2L_2	> 7 (8.20)	> 7 (7.55)
Eu_2L_3	–	–
Luminescence data		
EuL	6.57 ± 0.37	5.39 ± 0.49
EuL_2	4.55 ± 0.15	6.40 ± 0.21
Eu_2L	3.44 ± 0.12	5.66 ± 0.20
Eu_2L_2	> 7 (7.90)	6.10 ± 0.39
Eu_2L_3	–	–

A comparison between the log K values for the two isomers, **66** and **67**, showed that the trend towards higher stability constants for the **(*R,R*)** isomer compared with the **(*S,S*)** isomer, previously observed with the triflate, was also maintained using perchlorate and nitrate as the counterions. This was also evident from the titration profiles shown in Figures 4.36 and 4.37 for the luminescence emission at 616 nm for the two isomers. However, when the results from the titrations using perchlorate or nitrate as the counterions are compared to the corresponding values for the triflate salt (*cf.* Table 4.1 and 4.2), it is clear that the counterion is influencing the stability constants of the metal complexes formed in solution. Perchlorate is the least coordinating anion and therefore provides very high stability constants for the mononuclear species EuL and EuL_2. This has a very large effect on the stability of the other Eu^{III} complexes and hence on their speciation in solution. Owing to the fact that the log K values for the EuL and EuL_2 species were so high, the data derived from titration in the presence of $Eu(ClO_4)_3$ could only be fitted to the following complexation models; 1:1 (EuL), 1:2 (EuL_2) for the **(*R,R*)** isomer; 1:1 (EuL), 1:2 (EuL_2), 2:2 (Eu_2L_2) for the **(*S,S*)** isomer. The difference between the two isomers can be ascribed to the lower stability constants of the **(S,S)** isomer, which allowed the formation of the Eu_2L_2 species. Conversely, nitrate is a more coordinating anion than triflate therefore lower stability constants were expected. This was proven to be the case, as evidenced by the log K values in Table 4.6 (*cf.* Table 4.1 for triflate). The data collected from the titrations with $Eu(NO_3)_3$ were fitted to the following complexation model; 1:1

(EuL), 1:2 (EuL_2), 2:1 (Eu_2L), 2:2 (Eu_2L_2). It should be noted that with both perchlorate and nitrate, the UV-Visible and luminescence data could not be fitted for the Eu_2L_3 species.

In conclusion, it can be stated that the use of Eu^{III} as a triflate salt represents a good compromise towards the formation of the dimetallic triple-stranded helicate in CH_3CN. With triflate the complexation model accounts for all the species (EuL, EuL_2, Eu_2L, Eu_2L_2 and Eu_2L_3), the monometallic species being less stable than with perchlorate thus allowing the formation of the dimetallic complexes. Conversely, a more coordinating anion, like nitrate, can prevent the formation of the desired Eu_2L_3, as the nitrate is able to fulfil the coordination sphere of the lanthanide ions in the Eu_2L_2 complex.

4.8 Speciation and data fit

The metal complex ion stability constants can be used to calculate the concentration of all species present in solution at any concentration of Eu^{III}. The concentration of the species is expressed as a percentage relative to the total amount of ligand present in solution. The speciation diagrams for the various Eu^{III} complexes formed for ligands **66** ***(R,R)*** and **67** ***(S,S)*** in CH_3CN and the speciation diagram for ligand **67** ***(S,S)*** in $CH_3CN/CHCl_3$ (50:50, v/v), all derived from the UV-Visible absorption titrations with **method B**, are shown in Figures 4.38, 4.40, 4.42, respectively. In Figures 4.39, 4.41, 4.43, the changes observed in the corresponding absorbance data at 320 nm are shown along with the fitted data obtained from SPECFIT.

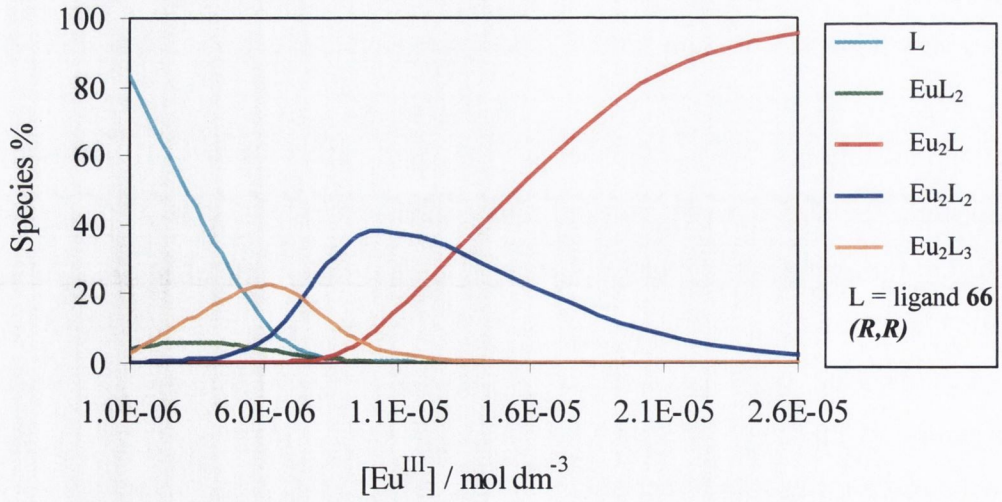

Figure 4.38 Speciation variation of ligand 66 (R,R) derived from UV-Vis data, showing the species present in CH_3CN at various $Eu(CF_3SO_3)_3$ concentrations in which [66] = 1.0 × 10-5 M at 298.2 K. Speciation is shown relative to the total concentration of ligand 66.

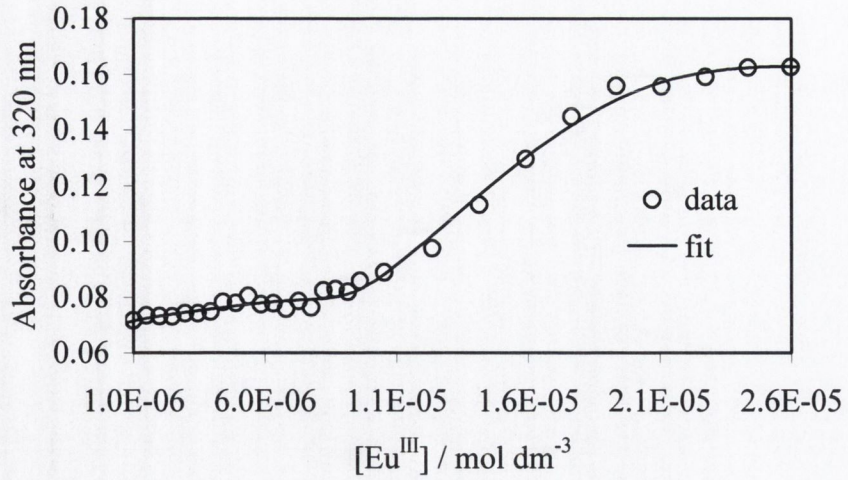

Figure 4.39 Experimental binding isotherm for the UV-Visible absorption titration of ligand 66 *(R,R)* with $Eu(CF_3SO_3)_3$ in CH_3CN at 298.2 K (○) and corresponding fitting from SPECFIT (continuous line).

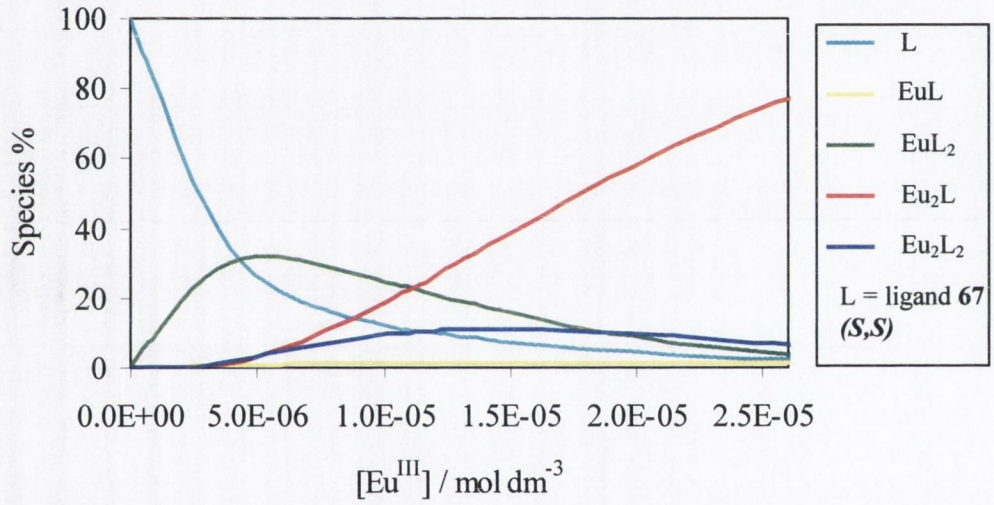

Figure 4.40 Speciation variation of ligand 67 *(S,S)* derived from UV-Vis data, showing the species present in CH_3CN at various $Eu(CF_3SO_3)_3$ concentrations in which [67] = 1.0 × 10^{-5} M at 298.2 K. Speciation is shown relative to the total concentration of ligand 67.

The main difference in the speciation diagrams for the two isomers lies in the Eu_2L_3 species, which is only present for the ***(R,R)*** isomer. This can be ascribed to the lower stability constants for the precursor of this species, Eu_2L_2, for ligand **67** ***(S,S)***. The monometallic species EuL forms only in very low percentage for the ***(R,R)*** isomer, so low that it is not visible in the diagram. Also, the EuL_2 complex is present in a much higher percentage in the ***(S,S)*** isomer than in the ***(R,R)***. However, for both isomers the predominant species in the presence of excess of Eu^{III} is the Eu_2L complex.

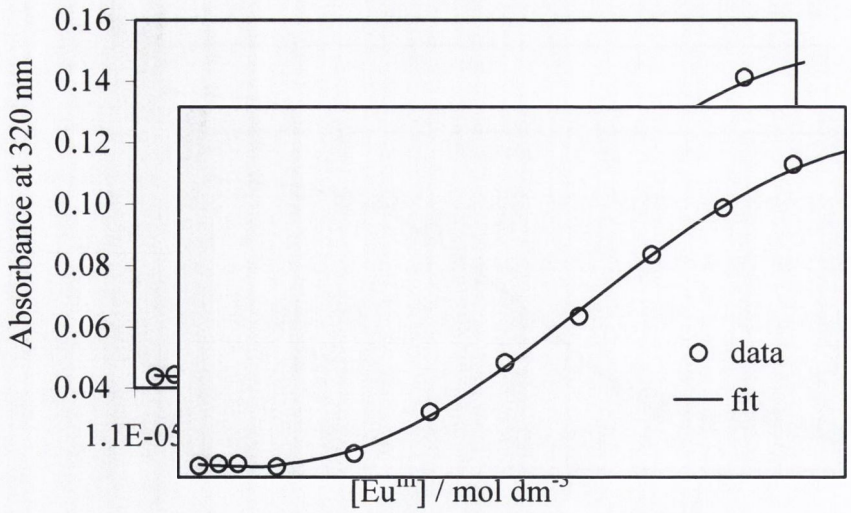

Figure 4.41 Experimental binding isotherm for the UV-Visible absorption titration of ligand 67 *(S,S)* with $Eu(CF_3SO_3)_3$ in CH_3CN at 298.2 K (○) and corresponding fitting from SPECFIT (continuous line). In order to minimise the experimental error associated with the log *K* calculated, data points below [Eu^{III}] = 1.1 × 10-5 M were excluded from the fitting, as below this concentration, no spectral changes were observed.

From Figure 4.39 and 4.41, it is clear that the experimental data obtained from the UV-Visible titration in CH_3CN and the fitted data obtained from SPECFIT are in good agreement for both isomers.

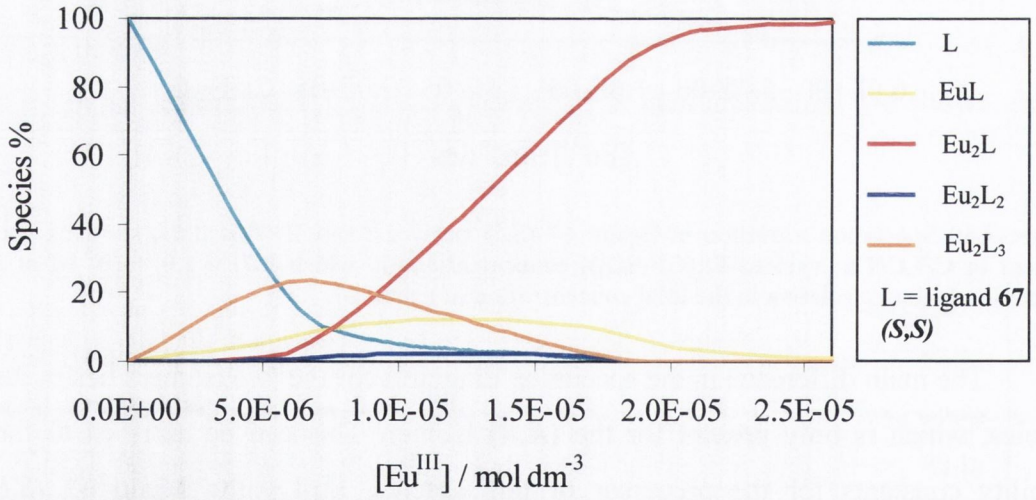

Figure 4.42 Speciation variation of ligand 67 *(S,S)* derived from UV-Vis data, showing the species present in $CH_3CN/CHCl_3$ (50:50, v/v) at various $Eu(CF_3SO_3)_3$ concentrations in which [67] = 1.0 × 10^{-5} M at 298.2 K. Speciation is shown relative to the total concentration of ligand 67.

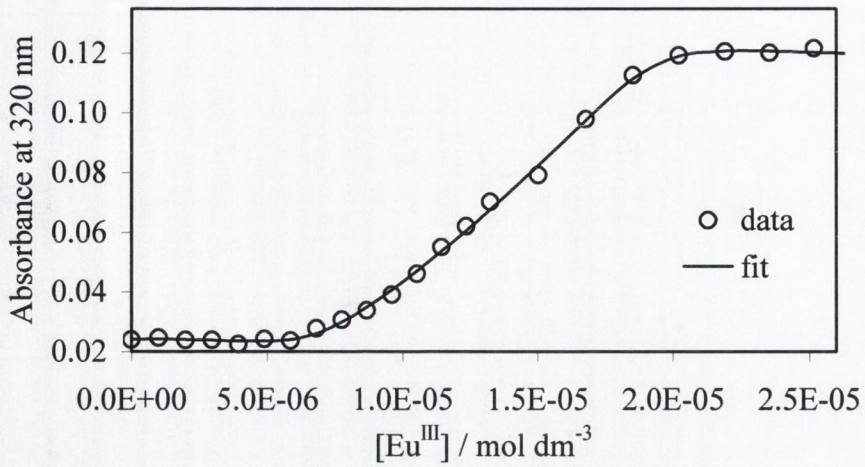

Figure 4.43 Experimental binding isotherm for the UV-Visible absorption titration of ligand 67 *(S,S)* with $Eu(CF_3SO_3)_3$ in $CH_3CN/CHCl_3$ (50:50, v/v) at 298.2 K (○) and corresponding fitting from SPECFIT (continuous line).

The speciation diagram for ligand **67** ***(S,S)***, derived from the stability constants corresponding to the UV-Visible titration in $CH_3CN/CHCl_3$ (50:50, v/v), shows the presence of the Eu_2L_3. Therefore, it is possible to conclude that a less polar solvent system (*i.e.* less competitive in the coordination of the Eu^{III} metal ions) aids the formation of the desired Eu_2L_3 species.

Figures 4.44-4.45 illustrate the speciation diagrams for the various Eu^{III} complexes formed for ligand **67** ***(S,S)*** in CH_3CN, derived from the UV-Visible absorption titrations with $Eu(ClO_4)_3$ and $Eu(NO_3)_3$, respectively.

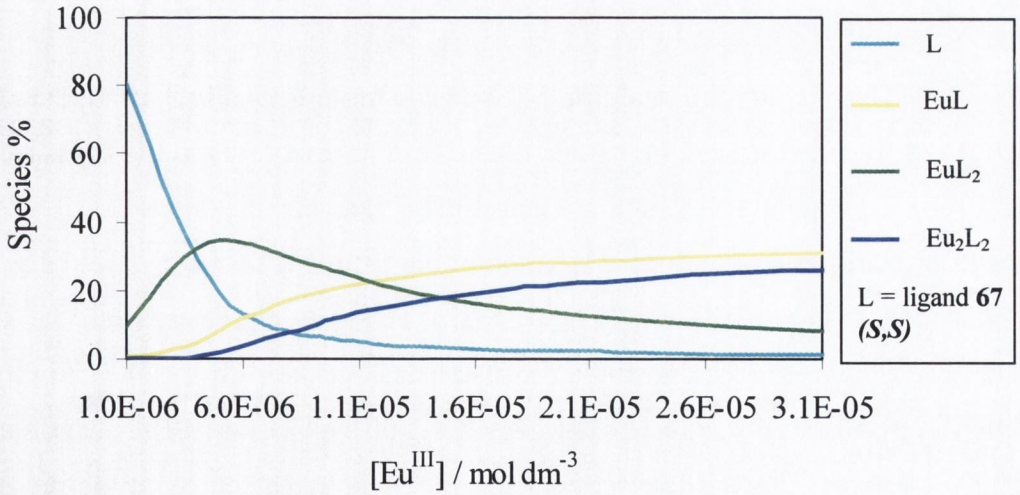

Figure 4.44 Speciation variation of ligand 67 *(S,S)* derived from UV-Vis data, showing the species present in CH_3CN at various $Eu(ClO_4)_3$ concentrations in which [67] = 1.0 × 10^{-5} M at 298.2 K. Speciation is shown relative to the total concentration of ligand 67.

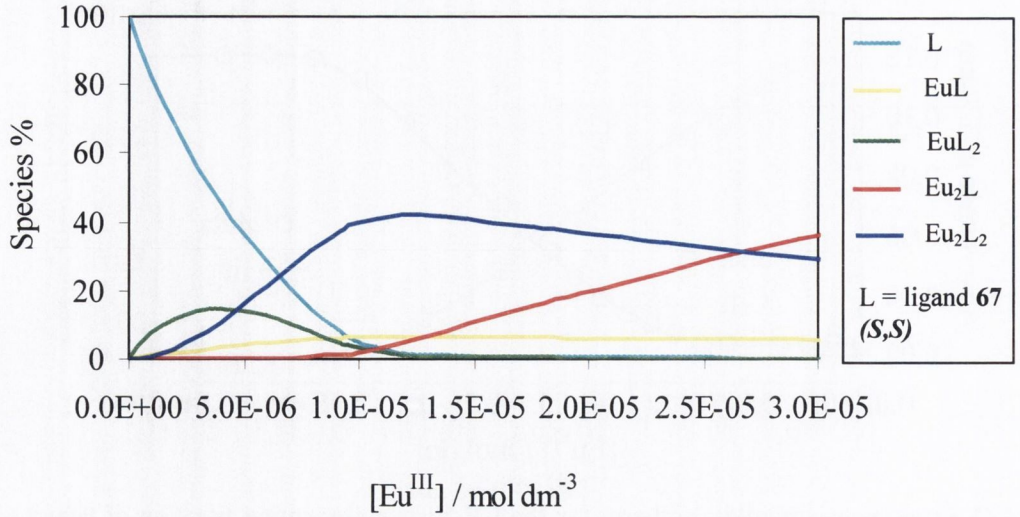

Figure 4.45 Speciation variation of ligand 67 *(S,S)* derived from UV-Vis data, showing the species present in CH_3CN at various $Eu(NO_3)_3$ concentrations in which [67] = 1.0 × 10^{-5} M at 298.2 K. Speciation is shown relative to the total concentration of ligand 67.

As anticipated from the examination of the stability constants for ligand **67**, titration with $Eu(ClO_4)_3$ leads mainly to the formation of the monometallic species EuL and EuL_2, the dimetallic species Eu_2L_2 forming in the lowest percentage (*cf.* Figure 4.44). This may be ascribed to the non-coordinating features of the perchlorate ion. Conversely, as evidenced by the diagram in Figure 4.45, the dimetallic complex Eu_2L_2 is the major species in the case of the titration with $Eu(NO_3)_3$, whereas the monometallic species form only in small amounts (EuL less than 10%, EuL_2 *ca.*17 %).

4.9 Conclusions

In this chapter the formation of the dinuclear triple helical Eu^{III} complexes **74 (*R,R*)** and **75 (*S,S*)** has been studied in organic media with a variety of spectroscopic techniques. The ^{1}H-NMR titration experiments demonstrated that complexation in $CD_3CN/CDCl_3$ (50:50) was fully achieved after the addition of 0.6 equiv. of $Eu(CF_3SO_3)_3$ to a solution of either of the two ligands **66 (*R,R*)** or **67 (*S,S*)**. This was consistent with the 2:3, Eu:L stoichiometry of the desired dimetallic triple stranded helicates Eu_2L_3. The chirality of both the ligands and the Eu^{III} complexes was confirmed by CD and CPL measurements. In particular, the CPL spectra displayed strong effects in agreement with the presence of a large excess of only one helical diastereoisomer (*P* or *M*) in solution. This also confirmed that the observation of only one set of signals in the ^{1}H-NMR spectrum could be ascribed

to the presence of only one helical species in solution, rather than to a fast $P \rightleftharpoons M$ interconversion on the NMR time scale.

Job's method (or method of continuous variations) was used to assess the stoichiometry of the complexes in solution, which was shown to be 2:3, Eu:L (**66** or **67**) in both CH_3CN and in $CH_3CN/CHCl_3$ (50:50) solutions.

The UV-Vis and luminescence behaviour of both isomers **66** (***R,R***) and **67** (***S,S***) was evaluated through metal ion complexation studies in CH_3CN and in $CH_3CN/CHCl_3$ (50:50) solution. The measurements were carried out using two different methods, **method A** and **method B**. The results obtained from these two methods highlighted that the kinetics of the complexation process plays a very important role, suggesting that, allowed to equilibrate, only the most stable species are detected in solution.

Moreover, determination of the metal complex ion stability constants delineated a difference in stability between the two isomers. Hence it was established that the (***R,R***) isomer formed more stable complexes than the (***S,S***) isomer. Such a difference was not encountered in the ^{1}H-NMR studies, suggesting that a highly sensitive technique is required to detect the different behaviour between the two isomers. Only by UV-Vis and luminescence studies (~ 10^{-5} M), the influence of the chirality of the ligands on the formation of the Eu^{III} complex species, becomes detectable. The difference in stability constants implies the presence of different metal complex species for the two isomers in solution, as illustrated in detail by the speciation diagrams (see Section 4.8). It was found that only the (***R,R***) isomer form the desired Eu_2L_3 species in CH_3CN, whereas both isomers form the triple helicates in $CH_3CN/CHCl_3$ (50:50).

In addition, the change in the polarity of the solvent used in the UV-Vis and luminescence measurements, *i.e.* CH_3CN vs $CH_3CN/CHCl_3$ (50:50), had a significant effect on the formation of the Eu^{III} complex species, that is, the lower the polarity the higher the stability constants. Furthermore, in less polar media, such as $CH_3CN/CHCl_3$ (50:50) solution, the difference in stability between the metal complexes formed by the two isomers is significantly reduced.

Finally, the effect of the counterion on the stability constants of the metal complex species was investigated. UV-Vis and luminescence titrations in CH_3CN were carried out with three different anions; triflate, perchlorate and nitrate. The corresponding metal complex ion stability constants showed that the counterion has a large influence on the formation of the species present in solution. By analysis of the results, triflate was shown

to be the best compromise towards the formation of the desired dimetallic triple helicate species Eu_2L_3.

Based on the observations detailed in Chapter 3 and Chapter 4, it is possible to conclude that both ligands **66** (***R,R***) and **67** (***S,S***) form the desired triple helicates in the presence of Eu^{III}, although definitive proof can come only from an X-ray crystal structure analysis of the complexes. However, to date, no crystals suitable for X-ray structural analysis have been successfully isolated. Moreover, formation of such helical complexes is affected by the time scale of the experiment, the polarity of the solvent and the counterion. Also, the chirality of the ligands has a significant effect on the helicate formation at low concentration.

4.10 Future work

With the aim of further investigating the formation of supramolecular self-assemblies in the presence of luminescent lanthanide ions, the simple synthetic strategy employed for the preparation of ligands **66** and **67** may be exploited to develop new families of ligands. A good basis for future investigations would be provided by enhancing the flexibility of the ligands, or inducing more rigidity, by incorporating a variety of functional groups in the ligand structure (*e.g. via* functionalisation of the 4-position of the pyridyl unit), or by modifying the *antenna*. Future studies should focus on the design of these ligands and on the role that different functional groups play in altering the thermodynamic and the kinetic stability of the resulting supramolecular assemblies. Such modifications could lead to systems which are highly selective towards target species. Moreover, the incorporation of hydrophilic groups would increase the water solubility of these systems, which may aid the development of novel biological probes.

5 EXPERIMENTAL

5.1 General experimental details

All chemicals were obtained from Sigma-Aldrich, Fluka, Lancaster or Acros Organics and unless specified, were used without further purification. Deuterated solvents for NMR use were purchased from Apollo. Dry solvents were prepared using standard procedures, according to Vogel,[209] with distillation prior to each use. Chromatographic columns were run using Silica gel 60 (230-400 mesh ASTM) or Aluminum Oxide (activated, Neutral, Brockmann I STD grade 150 mesh). Solvents for synthesis purposes were used at GPR grade unless otherwise stated. Analytical TLC was performed using Merck Kieselgel 60 F_{254} silica gel plates or Polygram Alox N/UV_{254} aluminium oxide plates. Visualisation was by UV light (254 nm), by exposure to iodine vapour, immersion in aqueous alkaline $KMnO_4$ solution, or with 2% ninhydrin in ethanol spray reagent. NMR spectra were recorded using a Bruker DPX-400 Avance spectrometer, operating at 400.13 MHz and 600.1 MHz for ^{1}H-NMR and 100.6 MHz and 150.9 MHz for ^{13}C-NMR. Shifts are referenced relative to the internal solvent signals. NMR data were processed using Bruker Win-NMR 5.0 software. Electrospray mass spectra were recorded on a Mass Lynx NT V 3.4 on a Waters 600 controller connected to a 996 photodiode array detector with HPLC-grade methanol, water or acetonitrile as carrier solvents. Accurate molecular weights were determined by a peak-matching method, using leucine enkephaline (H-Tyr-Gly-Gly-Phe-Leu-OH) as the standard internal reference (m/z = 556.2771); all accurate mass were calculated to $\leq$ 5 ppm. Samples were prepared as solutions in methanol, acetonitrile or water. Melting points were determined using an Electrothermal IA9000 digital melting point apparatus. Infrared spectra were recorded on a Mattson Genesis II FTIR spectrometer equipped with a Gateway 2000 4DX2-66 workstation and on a Perkin Elmer Spectrum One FT-IR Spectrometer equipped with Universal ATR sampling accessory. Oils were analysed using NaCl plates; solid samples were dispersed in KBr and recorded as clear pressed discs or as neat samples. Elemental analysis was carried out at the Microanalysis Laboratory, School of Chemistry and Chemical Biology, University College Dublin.

5.2 General physical methods

Deionised water that had been purified with the MilliQ-Reagent system to produce water with a specific resistance of >15 MΩ cm^{-1}, boiled for 30 min to remove CO_2, and cooled under a drying tube filled with soda lime, was used in the preparation of all aqueous solutions.

The metal salts $Eu(ClO_4)_3$, $Eu(CF_3SO_3)_3$, $Tb(CF_3SO_3)_3$, $Sm(CF_3SO_3)_3$, $Eu(NO_3)_3$ were purchased from Aldrich and the lanthanide triflate and nitrate salts were dried under high vacuum over P_2O_5.

Tetraethylammonium perchlorate (NEt_4ClO_4) was prepared by addition of excess $HClO_4$ (1.0 M, 1.7 dm^3) to NEt_4Br (300 g, 1.4 mol) in H_2O. The resulting NEt_4ClO_4 was recrystallised from perchloric acid (1.0 M, 100 ml) and ethanol (3 × 150 mL) until free of bromide and acid. The white crystalline NEt_4ClO_4 was then dried under high vacuum over P_2O_5 for 2 days. (CAUTION: Anhydrous perchlorates are potentially explosive and should be handled with caution).

The ligands used were prepared as described in Chapter 2 and Chapter 3 and they were dried over P_2O_5 under vacuum for a minimum of 6 hrs prior to use.

5.3 Potentiometric titrations

Potentiometric titrations were performed using an automatic titrator system, MOLSPIN, equipped with a glass electrode (Orion Ross Sureflow 81-72 BN combination electrode) and connected to a Dell PC. The titrations were carried out at 298.2 ± 0.1 K in a water-jacketed vessel. Argon was bubbled firstly through a 1 M KOH solution and then through a solution of 0.1 M NEt_4ClO_4. Dry Argon was then bubbled through the cell to exclude CO_2 and O_2. Milli-Q water and NEt_4ClO_4 were prepared as described in Section 5.2. The solutions used for the measurements described in Chapter 2 were prepared using 100% water with constant ionic strength I = 0.1 M (NEt_4ClO_4). The solutions for the experiments detailed in Chapter 3 were prepared in an acetonitrile/water solvent system (80:20; v/v), with constant ionic strength, I = 0.1 M (NEt_4ClO_4).

The glass electrode was calibrated daily by titrating 0.1 M NEt_4OH with 10 cm^3 of a solution of 0.1 M NEt_4ClO_4 and 0.0065 M $HClO_4$. The resulting data was fitted to the Nernst equation to determine E_0 and pK_w, Equation 5.1.

$$E = E_0 + \frac{RT}{F} \ln [H^+] \quad \textbf{(5.1)}$$

where E = observed potential (V)

E_0 = standard electrode potential (V)

R = gas constant (8.314 J mol^{-1} K^{-1})

T = temperature (K)

F = Farady's constant (9.6487×10^4 Coulombs mol^{-1})

At 298.2 K, with E in millivolts and converting to logarithm base 10:

$$pH = \frac{(E_0 - E)}{59.15} \quad \textbf{(5.2)}$$

where E = observed potential (mV)

$pH = - \log [H^+]$

and

$$pK_w = \frac{(E_0 - E)}{59.15} + pOH \quad \textbf{(5.3)}$$

The program GLEE was used to calculate the endpoint of the titration (and hence the exact concentration of H^+ used) and the calibration parameters E_0 and pK_w. At least two titrations were performed for each system. The protonation constants were determined by the titration of NEt_4OH with a 10 cm^3 solution of a ligand and $HClO_4$. The NEt_4OH (~ 0.1 M or 0.2 M) was previously standardised against potassium hydrogen phthalate. The concentration of the ligand of interest and $HClO_4$ in solution varied for each ligand; the following concentrations were used [ligand, ($HClO_4$), (NEt_4OH)]: [**51**, 6.4×10^{-4} M (6.5×10^{-3} M), (0.103 M)], [**64**, 8.91×10^{-4} M (3.49×10^{-3} M), (0.096 M)], [**65**, 7.00×10^{-4} M (3.48×10^{-3} M), (0.096 M)], [**66**, 1.00×10^{-3} M (7.91×10^{-3} M), (0.188 M)], [**67**, 1.18×10^{-3} M (6.50×10^{-3} M), (0.096 M)].

The determination of the metal complex ion stability constants for each ligand was carried out by addition of a metal salt solution (varying concentration) to the acidified titration solution. [ligand, (Eu^{III}), ($HClO_4$), (NEt_4OH)]: [**51**, 6.4×10^{-4} M, [$Eu(CF_3SO_3)_3$] 6.4×10^{-4} M, (6.5×10^{-3} M), (0.103 M)], [**51**, 6.4×10^{-4} M, [$Eu(ClO_4)_3$] 6.4×10^{-4} M, (6.5×10^{-3} M), (0.103 M)], [**66**, 1.00×10^{-3} M, [$Eu(CF_3SO_3)_3$] 1.00×10^{-3} M, (7.91×10^{-3} M), (0.188 M)], [**66**, 1.00×10^{-3} M, [$Eu(CF_3SO_3)_3$] 5.00×10^{-4} M, (7.91×10^{-3} M), (0.188 M)], [**67**, 1.18×10^{-3} M, [$Eu(CF_3SO_3)_3$] 1.00×10^{-3} M (6.50×10^{-3} M), (0.096 M)], [**67**, 1.18×10^{-3} M, [$Eu(CF_3SO_3)_3$] 5.00×10^{-4} M (6.50×10^{-3} M), (0.096 M)].

By means of the MOLSPIN Autoburette, constant volume aliquots of the titrant were delivered during the titrations, during which the emf decreased by a maximum of 5 mV. For all titrations a maximum delay of 100 seconds between each titrant addition was sufficient for equilibrium to be established. The stability constants for each metal complex ion were determined by means of the FORTRAN program HYPERQUAD.[141] The final constants represent an average from two calculated titrations where the chi-squared (χ^2) of each run was less than 12.6 at the 95% confidence level.

5.4 Ultraviolet-visible spectroscopy

UV-visible absorption spectra were recorded by means of a Varian CARY 50 spectrophotometer. The solvents used were of HPLC grade. The wavelength range was 220-450 nm with a scan rate of 600 nm min^{-1}. The blank used was different depending on the compound under study:

- H_2O, 0.1 M NEt_4ClO_4 for titrations described in Chapter 2;
- CH_3CN/H_2O (80:20; v/v), 0.1 M NEt_4ClO_4, for titrations described in Chapter 3;
- CH_3CN or $CH_3CN/CHCl_3$ (50:50, v/v), for titrations described in Chapter 4.

Baseline correction measurements were used for all spectra. All solutions were equilibrated at 298.2 ± 0.2 K in a thermostated block throughout the measurements. The concentration of the ligand solution was 5×10^{-5} M, for the titrations described in Chapter 2, and 10^{-5} M for the experiments in Chapter 3 and Chapter 4. All solutions were prepared freshly prior to measurement, except for the measurements carried out with method A described in Chapter 4.

5.5 Fluorescence and luminescence measurements

Fluorescence and luminescence measurements were made with a Varian Carey Eclipse Fluorimeter equipped with a 1.0 cm path length quartz cell. The solvents used were of HPLC grade. For the fluorescence titrations, data was obtained between 332 and 500 nm (Chapter 2) or between 300 and 400 nm (Chapter 3). As for the luminescence titrations, data was collected between 560 and 720 nm. All solutions were equilibrated at 298.2 ± 0.2 K in a thermostated block throughout the measurements. The concentrations of the ligands and complexes investigated were the same as those used for the UV-visible absorption measurements (Section 5.4). The settings of the fluorimeter for the fluorescence and luminescence measurements, carried out in Chapters 2-4, are reported in Tables 5.1-5.4.

Table 5.1 Fluorescence settings for titrations in Chapter 2 (100% H_2O with constant ionic strength I = 0.1 M, NEt_4ClO_4)

Fluorescence Settings	
Mode: Fluorescence	**Excitation**: 330 nm
Flash count: 1	**Scan**: 332-500 nm
Scan Control: medium	**PMT Voltage**: Medium
Excitation slit width: 10 nm	**Emission slit width**: 5 nm

Table 5.2 Luminescence settings for titrations in Chapter 2 (100% H_2O with constant ionic strength I = 0.1 M, NEt_4ClO_4)

Luminescence Settings	
Mode: Phosphorescence	**Excitation**: 330 nm
Total Decay: 0.02 ms	**Scan**: 560-720 nm
Flash: 1	**Delay**: 0.1 ms
Gate: 10 ms	**PMT Voltage**: High
Excitation slit width: 10 nm	**Emission slit width**: 5 nm

Table 5.3 Fluorescence settings for titrations in Chapter 3 (CH_3CN/H_2O (80 : 20, v/v) with constant ionic strength I = 0.1 M, NEt_4ClO_4)

Fluorescence Settings	
Mode: Fluorescence	**Excitation**: 281 nm
Flash count: 1	**Scan**: 300-450 nm
Scan Control: medium	**PMT Voltage**: 700 V
Excitation slit width: 10 nm	**Emission slit width**: 10 nm

Table 5.4 Luminescence settings for titrations in Chapter 3 (CH_3CN/H_2O (80 : 20, v/v) with constant ionic strength I = 0.1 M, NEt_4ClO_4) and Chapter 4 (CH_3CN or $CH_3CN/CHCl_3$ (50 : 50, v/v))

Luminescence Settings	
Mode: Phosphorescence	**Excitation**: 281 nm
Total Decay: 0.02 ms	**Scan**: 560-720 nm
Flash: 1	**Delay**: 0.1 ms
Gate: 10 ms	**PMT Voltage**: High
Excitation slit width: 5 nm	**Emission slit width**: 5 nm

5.6 Lifetime determination for Eu^{III} complexes

Luminescence lifetime measurements of **Eu.51** were carried out in H_2O and D_2O at neutral pH, on a Varian Carey Eclipse Fluorimeter. Lifetime measurements of **74 (R,R)** and **75 (S,S)** were carried out in CH_3CN/H_2O (80 : 20, v/v) and CD_3CN/D_2O (80 : 20, v/v). The settings for the Varian Carey Eclipse Fluorescence spectophotometer are displayed below.

Lifetime Settings

Direct excitation: Eu^{III} – 395 nm
Emission: Eu^{III} – 615 nm

No. Cycles: 1000	**Total Decay**: 10 ms
Flash: 1	**Delay**: 0.1 ms
Gate: 0.1 ms	**PMT Voltage**: High
Excitation slit width: 10 or 20 nm	**Emission slit width**: 10 or 20 nm

5.7 Determination of Equilibrium Water Content of hydrogel sensor materials

Complex-incorporated hydrogel films prepared with different ratios of HEMA and MMA were cut (1cm x 1cm) in their water-swollen state. The samples were dehydrated at 60 °C to constant weight. The samples were then immersed in deionised water and reweighed, following gentle removal of excess surface water with a tissue, at intervals until a constant weight was achieved. All measurements were made in triplicate and values are quoted as the mean ± 1 standard deviation. The equilibrium water content (EWC), defined as a ratio of the mass of water taken up to the mass of dry sample, was calculated using the following equation:

$$\textbf{EWC (\%)} = \frac{\text{mass of hydrated sample} - \text{mass of dehydrated sample}}{\text{mass of dehydrated sample}} \times 100$$

5.8 Luminescence measurements of hydrogel sensor materials

Confocal laser scanning microscopic (CLSM) examination of hydrogel samples was carried out with a Leica TCS SP2 confocal laser scanning microscope in the School of Pharmacy at Queen's University Belfast. After focusing, the sample surface was excited using the 458 nm line from a Ar/ArKr laser and luminescence data collected over the range 500-800 nm. Luminescence emission micrographs show summed photomultiplier

intensities across the full wavelength range detected with a look-up table assigning color to overall intensity ranging from black (zero intensity) to bright red (highest intensity). Increasing itermediate intensities are shown with increasing shades of red. Steady-state fluorescence measurements were recorded on a Varian Carey Eclipse Fluorimeter using a modified quartz cell.

5.9 CD measurements

CD spectra were recorded in MeOH on a Jasco J-810-150S spectropolarimeter. All CD spectra are represented as mdeg *vs* λ (nm). The baseline of the solvent was taken and removed from all spectra shown.

5.10 CPL measurements

Circularly polarised luminescence spectra were recorded at the University of Glasgow. Excitation of the Eu^{III} (560-581 nm) was accomplished by using a Coherent 599 tunable dye laser (0.03 nm resolution) with an argon ion laser as a pump source. The laser dye used in the measurement was Rhodamine 110 in ethylene glycol. Calibration of the emission monochromator (and subsequently the dye laser) was accomplished by passing scattered light from a low power He-Ne laser through the detection system. The error in the dye laser wavelength was assumed to be equal to the resolution of the emission detection. The optical detection system consisted of a photoelastic modulator (PEM, Hinds Int.) operating at 50 kHz and a linear polariser, which together act as a circular analyser, followed by a long pass filter, focusing lens and a 0.22 m double monochromator. The emitted light was detected by a cooled EM1-9558QB photomultiplier tube operating in photon counting mode. The output pulses from the photomultiplier tube were passed through a variable gain amplifier/ discriminator and input into a specially built differential photon counter. The 50 KHz reference signal from the photoelastic modulator was used to direct the incoming pulses into two separate counters, an up-counter, which counts every photon pulse and thus is a measure of the total luminescence signal $I = I_{left} + I_{right}$, and an up/down counter, which adds pulses when the analyser is transmitting left circularly polarised light and subtracts when the analyser is transmitting right circularly polarised light. This second counter provides a measure of the differential emission intensity $\Delta I = I_{left} - I_{right}$. The differential photon counter allows for the selection of a time window for

counting, which is centred around the maximum in the modulation cycle. For the measurements reported in this thesis, the window was set to 50%.

5.11 Molecular mechanics modelling studies

Molecular mechanics calculations were undertaken with Hyperchem Version 7.52. Molecular mechanics calculations were carried out using MM+ with the Polak-Ribiere algorithm of Hyperchem. The target configuration was arranged roughly by eye and the energy minimised at an RMS gradient of 0.01. Molecular dynamics was also used (simulated heating at 100 K) to ensure that the true energy minima had been reached. Guided by elemental analysis and ^{1}H-NMR, UV-visible and luminescence spectroscopic data, the modelling studies were limited to dinuclear species of general formula $[Eu_2L_3]^{6+}$ of *rac*- and *meso*-configuration. The energy structures for the *rac*-configurations of the (*R,R*) and (*S,S*) isomers minimised to a lower energy than the corresponding *meso*-configuration.

5.12 General synthetic procedures for Chapter 2

5.12.1 Procedure 1: primary and secondary amine substitution reactions

Chloro-1,8-naphthalimide derivative (1 equiv.) was suspended in an excess of amine. The resulting solution was heated to 80 °C for 12 h. The product was precipitated out by pouring the resulting mixture onto an iced water solution with vigorous stirring. The product was filtered off and washed with 1 N HCl solution. No further purification was necessary.

5.12.2 Hydrogel preparation for 43 and 44

Crosslinked poly[methylmethacrylate-*co*-2-(hydroxyethylmethacrilate)] hydrogels were prepared by stirring a mixture of methylmethacrylate (7.35 g), 2-(hydroxyethylmethacrylate) (2.45 g), ethyleneglycol dimethacrylate (0.1 g), azo-bis-isobutyronitrile (0.1g) and either sensor **6** or **7** (0.005 g) until dissolution was complete, followed by injection of the monomer mixture into a 1 mm mould with release liner. The mould was heated at 90°C for 6 hours and the resulting material washed 3 times with deionised water.

5.12.3 Hydrogel preparation for Eu.51

Crosslinked poly[methylmethacrylate-*co*-2-(hydroxyethylmethacrylate)] hydrogels were prepared by stirring a mixture of methylmethacrylate (5.0 or 2.45g), 2-(hydroxyethylmethacrylate) (5.0 or 7.35g respectively), ethyleneglycol dimethacrylate (0.1 g), benzoyl peroxide (0.1 g) and **Eu.51** (0.005 g) until dissolution was complete. The same procedure was followed in preparing crosslinked poly(2(hydroxyethylmethacrylate)) (pHEMA), but in this case crosslinker, initiator and europium complex were added to 9.8 g of HEMA. For all hydrogel compositions, the homogeneous solutions, prepared as above described, were then injected into a 1 mm mould with release liner. The mould was heated at 90 °C for 4 hours and the resulting material washed with deionised water. The hydrogel films obtained were then soaked in deionised water.

5.13 Experimental details for Chapter 2

***N*-(1- Methoxycarbonyl-methyl)-4-chloro-1,8-naphthalimide (46)**

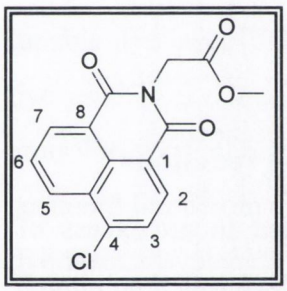

Glycine methyl ester hydrochloride (1.6 g, 12.7 mmol), 4-chloro-1,8-naphthalic anhydride (2 g, 8.6 mmol) and triethylamine (1.3 g, 1.8 ml, 12.7 mmol) were refluxed in toluene (100 ml). After filtration through celite the mixture was reduced to dryness under reduced pressure. The resulting residue was dissolved in DCM and washed twice with 1.0 M HCl and once with water. The organic layer was then dried over $MgSO_4$ and the solvent removed under reduced pressure, to give the desired product as a brown crystalline solid after recrystallisation from MeOH (2.0 g), in 77.0 % yield. m.p. 158-159 °C; Calculated for $C_{15}H_{10}NO_4Cl$: $(M+H)^+$ *m/z* = 304.0371; Found: 304.0377; δ_H (400 MHz, $CDCl_3$, 298.2 K) 8.67 (1H, d, *J* = 8.0 Hz, Ar-H7), 8.63 (1H, d, *J* = 8.0 Hz, Ar-H2), 8.48 (1H, d, *J* = 8.0 Hz, Ar-H5), 8.09 (1H, d, *J* = 8.0 Hz, Ar-H3), 8.05 (1H, t, *J* = 8.0 Hz, Ar-H6), 4.84 (2H, s, CH_2), 3.71 (3H, s, OCH_3); δ_c (100 MHz, $CDCl_3$, 298.2 K) 168.4, 163.4, 139.6, 133.7, 132.4, 131.6, 131.5, 131.2, 131.1, 129.4, 129.3, 128.1, 127.9, 127.4, 122.6, 121.1, 52.5, 41.3; m/z: 327.2 $(M + Na)^+$, 630.5 $(2M+ Na)^+$; IR (KBr) υ_{max} (cm^{-1}) 1753, 1702, 1661, 1589, 1216, 1178.

_N_-[1-(2-piperidino-ethyl)-carboxamido-methyl]-4-(2-piperidino-ethylamino)-1,8-naphthalimide (43)

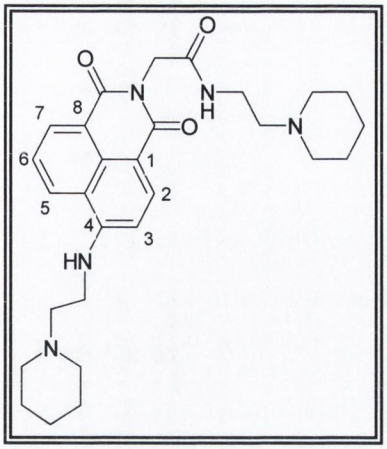

Compound **43** was synthesised by refluxing _N_-(1-methoxycarbonyl-methyl)-4-chloro-1,8-naphthalimide, **46** (0.5 g, 1.6 mmol) in 1-(2-aminoethyl)-piperidine (2 ml) according to **Procedure 1**. The product was isolated after recrystallisation from EtOH as a bright orange powder (0.55g, 74.3 % yield). m.p. 135-136 °C; Calculated for $C_{28}H_{38}N_5O_3$: $(M+H)^+$ *m/z* = 429.2975; Found: 429.2971; δ_H (400 MHz, $(CD_3)_2SO$, 298.2 K) 8.89 (1H, d, *J* = 8.0 Hz, Ar-H7), 8.44 (1H, d, *J* = 8.0 Hz, Ar-H2), 8.31 (1H, d, *J* = 8.0 Hz, Ar-H5), 7.99 (1H, t, *J* = 5.5 Hz, NH), 7.67 (1H, t, *J* = 8.0 Hz, Ar-H6), 7.62 (1H, t, *J* = 5.5 Hz, NH), 6.78 (1H, d, *J* = 8.0 Hz, Ar-H3), 4.62 (2H, s, CH_2CO), 3.51 (2H, q, *J* = 6.5, 6.0 Hz, CH_2), 3.31 (2H, q, *J* = 7.0, 6.0 Hz, CH_2), 2.58 (10H, m, $(CH_2)\times5$), 1.45-1.40 (14H, m, $(CH_2)\times7$); δ_c (100 MHz, $(CD_3)_2SO$, 298.2 K) 166.8, 163.6, 162.7, 150.6, 134.2, 130.6, 129.5, 128.4, 124,2, 121.8, 120.1, 107.5, 103.8, 57.5, 56.4, 54.1, 54.0, 41.9, 40.5, 36.3, 25.5, 25.4, 23.9; IR (KBr) υ_{max} (cm^{-1}) 3396, 3381, 3300, 2937, 1693, 1653, 1589, 1397, 1106.

_N_-[1-(2-morpholino-ethyl)-carboxamido-methyl]-4-(2-morpholino-ethylamino)-1,8-naphthalimide (44)

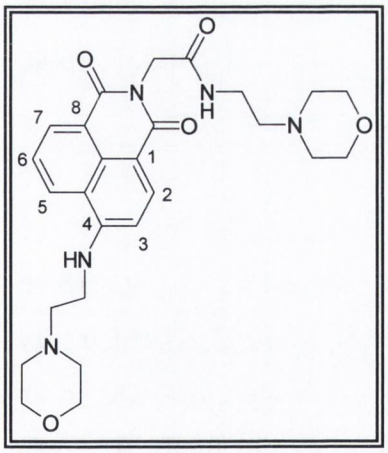

Compound **44** was synthesised by refluxing _N_-(1-methoxycarbonyl-methyl)-4-chloro-1,8-naphthalimide, **46** (0.5 g, 1.6 mmol) in 4-(2-aminoethyl)-morpholine (2 ml) according to **Procedure 1**. The product was isolated after recrystallisation from DMF as a bright orange powder (0.62g, 80% yield). m.p. 242-243 °C; Calculated for $C_{26}H_{33}N_5O_5$: C, 62.76; H, 7.12; N, 14.07 %; Found: C, 62.80; H, 6.69; N, 14.09 %; δ_H (400 MHz, $CDCl_3$, 298.2 K) 8.51 (1H, d, *J* = 8.0 Hz,Ar-H7), 8.40 (1H, d, *J* = 8.0 Hz, Ar-H2), 8.13 (1H, d, *J* = 8.0 Hz, Ar-H5), 7.58 (1H, t, *J* = 8.0 Hz, Ar-H6), 6.62 (1H, d, *J* = 8.0 Hz, Ar-H3), 6.46 (2H, br. s, NH), 4.87 (2H, s, NCH_2), 3.80 (4H, s, $N(CH_2CH_2)_2O$), 3.54 (4H, s, $N(CH_2CH_2)_2O$), 3.42 (4H, br m, $NHCH_2$), 2.84 (2H, t, *J* = 5.5 Hz, CH_2N), 2.60 (4H, br s, $N(CH_2CH_2)_2O$), 2.51 (2H, t, *J* = 5.5 Hz, CH_2N), 2.43 (4H, br s, $N(CH_2CH_2)_2O$); δ_c (100 MHz, $CDCl_3$, 298.2 K) 167.2, 164.0, 163.2, 149.5, 139.2, 137.6, 134,4, 131.0,

129.4, 126.2, 124.3, 121.9, 119.9, 108.9, 1`04.0, 66.6, 66.3, 56.2, 55.6, 52.8, 52.7, 42.6, 38.7,35.2; *m/z*: 495.8 $(M+H)^+$, 517.8 $(M+Na)^+$; IR (KBr) υ_{max} (cm^{-1}) 3374, 3300, 2942, 2825, 1691, 1652, 1588, 1397, 1109.

_N_-[1-(2-buthyl-ethyl)-carboxamido-methyl]-4-(2-buthyl-ethylamino)-1,8-naphthalimide (50)

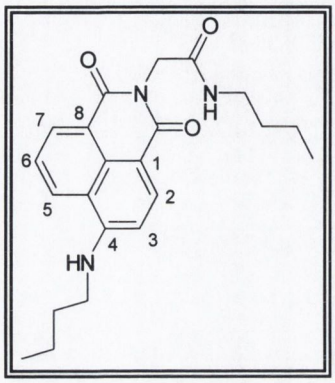

Compound **50** was synthesised by refluxing N-(1-methoxycarbonyl-methyl)-4-chloro-1,8-naphthalimide, 10 (0.3 g, 0.94 mmol) in n-butylamine (3 ml) according to **Procedure 1**. The product was isolated after recrystallisation from DMF/water as a bright orange powder (0.25g, 69.4 % yield). m.p. 239-240 °C; Calculated for $C_{22}H_{27}N_3O_3$: C, 68.46; H, 7.18; N, 10.89 %; Found: C, 68.54; H, 7.08; N, 10.87 %; δH (400 MHz, $(CD_3)_2SO$, 298.2 K) 8.78 (1H, d, *J* = 8.5 Hz, Ar-H7), 8.44 (1H, d, *J* = 8.5 Hz, Ar-H2), 8.32 (1H, d, *J* = 8.5 Hz, Ar-H5), 8.01 (1H, br s, NH), 7.67 (1H, t, *J* = 8.5 Hz Ar-H6); 6.83 (1H, d, *J* = 8.5 Hz, Ar-H3), 4.56 (2H, s, CH_2CO), 3.42 (2H, dd, *J* = 7.0, 6.0 Hz, $CONHCH_2$), 3.10 (2H, dd, *J* = 7.0, 6.0 Hz, $NHCH_2$), 1.67 (2H, quin, *J* = 7.0 Hz, $CONHCH_2CH_2$) 1.51 (4H, m, $CONH(CH_2)_2CH_2$ and $NHCH_2CH_2$), 1.33 (2H, sextet, *J* = 7.0 Hz, $NH(CH_2)_2CH_2$), 1.03 (3H, t, *J* = 7.0 Hz, $CONH(CH_2)_3CH_3$), 0.89 (3H, t, *J* = 7.0 Hz, $NH(CH_2)_3CH_3$); δc (100 MHz, $(CD_3)_2SO$, 298.2 K) 166.7, 163.6, 162.7, 150.7, 134.2, 130.6, 129.6, 128.6, 124.1, 121.8, 120.1, 107.4, 103.7, 42.5, 41.9, 38.2, 31.1, 29.9, 19.7, 19.4, 13.7, 13.6; *m/z*: 382.1 $(M+H)^+$, 309.0 $(M-NH(CH_2)_3CH_3)^+$; IR (KBr) ν_{max} (cm^{-1}) 3443, 3316, 2955, 1690, 1664, 1629, 1583, 1534, 1777.

Chloro-_N_-(2-methyl-4-quinolyl)ethanamide (54)

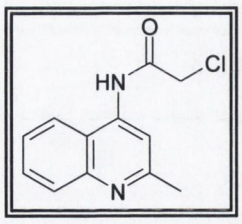

4-Amino-2-methylquinoline (4-aminoquinaldine) (3g, 18.96 mmol) and triethylamine (2.1 g, 20.86 mmol) were dissolved in dry dichloromethane (60 ml) and the mixture was cooled to -10°C in an ice/salt bath. To this mixture, chloroacetyl chloride (2.35 g, 20.86 mmol) in dry CH_2Cl_2 (20 ml) was added over a period of 20 min. The resulting suspension was stirred for a further hour at -10 °C and for two hours at room temperature under an inert atmosphere. The resulting triethylammonium chloride was filtered off and the organic layer was washed once with 1.0 M HCl solution (20 ml). The

aqueous acid solution was washed with CH_2Cl_2 (25 ml), the pH brought to 7.5 using $NaHCO_3$ and the solution extracted three times with CH_2Cl_2 (30 ml). The combined organic layers were dried over K_2CO_3 and the solvent was removed under reduced pressure to give **54** as an off-white solid in 40% yield. Calculated for $C_{12}H_{11}N_2OCl$: C, 61.41; H, 4.72; N, 11.93 %; Found: C, 59.98; H, 4.70; N, 11.69 %; δ_H (400 MHz, $CDCl_3$, 298.2 K) 9.17 (1H, br s, NH), 8.21 (1H, s, Ar-H), 8.08 (1H, d, J = 8.5 Hz, Ar-H), 7.81 (1H, d, J = 8.5 Hz, Ar-H), 7.75 (1H, t, J = 8.5 Hz Ar-H), 7.59 (1H, t, J = 8.5 Hz, Ar-H), 4.37 (2H, s, CH_2), 2.77 (3H, s, Ar-CH_3); δ_c (100 MHz, $CDCl_3$, 298.2 K) 164.2, 160.1, 129.8, 129.7, 126.1, 118.5, 111.4, 43.4, 25.8; *m/z*: 234.66 $(M+H)^+$; IR (KBr) υ_{max} (cm^{-1}) 3264, 1679, 1618, 1605, 1560, 1534, 1350, 1121, 780, 755, 531.

2-(4,10-Bis-dimethylcarbamoylmethyl-1,4,7,10-tetraaza-cyclododec-1-yl)-N,N-dimethyl-acetamide (57)

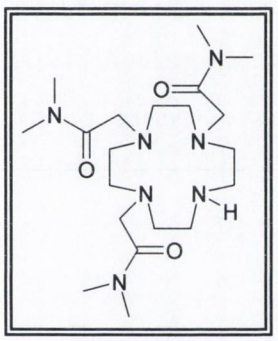

1,4,7,10 tetraazacyclododecane (98 %) (0.5 g, 2.85 mmol) was placed in a 50 ml single neck RBF. To this was added $NaHCO_3$ (0.72 g, 8.57 mmol) and dry MeCN (15 mL). 2-Chloro-N,N-dimethyl-acetamide **56** (1.08 g, 8.87 mmol) was added and the mixture was stirred at 65 °C for 72 hours. The resulting solution was then cooled and passed through a celite filter. The yellow solution was reduced to a dark yellow oil and dried under vacuum overnight to produce 1.35 g of a mixture of products, as shown by TLC. The crude mixture was purified by alumina column chromatography using 100% CH_2Cl_2, with a gradient elution to 40:60 CH_2Cl_2: MeOH(NH_3) mobile phase. The desired product was collected as a white solid after drying under vacuum (0.420 g, 0.98 mmol, 34.5% yield). Calculated for $C_{20}H_{41}N_7O_3$: $(M+H)^+$ *m/z*=428.3344, Found: 428.3349; δ_H (400 MHz, $CDCl_3$, 298.2 K) 10.00 (1H, br s, NH), 3.61 (2H, s, $COCH_2$), 3.58 (4H, s, $COCH_2$), 3.09 (8H, s), 3.04 (3H, s) 2.96 (6H, s), 2.90 (10H, s), 2.84 (7H, s); δ_c (100 MHz, $CDCl_3$, 298.2 K), 170.25, 170.15, 55.51, 53.80, 51.70, 50.57, 49.72, 46.70, 36.39, 35.27; *m/z*: 428.18 $(M+H)^+$, 450.15 $(M+Na)^+$; IR (KBr) υ_{max} (cm^{-1}) 3434, 2927, 2852, 1637, 1508, 1475, 1402, 1338, 1261, 1103, 1064, 1022, 881, 806, 769, 667, 649, 574, 484.

2-{4,7-Bis-dimethylcarbamoylmethyl-10-[(2-methyl-quinolin-4-ylcarbamoyl)-methyl]-1,4,7,10tetraaza-cyclododeca-yl}-*N,N*-dimethyl-acetamide (51)

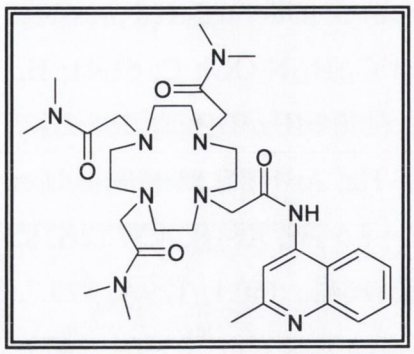

To DMF (35 mL), **57** (0.272 g, 0.636 mmol), Cs_2CO_3 (0.228 g, 0.7 mmol), KI (0.116 g, 0.7 mmol) and **54** (0.164 g, 0.7 mmol) were added. The mixture was heated at 80 °C under inert atmosphere for 72 hours. The solution was filtered and the solvent removed under reduced pressure. A dark orange viscous residue was obtained (0.359 g, 0.57 mmol) and then purified by precipitation from diethyl ether to give a brown solid in 53 % yield. Calculated for $C_{32}H_{51}N_9O_4$: $(M+H)^+$ *m/z:* 626.4142 ; Found: 626.4163; δ_H (400 MHz, $CDCl_3$, 298.2 K) 10.5 (1H, s, NH), 8.75 (1H, d, J = 8.5 Hz, Ar-H), 7.93 (1H, s, Ar-H), 7.89 (1H, d, J = 8.5 Hz, Ar-H), 7.57 (1H, t, J = 8.5 Hz, Ar-H), 7.43 (1H, t, J = 8.5 Hz, Ar-H), 3.86 (2H, s, $HNCOCH_2$), 2.7 (43H, m, N-CH_3, $CH_2CON(CH_3)_2$, cyclen CH_2, CH_3); δ_c (100 MHz, $CDCl_3$, 298 K) 172.1, 170.4, 170.3, 158.3, 148.0, 141.8, 128.7, 127.7, 124.6, 123.4, 119.7, 112.6, 57.6, 54.5, 54.4, 35.7, 35.6, 35.0, 28.8, 26.5, 25.2; *m/z:* 626.33 $(M+H)^+$, 313.67 $(M+2H)^{2+}$; IR (KBr) υ_{max} (cm^{-1}) 3434, 2949, 2818, 2363, 1645, 1531, 1499, 1451, 1407, 1348, 1299, 1266, 1185, 1102, 1005, 769.

2-{4,7-Bis-dimethylcarbamoylmethyl-10-[(2-methyl-quinolin-4-ylcarbamoyl)-methyl]-1,4,7,10tetraaza-cyclododeca-yl}-*N,N*-dimethyl-acetamide Eu(III) (Eu.51)

51 (0.095 g, 0.15 mmol) and $Eu(CF_3SO_3)_3$ (0.1 g, 0.16 mmol) were added to a 25 mL single neck RBF that contained freshly dried CH_3CN (10 mL). After three freeze-pump-thaw cycles, the solution was placed under an Argon atmosphere and left stirring at reflux for 24 hours. The resulting solution was cooled to room temperature and then added dropwise to a stirred solution of dry diethyl ether (100 mL). The mixture was left and then the solvent was subsequently decanted; this operation was repeated several times until **Eu.51** was yielded as a pale green solid (83.6% yield). δ_H (400 MHz, CD_3COCD_3, 298.2 K) 12.7, 10.4, 8.0, 6.9, 3.1, 2.2, 1.6, -5.5, -6.2, -7.0, -8.5; *m/z*: 463.5 $(M+[Triflate])^{2+}$, 259.4 $(M)^{3+}$, 388.6 $(M)^{2+}$; IR (KBr) υ_{max} (cm^{-1}) 3434, 2361, 2343, 1624, 1255, 1164, 1030, 639.

5.14 General procedures for Chapter 3

5.14.1 Procedure 2: EDCI·HCl coupling of 2,6-pyridinedicarboxylic acid derivatives with an amine

To a solution of the 2,6-pyridinedicarboxylic derivative (1 equiv.) in dry THF was added hydroxybenzotriazole (HOBt) (1 equiv.) and the amine (1 equiv.). The stirring solution was cooled in an ice-bath for 15 min while kept under an inert atmosphere of argon. EDCI·HCl (1.05 equiv.) and triethylamine (1.05 equiv.) were then added and the reaction mixture left stirring at 0 °C for 30 min. The ice-bath was removed and the mixture left stirring at room temperature for 18 h. The insoluble residue was filtered off and the solvent removed under reduced pressure. DCM was added to the crude oil and washed twice with 1 M HCl, a saturated solution of $NaHCO_3$ and finally with water. The organic layer was dried over $MgSO_4$, filtered and evaporated to dryness. If necessary, purification of the crude product by flash column chromatography using neutral silica was carried out.

5.14.2 Procedure 3: removal of benzyl ester protecting group

The removal of the benzyl ester protecting group was carried out in CH_3OH, using a Parr hydrogen shaker apparatus with a 10 % Pd/C catalyst (0.1 equiv.) under 3 atm of hydrogen gas. The solution was shaken until no more hydrogen was consumed. The resulting solution was passed through a celite filter and the solvent evaporated to dryness under reduced pressure.

5.15 Experimental details for Chapter 3

2,6-Pyridinedicarboxylic acid, monobenzyl ester (69)[182]

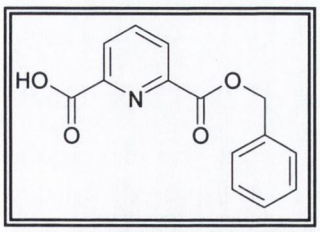

A mixture of 2,6-pyridinedicarboxylic acid (16.7 g, 0.1 mol), water (40 mL), benzyl alcohol (115 mL), and concentrated H_2SO_4 (5.5 mL) was refluxed for 2 h and allowed to stir at room temperature overnight. The mixture was neutralized with 1 L of saturated aqueous $NaHCO_3$, and extracted with $CHCl_3$, to remove the diester. The aqueous layer was acidified to pH 3.8, at which point the monoester crystallized as white needles in 22 % yield. m.p. 132-134 °C (Lit. m.p. 132-133 °C).[183] δH (400 MHz, CDCl3, 298.2 K) 8.42 (2H, dd, J = 8.0 Hz, J = 16.0 Hz, pyridine H3 and H5), 8.14 (1H, t, J = 8.0 Hz, pyridine H4), 7.50 (2H, dd, Ar-H), 7.43 (3H, m, Ar-H), 5.48 (2H, s, CH2).

6-(1-Naphthalen-1-yl-ethylcarbamoyl)-pyridine-2-carboxylic acid benzyl ester, (70 (*R*), 71 (*S*))

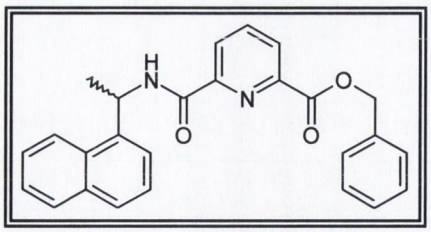

To a stirred solution of the appropriate 1-(1-naphthyl)-ethylamine (*R* or *S* isomer, 0.630 mL, 3.9 mmol) in 30 mL anhydrous THF, HOBt (0.527 g, 3.9 mmol) and monobenzyl ester **69** (1 g, 3.9 mmol) were added. This solution was then stirred for further 30 min at 0 °C before the coupling reagent EDCI·HCl (0.785 g, 4.1 mmol) and triethylamine (0.571 mL, 4.1 mmol) were added according to **Procedure 2**. In each case a pale yellow oil was obtained.

70 (*R*), 1.30 g, 81% yield. Calculated for $C_{26}H_{22}N_2O_3Na$: $(M+Na)^+$ *m/z* = 433.1528; Found: 433.1532; δ_H (400 MHz, $CDCl_3$, 298.2 K) 8.54 (1H, d, *J* = 8.5 Hz, NH), 8.44 (1H, d, *J* = 8.0 Hz, pyridine-H), 8.24 (1H, d, *J* = 8.5 Hz, nap-H), 8.20 (1H, t, *J* = 8.0 Hz, pyridine-H), 7.99 (1H, t, *J* = 8.0 Hz, pyridine-H), 7.89 (1H, d, *J* = 7.5 Hz, nap-H), 7.83 (1H, d, *J* = 7.5 Hz, nap-H), 7.64 (1H, d, *J* = 7.0 Hz, nap-H), 7.58-7.38 (8H, m, 3 napH, 5 Ar-H), 6.20 (1H, m, CH), 5.42 (2H, s, (CH_2), 1.82 (3H, d, 7.0 Hz, CH_3); δ_c (100 MHz, ($CDCl_3$, 298.2 K) 163.7, 161.9, 149.7, 146.1, 138.1, 137.9, 134.9, 133.5, 130.6, 128.4, 128.2, 128.0, 127.8, 126.8, 126.0, 125.3, 125.1, 124.9, 122.9, 122.2, 67.0, 44.5, 20.9; IR (NaCl) υ_{max} (cm^{-1}) 3381, 1724, 1667, 1587, 1508, 1305, 1291, 1236, 1131, 1078, 1029, 997, 963, 909, 843, 800, 777, 750, 696, 647.

71 (*S*), 1.26 g, 79% yield. Calculated for $C_{26}H_{22}N_2O_3Na$: $(M+Na)^+$ *m/z* = 433.1528; Found: 433.1549; δ_H (400 MHz, $CDCl_3$, 298.2 K) 8.51 (1H, d, *J* = 8.5 Hz, NH), 8.44 (1H, d, *J* = 7.5 Hz, pyridine-H), 8.23 (2H, d, nap-H, pyridine-H), 8.00 (1H, t, *J* = 7.5 Hz, pyridine-H), 7.89 (1H, d, *J* = 8.5 Hz, nap-H), 7.83 (1H, d, *J* = 8.5 Hz, nap-H), 7.64 (1H, d, *J* = 7.0 Hz, nap-H), 7.57-7.38 (8H, m, 3 nap-H, 5 Ar-H), 6.19 (1H, m, CH), 5.42 (2H, s, (CH_2), 1.82 (3H, d, 7.0 Hz, CH_3); δ_c (100 MHz, ($CDCl_3$, 298.2 K) 163.7, 161.9, 149.7, 146.0, 138.0, 137.9, 134.9, 133.5, 130.6, 128.4, 128.2, 128.0, 127.8, 127.7, 126.8, 126.0, 125.3, 125.1, 124.9, 122.9, 122.2, 67.0, 44.5, 20.9; IR (NaCl) υ_{max} (cm^{-1}) 3381, 1718, 1651, 1588, 1305, 1155, 1077, 966, 722.

6-(1-Naphthalen-1-yl-ethylcarbamoyl)-pyridine-2-carboxylic acid, (72 (*R*), 73 (*S*))

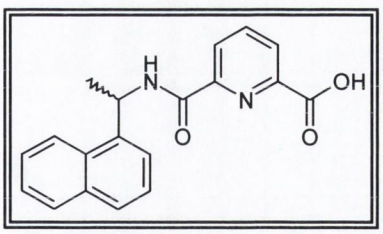

The two isomers **72 (*R*)** and **73 (*S*)** were obtained by hydrogenation of **70 (*R*)** (1.24 g) and **71 (*S*)** (1.22 g), respectively, according to **Procedure 3**, without further purification. The reaction furnished the two carboxylic acid derivatives **72 (*R*)** and **73 (*S*)** as yellow solids.

72 (*R*), (0.94 g, 98%), m.p. 116-120 °C. Calculated for $C_{19}H_{16}N_2O_3 \cdot ½\ H_2O$: C, 69.29; H, 5.20; N, 8.51%; Found: C, 69.43; H, 5.06; N, 8.31 %; Calculated for $C_{19}H_{16}N_2O_3Na\ (M+Na)^+$ *m/z* = 343.1059; Found: 343.1062; δ_H (400 MHz, $CDCl_3$, 298.2 K) 8.51 (1H, d, *J* = 8.5 Hz, NH), 8.38 (1H, d, *J* = 7.5 Hz, pyridine-H), 8.21 (1H, d, *J* = 7.5 Hz, pyridine-H), 8.08 (1H, d, *J* = 8.5 Hz, nap-H), 7.97 (1H, t, *J* = 7.5 Hz, pyridine-H), 7.78 (1H, d, *J* = 8.0 Hz, nap-H), 7.69 (1H, d, *J* = 8.0 Hz, nap-H), 7.50 (2H, m, 2 nap-H), 7.45 (1H, t, *J* = 8.0 Hz, nap-H,), 7.33 (1H, t, *J* = 7.5 Hz, nap-H,), 6.03 (1H, m, CH), 1.67 (3H, d, 7.0 Hz, CH_3); δ_c (100 MHz, ($CDCl_3$, 298.2 K) 164.8, 162.7, 148.5, 145.0, 138.5, 137.6, 133.0, 130.3, 128.2, 127.5, 126.2, 125.9, 125.7, 125.2, 124.7, 122.7, 122.2, 44.7, 20.3; IR (neat sample) υ_{max} (cm^{-1}) 3271, 3050, 2977, 2936, 1752, 1651, 1524, 1452, 1345, 1255, 1172, 1118, 1076, 1000, 921, 846, 799, 776, 745, 681.

73 (*S*), (0.85 g, 90%), m.p. 116-120 °C. Calculated for $C_{19}H_{16}N_2O_3 \cdot ½\ H_2O$: C, 69.29; H, 5.20; N, 8.51%; Found: C, 69.23; H, 5.13; N, 8.34 %; Calculated for $C_{19}H_{16}N_2O_3Na\ (M+Na)^+$ *m/z* = 343.1059; Found: 343.1061; δ_H (400 MHz, $CDCl_3$, 298.2 K) 8.49 (1H, d, *J* = 8.5 Hz, NH), 8.44 (1H, d, *J* = 7.5 Hz, pyridine-H), 8.23 (1H, d, *J* = 8.5 Hz, nap-H), 8.19 (1H, d, *J* = 7.5 Hz, pyridine-H), 7.99 (1H, t, *J* = 7.5 Hz, pyridine-H), 7.88 (1H, d, *J* = 8.0 Hz, nap-H), 7.82 (1H, d, *J* = 8.0 Hz, nap-H), 7.65 (1H, d, *J* = 7.0 Hz, nap-H), 7.56 (1H, t, *J* = 7.0 Hz, nap-H,), 7.49 (2H, m, 2 nap-H,), 6.20 (1H, m, CH), 1.83 (3H, d, 7.0 Hz, CH_3); δ_c (100 MHz, ($CDCl_3$, 298.2 K) 163.3, 161.5, 148.8, 144.5, 139.1, 137.2, 133.4, 130.6, 128.4, 128.1, 126.4, 126.2, 126.2, 125.4, 124.8, 122.7, 122.4, 44.6, 20.3; IR (neat sample) υ_{max} (cm^{-1}) 3282, 3049, 2977, 2936, 1751, 1651, 1524, 1452, 1345, 1255, 1172, 1118, 1076, 1000, 921, 846, 799, 776, 745, 681.

_N,N'_-[Methylenebis(phen-1,4-ylene)]bis(6-(_R_)-1-Naphthalen-1-yl-ethylcarbamoyl)-pyridine-2-carboxamide) (66 (_R,R_))

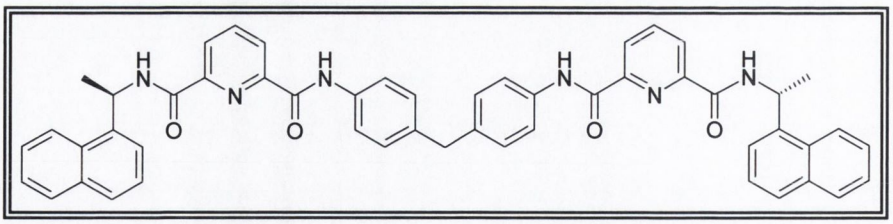

The (*R,R*) isomer of the bis-tridentate ligand **66** was prepared according to **Procedure 2**. To a mixture of 4,4'-diaminodiphenylmethane (0.195 g, 0.985 mmol), **72 (*R*)** (0.630 g, 1.97 mmol), HOBt (0.280 g, 2.07 mmol) in THF (*ca.* 25 mL), EDCI·HCl (0.397 g, 2.07 mmol), triethylamine (0.288 mL, 2.07 mmol) and DMAP (0.144 g, 1.18 mmol) were added, after cooling the reaction mixture at 0 °C. DMAP is a strong base and was added to insure the completion of the reaction. The work-up carried out was the same as that described in **Procedure 2** and resulted in an orange oil (94.5% yield). The crude oil was dissolved in DCM and then dropped slowly onto dry diethyl ether (60-70 mL).The final product was collected as an off-white solid by filtration through a hirsch funnel in 60% yield. m.p. decomposes above 148 °C. Calculated for $C_{51}H_{42}N_6O_4 \cdot ½\ H_2O \cdot ½$ DCM: C, 72.40; H, 5.19; N, 9.84%; Found: C, 72.56; H, 5.43; N, 9.75 %; δ_H (400 MHz, $CDCl_3$, 298.2 K) 9.30 (2H, s, 2 NH), 8.44 (2H, d, J = 7.5 Hz, pyridine-H), 8.41 (2H, d, J = 7.5 Hz, pyridine-H), 8.22 (2H, d, J = 8.0 Hz, nap-H), 8.09 (2H, t, J = 7.5 Hz, pyridine-H), 8.06 (2H, d, J = 8.0 Hz, 2 NH), 7.91 (2H, d, J = 7.5 Hz, nap-H), 7.85 (2H, d, J = 8.0 Hz, nap-H), 7.65 (2H, d, J = 7.0 Hz, nap-H,), 7.60-7.47 (6H, m, 6 nap-H,), 7.43 (4H, d, J = 8.0 Hz, Ar-H), 7.14 (4H, d, J = 8.0 Hz, Ar-H), 6.12 (2H, m, 2 CH), 3.95 (2H, s, CH_2), 1.85 (6H, d, 7.0 Hz, 2 CH_3); δ_c (100 MHz, ($CDCl_3$, 298.2 K) 162.0, 160.6, 148.4, 148.2, 138.8, 137.5, 137.2, 134.6, 133.6, 130.5, 129.0, 128.5, 128.2, 126.3, 125.5, 125.0, 124.8, 124.7, 122.8, 122.5, 119.9, 45.3, 40.3, 20.5; IR (neat sample) υ_{max} (cm^{-1}) 3298, 3049, 2979, 2934, 2079, 1661, 1588, 1517, 1444, 1411, 1320, 1234, 1179, 1118, 1075, 999, 944, 916, 842, 800, 776, 749, 677.

_N,N'_-[Methylenebis(phen-1,4-ylene)]bis(6-(_S_)-1-Naphthalen-1-yl-ethylcarbamoyl)-pyridine-2-carboxamide) (67 (_S,S_))

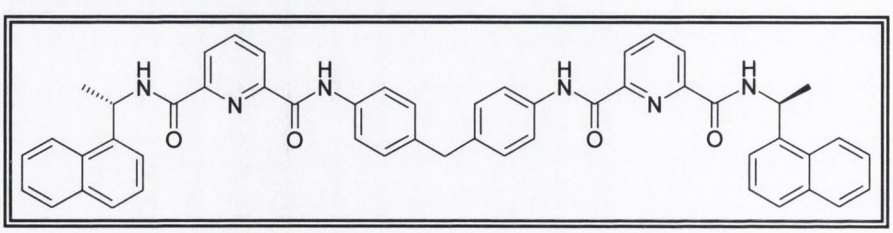

The (*S,S*) isomer of the bis-tridentate ligand **67** was prepared

according to **Procedure 2**. To a mixture of 4,4'-diaminodiphenylmethane (0.165 g, 0.83 mmol), **72 (*R*)** (0.545 g, 1.70 mmol), HOBt (0.235 g, 1.74 mmol) in THF (*ca.* 20 mL), EDCI·HCl (0.334 g, 1.74 mmol), triethylamine (0.245 mL, 1.74 mmol) and DMAP (0.122 g, 1.00 mmol) were added, after cooling the reaction mixture at 0 °C. DMAP is a strong base and was added to insure the completion of the reaction. The work-up carried out was the same as that described in **Procedure 2** and resulted in an off-white fluffy solid (52% yield). The crude product was purified by column chromatography on silica using 100% CH_2Cl_2, with a gradient elution to 95:5, DCM:MeOH mobile phase. The final product was collected as an off-white solid in 44% yield. m.p. decomposes above 149 °C. Calculated for $C_{51}H_{42}N_6O_4 \cdot H_2O \cdot ½$ DCM: C, 71.64; H, 5.25; N, 9.73%; Found: C, 71.65; H, 5.03; N, 9.59 %; δ_H (400 MHz, $CDCl_3$, 298.2 K) 9.36 (2H, s, 2 NH), 8.42 (2H, d, J = 7.5 Hz, pyridine-H), 8.37 (2H, d, J = 7.5 Hz, pyridine-H), 8.18 (4H, 2 d (overlapping), 2 NH and 2 nap-H), 8.06 (2H, t, J = 7.5 Hz, pyridine-H), 7.88 (2H, d, J = 8.0 Hz, nap-H), 7.81 (2H, d, J = 8.5 Hz, nap-H), 7.61 (2H, d, J = 7.0 Hz, nap-H), 7.57-7.42 (6H, m, 6 nap-H,), 7.41 (4H, d, J = 8.5 Hz, Ar-H), 7.08 (4H, d, J = 8.5 Hz, Ar-H), 6.08 (2H, m, 2 CH), 3.91 (2H, s, CH_2), 1.81 (6H, d, 7.0 Hz, 2 CH_3); δ_c (100 MHz, ($CDCl_3$, 298.2 K) 162.5, 161.3, 148.3, 147.9, 137.9, 137.8, 137.0, 134.3, 133.1, 130.4, 128.3, 128.2, 127.5, 125.9, 125.3, 124.9, 124.4, 124.2, 122.8, 122.3, 121.1, 44.8, 40.1, 20.5; IR (neat sample) υ_{max} (cm^{-1}) 3298, 3049, 2977, 2934, 2084, 1655, 1588, 1521, 1444, 1411, 1320, 1233, 1179, 1118, 1075, 999, 944, 916, 842, 800, 776, 749, 678.

3{*N,N*'-[Methylenebis(phen-1,4-ylene)]bis(6-(*R*)-1-Naphthalen-1-yl-ethylcarbamoyl)-pyridine-2-carboxamide)}. 2Eu. 6(CF_3SO_3) (74 (*R,R*))

Ligand **66 (*R,R*)** (0.03 g, 0.037 mmol) and $Eu(CF_3SO_3)_3$ (0.0148 g, 0.025 mmol) were added to a 5 mL single neck RBF that contained 3 mL of $CH_3CN/CHCl_3$ (50 : 50, v/v). The solution was then refluxed for 24 hrs. The resulting solution was cooled to room temperature and then dropped slowly onto dry diethyl ether. A pale brown solid precipitated out of solution and was collected by Hirsch filtration in 48.5% yield. m.p. decomposes above 280 °C. Calculated for $C_{159}H_{126}N_{18}O_{30}Eu_2F_{18}S_6 \cdot 2\ CHCl_3$: C, 50.28; H, 3.35; N, 6.56%; Found: C, 49.77; H, 3.55; N, 6.48 %; δ_H (600 MHz, CD_3CN, 298.2 K) 8.99 (3 × 2H, br. s, nap-H), 8.21 (3 × 4H, br. s, Ar-H), 8.06 (3 × 2H, br. s, CH), 7.98 (3 × 2H, br. s, nap-H), 7.81 (3 × 4H, br. s, Ar-H), 7.62 (3 × 4H, br. s, nap-H), 7.16 (3 × 2H, br. s, nap-H), 6.78 (3 × 2H, br. s, 2 NH), 6.58 (3 × 2H, br. s, nap-H), 6.41 (3 × 2H, br. s,

pyridine-H), 6.24 (3 × 2H, br. s, nap-H), 5.73 (3 × 2H, br. s, pyridine-H), 5.26 (3 × 2H, br. s, pyridine-H), 4.38 (3 × 2H, br. s, CH_2), 4.08 (3 × 2H, br. s, 2 NH), CH_3 obscured by solvent peak at 1.99 ppm; δ_c (CD_3CN, 298.2 K obtained by inverse detection through HSQC experiment, quaternary excluded) 153.3, 129.7, 128.8, 127.0, 126.7, 125.9, 124.4, 124.4, 122.1, 120.0, 91.0, 90.6, 40.4, 21.6; IR (neat sample) υ_{max} (cm^{-1}) 3267, 3087, 2096, 1629, 1585, 1553, 1511, 1457, 1416, 1380, 1348, 1275, 1243, 1225, 1162, 1028, 956, 918, 839, 801, 778, 754, 699, 677, 662.

3{*N,N*'-[Methylenebis(phen-1,4-ylene)]bis(6-(*S*)-1-Naphthalen-1-yl-ethylcarbamoyl)-pyridine-2-carboxamide)}. 2Eu. 6(CF_3SO_3) (75 (*S,S*))

Ligand **67 (*S,S*)** (0.0835 g, 0. 1 mmol) and $Eu(CF_3SO_3)_3$ (0.0415 g, 0.07 mmol) were added to a 50 mL single neck RBF that contained 15 mL of MeOH. The solution was then refluxed for 24 hrs under an argon atmosphere. The resulting solution was cooled to room temperature and then dropped slowly onto dry diethyl ether. A pale yellow solid precipitated out of solution and was collected by Hirsch filtration in 92% yield. m.p. decomposes above 280 °C. Calculated for $C_{159}H_{126}N_{18}O_{30}Eu_2F_{18}S_6 \cdot 2\ H_2O \cdot 2MeOH$: C, 52.16; H, 3.75; N, 6.80%; Found: C, 51.95; H, 3.61; N, 6.90 %; δ_H (400 MHz, CD_3CN, 298.2 K) 9.04 (3 × 2H, br. s, nap-H), 8.28 (3 × 4H, br. s, Ar-H), 8.18 (3 × 2H, br. s, CH), 7.98 (3 × 2H, br. s, nap-H), 7.84 (3 × 4H, br. s, Ar-H), 7.58 (3 × 4H, br. s, nap-H), 7.10 (3 × 2H, br. s, nap-H), 6.69 (3 × 2H, br. s, 2 NH), 6.49 (3 × 2H, br. s, nap-H), 6.29 (3 × 2H, br. s, pyridine-H), 6.12 (3 × 2H, br. s, nap-H), 5.59 (3 × 2H, br. s, pyridine-H), 5.12 (3 × 2H, br. s, pyridine-H), 4.37 (3 × 2H, br. s, CH_2), 3.96 (3 × 2H, br. s, 2 NH), CH_3 obscured by solvent peak at 1.97 ppm; IR (neat sample) υ_{max} (cm^{-1}) 3266, 3088, 1629, 1585, 1552, 1511, 1457, 1416, 1379, 1348, 1274, 1242, 1225, 1161, 1028, 956, 917, 838, 801, 778, 754, 728, 699, 678, 662.

REFERENCES

1. Matsumoto, K.; Yuan, J. *Metal ions in biological systems*; Marcel Dekker Inc.: New York, 2003; Vol. 40.
2. Faulkner, S.; Pope, S. J. A.; Burton-Pye, B. P. *Appl. Spectrosc. Rev.* **2005**, *40*, 1.
3. Kido, J.; Okamoto, Y. *Chem. Rev.* **2002**, *102*, 2357.
4. Bunzli, J. C. G. *Acc. Chem. Res.* **2006**, *39*, 53.
5. Bünzli, J.-C. G.; Piguet, C. *Chem. Soc. Rev.* **2005**, *34*, 1048.
6. Desreux, J. F. *Inorg. Chem.* **1980**, *19*, 1319.
7. Lauffer, R. B. *Chem. Rev.* **1987**, *87*, 901-927.
8. Parker, D.; Williams, J. A. G. *Metal ions in biological systems*; Marcel Dekker Inc.: New York, 2003; Vol. 40.
9. Melhuish, W. H. *Pure Appl. Chem.* **1984**, *56*, 231.
10. http://perso.univ-rennes1.fr/martinus.werts/lanthanides/ln_shine.html.
11. Carnall, W. T.; Fields, P. R.; Rajnak, K. *J. Chem. Phys.* **1968**, *49*, 4424.
12. Hemmilä, I.; Stählberg, T.; P., M. *Bioanalytical Applications of Labelling Technologies*; Wallac Oy: Turku, 1995.
13. Hemmilä, I.; Mukkala, V. M. *Crit. Rev. Clin. Lab. Sci.* **2001**, *38*, 441.
14. Voloshin, A. I.; Shavaleev, N. M.; Kazakov, V. P. *J. Lumin.* **2001**, *93*, 199-204.
15. Auzel, F. *Chem. Rev.* **2004**, *104*, 139-174.
16. Stouwdam, J. W.; Hebbink, G. A.; Huskens, J.; vanVeggel, F. C. J. M. *Chem. Mater.* **2003**, *15*, 4604-4616.
17. Shavaleev, N. M.; Pope, S. J. A.; Bell, Z. R.; Faulkner, S.; Ward, M. D. *Dalton Trans.* **2003**, 808 - 814.
18. Werts, M. H. V.; Woudenberg, R. H.; Emmerink, P. G.; Gassel, R. v.; Hofstraat, J. W.; Verhoeven, J. W. *Angew. Chem. Int. Ed.* **2000**, *39*, 4542-4544.
19. Imbert, D.; Cantuel, M.; Bunzli, J. C. G.; Bernardinelli, G.; Piguet, C. *J. Am. Chem. Soc.* **2003**, *125*, 15698-15699.
20. Parker, D. *Coord. Chem. Rev.* **2000**, *205*, 109-130.
21. Wolbers, M. P. O.; Veggel, F. C. J. M. v.; Snellink-Ruel, B. H. M.; Hofstraat, J. W.; Geurts, F. A. J.; Reinhoudt, D. N. *J. Chem. Soc., Perkin Trans. 2* **1998**, 2141.
22. Atkins, P. W. *Physical Chemistry*, 6th edition ed.; W. H. Freeman & Co. and Sumanas, Inc., 1998.

23. Forster, T. *Ann. Phys.(Leipzig)* **1984**, *2*, 55.
24. Barigelletti, F.; Flamigini, L.; Balzani, V.; Collin, J. P.; Sauvage, J. P.; Sour, A.; Constable, E. C.; Thompson, A. M. W. C. *Coord. Chem. Rev.* **1994**, *132*, 209.
25. Dexter, D. *J. Phys. Chem.* **1953**, *21*, 836.
26. Gunnlaugsson, T.; Mac Donaill, D.; Parker, D. *J. Am. Chem. Soc.* **2001**, *123*, 12866.
27. Gunnlaugsson, T.; Harte, A. J.; Leonard, J. P.; Nieuwenhuyzen, M. *Supramol. Chem.* **2003**, *15*, 505.
28. Shinoda, S.; Miyake, H.; Tsukube, H. *Handbook of the Physics and Chemistry of Rare Earths*; Elsevier North Holland, 2005; Vol. 35.
29. Beeby, A.; Clarkson, I. M.; Dickins, R. S.; Faulkner, S.; Parker, D.; Royle, L.; Sousa, A. S. d.; Williams, J. A. G.; Woods, M. *J. Chem. Soc., Perkin Trans. 2* **1999**, 493 - 504.
30. Supkowski, R. M.; Horrocks, J. W. D. *Inorg. Chim. Acta* **2002**, *340*, 44-48.
31. Lehn, J.-M. *Angew. Chem. Int. Ed.* **1990**, *29*, 1304-1319.
32. de Silva, A. P.; Gunaratne, H. Q. N.; Rice, T. E. *Angew. Chem. Int. Ed.* **1996**, *35*, 2116-2118.
33. Dickins, R. S.; Howard, J. A. K.; Maupin, C. L.; Moloney, J. M.; Parker, D.; Riehl, J. P.; Siligardi, G.; Williams, J. A. G. *Chem. Eur. J.* **1999**, *5*, 1095-1105.
34. Beeby, A.; Parker, D.; Williams, J. A. G. *J. Chem. Soc., Perkin Trans. 2* **1996**, 1565 - 1579.
35. Cotton, F. A.; Wilkinson, G. *Advanced Inorganic Chemistry*, 5th ed.; Wiley Interscience, 1988.
36. Cabbiness, D. K.; Margerum, D. W. *J. Am. Chem. Soc.;* **1970**, *92*, 2151 - 2153.
37. Zucchi, G.; Ferrand, A. C.; Scopelliti, R.; Bunzli, J. C. G. *Inorg. Chem.* **2002**, *41*, 2459-2465.
38. Gunnalugsson, T. *Tetrahedron Lett.* **2001**, *42*, 8901.
39. Lowe, M. P.; Parker, D.; Reany, O.; Aime, S.; Botta, M.; Castellano, G.; Gianolio, E.; Pagliarin, R. *J. Am. Chem. Soc.* **2001**, *123*, 7601-7609.
40. Weller, A. *Pure Appl. Chem.* **1968**, *16*, 115-121.
41. Woods, M.; Sherry, A. D. *Inorg. Chem.* **2003**, *42*, 4401-4408.
42. Woods, M.; Zhang, S.; Ebron, V. H.; Sherry, A. D. *Chem. Eur. J.* **2003**, *9*, 4634-4640.
43. Reany, O.; Gunnlaugsson, T.; Parker, D. *Chem. Commun.* **2000**, 473-474.

44. Gunnlaugsson, T.; Leonard, J. P.; Sénéchal, K.; Harte, A. J. *Chem. Commun.* **2004**, 782-783.
45. Gunnalugsson, T.; Leonard, J. P. *Dalton Trans.* **2005**, 3204-3212.
46. Beeby, A.; Dickins, R. S.; FitzGerald, S.; Govenlock, L. J.; Parker, D.; Williams, J. A. G.; Maupin, C. L.; Riehl, J. P.; Siligardi, G. *Chem. Commun.* **2000**, 1183-1184.
47. Faulkner, S.; Pope, S. J. A. *J. Am. Chem. Soc.* **2003**, *125*, 10526-10527.
48. Gunnalugsson, T.; Harte, A. J.; Leonard, J. P.; Nieuwenhuyzen, M. *Chem. Commun.* **2002**, 2134.
49. Dickins, R. S.; Aime, S.; Batsanov, A. S.; Beeby, A.; Botta, M.; Bruce, J. I.; Howard, J. A. K.; Love, C. S.; Parker, D.; Peacock, R. D.; Puschmann, H. *J. Am. Chem. Soc.* **2002**, *124*, 12697-12705.
50. Dickins, R. S.; Gunnlaugsson, T.; Parker, D.; Peacock, R. D. *Chem. Commun.* **1998**, 1643-1644.
51. Liu, Y.; Han, B. H.; Li, Y. M.; Chen, R. T.; Ouchi, M.; Inoue, Y. *J. Phys. Chem.* **1996**, *100*, 17361-17364.
52. Gonzalez-Lorenzo, M.; Platas-Iglesias, C.; Avecilla, F.; Faulkner, S.; Pope, S. J. A.; deBlas, A.; Rodriguez-Blas, T. *Inorg. Chem.* **2005**, *44*, 4254-4262.
53. Beer, P. D.; Szemes, F.; Passaniti, P.; Maestri, M. *Inorg. Chem.* **2004**, *43*, 3965-3975.
54. de Silva, A. P.; Gunaratne, H. Q. N.; Rice, T. E.; Stewart, S. *Chem. Commun.* **1997**, 1891-92.
55. Klink, S. I.; Hebbink, G. A.; Grave, L.; Peters, F. G. A.; vanVeggel, F. C. J. M.; Reinhoudt, D. N.; Hofstraat, J. W. *Eur. J. Org. Chem.* **2000**, *2000*, 1923-1931.
56. Werts, M. H. V.; Hofstraat, J. W.; Geurts, F. A. J.; Verhoeven, J. W. *Chem. Phys. Lett.* **1997**, *276*, 196-201.
57. Glover, P. B.; Ashton, P. R.; Childs, L. J.; Rodger, A.; Kercher, M.; Williams, R. M.; DeCola, L.; Pikramenou, Z. *J. Am. Chem. Soc.* **2003**, *125*, 9918-9919.
58. Yamada, T.; Shinoda, S.; Tsukube, H. *Chem. Commun.* **2002**, 1218-1219.
59. Charbonniere, L.; Ziessel, R.; Guardigli, M.; Roda, A.; Sabbatini, N.; Cesario, M. *J. Am. Chem. Soc.* **2001**, *123*, 2436-2437.
60. Elhabiri, M.; Scopelliti, R.; Bunzli, J. C. G.; Piguet, C. *J. Am. Chem. Soc.* **1999**, *121*, 10747-10762.
61. Coppo, P.; Duati, M.; Kozhevnikov, V. N.; Hofstraat, J. W.; Cola, L. D. *Angew. Chem. Int. Ed.* **2005**, *44*, 1806-1810.

62. Klink, S. I.; Keizer, H.; Hofstraat, H. W.; van Veggel, F. C. J. M. *Synth. Met.* **2002**, *127*, 213-216.

63. Senechal-David, K.; Leonard, J. P.; Plush, S. E.; Gunnlaugsson, T. *Org. Lett.* **2006**, *8*, 2727-2730.

64. Bassett, A. P.; Magennis, S. W.; Glover, P. B.; Lewis, D. J.; Spencer, N.; Parsons, S.; Williams, R. M.; DeCola, L.; Pikramenou, Z. *J. Am. Chem. Soc.* **2004**, *126*, 9413-9424.

65. Floquet, S.; Borkovec, M.; Bernardinelli, G.; Pinto, A.; Leuthold, L.-A.; Hopfgartner, G.; Imbert, D.; Bünzli, J.-C. G.; Piguet, C. *Chem. Eur. J.* **2004**, *10*, 1091-1105.

66. Mamula, O.; Lama, M.; Telfer, S. G.; Nakamura, A.; Kuroda, R.; Stoeckli-Evans, H.; Scopelitti, R. *Angew. Chem. Int. Ed.* **2005**, *44*, 2527-2531.

67. Kopeček, J. *Eur. J. Pharm. Sci.* **2003**, *20*, 1-16.

68. Wichterle, O.; Lím, D. *Nature* **1960**, *185*, 117-118.

69. Güven, O.; Şen, M.; Karadağ, E.; Saraydin, D. *Rad. Phys. Chem.* **1999**, *56*, 381-386.

70. Yaung, J. F.; Kwei, T. K. *J. Appl. Pol. Sci.* **1998**, *69*, 921-930.

71. Šprincl, L.; Vacík, J.; Kopeček, J.; Lím, D. *J. Biomed. Mater. Res.* **1973**, *7*, 123-136.

72. Peppas, N. A.; Bures, P.; Leobandung, W.; Ichikawa, H. *Eur. J. Pharm. Biopharm.* **2000**, *50*, 27-46.

73. Tew, G. N.; Sanabria-DeLong, N.; Agrawal, S. K.; Bhatia, S. R. *Soft Matter* **2005**, *1*, 253-258.

74. Hsiue, G.-H.; Guu, J.-A.; Cheng, C.-C. *Biomaterials* **2001**, *22*, 1763-1769.

75. Alvarez-Lorenzo, C.; Hiratani, H.; Gómez-Amoza, J. L.; Martínez-Pacheco, R.; Souto, C.; Concheiro, A. *J. Pharm. Sci.* **2002**, *91*, 2182-2192.

76. Gehrke, S. H.; Lee, P. I. *Specialized drug delivery systems*; Marcal Dekker, P. Tyle, 1990.

77. Gunnlaugsson, T.; MacCoy, C. P.; Morrow, R. J.; Phelan, C.; Stomeo, F. *Arkivoc* **2003**, 216-228.

78. Amsden, B. *Polymer Gels and Networks* **1998**, *6*, 13-43.

79. Osada, Y.; Gong, J.-P. *Adv. Mater.* **1998**, *10*, 827-837.

80. Lowman, A. M.; Peppas, N. A. *Encyclopedia of Controlled Drug Delivery*; Wiley: New York, 1999.

81. Berger, J.; Reist, M.; Mayer, J. M.; Felt, O.; Peppas, N. A.; Gurny, R. *Eur. J. Pharm. Biopharm.* **2004**, *57*, 19-34.
82. Rosiak, J. M.; Ulanski, P.; Rzeznicki, A. *Nucl. Instrum. Methods Phys. Res., Sect. B* **1995**, *105*, 335-339.
83. Rosiak, J. M.; Yoshii, F. *Nucl. Instrum. Methods Phys. Res., Sect. B* **1999**, *151*, 56-64.
84. Dagani, R. *Chem. Eng. News* **1997**, *9*, 26-30.
85. Jen, A. C.; Wake, M. C.; Mikos, A. G. *Biotechnol. Bioeng.* **1996**, *50*, 357-364.
86. Byrne, M. E.; Park, K.; Peppas, N. A. *Adv. Drug Delivery Rev.* **2002**, *54*, 149-161.
87. Brannon-Peppas, L.; Peppas, N. A. *Biomaterials* **1990**, *11*, 635-644.
88. Liu, Q.; Hedberg, E. L.; Liu, Z.; Bahulekar, R.; Meszlenyi, R. K.; Mikos, A. G. *Biomaterials* **2000**, *21*, 2163-2169.
89. Kim, S. H.; Opdahl, A.; Marmo, C.; Somorjai, G. A. *Biomaterials* **2002**, *23*, 1657-1666.
90. Beruto, D. T.; Botter, R. *Biomaterials* **2004**, *25*, 2877-2883.
91. Denizli, A.; Kiremitci, M.; Piskin, F. *Biomaterials* **1988**, *9*, 363-6.
92. Kiremitci-Gumusderelioglu, M.; Gokce, M.; Fikret, R. A. *J. Biomater. Sci. Polymer Edn.* **1996**, *7*, 857-869.
93. Trigo, R. M.; Blanco, M. D.; Teijon, J. M.; Sastre, R. *Biomaterials* **1994**, *15*, 1181-6.
94. Maitra, U.; Mukhopadhyay, S.; Sarkar, A.; Rao, P.; Indi, S. S. *Angew. Chem. Int. Ed.* **2001**, *40*, 2281-2283.
95. Yoshimura, I.; Miyahara, Y.; Kasagi, N.; Yamane, H.; Ojida, A.; Hamachi, I. *J. Am. Chem. Soc.* **2004**, *126*, 12204-12205.
96. Sangeetha, N. M.; Maitra, U. *Chem. Soc. Rev.* **2005**, *34*, 821-836.
97. Kim, J.; Nayak, S.; Lyon, L. A. *J. Am. Chem. Soc.* **2005**, *127*, 9588-9592.
98. Amendola, V.; Fabbrizzi, L.; Mangano, C.; Pallavicini, P. *Acc. Chem. Res.* **2001**, *34*, 488.
99. de Silva, A. P.; Fox, D. B.; Huxley, A. J. M.; Moody, T. S. *Coord. Chem. Rev.* **2000**, *205*, 41-57.
100. Sigel, A.; Sigel, H. *The lanthanides and their interrelations with biosystems*; Marcel Dekker, Inc.: New York, 2003; Vol. 40.
101. de Silva, A. P.; Gunaratne, H. K. N.; Gunnlaugsson, T.; Huxley, A. J. M.; MacCoy, C. P.; Rademacher, J. T.; Rice, T. E. *Chem. Rev.* **1997**, 1515-1566.

102. Parker, D.; Williams, J. A. G. *J. Chem. Soc., Dalton Trans.* **1996**, 3613-3628.

103. Ji, H. F.; Dabestani, R.; Brown, G. M.; Hettich, R. L. *Photochem. Photobiol.* **1999**, *69*, 513-516.

104. www.shsu.edu/~chemistry/chemiluminescence/.

105. Wayne, R. P. *Principles and Applications of Photochemistry*; Oxford Science Publications, 1988.

106. Bissel, R. A.; de Silva, A. P.; Gunaratne, H. Q. N.; Lynch, P. L. M.; Maguire, G. E. M.; Sandanayake, K. R. A. S. *Chem. Soc. Rev.* **1992**, 187.

107. de Silva, A. P.; de Silva, S. A. *J. Chem. Soc., Chem. Commun.* **1986**, 1709.

108. Valeur, B.; Leray, I. *Coord. Chem. Rev.* **2000**, *205*, 3-40.

109. Leonard, J. P., University of Dublin, TCD, 2003.

110. Gunnlaugsson, T.; Davis, A.; Glynn, M. *Chem. Comm.* **2001**, 2556.

111. de Silva, A. P.; Gunaratne, H. Q. N.; Gunnlaugsson, T.; Niewenhuyzen, M. *Chem. Comm.* **1996**, 1967-68.

112. Gunnlaugsson, T.; Davis, A. P.; O'Brien, J. E.; Glynn, M. *Org. Lett.* **2002**, *4*, 2449-2452.

113. Callan, J. F.; de Silva, A. P.; Magri, D. C. *Tetrahedron* **2005**, *61*, 8551-8588.

114. Tusa, J. K.; He, H. *J. Mater. Chem.* **2005**, *15*, 2640 - 2647.

115. Andersson, B. S.; Beran, M.; Bakic, M.; Silberman, L. E.; Newman, R. A.; Zwelling, L. A. *Cancer Res.* **1987**, *47*, 1040.

116. Allens, R. L. M. *Colour Chemistry*; Eds, Thomas Nelson: London, 1971.

117. Zollinger, H. *Synthesis, Properties and Applications of Organic Dyes and Pigments*; Eds, Thomas Nelson: London, 1987.

118. Krishna, K. D.; Ramendra, K. S.; Misre, K. *Ind. J. Chem.* **1995**, *34B*, 876.

119. de Silva, A. P.; Gunaratne, H. Q. N.; Habib-Jiwan, J. L.; MacCoy, C. P.; Rice, T. E.; Soumillion, J. P. *Angew. Chem. Int. Ed.* **1995**, *34*, 1728.

120. Quin, X.; Zhu, Z.; Chen, K.; Yin, Q.; Zhu, G. *Mater. Chem. Phys.* **1989**, *23*, 335.

121. Pardo, A.; Poyato, J. M. L.; Camacho, J. J.; Brana, M. F.; Castellano, J. M. *J. Photochem.* **1986**, *36*, 323.

122. Bailly, C.; Brana, M.; Waring, M. J. *Eur. J. Biochem.* **1996**, *240*, 195.

123. Gunnlaugsson, T.; Kruger, P. E.; Lee, T. C.; Parkesh, R.; Pfeffer, F. M.; Hussey, G. M. *Tetrahedron Lett.* **2003**, *44*, 6575.

124. Czarnik, A. W. *Chemistry & Biology* **1995**, *2*, 423.

125. He, H.; Mortellaro, M. A.; Leiner, M. J. P.; Young, S. T.; Fraatz, R. J.; Tusa, J. K. *Anal. Chem.* **2003**, *75*, 549-555.

126. He, H.; Mortellaro, M. A.; Leiner, M. J. P.; Fraatz, R. J.; Tusa, J. K. *J. Am. Chem. Soc.* **2003**, *125*, 1468-1469.

127. Grabchev, I.; Qian, X.; Xiao, Y.; Zhang, R. *New J. Chem.* **2002**, *26*, 920 - 925.

128. Tian, H.; Gan, J.; Chen, K.; He, J.; Song, Q. L.; Hou, X. Y. *J. Mater. Chem.* **2002**, *12*, 1262 - 1267.

129. de Silva, A. P.; Rice, T. E. *Chem. Commun.* **1999**, 163-164.

130. Kunioka, M.; Choi, H. J. *Polymer degradation and stability* **1998**, *59*, 33.

131. Paddock, S. W. *Mol. Biotechnol.* **2000**, *16*, 127.

132. Georges, J. *Analyst* **1993**, *118*, 1481.

133. Wainwright, K. P. *Coord. Chem. Rev.* **1997**, *166*, 35-90.

134. Lincoln, S. F. *Coord. Chem. Rev.* **1997**, *166*, 255-289

135. Meyer, M.; Dahaoui-Gindrey, V.; Lecomte, C.; Guilard, R. *Coord. Chem. Rev.* **1998**, *178-180*, 1313-1405.

136. Lukes, I.; Kotek, J.; Vojtisek, P.; Hermann, P. *Coord. Chem. Rev.* **2001**, *216-217*, 287-312.

137. Stein, G.; Würzberg, E. *J. Chem. Phys.* **1975**, *62*, 208.

138. Aime, S.; Botta, M.; Ermondi, G. *Inorg. Chem.* **1992**, *31*, 4291-4299.

139. Bencini, A.; Bianchi, A.; Garcia-Espana, E.; Micheloni, M.; Ramirez, J. A. *Coord. Chem. Rev.* **1999**, *188*, 97-156.

140. Hartley, F. R.; Burgess, C.; Alcock, R. *Solution Equilibria*; Ellis Horwood Publishers, 1980.

141. Gans, P.; Sabatini, A.; Vacca, A. *Talanta* **1996**, *43*, 1739-1753.

142. Izatt, R. M.; Eatough, D. J.; Christensen, J. J. *Structure and bonding*, 1973.

143. Lehn, J. M.; Sauvage, J. P. *J. Am. Chem. Soc.* **1975**, 6700.

144. Gunnlaugsson, T.; Brougham, D. F.; Fanning, A. M.; Nieuwenhuyzen, M.; O'Brien, J. E.; Viguier, R. *Org. Lett.* **2004**, *6*, 4805-4808.

145. Horrocks, W. D.; Sudnick, D. R. *J. Am. Chem. Soc.* **1979**, *101*, 334 - 340.

146. Haas, Y.; Stein, G. *J. Phys. Chem.* **1971**, *75*, 3668 - 3677

147. Connor, K. A. *Binding Constants*; John Wiley & Sons New York, 1987.

148. Jaffe`, H. H.; Orchin, M. *Theory and Applications of Ultraviolet Spectroscopy*; Wiley: New York, 1962.

149. Konopelski, J. P.; Kotzyba-Hibert, F.; Lehn, J.-M.; Desvergne, J.-P.; Fagès, F.; Castellan, A.; Bouas-Laurent, H. *J. Chem. Soc., Chem. Commun.* **1985**, 433 - 436.

150. Huston, M. E.; Haider, K. W.; Czarnik, A. W. *J. Am. Chem. Soc.* **1988**, *110*, 4460-4462.

151. Cox, G. S.; Turro, N. J.; Yang, N. C. C.; Chen, M. J. *J. Am. Chem. Soc.* **1984**, *106*, 422-424.

152. de Silva, A. P.; Rupasinghe, R. A. D. D. *J. Chem. Soc., Chem. Commun.* **1985**, *23*, 1669-1670.

153. Mason, S. F.; Philp, J.; Smith, B. E. *J. Chem. Soc. A* **1968**, 3051-3056.

154. Weller, A. *Progress in reaction kinetics*; G. Porter, Pergamon: Oxford, 1961; Vol. 1.

155. Mason, S. F.; Smith, B. E. *J. Chem. Soc. A* **1969**, 325-328.

156. Förster, R. *Z. Electrochem.* **1950**, *54*, 531.

157. Tajima, S.; Tobita, S.; Shizuka, H. *J. Phys. Chem. A* **2000**, *104*, 11270-11277.

158. Sikorska, E.; Szymusiak, H.; Khmelinskii, I. V.; Koziolowa, A.; Spanget-Larsen, J.; Sikorski, M. *J. Photochem. Photobiol. A* **2003**, *158*, 45-53.

159. Parker, D.; Williams, J. A. G. *J. Chem. Soc., Dalton Trans.* **1996**, 3613 - 3628.

160. http://faraday.physics.uiowa.edu/heat/2B40.20.htm.

161. Ding, Y.; Jiang, S.; Hwang, B.-C.; Luo, T.; Peyghambarian, N.; Himei, Y.; Ito, T.; Miura, Y. *Optical Materials* **2000**, *15*, 123-130.

162. Lessmann, J. J.; Horrocks, W. D. *Inorg. Chem.* **2000**, *39*, 3114-3124.

163. Lehn, J.-M. *Science* **1993**, *260*, 1762-63.

164. Lawrence, D. S.; Jiang, T.; Levett, M. *Chem. Rev.* **1995**, *95*, 2229-2260.

165. Sabbatini, N.; Guardigli, M.; Lehn, J.-M. *Coord. Chem. Rev.* **1993**, *123*, 201-228.

166. Theil, A.; Mauve, C.; Adeline, M.-T.; Marinetti, A.; Sauvage, J.-P. *Angew. Chem. Int. Ed.* **2006**, *45*, 2104-2107.

167. Hutin, M.; Schalley, C. A.; Bernardinelli, G.; Nitschke, J. R. *Chem. Eur. J.* **2006**, *12*, 4069-4076.

168. Flood, A. H.; Wong, E. W.; Stoddart, J. F. *Chem. Phys.* **2006**, *324*, 280-290.

169. Dichtel, W. R.; Miljanic, O. S.; Spruell, J. M.; Heath, J. R.; Stoddart, J. F. *J. Am. Chem. Soc.* **2006**, *128*, 10388-10390.

170. Baxter, P. N. W.; Lehn, J.-M.; Kneisel, B. O.; Baum, G.; Fenske, D. *Chem. Eur. J.* **1999**, *5*, 113-120.

171. Lehn, J. M.; Rigault, A.; Siegel, J.; Harrowfield, J.; Chevrier, B.; Moras, D. *Proc. Natl. Acad. Sci. U.S.A.* **1987**, *84*, 2565.

172. Piguet, C.; Bernardinelli, G.; Hopfgartner, G. *Chem. Rev.* **1997**, *97*, 2005-2062.

173. Pfeil, A.; Lehn, J. M. *J. Chem. Soc., Chem. Commun.* **1992**, 838.

174. Constable, E. C.; Edwards, A. J.; Raithby, P. R.; Walker, J. V. *Angew. Chem. Int. Ed.* **1993**, *32*, 1465-1467.

175. Goetz, S.; Kruger, P. E. *Dalton Trans.* **2006**, 1277-1284.

176. Edder, C.; Piguet, C.; Bünzli, J.-C. G.; Hopfgartner, G. *J. Chem. Soc., Dalton Trans.* **1997**, 4657-4664.

177. Piguet, C.; Hopfgartner, G.; Williams, A. F.; Bünzli, J.-C. G. *J. Chem. Soc., Chem. Commun.* **1995**, 491-493.

178. Elhabiri, M.; Scopelliti, R.; Bünzli, J.-C. G.; Piguet, C. *Chem. Commun.* **1998**, 2347-2348.

179. Horrocks, W. D.; Sudnick, D. R. *Science* **1979**, *206*, 1194-1196.

180. Desreux, J. F.; Reilley, C. N. *J. Am. Chem. Soc.* **1976**, *98*, 2105-2109.

181. Senegas, J.-M.; Koeller, S.; Bernardinelli, G.; Piguet, C. *Chem. Commun.* **2005**, 2235-2237.

182. Reddy, K. V.; Jin, S. J.; Arora, P. K.; Sfeir, D. S.; Maloney, S. C. F.; Urbach, F. L.; Sayre, L. M. *J. Am. Chem. Soc.* **1990**, *112*, 2332- 2340.

183. Hamuro, Y.; Geib, S. J.; Hamilton, A. D. *J. Am. Chem. Soc.* **1997**, *119*, 10587-10593.

184. Akitt, J. W.; Mann, B. E. *NMR and Chemistry: an introduction to modern NMR spectroscopy*, 4th ed.; Stanley Thornes, 2000.

185. Frey, S. T.; Chang, C. A.; Carvalho, J. F.; Varadarajan, A.; Schultze, L. M.; Pounds, K. L.; Horrocks, W. D. *Inorg. Chem.* **1994**, *33*, 2882 - 2889.

186. Wu, S. L.; Horrocks, W. D. *Inorg. Chem.* **1995**, *34*, 3724-3732.

187. Wang, Y.; Horrocks, J. W. D. *Inorg. Chim. Acta* **1997**, *263*, 309-314.

188. Kobayashi, Y.; Komatsu, T.; Sumi, M.; Numajiri, S.; Miyamoto, M.; Kobayashi, D.; Sugibayashi, K.; Morimoto, Y. *Eur. J. Pharm. Sci.* **2004**, *21*, 471-478.

189. Middleton, A.; Partington, J. R. *Nature* **1938**, *141*, 516.

190. Berlman, I. B. *Handbook of Fluorescence Spectra of Aromatic Compounds*; Academic Press: London, 1965.

191. Murov, S. L.; Carmichael, I.; Hug, G. L. *Handbook of Photochemistry*, 2nd ed.; Marcel Dekker, Inc.: New York, 1993.

192. Vander Donckt, E.; Nasielski, J.; Thiry, P. *J. Chem. Soc. D* **1969**, 1249.

193. Lasser, N.; Feitelson, J. *J. Phys. Chem.* **1973**, *77*, 1011-1016.

194. Werts, M. H. V.; Jukes, R. T. F.; Verhoeven, J. W. *Phys. Chem. Chem. Phys.* **2002**, *4*, 1542-1548.

195. McCoy, C. P.; Stomeo, F.; Plush, S. E.; Gunnlaugsson, T. *Chem. Mater.* **2006**, 4336-4343.

196. Wang, Y.-M.; Wang, Y.-J.; Wu, Y.-L. *Polyhedron* **1998**, *18*, 109-117.

197. Suárez, S.; Mamula, O.; Scopelliti, R.; Donnio, B.; Guillon, D.; Terazzi, E.; Piguet, C.; Bünzli, J.-C. G. *New J. Chem.* **2005**, *29*, 1323-1334.

198. Maeder, M.; Zuberbuehler, A. D. *Anal. Chem.* **1990**, *62*, 2220-2224.

199. Rodger, A.; Nordén, B. *Circular Dichroism and Linear Dichroism*; Oxford Chemistry Press: New York, Tokyo, 1997.

200. Zarges, W.; Hall, J.; Lehn, J.-M.; Bolm, C. *Helv. Chim. Acta* **1991**, *74*, 1843-1852.

201. Krämer, R.; Lehn, J.-M.; Cian, A. D.; Fischer, J. *Angew. Chem. Int. Ed.* **1993**, *32*, 703-706.

202. Field, J. E.; Muller, G.; Riehl, J. P.; Venkataraman, D. *J. Am. Chem. Soc.* **2003**, *125*, 11808-11809.

203. Muller, G.; Maupin, C. L.; Riehl, J. P.; Birkedal, H.; Piguet, C.; Bünzli, J.-C. G. *Eur. J. Inorg. Chem.* **2003**, 4065-4072.

204. Job, A. *Annales de Chemie* **1928**, *9*, 113.

205. Geraldes, C. F. G. C.; Alpoim, M. C.; Marques, M. P. M.; Sherry, A. D.; Singh, M. *Inorg. Chem.* **1985**, *24*, 3876-3881.

206. Riedo, T. J.; Kaden, T. A. *Helv. Chim. Acta* **1979**, *62*, 1089-1096.

207. Häfliger, H.; Kaden, T. A. *Helv. Chim. Acta* **1979**, *62*, 683-688.

208. Martell, A. E.; Motekaitis, R. J. *The determination and use of stability constants*; VCH Publishers: Weinheim, 1988.

209. Furniss, B. S.; Hannaford, A. J.; Smith, P. W. G.; Tatchell, A. R. *Textbook of Practical Organic Chemistry*, 5th ed.; Longman Scientific & Technical: New York, 1989.

Soft Matter pH Sensing: From Luminescent Lanthanide pH Switches in Solution to Sensing in Hydrogels

Colin P. McCoy*

School of Pharmacy, Queen's University Belfast, Belfast BT9 7BL, U.K.

Floriana Stomeo, Sally E. Plush, and Thorfinnur Gunnlaugsson

School of Chemistry, Centre for Synthesis and Chemical Biology, Trinity College Dublin, Dublin 2, Ireland

Received March 13, 2006. Revised Manuscript Received June 23, 2006

The synthesis, complexation, and photophysical properties of the Eu(III)-based quinoline cyclen conjugate complex **Eu1** and its permanent, noncovalent incorporation into hydrogels as sensitive, interference-free pH sensing materials for biological media are described. The Eu(III) emission in both solution and hydrogel media was switched reversibly "*on*−*off*" as a function of pH with a large, greater than order of magnitude enhancement in Eu(III) emission. The irreversible incorporation of **Eu1** into water-permeable hydrogels was achieved using poly[methyl methacrylate-*co*-2-hydroxyethyl methacrylate]-based hydrogels, and the luminescent properties of the novel sensor materials, using confocal laser-scanning microscopy and steady state luminescence, were characterized and demonstrated to be retained with respect to solution behavior. Water uptake and dehydration behavior of the sensor-incorporated materials was also characterized and shown to be dependent on the material composition.

Introduction

In recent years the use of ions and molecules to modulate fluorescence through the construction of fluorescent−receptor moieties has led to the development of luminescent sensors and switches.[1] This area is now well-established within the field of supramolecular chemistry.[2] Even though such fluorescent sensors are highly desirable and are now important tools in environmental, health, and biological monitoring, there are still significant drawbacks to the use of fluorescence.[3] This is particularly evident for on-line or field monitoring of biological media where many biological substrates are also fluorescent, emitting in the nanosecond time frame, and hence can mask or "pollute" the detection signal (the so-called autofluorescence).[4] Furthermore, light scattering in biological media can interfere with the measured signal. Means of overcoming these drawbacks have involved the use of long wavelength absorbing and emitting fluorophores, which can overcome the short wavelength emission, but not the short emission lifetimes. Using metal complexes, however, often overcomes both these drawbacks.[5] Such complexes have proved important in the study of nucleic acids as they can be selectively functionalized to intercalate, or bind, to DNA, with concomitant changes in their characteristic long wavelength emission bands. Alternatives to these metal complexes are those based on lanthanide ions, which emit at long wavelengths, with characteristic line-like emission bands and lifetimes ranging from sub-microseconds to sub-milliseconds, hence overcoming both of the above-mentioned drawbacks.[6−8] We have developed several examples of lanthanide-based luminescent sensors for ions and molecules, where the emission of Tb(III), Eu(III), Nd(III), and Yb(III) have been modulated.[9] As the lanthanides have low extinction coefficients, direct excitation is not feasible

* Corresponding author. Tel.: +44 28 9097 2081. Fax: +44 28 9024 7794. E-mail: c.mccoy@qub.ac.uk.

(1) (a) Feringa, B. L., Ed. *Molecular Switches*; Wiley-VCH: Weinheim, 2001. (b) Giordani, S.; Cejas, M. A.; Raymo, F. M. *Tetrahedron* **2004**, *60*, 10973. (c) de Silva, A. P.; McCaughan, B.; McKinney, B. O. F.; Querol, M. *Dalton Trans.* **2003**, 1902. (d) Balzani, V. *Photochem. Photobiol. Sci.* **2003**, *2*, 459. (e) Balzani, V.; Credi, A.; Venturi, M. *Pure Appl. Chem.* **2003**, *75*, 541. (f) Balzani, V.; Gómez-López, M.; Stoddart, J F. *Acc. Chem. Res.* **1998**, *31*, 405.

(2) de Silva, A. P.; Gunaratne, H. Q. N.; Gunnlaugsson, T.; Huxley, A. J. M.; McCoy, C. P.; Rademacher, J. T.; Rice, T. E. *Chem. Rev.* **1997**, *97*, 1515.

(3) Faulkner, S.; Matthews, J. L. In *Application of Coordination Complexes*; Ward, M. D., Ed.; Comprehensive Coordination Chemistry, 2nd ed., Vol. 9; Elsevier: Amsterdam, 2003.

(4) Parker, D. *Coord. Chem. Rev.* **2000**, *205*, 109.

(5) (a) Gunnlaugsson, T.; Leonard, J. P. *Chem. Commun.* **2005**, 3114. (b) Leonard. J. P.; Gunnlaugsson, T. *J. Fluoresc.* **2005**, *15*, 585.

(6) (a) Pope, S. J. A.; Coe, B. J.; Faulkner, S. *Chem. Commun.* **2004**, 1550. (b) Bretonnière, Y.; Cann, M. J.; Parker, D.; Slater, R. *Org. Biomol. Chem.* **2004**, *2*, 1624. (c) Bobba, G.; Bretonnière, Y.; Frias, J.-C.; Parker, D. *Org. Biomol. Chem.* **2003**, *1*, 1870. (d) Li, C.; Wong, W.-T. *Chem. Commun.* **2002**, 2034. Faulkner, S.; Burton-Pye, B. P.; Khan, T.; Martin, L. R.; Wray, S. D.; Skabara, P. J. *Chem. Commun.* **2002**, 1668. (e) Govenlock, L. J.; Mathieu, C. E.; Maupin, C. L.; Parker, D.; Riehl, J. P.; Sligardi, C.; Williams, J. A. G. *Chem. Commun.* **1999**, 1699. (f) de Silva, A. P.; Gunaratne, H. Q. N.; Rice, T. E.; Stewart, S. *Chem. Commun.* **1997**, 1891. (g) Beeby, A.; Parker, D.; Williams, J. A. G. *J. Chem. Soc., Perkin Trans. 2* **1996**, 1565. (h) Dickins, R. S.; Gunnlaugsson, T.; Parker, D.; Peacock, R. D. *Chem. Commun.* **1998**, 1643.

(7) (a) Parker, D. *Chem. Soc. Rev.* **2004**, *33*, 156. (b) Bünzli, J.-C. G.; Piguet, C. *Chem. Rev.* **2002**, *102*, 1897. (c) Tsukube, H.; Shinoda, S. *Chem. Rev.* **2002**, *102*, 2389. (d) Tsukube, H.; Shinoda, S.; Tamiaki, H. *Coord. Chem. Rev.* **2002**, *226*, 227. (e) Bünzli, J.-C. G.; Piguet, C. *Chem. Soc. Rev.* **1999**, *28*, 347. (f) Parker, D.; Williams, J. A. G. *J. Chem. Soc., Dalton Trans.* **1996**, 3616. (g) Sammes, P. G.; Yahioglu, G. *Nat. Prod. Rep.* **1996**, 1. (h) Sabbatini, N.; Guardigli, M.; Lehn, J.-M. *Coord. Chem. Rev.* **1993**, *123*, 201. (i) Georges, J. *Analyst* **1993**, *118*, 1481.

(8) Parker, D.; Dickins, R. S.; Puschmann, H.; Cossland, C.; Howard, J. A. K. *Chem. Rev.* **2002**, *102*, 1977.

10.1021/cm060603v CCC: $33.50
Published on Web 08/01/2006

in competitive media.[5,10] Hence, the use of macrocyclic or acyclic conjugates, furnished with chromophores (antennae) that have high extinction coefficients, has been employed by us and others to achieve indirect excitation of the lanthanide excited states by sensitization, also called the *antenna affect*.[11] By appropriately incorporating a recognition moiety into the antenna we have been able to achieve sensing through selective modulation of the lanthanide luminescence.[9,12]

In this paper we describe the synthesis of one such Eu(III)-based sensor for protons (**Eu1**), incorporating quinoline-derivatized cyclen (1,4,7,10-tetraazacyclododecane)[13] **1**. Ligand **1** has been designed to only have a single antenna. The Eu(III) emission is highly pH dependent can be easily and reversibly switched "*off−on*" in water. With the aim of developing such luminescent sensors with medical and pharmaceutical monitoring applications, we have also achieved the permanent, noncovalent incorporation of **Eu1** into water-permeable hydrogels and investigated several physical and photophysical properties of the resulting responsive materials.[14] The demonstration of retention of behavior in nonsolution environments is important for the development of soft matter real-time sensors which can be used in clinical monitoring environments. The choice of soft matter immobilization allows development of materials which are responsive to complex liquid analytes, such as blood, but can be employed reversibly, as the material is permeable to water but not complex biomolecules or cells, and can be returned to its initial state of switching by flushing with water.

Experimental Section

General Method. Starting materials were obtained from Sigma Aldrich, Strem Chemicals, and Fluka. Solvents used were HPLC grade unless otherwise stated. Water was purified with a Waters Milli-Q system to give a specific resistance of >15 MΩ cm and was then boiled for 30 min to remove CO_2 and allowed to cool in flasks fitted with soda lime tubes. ^{1}H NMR spectra were recorded at 400 MHz using a Bruker Spectrospin DPX-400, with chemical shifts expressed in parts per million (ppm or δ) downfield from the standard. ^{13}C NMR were recorded at 100 MHz using a Bruker Spectrospin DPX-400 instrument. Infrared spectra were recorded on a Mattson Genesis II FTIR spectrophotometer equipped with a Gateway 2000 4DX2-66 workstation. Mass spectroscopy was carried out using HPLC grade solvents. Mass spectra were determined by detection using Electrospray on a Micromass LCT spectrometer, using a Shimadzu HPLC or Waters 9360 to pump solvent. The whole system was controlled by MassLynx 3.5 on a Compaq Deskpro workstation. UV−visible spectroscopy was carried out on a Shimadzu UV-2401 PC UV−visible spectrophotometer. Studies were carried out on fast scan mode with slit widths of 1.0 nm, using matched quartz cells. Excitations were carried out at 300 nm unless otherwise stated. Solution fluorescence and luminescence measurements were made on a Perkin-Elmer LS 50B or Varian Carey Eclipse.

Synthesis of Ligand 2-{4,7-Bis-dimethylcarbamoylmethyl-10-[(2-methyl-quinolin-4-ylcarbamoyl)-methyl]-1,4,7,10-tetraaza-cyclododecayl}-*N*,*N*-dimethyl-acetamide, 1. 2-(4,10-Bis-dimethylcarbamoylmethyl-1,4,7,10-tetraaza-cyclododec-1-yl)-*N*,*N*-dimethyl-acetamide (**3**) (0.272 g, 0.636 mmol), Cs_2CO_3 (0.228 g, 0.7 mmol), KI (0.116 g, 0.7 mmol), and chloro-*N*-(2-methyl-4-quinolyl)-ethanamide (**2**) (0.164 g, 0.7 mmol) were added to DMF (35 mL). The mixture was heated at 80 °C under inert atmosphere for 72 h. The solution was filtered and the solvent removed under reduced pressure. A dark orange viscous residue was obtained (0.359 g, 0.57 mmol) and then purified by precipitation from diethyl ether to give a brown solid in 53% yield. Calculated for $C_{32}H_{51}N_9O_4$, $(M + H)^+$ *m/z* (% ES^+): 626.4142; Found: 626.4163. δ_H (400 MHz, $CDCl_3$): 10.5 (1H, s, N*H*), 8.75 (1H, d, $J = 8.5$, Ar-*H*), 7.93 (1H, s, Ar-*H*), 7.89 (1H, d, $J = 8.5$ Hz, Ar-*H*), 7.57 (1H, t, $J = 6.0$ Hz, Ar-*H*), 7.43 (1H, t, $J = 6.0$ Hz, Ar-*H*), 3.86 (2H, s, HNCOCH_2), 2.70 (43H, m, N−CH_3, CH_2CON(CH_3)$_2$, cyclen CH_2). δ_c (100 MHz, $CDCl_3$): 172.1, 170.4, 170.3, 158.3, 148.0, 141.8, 128.7, 127.7, 124.6, 123.4, 119.7, 112.6, 57.6, 54.5, 54.4, 35.7, 35.6, 35.0, 28.8, 26.5, 25.2. *m/z*: 626.33 $(M + H)^+$, 313.67 $(M + 2H/2)^+$. υ(KBr)/ cm^{-1}: 3434, 2949, 2818, 2363, 1645, 1531, 1499, 1451, 1407, 1348, 1299, 1266, 1185, 1102, 1005, 769.

Synthesis of Eu(III) Complex of 1, Eu1. 2-{4,7-Bis-dimethylcarbamoylmethyl-10-[(2-methyl-quinolin-4-ylcarbamoyl)-methyl]-1,4,7,10 tetraaza-cyclododeca-yl}-*N*,*N*-dimethyl-acetamide (**1**) (0.095 g, 0.15 mmol) and Eu(III) trifluoromethane sulfonate (0.1 g, 0.16 mmol) were added to a 25 mL single-neck round-bottom flask that contained freshly dried MeCN (10 mL). After three freeze−pump−thaw cycles, the solution was placed under an argon atmosphere and left stirring at reflux for 24 h. The resulting solution was cooled to room temperature and then added dropwise to dry diethyl ether (100 mL) with stirring. The resulting precipitate was isolated to give **Eu1** as a pale green solid in 84% yield. δ_H (400 MHz, CD_3OCD_3): 12.7, 10.4, 8.0, 6.9, 3.1, 2.2, 1.6, −5.5, −6.2, −7.0, −8.5. *m/z*: 463.5 $([M + CF_3SO_3]/2)^+$, 259.4 $(M/3)^+$, 388.6 $(M/2)^+$. υ(KBr)/ cm^{-1}: 3434, 2361, 2343, 1624, 1255, 1164, 1030, 639.

Ground and Excited State pK_a Determinations. Titration solutions were saturated with argon by passing a fine stream of bubbles (previously passed through aqueous 0.1 M KOH followed by 0.1 M NEt_4ClO_4) through them for at least 15 min before the commencement of titration. (CAUTION: Anhydrous perchlorates are potentially explosive and should be handled with caution.) During the titrations a fine stream of argon bubbles was passed through the titration vessel that was closed to the atmosphere except for a small vent for the argon stream. The titrations were carried out using a MOLSPIN titrimator, MOLSPIN potentiometer, and an Orion 8172 Ross Sureflow combination pH electrode. Values of E_0 and pK_w were determined using the program GLEE. At least three runs were carried out for each system, and at least two of these runs were averaged; the criterion for selection for this averaging being that χ^2 for each run was <12.6 at the 95% confidence level. Values for each pK_a and K were determined using the program HYPERQUAD. The ground state pK_as (S_0) where calculated from the following formula:[21]

(9) (a) Gunnlaugsson, T.; Leonard, J. P.; Sénéchal, K.; Harte, A. J. *J. Am. Chem. Soc.* **2003**, *125*, 12062. (b) Gunnlaugsson, T.; Leonard, J. P.; Sénéchal, K.; Harte, A. J. *Chem. Commun.* **2004**, 782. (c) Gunnlaugsson, T.; Leonard, J. P. *Chem. Commun.* **2003**, 2424. (d) Gunnlaugsson, T.; MacDónaill, D. A.; Parker, D. *Chem. Commun.* **2000**, 93. (e) Gunnlaugsson, T.; Parker, D. *Chem. Commun.*, **1998**, 511.

(10) Bünzli, J.-C. G., Choppin, G. R., Eds. *Lanthanide Probes in Life, Chemical and Earth Sciences, Theory and Practice*; Elsevier: New York, 1989; p 219.

(11) (a) Merbach, A. E.; Tóth, E. *The chemistry of contrast agents in medical magnetic resonance imaging*; Wiley: West Sussex, England, 2001. (b) DeW Horrocks, W.; Sudnick, D. R. *Science* **1979**, *206*, 1194.

(12) Gunnlaugsson, T. *Tetrahedron Lett.* **2001**, *42*, 8901.

(13) Gunnlaugsson, T.; McCoy, C. P.; Stomeo, F. *Tetrahedron Lett.* **2004**, *45*, 8403.

(14) Gans, P.; Sabatini, A.; Vacca, A. *Talanta* **1996**, *43*, 1739.

(15) Gunnlaugsson, T.; Mac Dónaill, D. A.; Parker, D. *J. Am. Chem. Soc.* **2001**, *123*, 12866.

$$pK_a(S_0) = pH - \log\frac{(Abs_{AH} - Abs_A)}{(Abs_A - Abs_{A-})}$$

where Abs_{AH}, Abs_A, and Abs_{A-} are the absorbances of every solution, the absorbance of the protonated species, and the absorbance of the deprotonated species.

The excited state pK_as (S_1) were determined from the Förster cycle as follows:[22]

$$pK_a(S_1) = pK_a(S_0) + \frac{0.625}{T}\Delta\nu$$

where $\Delta\nu$ is the difference between the energy of the protonated and deprotonated form in reciprocal centrimeters and T is the absolute temperature.

Preparation of Sensor-Incorporated and Control Hydrogels. Complex **Eu1** was nonconvalently incorporated into three different hydrogel matrixes comprised of cross-linked poly[methyl methacrylate-*co*-2-hydroxyethyl methacrylate]. The control hydrogel matrixes were prepared using methyl methacrylate (MMA) and 2-hydroxyethyl methacrylate (HEMA) in three different ratios: 1:1 (MMA:HEMA, w/w), 1:3 (MMA:HEMA, w/w), and 100% HEMA. For all of these, monomers were stirred with ethylene glycol dimethacrylate (1% w/w) (used as a cross-linker) and azo-bis-isobutyronitrile as a radical initiator (1% w/w) until dissolved. In all cases, the total mass of polymer prepared was 10 g. Sensor-incorporated hydrogels were prepared in an analogous manner as control polymers, with Eu1 (0.05% w/w) being dissolved in the monomer mixture prior to polymerization. The mixture was injected into a mould using a 1 mm spacer between two glass places at 90 °C for 6 h, and the resulting polymer sheets were soaked in deionized water for 3 days.

Determination of Equilibrium Water Content of Hydrogel Sensor Materials. Complex-incorporated hydrogel films prepared with different ratios of HEMA and MMA were cut (1 cm × 1 cm) in their water-swollen state. The samples were dehydrated at 60 °C to constant weight. The samples were then immersed in deionized water and reweighed, following gentle removal of excess surface water with a tissue, at intervals until a constant weight was achieved. All measurements were made in triplicate, and values are quoted as the mean ± 1 standard deviation. The equilibrium water content (EWC), defined as a ratio of the mass of water taken up to the mass of dry sample, was calculated using the following equation:

$$\text{EWC (\%)} = \frac{\text{mass of hydrated sample} - \text{mass of dehydrated sample}}{\text{mass of dehydrated sample}} \times 100$$

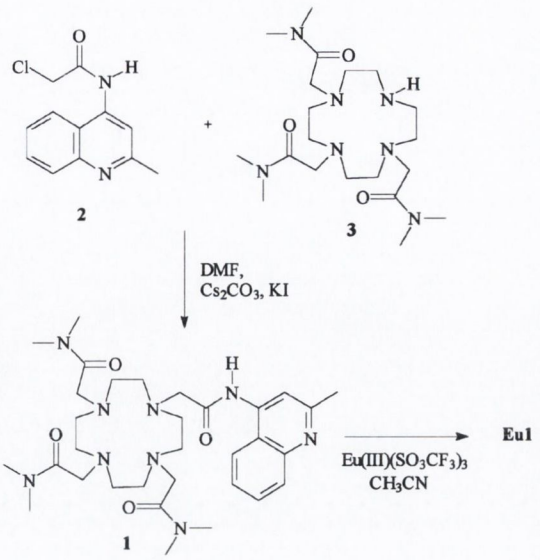

Figure 1. Synthesis of ligand **1** and the corresponding Eu(III) complex **Eu1**.

Luminescence Measurements of Hydrogel Sensor Materials. Confocal laser scanning microscopic (CLSM) examination of hydrogel samples was carried out with a Leica TCS SP2 confocal laser scanning microscope. After focusing, the sample surface was excited using the 458 nm line from a Ar/ArKr laser and luminescence data collected over the range 500−800 nm. Luminescence emission micrographs show summed photomultiplier intensities across the full wavelength range detected with a look-up table assigning color to overall intensity ranging from black (zero intensity) to bright red (highest intensity). Steady state luminescence measurements were made using a front-surface accessory to clamp hydrogel sections in a Perkin-Elmer LS 50B.

Results and Discussion

Synthesis of Sensor 1 and Its Eu(III) Complex, Eu1. The synthesis of ligand **1** is shown in Figure 1. The synthesis involved the formation of the α-chloroamide derivative of the corresponding quinoline amine. The α-chloroamide **2** was made in one step by reacting chloroacetyl chloride with 4-aminoquinoline at −10 °C in dry THF for 12 h. Filtration of the inorganic salts followed by acid−base extraction and trituration of the resulting off-white solid with DCM gave **2** in 65% yield. The trisubstituted ligand **3**, 2-(4,10-bis-dimethyl-carbamoylmethyl-1,4,7,10-tetraaza-cyclododec-1-yl)-*N*,*N*-dimethyl-acetamide, which had been formed in a single step from cyclen, was then reacted with **2** in DMF at 85 °C in the presence of Cs_2CO_3 and KI for 3 days. The resulting ligand **1** was purified by precipitation from dry diethyl ether in a 53% yield. The Eu(III) complex of **1** was made by refluxing **1** and $Eu(CF_3SO_3)_3$ in dry MeCN under an inert atmosphere for 24 h, followed by precipitation from dry diethyl ether, and isolation of the desired off-white powder in 84% yield. The ^1H NMR of **Eu1** ((CD_3COCD_3)) showed the characteristic europium shifted axial and equatorial cyclen protons, confirming that in solution the complex adopts a square prismatic geometry. The ESMS also showed that complexation had occurred. An Eu(III) isotopic distribution pattern was observed for the complex which matched that of the calculated spectra.

(16) (a) Special issue, "Recent Advances in Rare Earth Chemistry": Kobayashi, S. *Tetrahedron* **2003**, *52*, 10349. (b) Special issue, "Frontiers in Lanthanide Chemistry": Kagan, H. B., Guest Ed. *Chem. Rev.* **2002**, *102*, 1805.
(17) (a) Gunnlaugsson, T.; Harte, A.; Leonard, J. P.; Nieuwenhuyzen, M. *Supramol. Chem.* **2003**, *15*, 505. (b) Gunnlaugsson, T.; Harte, A.; Leonard, J. P.; Nieuwenhuyzen, M. *Chem. Commun.* **2002**, 2134.
(18) DeW Horrocks, W.; Sudnick, D. R *J. Am. Chem. Soc.* **1979**, *101*, 334.
(19) (a) Beeby, A.; Clarkson, I. M.; Dickins, R. S.; Faulkner, S.; Parker, D.; Royle, L.; de Sousa, A. S.; Williams, J. A. G.; Woods, M. *J. Chem. Soc., Perkin Trans. 2.* **1999**, 493 (b) Dickins, R. S.; Parker, D.; de Sousa, A. S.; Williams, J. A. G. *Chem. Commun.* **1997**, 697.
(20) Bruce, J. I.; Dickins, R. S.; Govenlock, L. J.; Gunnlaugsson, T.; Lopinski, S.; Lowe, M. P.; Parker, D.; Peacock, R. D.; Perry, J. J. B.; Aime, S.; Botta, M. *J. Am. Chem. Soc.* **2000**, *122*, 9674.
(21) Jaffé, H. H.; Orchin, M. *Theory and Applications of Ultraviolet Spectroscopy*; Wiley: New York, 1962.
(22) Förster, R.; *Z. Electrochem.* **1950**, *54*, 531.

Table 1. pK_a Values of the Protonated Ligand 1 at 298.2 K and I = 0.1 M (NEt_4ClO_4) in Water

equilibrium quotient	pK_a	designation
$[\mathbf{1}][H^+]/[H_1\mathbf{1}^+]$	10.65 ± 0.02	pK_{a1}
$[H\mathbf{1}^+][H^+]/[H_2\mathbf{1}^{2+}]$	8.96 ± 0.04	pK_{a2}
$[H_2\mathbf{1}^{2+}][H^+]/[H_3\mathbf{1}^{3+}]$	6.84 ± 0.05	pK_{a3}
$[H_3\mathbf{1}^{3+}][H^+]/[H_4\mathbf{1}^{4+}]$	4.95 ± 0.07	pK_{a4}
$[H_4\mathbf{1}^{4+}][H^+]/[H_5\mathbf{1}^{5+}]$	low	pK_{a5}

Potentiometric Measurements of 1 and Eu1. The pK_a values of the protonated ligand **1** were determined by potentiometric pH titration of the acidified ligand (L = 6.4 × 10^{-4} M, H^+ = 6.5 × 10^{-3} M) against 0.103 M NEt_4OH with I = 0.1 M (NEt_4ClO_4) in water. Four pK_a values were determined for ligand **1** using the program HYPERQUAD (Table 1).[15] The two larger pK_a values, pK_{a1} and pK_{a2}, and the smallest determined pK_a, pK_{a4}, of ligand **1** are assigned to the protonation of the macrocyclic ring amines. It is assumed that the fourth pK_a of the macrocyclic ring, pK_{a5}, is too small to be determined. The remaining pK_a value of 6.84 ± 0.05 (pK_{a3}) was assigned to the protonation of the quinoline nitrogen. For similar systems, large pK_a values for protoned quinoline nitrogens have also been observed.[16]

The complexation constants for ligand **1** were determined in an analogous manner to the protonation constants except that an equimolar quantity of $Eu(CF_3SO_3)_3$ was also present in solution, as shown in the titration curve in Figure 2. The derived complexation constants and pK_as for the protonated ligand complexes, determined using the program HYPERQUAD,[15] are shown in Table 2.

The pK_a of the MLH complex, 6.13 ± 0.09, can be assigned to the deprotonation of the quinoline nitrogen. This value is similar to the pK_{a3} value of the free ligand **1**. It was anticipated that the pK_a values would be similar because the quinoline nitrogen is not expected to be involved directly in metal ion coordination.

The deprotonation of the metal bound water was also observed with a pK_a of 7.47 ± 0.05 determined. This was expected because ligand **1** has only eight coordination sites and europium is capable of forming nine-coordinate complexes. The pK_a value of 8.77 ± 0.09 can be assigned to the deprotonation of the quinoline carboxylic amide. This value is lower than generally observed for carboxylic amides but this can be attributed to the effect of the strong Lewis acid europium metal ion center.

Determination of the Coordination Numbers of Eu1. The coordination numbers of lanthanides are usually high and hence require polydentate ligands.[17] Ligand **1** can provide eight such coordination sites, four from the nitrogens of the cyclen structure, and four from the carboxylic amides. Europium generally has a coordination number of nine in such tetrasubstituted cyclen complexes, with the axial ninth site being occupied by a coordinated solvent molecule or an anion.[18] The way of estimating q was first determined by Horrocks and Sudnick by measuring the excited state lifetimes of Eu(III) and Tb(III) in H_2O and D_2O, respectively.[19] This method was reviewed by Parker et al., which is the method of choice herein. In the case of **Eu1**, the presence of the coordinated water molecule was determined

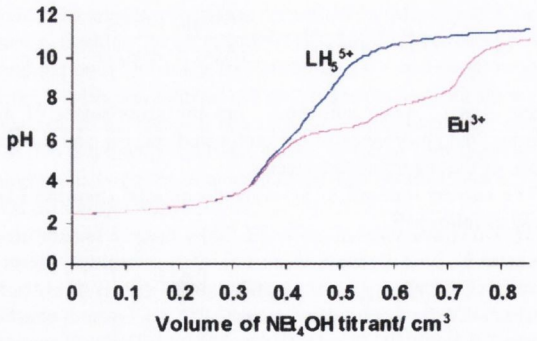

Figure 2. Titration curve for ligand **1** (LH_5^{5+}), formed in a solution, where [**1**] = 6.4 × 10^{-4} M and $[H^+]$ = 6 × 10^{-3} M at 298.2 K and I = 0.1 M (NEt_4ClO_4). The titration curve is also shown for the same solution except that $[Eu^{3+}]$ = 6.4 × 10^{-4} M was also present. Titrant [NEt_4OH] = 0.103 M.

Table 2. Complexation Constants, log K/dm^3 mol^{-1}, and pK_a Values for the Complexation of Eu^{3+} with Ligand 1 at 298.2 K and I = 0.1 M (NEt_4ClO_4)

equilibrium quotient	log K/dm^3 mol^{-1}
$[Eu(\mathbf{1})^{3+}]/[Eu^{3+}][\mathbf{1}]$	9.59 ± 0.02
equilibrium quotient	**pK_a**
$[Eu\mathbf{1}^{3+}][H^+]/[Eu(H\mathbf{1})^{4+}]$	6.13 ± 0.09
$[Eu\mathbf{1}OH^{2+}][H^+]/[Eu\mathbf{1}^{3+}]$	7.47 ± 0.05
$[Eu\mathbf{1}H_{-1}^{2+}][H^{-1}]/[Eu\mathbf{1}^{3+}]$	8.77 ± 0.09

by measuring the lifetimes of the Eu(III) emission in H_2O and D_2O, using the Parker modified equation:[20]

$$q_{Eu} = 1.2[(1/\tau_{H2O} - 1/\tau_{D2O}) - 0.25 - 0.075x]\ (\pm 0.3)$$

where x takes into account the effect of exchangeable amide N−H oscillators. The lifetime of the Eu(III) excited state was measured in neutral media. For **Eu1** τ_{H2O} was measured to be 429 μs whereas τ_{D2O} = 758 μs, yielding q = 0.91 (inner + outer sphere, after correcting for the amide NH oscillators). This indicates that the complex has a single bound water molecule, hence the complex is nine coordinate. This is in agreement with the potentiometric titrations.

Ground State Investigations. The ground, singlet excited state and the Eu(III) emission were evaluated for **Eu1** in water and in the presence of tetraethylammonium perchlorate (I = 0.1 M) to maintain a constant ionic strength. The ground state and the singlet excited state pK_a values were calculated according to the formulas described in the Experimental Section.[21,22]

For **Eu1**, the absorption spectra, when recorded first in acidic solution, displayed a maximum peak at 320 nm, with a shoulder at about 330 nm. Upon basification there was a significant hypsochromic and hypochromic shift to a broad absorption band due to the $\pi \rightarrow \pi^*$ transition centered at 305 nm, as shown in Figure 3. Two isosbestic points are observable in the spectra at ca. 263 and 303 nm, which suggests the presence of more than two species in equilibrium, as is reasonable with two deprotonation steps occurring across the range titrated.

The changes in the absorption spectra were plotted as a function of pH at 330 nm, as shown in Figure 4. This clearly shows that there is a significant decrease in the absorbance of the complex above pH 8. A pK_a of 8.82 ± 0.1 was

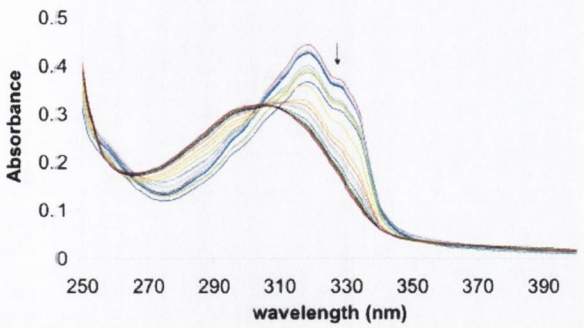

Figure 3. UV−visible spectra for the pH titration of **Eu1**. The arrow indicates the spectral trend with increasing pH between pH 3−11.5.

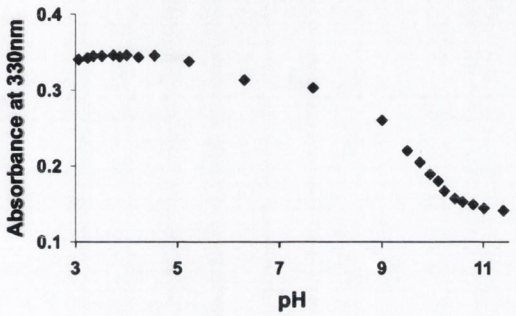

Figure 4. Changes in absorbance at 330 nm as a function of pH for **Eu1**.

calculated for this change. This coincides with the pK_a of 8.77 ± 0.09 determined for the deprotonation of the quinoline carboxylic amide. A slight decrease in absorbance is also noted above pH 5. A pK_a of 5.93 ± 0.1 was calculated. This change is therefore most likely due to the deprotonation of the quinoline nitrogen (pK_a 6.13 ± 0.09). As expected, deprotonation of the metal-bound water did not have an observable effect on the absorption of the complex. Therefore, only two pK_as where calculated as anticipated by the isosbestic points observed in Figure 3.

Singlet Excited State Investigations. The changes in the fluorescence emission spectra of the complex were investigated as a function of pH in water in the presence of tetraethylammonium perchlorate (I = 0.1 M). The changes were monitored following excitation at 330 nm, where there was a significant difference in the magnitude of the extinction coefficient in alkaline (low ϵ) and acidic solution (high ϵ). The changes in the emission spectra of **Eu1** when excited at 330 nm gave rise to spectral changes that mirror those seen in the absorption spectrum. In alkaline solution there was a structural band centered at 375 nm. Upon acidification there was a distinctive shift in the emission spectra from 375 nm to shorter wavelengths with the formation of a band with maximum at 357 nm, and two shoulders at 345 and 375 nm with concomitant enhancement of the emission intensity, as shown in Figure 5.

When the changes at 356 nm were plotted as a function of pH, a sigmoidal curve was observed, as shown in Figure 6. The changes observed show that the singlet state is only slightly affected below pH 8 and that the emission was switched "*off*" in alkaline solution. It is well-known that the acid−base behavior of many organic molecules can be strongly affected by electronic excitation.[23]

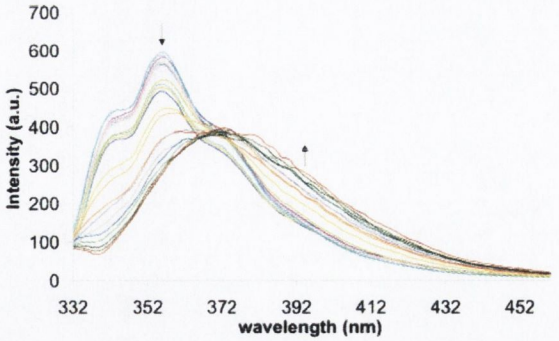

Figure 5. Overlaid fluorescence emission spectra for the pH titration of **Eu1**. Arrows indicate the spectral trend with increasing pH between pH 3−11.5.

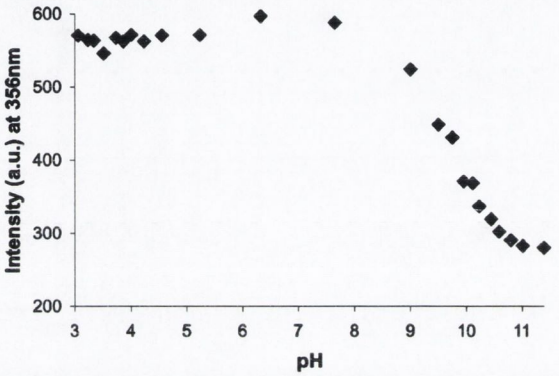

Figure 6. Changes in emission intensity at 356 nm as a function of pH for **Eu1**.

From the changes above pH 8, using the Förster equation given in the Experimental Section,[22] a pK_a of 9.47 ± 0.1 was calculated. This indicates that the basicity of **Eu1** is increased upon excitation to the first singlet state. There is a slight increase in the fluorescence intensity above pH 5; small changes in the absorption spectra were also noted above pH 5. The calculation of an excited state pK_a value using the Förster equation requires a change in wavelength; as this did not occur the excited state pK_a value for the changes between pH 5−8 cannot be determined in this manner. Excited state pK_a values and hence the assignment of the deprotonation steps cannot be determined with the same degree of accuracy as those for the ground state.[24] It is, however, expected that the changes between pH 5−8 are caused by the deprotonation of the quinoline nitrogen, while the changes above pH 8 are associated with the deprotonation of the quinoline carboxylic amide.

Eu(III) Excited State Investigations. The changes in the Eu(III) emission were investigated as a function of pH. In a similar manner as described above, the quinoline moiety of **Eu1** was excited at 330 nm in alkaline solution, and the changes in the Eu(III) emission were recorded as a function of pH.

In acidic solution, the Eu(III) emission, when excited at 330 nm (where the difference between the absorption in alkaline vs acid solution is the greatest), was clearly

(23) Tajima, S.; Tobita, S.; Shizuka, H. *J. Phys. Chem. A* **2000**, *104*, 11270.
(24) Sikorska, E.; Szymusiak, H.; Khmelinskii, I. V.; Koziolowa, A.; Spanget-Larsen, J.; Sikorski, M. *J. Photochem. Photobiol. A* **2003**, *158*, 45.

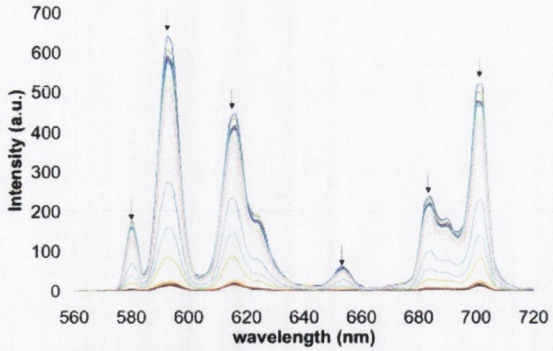

Figure 7. Changes in the Eu(III) emission of **Eu1** as a function of pH in solution, showing the deactivation of the $^5D_0 \rightarrow {}^7F_J$ ($J = 0$, 1, 2 (split), 3, and 4 (split)). Arrows indicate the spectral trend with increasing pH between pH 3−11.5. These changes are fully reversible.

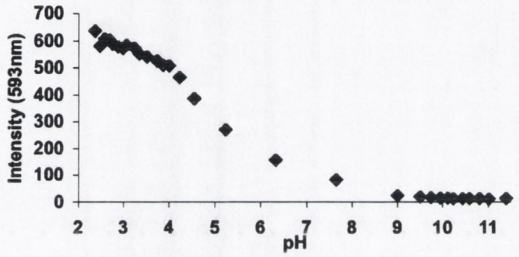

Figure 8. Changes in the Eu(III) emission of **Eu1** at 593 nm as a function of pH in solution.

"*switched on*" with large (up to a factor of 30) enhancements in the 580, 593, 615, 624, 654, 683, and 701 nm bands, representing the deactivation of the $^5D_0 \rightarrow {}^7F_J$ ($J = 0$ (580 nm), 1 (593 nm), 2 (split; 615 and 624 nm), 3 (654 nm), and 4 (split; 683 and 701 nm)),[7f] as shown in Figure 7.

These luminescence enhancements highlight the ability of the antenna to populate the lanthanide excited state by sensitization and that this process is highly pH-dependent. Moreover, the luminescence switching was fully reversible, since addition of strong base (pH ~ 10) quenches the emission, which could be subsequently "*switched on*" again by the addition of acid (pH = 1.6). The changes to the Eu(III) emission when plotted as a function of pH gave rise to a sigmoidal curve, shown in Figure 8.

Above pH 4.5 the Eu(III) emission significantly decreased until it was completely quenched above pH 9. The pK_a of the quinoline nitrogen as determined by potentiometric titration (6.13), absorption, and fluorescence spectroscopy (5.93) is in the pH range of 4−8. Therefore the decrease in the Eu(III) emission above pH 4.5 can be associated with the deprotonation of the quinoline nitrogen. Above ca. pH 8, it would be expected that the effect due to the quinoline nitrogen deprotonation would be insignificant. However the Eu(III) emission is not fully quenched at this pH. It may be anticipated that the emission is affected by the deprotonation of either the metal bound water, the quinoline carboxylic amide, or a combination of the two. Deprotonation of the metal bound water molecule would affect the O−H harmonic quenching of the Eu(III) excited state. The small change in Eu(III) emission that occurs between pH 2.5−4 cannot be readily explained through ligand or complex deprotonation. Potentiometric titration, absorption, and fluorescence spectroscopy of the complex had shown no evidence of deprotonations in this pH range. The anion effect has also been discounted as a plausible explanation for the observed quenching between pH 2.5−4, as the luminescence titrations were repeated using a variety of counterions, i.e. ClO_4^-, $CF_3SO_3^-$, and Cl^-. The effect is therefore associated with the metal ion. We are currently exploring this low-pH Eu(III) emission quenching effect with different analogues.

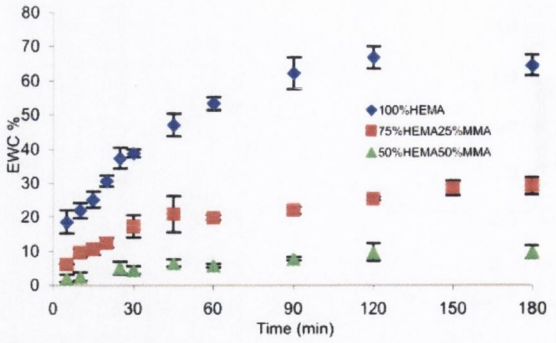

Figure 9. EWC (%) of the three different compositions of hydrogel with 0.1% (w/w) of **Eu1** during uptake from xerogels. Results are shown as the mean of three replicates ± one standard deviation.

From these results it is evident that the Eu(III) emission for **Eu1** is sensitive to changes in pH and that the changes shown in Figure 6 occur over a large pH range. Hence, **Eu1** can be used to monitor pH changes from ca. 2.5 to 8, mimicking pH electrodes.

Having established that the Eu(III) emission for**Eu1** was highly pH sensitive in competitive media, we choose to incorporate **Eu1** into water-permeable polymers.

Characterization of Eu1-Incorporated Water-Permeable Polymers. The Eu(III) complex **Eu1** was noncovalently incorporated into three different hydrogel matrixes comprised of poly[methyl methacrylate-*co*-2-hydroxyethyl methacrylate], denoted 1:1 (MMA:HEMA, w/w), 1:3 (MMA:HEMA, w/w), and 100% HEMA. The sensor was homogeneously incorporated at a concentration of 0.05% w/w.

Equilibrium Water Content. The water uptake kinetics and content of sensor-incorporated films was investigated using dehydrated samples of the materials (xerogels). When immersed into a hydrating medium, water enters and an equilibrium is eventually established between solvation of the copolymer and the forces holding the chains together. The degree of water uptake at equilibrium is a function of both the nature of the copolymer and the degree of cross-linking within that copolymer. Once this equilibrium is reached, the equilibrium water content (EWC) can be determined. The EWC of a material is an important parameter that has an influence on the physical properties of the hydrogels; the more hydrophilic the hydrogel the higher its EWC value. The EWC results for complex-incorporated films using the three different ratios of HEMA and MMA clearly demonstrate that increasing the HEMA content of the film significantly increased the equilibrium water content, as shown in Figure 9.

The EWCs for 1:1 MMA:HEMA, 1:3 MMA:HEMA, and 100% HEMA copolymers containing 0.05% (w/w) **Eu1** were determined to be 22.9 ± 1.7%, 39.6 ± 1.4%, and 58.2 ± 1.0%, respectively. All materials are fully equilibrated within

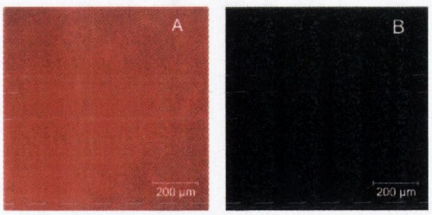

Figure 10. Confocal laser-scanning microscopy images of a section of hydrogel (MMA/HEMA, 1:3 w/w) incorporating 0.05% w/w **Eu1** in acidic (A) and basic (B) media.

90 min of immersion. An increase in EWC as the relative proportion of HEMA in the copolymers increases is expected due to the high hydrophilicity of HEMA relative to MMA, resulting from the pendant hydroxyl moiety of HEMA, which can participate in hydrogen bonding with water. The ability to control the EWC of the copolymer within which the complex resides is of considerable importance. High EWC hydrogels with immobilized sensors are expected to show enhanced response times compared to low EWC hydrogels due to their relatively high permeability to water; however, very high EWC gels, with resulting highly expanded polymer network structure, will facilitate the release of noncovalently incorporated sensors such as those employed here. Importantly, it was observed that all the hydrogels retained the **Eu1** complex entirely within the matrix for >1 month, as both absorbance and luminescence measurements of the solution in which the hydrogels were soaked showed no detectable levels of complex. The ability of all the matrixes to physically retain the **Eu1** complex is ascribed to hydrogen bonding interactions between the polymer chains and the complex. This interaction is proposed to take place through the free, ninth coordination site, which may be occupied by either a water solvent molecule (as demonstrated in solution) or a complex−polymer hydrogen bond. The irreversible retention of the complex in all the matrixes examined is attributable to the latter interaction.

Luminescence Measurements of Eu1 in Hydrogels. Hydrogel films were investigated using confocal laser-scanning microscopy (CLSM) and steady state luminescence.

CLSM allows direct, noninvasive measurement of fluorescence from the surface of a sample following excitation from an appropriate laser source. To build up a single image, data is collected pixel by pixel with the laser rastering over the sample, with measurement of overall fluorescence intensity within a defined wavelength range being translated into a false color for each pixel which correlates with that intensity. A full spectrophotometric measurement of luminescence emission from any defined area within a collected series of images can thus be obtained. This allowed characterization of both the distribution of the sensors within the hydrogel matrixes and the luminescence emission characteristics of the sensors on a macro (from square micrometer up to square millimeter) scale.

For all films the Eu(III) emission from the films was modulated by changing from an alkaline to an acidic medium. After the strips were soaked in acidic or alkaline solution for 1 h, the changes in the Eu(III) emission were recorded using CLSM as shown in the luminescence emission micrographs in Figure 10. Figure 10, which effectively maps Eu emission from the hydrogel surface, demonstrates the pH-dependent changes in the Eu(III) emission. These results show that the sensor is homogeneously dispersed within the medium and that in acidic solution the emission is switched "*on*" (Figure 10A), whereas in basic solution the Eu(III) was not observed and emission is switched "*off*" (Figure 10B). Hence, the luminescence of the films is highly sensitive to pH, as in solution.

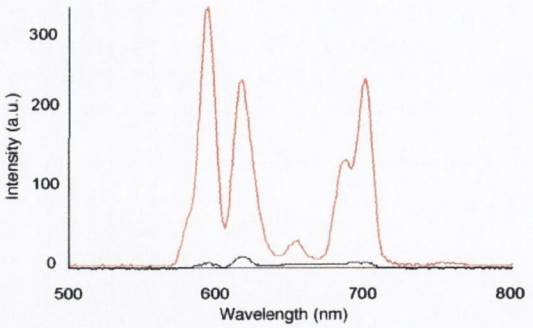

Figure 11. Eu(III) emission of the 1:3 MMA/HEMA film after soaking in pH 2 (red line) and pH 9 (black line) solutions for 24 h.

All the hydrogels showed a significant (>1 order of magnitude) difference in their Eu(III) emission intensities as a function of pH. These results mirror that seen in the aqueous solution; e.g. the emission was switched *"on"* in acid whereas in a basic environment the emission was switched *"off"*. The steady state fluorescence results for the 1:3 w/w MMA/HEMA hydrogel are shown in Figure 11.

By comparison with Figure 7, the relative intensities of each luminescence band ($\Delta J = 0$, 1, 2, 3, and 4) are, within experimental error, in agreement, indicating the close similarity of the europium environment in solution and hydrogel matrixes. Due to the experimental method, the resolution of spectra obtained for hydrogels is slightly lower than in solution, with the $\Delta J = 0$ band (580 nm) observed as a shoulder on the $\Delta J = 1$ band (593 nm). These results clearly demonstrate that such "*on−off*" pH dependent switching is possible both in hydrogels and in solution. The maximum switching factor (luminescent enhancement), observed for the MMA/HEMA, 1:3 w/w material, is 53, which is greater than the factor of 30 observed in solution and is a clear "*on−off*" signal. However, the time taken to achieve the fully switched *"on"* equilibrium was significantly different in the films to that observed in solution. In solution, the response is instantaneous; the hydrogel media respond more slowly, as the aqueous medium to be analyzed must diffuse into the hydrogel matrix. Nevertheless, the materials studied all give measurable *"on−off"* switching on the minute time scale.

Conclusion

In this paper we have described the synthesis and the characterization of the pH sensor **Eu1**. The Eu(III) emission of the complex was shown to be highly pH sensitive, and the emission could be reversibly switched "*off-on*" as a function of pH in solution. The permanent incorporation of **Eu1** in a noncovalent manner into three hydrogels of composition 1:1 (MMA:HEMA, w/w), 1:3 (MMA:HEMA,

w/w), and 100% HEMA was achieved. Of significant importance, the emission of these water-permeable materials was on all occasions found to be highly pH sensitive and reversible, as in solution. These materials thus represent matrixes which can be switched *"on"* or *"off"*, with potential application in the interference-free analysis of biological media.

We are currently improving on these design principles with the aim of achieving the sensing of other cations.

Acknowledgment. We thank Trinity College Dublin, Centre for Synthesis and Chemical Biology, the Queen's University Belfast, and The Royal Society (for a University Research Fellowship to McCoy) for financial support, Dr. John E. O'Brien for assisting with NMR, and Dr. Ryan J. Morrow for help with the preparation of hydrogels.

CM060603V

Available online at www.sciencedirect.com
SCIENCE DIRECT®
Tetrahedron Letters
ELSEVIER
Tetrahedron Letters 45 (2004) 8403–8407

Towards the development of Eu(III) luminescent switching/sensing in water-permeable hydrogels

Thorfinnur Gunnlaugsson,[a,*] Colin P. McCoy[b,*] and Floriana Stomeo[a]

[a]*Department of Chemistry, Centre for Synthesis and Chemical Biology, Trinity College Dublin, Dublin 2, Ireland*
[b]*School of Pharmacy, The Queen's University of Belfast, 97 Lisburn Road, Belfast BT9 7BL, UK*

Received 1 July 2004; revised 26 August 2004; accepted 3 September 2004
Available online 25 September 2004

Abstract—The synthesis of the Eu(III) complex **1.Eu** and photophysical studies of this complex in solution are described. In water, the Eu(III) luminescence was 'switched on' in the presence of H^+, with large enhancements in the Eu(III) luminescence. The complex was then incorporated into poly[methylmethacrylate-*co*-2-(hydroxyethylmethacrylate)]-based hydrogels and the luminescent properties of the resulting polymeric films were investigated using confocal laser-scanning microscopy as well as using steady-state luminescence. The luminescence was shown to be 'switched on' in the soft material after adjusting the pH of the solution in which the **1.Eu**-incorporated film was immersed from alkaline to acid.

The development of luminescent devices is an active area of research. A large number of examples of luminescent switches, sensors and logic gates have been reported over the last few years.[1,2] These examples are usually studied in solution where the change in the luminescent properties of the device is caused by the use of external 'inputs' such as ions or molecules,[3] though several excellent examples exist of 'fully' optically-based devices, where both the 'input' and the 'output' are optical.[4] Examples of the former include chemosensors, where the recognition or sensing of a particular analyte causes the modulation of one or more of the physical properties of the sensors.[5] For practical purposes the incorporation of such a chemosensor into materials is highly desirable, giving it a platform for continuous flow analysis, as well as of on-line monitoring of essential electrolytes in critical care analysis.[6] We are interested in the development of such chemosensors for ions and molecules,[7,8] and recently we have incorporated several fluorescent 1,8-naphthalimide derivatives into poly[methylmethacrylate-*co*-2-(hydroxyethylmethacrylate)]-based hydrogels with the aim of developing novel luminescent devices.[9] Even though this approach was successful, the drawback to the use of such fluorescent materials is the short excited state lifetimes that can easily coincide with that of any biological background emission, that is autofluorescence. One way to overcome this is by employing long-lived and long wavelength emitting probes. For such purposes the use of lanthanide luminescence[10,11] is particularly attractive as the ions emit at long wavelengths and have relatively long-lived excited states (in the μs–ms time frame). However, the main drawback in the use of these emitting moieties is the difficulty of producing their excited state by direct excitation. This can be overcome by population of their excited state via sensitization from an appropriately energy-matched antenna.[10–12] This opens up the avenue of developing combined antenna–receptor moieties where the sensitization process can be modulated by a recognition event at the receptor part.[10,11] We, and others, have demonstrated such delayed luminescent switching and sensing in aqueous solutions, using synthetic lanthanide-based conjugates and self-assembly processes.[10–12] However, to the best of our knowledge, the incorporation of such 'switchable' lanthanide luminescent devices into

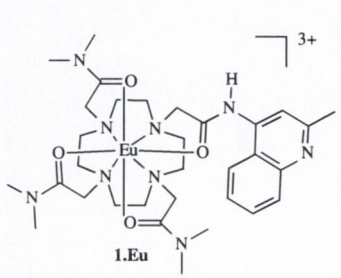

1.Eu

* Corresponding authors. Tel.: +353 1 608 2345; fax: +353 1 671 2826; e-mail: gunnlaut@tcd.ie

0040-4039/$ - see front matter © 2004 Elsevier Ltd. All rights reserved.
doi:10.1016/j.tetlet.2004.09.042

water-permeable hydrogels has not been achieved.[13] Here we describe the development of a lanthanide luminescent pH sensor **1.Eu** which shows reversible luminescence 'off–on' switching as a function of pH and the preliminary results of the noncovalent incorporation of this sensor into water-permeable hydrogels,[14] and the luminescent properties within the gel.

The design of **1.Eu** is based on the use of the tetraaza macrocycle cyclen (1,4,7,10-tetraazacyclododecane), which upon incorporation of four pendant arms such as carboxylates or carboxylic amides can form kinetically and thermodynamically stable complexes with lanthanide ions. It is also possible to functionalize selectively one (or more) of these pendant arms to allow for the incorporation of antenna moieties. We have used this metal coordination core for the incorporation of various antennae using combined antenna–receptor moieties. To demonstrate the feasibility of the incorporation of such a luminescent lanthanide complex into the hydrogels, we chose to use quinaldine chromophores, where the nitrogen moiety acts as a proton acceptor.[15] However, this is the first time that such a combined antenna–receptor is incorporated into a monofunctionalized cationic tetraamide Eu(III) complex, that is, only one antenna is incorporated.

The synthesis of **1.Eu** is shown in Scheme 1, and involves the reaction of the 2-(4,10-bis-dimethyl-carbamoylmethyl-1,4,7,10-tetraaza-cyclododec-1-yl)-*N*,*N*-dimethylacetamide **2**[16] with chloro-*N*-(2-methyl-4-quinolyl)ethanamide (**3**)[15] in DMF at 85 °C in the presence of Cs_2CO_3 and KI for 3 days. The ligand **1** was purified by precipitation from dry diethyl ether, giving **1** in 53% yield.[17] The two starting materials **2** and **3** have recently been reported by us.[15,16] The former was made in a single step by reacting the α-chloroamide of *N*,*N*-dimethyl-acetamide with cyclen in dry CH_3CN (in a 3:1 molar ratio of acetamide–cyclen) at 65 °C for 72 h in the presence of $NaHCO_3$. The product was then purified by column chromatography on alumina (gradient elution from CH_2Cl_2 to 60% NH_3 saturated MeOH/CH_2Cl_2 solution). The Eu(III) complex of **1** was made by refluxing together equivalent amounts of **1** and $Eu(CF_3SO_3)_3$ in dry CH_3CN under an inert atmosphere for 24 h. Upon cooling to room temperature the solution was poured into a stirring solution of dry diethyl ether, which resulted in a pale green solid in 84% yield.[18] The ^1H NMR of **1.Eu** in acetone-d_6 showed the characteristic europium shifted axial and equatorial cyclen protons, showing that the complex had been formed, and had adopted a square prismatic geometry in solution.[10] The ESMS of **1.Eu** also showed that complexation had occurred as a Eu(III) isotope pattern was observed for the complex as demonstrated for $(M + [triflate]/2)^+$ in Figure 1. By evaluating the lifetime of the Eu(III) excited state in both D_2O and H_2O, the complex was found to have one metal-bound water molecule.[10]

The **1.Eu** complex was finally incorporated into hydrogel matrices comprised of poly[methylmethacrylate-*co*-2-(hydroxyethylmethacrylate)] in a noncovalent manner,[9] using methylmethacrylate (MMA) and 2-(hydroxyethylmethacrylate) (HEMA) in three different ratios: 1:1 (MMA–HEMA, w/w), 1:3 (MMA–HEMA, w/w) and 100% HEMA. In all cases, ethylene glycol dimethacrylate was used as crosslinker and benzoyl peroxide as a radical initiator (both as 1% w/w of the total polymer). As **1.Eu** is cationic and hydrophilic, we chose to use a more water-permeable hydrogel matrix, by using higher percentages of HEMA, in comparison to our naphthalimide work.[9] The increased permeability to water was expected to decrease the time required for equilibration in response to pH changes. In order to achieve a homogeneous dispersion of **1.Eu** in the hydrogel, the complex (0.05% w/w) was dissolved in the appropriate monomer mixture prior to polymerization. After formation of the polymeric films, these were stored in neutral aqueous

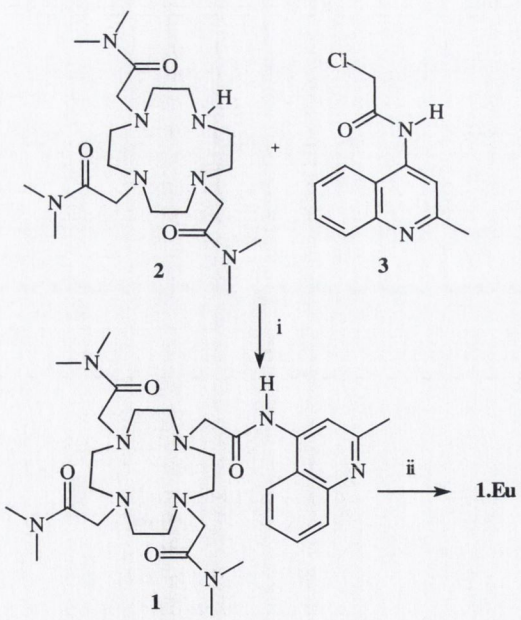

Scheme 1. Synthesis of **1** and the Eu(III) complex **1.Eu**. Reagents and conditions: (i) DMF, 85 °C, Cs_2CO_3, KI, 3 days; (ii) $Eu(CF_3SO_3)_3$, dry CH_3CN, reflux.

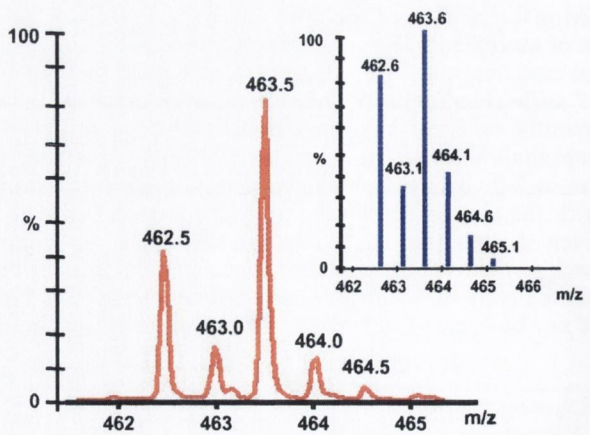

Figure 1. The electrospray mass spectrum of **1.Eu**, showing the isotopic distribution for $m/z = (M + [triflate]/2)^+$. Insert is the calculated isotopic distribution pattern for the same.

solution. Due to the different permeability grades of the films, a certain amount of **1.Eu** was found in the water where the hydrogel films were soaked over long-time storage (a period of days). Further investigations are required to determine the exact amount of the **1.Eu** released into solution as well as the kinetics of this process as a function of the hydrogel composition, but we do not believe that this is a major effect in the current study.

The photophysical properties of **1.Eu** were investigated both in water solution and in the above hydrogels. The changes in the absorption spectrum of the complex in water and in the presence of tetramethylammonium chloride (0.1 M, to maintain a constant ionic strength), as a function of pH are shown in Figure 2. In alkaline solution the complex has a broad absorption band due to the $\pi \rightarrow \pi^*$ transition which occurred at 300 nm. Upon acidification there was a significant shift to 319 nm, with a new band appearing at 261 nm, and with isosbestic points at 295 and 270 nm, respectively. In contrast to these results, the fluorescence emission spectra of **1.Eu** when excited at 330 nm gave rise to spectral changes that mirror those seen in the absorption spectrum, hence upon acidification (from alkaline solution) there was a distinctive shift in the emission spectra from 375 to 357 nm, and a subsequent enhancement of the emission intensity (from 350 to 700 a.u.). As stated above the efficiency of the population of the Eu(III) excited state is dependent on the ability of the antenna to sensitize the $^5D_0$ excited state. This will subsequently be seen in the intensity of the lanthanide luminescence that is due to the deactivation of the excited state to ^7F_J ($J = 1$, 2, 3 and 4) ground states. Hence, we chose 330 nm, where the difference between the absorption in alkaline versus acid solution is the greatest (cf. Fig. 2). Hence at this wavelength the efficiency of the sensitization of the $^5D_0$ excited state would be significantly pH dependent. The changes in the Eu(III) emission in solution as a function of pH are shown in Figure 3. Here the Eu(III) emission is clearly 'switched on' with large enhancements in the 580, 593, 615, 624, 654, 683 and 701 nm bands, respectively, representing the deactivation of the $^5D_0 \rightarrow {}^7F_J$ ($J = 0$, 1, 2, 3 and 4). Moreover, the luminescence switching was fully reversible, since addition of strong base (pH $\sim$ 10) quenched the emission, which could be subsequently 'switched on' again

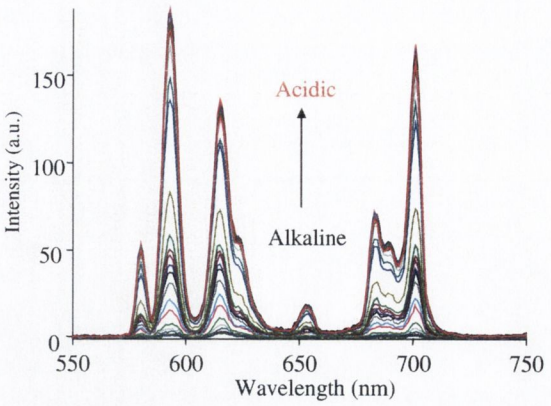

Figure 3. The changes in the Eu(III) emission of **1.Eu** in water as a function of pH.

by the addition of acid (pH = 1.6). By plotting the changes of any of these wavelengths as a function of pH (Fig. 4) it is clear that the emission changes almost linearly from ca. pH 3 to 8. These changes are mostly due to the protonation of the quinoline nitrogen moiety (between ca. 2.5 and 5) whereas the changes between ca. 6 and 8 are due to deprotonation of the quinoline carboxylic amide moiety, and mirror those seen in the fluorescence emission titration.[15a]

Having established the solution behaviour of **1.Eu** we analyzed the luminescent properties of the three lanthanide complex-incorporated hydrogel films. These were tested, in order of increasing hydrophilicity: 1:1 MMA/HEMA, 1:3 MMA/HEMA and 100% HEMA. For all films the Eu(III) emission was affected by going from alkaline to acidic media. This was achieved by soaking strips of the films in acidic or basic solutions for 1 h. The most hydrophilic (100% HEMA) and the most hydrophobic (1:1 MMA/HEMA) films showed an appreciable difference in the Eu(III) emission intensity, mirroring the behaviour in aqueous solution, where the emission was 'switched on' in acid (Fig. 5). It is worth remarking that the spectral fine structure obtained in solution is not so apparent in spectra recorded from films. We also recorded the changes in the Eu(III) emission after 24 h. The results for the 1:3,

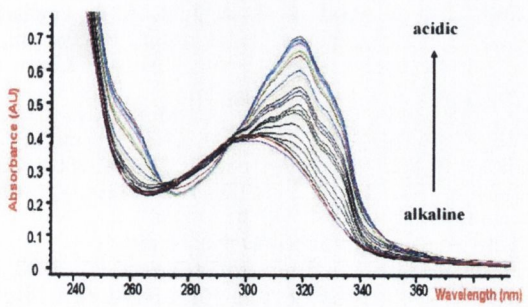

Figure 2. The changes in the absorption spectrum of **1.Eu** as a function of pH in water.

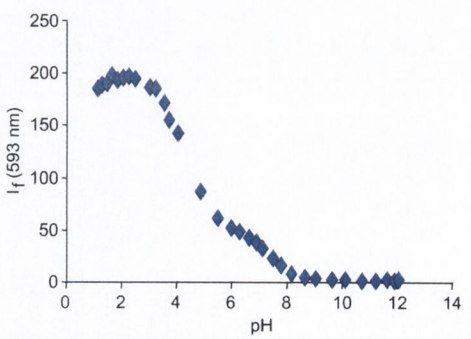

Figure 4. Changes in the Eu(III) emission at 593 nm as a function of pH.

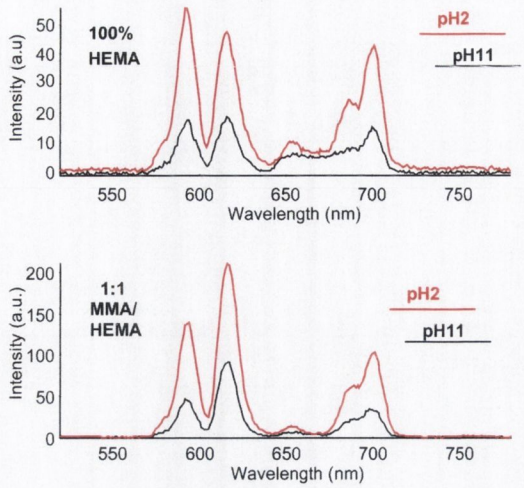

Figure 5. The change in the Eu(III) emission of the (top) 100% HEMA and 1:1 MMA/HEMA gels after 1 h soaking in either pH 2 or 11 solutions.

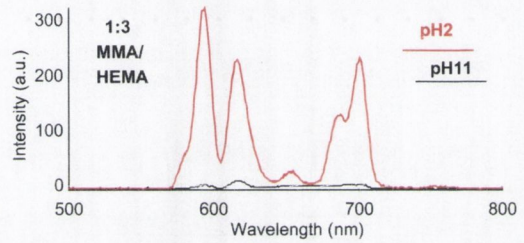

Figure 6. Luminescence emission spectra of **1.Eu** incorporated into MMA/HEMA (1:3) after soaking for 24 h.

MMA/HEMA hydrogel are shown in Figure 6. Here the Eu(III) emission has been fully 'switched off'. These results demonstrate that such 'off–on' pH dependent switching is possible both in solution and in the hydrogels. However, after such prolonged soaking some leaching had occurred as the solution gave rise to Eu(III) emission, indicating that the complex had diffused from the film. However, we did not quantify the degree of this leaching and it was not observed for the other films.

Luminescent measurements were also performed using confocal laser-scanning microscopy (CLSM) on **1.Eu** incorporated into the MMA/HEMA (1:3) hydrogel. Reflectance images showed that the complex was not homogeneously spread throughout the hydrogel. However, it was possible to observe the difference in emission between the films after soaking in acidic and basic solution for 24 h. As can be seen from the two images in Figure 7, the hydrogel incorporating 0.05% w/w of **1.Eu** at pH 2 shows the typical red emission of Eu(III), whereas at pH 11 the red emission is almost entirely quenched.

In conclusion, we have demonstrated that a cationic Eu(III)-based pH sensor can be incorporated into a soft material such as hydrogels. To the best of our knowledge this is the first time that such lanthanide based sensors have been incorporated into these types of

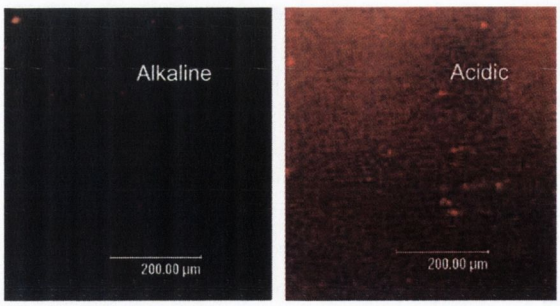

Figure 7. CLSM image of a section of hydrogel (MMA/HEMA, 1:3) incorporating 0.05% w/w **1.Eu** in acidic and basic media.

hydrogels. As **1.Eu** was not covalently bonded to any of the monomers used, there is a significant danger of leaching, where the water-soluble complex can diffuse from the gel into the environment, particularly upon prolonged storage. We are currently working towards overcoming this problem as well as working towards improving the 'switching' time between the 'off' and the 'on' stages, which are dependent on the diffusion rate of the analytes within the gel.

Acknowledgements

We thank Trinity College Dublin and the Queen's University Belfast, Center for Synthesis and Chemical Biology, Kinerton Ltd and The Royal Society (for a University Research Fellowship to McCoy) for financial support and Dr. John E. O'Brien for assisting with NMR and Dr. Ryan J. Morrow with the formation of hydrogels. We particularly thank Dr. Joseph P. Leonard for his continuous help.

References and notes

1. Rurack, K.; Resch-Genger, U. *Chem. Soc. Rev.* **2002**, *31*, 116; Rurack, K. *Spectrochem. Acta A* **2001**, *57*, 2161; Lavigne, J. J.; Anslyn, E. V. *Angew. Chem., Int. Ed.* **2001**, *40*, 3119; Beer, P. D.; Gale, P. A. *Angew. Chem., Int. Ed.* **2001**, *40*, 486; Fabbrizzi, L.; Licchelli, M.; Rabaioli, G.; Taglietti, A. F. *Coord. Chem. Rev.* **2000**, *205*, 85; Czarnik, A. W. *Acc. Chem. Res.* **1994**, *27*, 302.
2. Balzani, V. *Photochem. Photobiol. Sci.* **2003**, *2*, 459; Balzani, V.; Credi, A.; Venturi, M. *Pure Appl. Chem.* **2003**, *75*, 541; Brown, G. J.; de Silva, A. P.; Pagliari, S. *Chem. Commun.* **2002**, 2461; Ballardini, R.; Balzani, V.; Credi, A.; Gandolf, M. T.; Venturi, M. *Acc. Chem. Res.* **2001**, *36*, 445.
3. de Silva, A. P.; McCaughan, B.; McKinney, B. O. F.; Querol, M. *Dalton Trans.* **2003**, 1902; Raymo, F. M.; Giordani, S. *J. Am. Chem. Soc.* **2002**, *124*, 2004; Gunnlaugsson, T.; MacDónaill, D. A.; Parker, D. *Chem. Commun.* **2000**, 93.
4. Raymo, F. M. *Adv. Mater.* **2002**, *14*, 401.
5. Martínez-Máñez, R.; Sancenón, F. *Chem. Rev.* **2003**, *103*, 4419; Gale, P. A. *Coord. Chem. Rev.* **2000**, *199*, 181–233; Beer, P. D.; Gale, P. A. *Angew. Chem., Int. Ed.* **2001**, *40*, 486; Beer, P. D. *Chem. Commun.* **1996**, 689; de Silva, A. P.; Fox, D. B.; Huxley, A. J.; Moody, T. S. *Coord. Chem.*

Rev. **2000**, *205*, 41; de Silva, A. P.; Gunaratne, H. Q. N.; Gunnlaugsson, T.; Huxley, A. J. M.; McCoy, C. P.; Rademacher, J. T.; Rice, T. E. *Chem. Rev.* **1997**, *97*, 1515.

6. He, H.; Mortellaro, M. A.; Leiner, M. J. P.; Young, S. T.; Fraatz, R. J.; Tusa, J. K. *Anal. Chem.* **2003**, *75*, 549.
7. Gunnlaugsson, T.; Lee, T. C.; Parkesh, R. *Org. Biomol. Chem.* **2003**, *1*, 3265; Gunnlaugsson, T.; Kruger, P. E.; Lee, T. C.; Parkesh, R.; Pfeffer, F. M.; Hussey, M. G. *Tetrahedron Lett.* **2003**, *44*, 6575; Gunnlaugsson, T.; Nieuwenhuyzen, M.; Richard, L.; Thoss, V. *J. Chem. Soc., Perkin Trans. 2* **2002**, 141; Gunnlaugsson, T.; Davis, A. P.; Glynn, M. *Org. Lett.* **2002**, *4*, 2449; Gunnlaugsson, T.; Bichell, B.; Nolan, C. *Tetrahedron Lett.* **2002**, *43*, 4989; Gunnlaugsson, T.; Davis, A. P.; Glynn, M. *Chem. Commun.* **2001**, 2556.
8. Gunnlaugsson, T.; Kruger, P. E.; Jensen, P.; Pfeffer, F. M.; Hussey, M. G. *Tetrahedron Lett.* **2003**, *44*, 8909; Gunnlaugsson, T.; Kelly, J. M.; Nieuwenhuyzen, M.; O'Brien, A. M. K. *Tetrahedron Lett.* **2003**, *44*, 8571; Gunnlaugsson, T.; Leonard, J. P. *J. Chem. Soc., Perkin Trans. 2* **2002**, 1980; Gunnlaugsson, T.; Nieuwenhuyzen, M.; Richard, L.; Thoss, V. *Tetrahedron Lett.* **2001**, *42*, 4725.
9. Gunnlaugsson, T.; McCoy, C. P.; Morrow, R. J.; Phelan, C.; Stomeo, F. *Arkivoc* **2003**, *8*, 216 http://www.arkat-usa.org/ark/journal/2003/McKervey/McKervey_index.htm.
10. Pope, S. J. A.; Faulkner, S. *J. Am. Chem. Soc.* **2003**, *125*, 10526; Shavaleev, N. M.; Moorcraft, L. P.; Pope, S. J. A.; Bell, Z. R.; Faulkner, S.; Ward, M. D. *Chem. Commun.* **2003**, 1134; Parker, D.; Dickins, R. S.; Puschmann, H.; Cossland, C.; Howard, J. A. K. *Chem. Rev.* **2002**, *102*, 1977; Parker, D. *Coord. Chem. Rev.* **2000**, *205*, 109; Parker, D.; Williams, J. A. G. *J. Chem. Soc., Perkin Trans. 2* **1995**, 1305.
11. Gunnlaugsson, T.; Leonard, J. P. *Chem. Commun.* **2003**, 2424; Gunnlaugsson, T.; Harte, A. J.; Leonard, J. P.; Nieuwenhuyzen, M. *Supramol. Chem.* **2003**, *15*, 505; Gunnlaugsson, T.; Harte, A. J.; Leonard, J. P.; Nieuwenhuyzen, M. *Chem. Commun.* **2002**, 2134.
12. Gunnlaugsson, T.; Harte, A. J.; Leonard, J. P.; Senechal, K. *Chem. Commun.* **2004**, 782; Gunnlaugsson, T.; Harte, A. J.; Leonard, J. P.; Senechal, K. *J. Am. Chem. Soc.* **2003**, *125*, 12062; Faulkner, S.; Burton-Pye, B. P.; Kahn, T.; Martin, L. R.; Wray, S. D.; Skabara, P. J. *Chem. Commun.* **2002**, 1668.
13. Parker and co-workers have recently incorporated luminescent sensors into sol gels: Blair, S.; Kataky, R.; Parker, D. *New J. Chem.* **2002**, *26*, 530; Blair, S.; Lowe, M. P.; Mathieu, C. E.; Parker, D.; Senanayake, P. K.; Kataky, R. *Inorg. Chem.* **2001**, *40*, 5860.
14. (a) There are a few reports on the use of lanthanide ions in polyelectrolyte hydrogels and in polymer gels: Smirnov, V. A.; Sudhadolski, G. A.; Philippova, O. E.; Khokhlov, A. R. *J. Phys. Chem. B.* **1999**, *103*, 7621; Smirnov, V. A.; Philippova, O. E.; Sudhadolski, G. A.; Khokhlov, A. R. *Macromolecules* **1998**, *31*, 1162; (b) Other reports on the use of lanthanide ions in polymeric systems include: Liu, H. G.; Lee, Y. I.; Qin, W. P.; Jang, K. W.; Kim, S. S.; Feng, X. S. *J. Appl. Polym. Sci.* **2004**, *92*, 3524; Itaya, T.; Honda, T.; Kusumoto, N.; Matsumoto, A.; Inoue, K. *Polymer* **2003**, *44*, 2927; Beltran, J. B.; Cordoncillo, E.; Escribano, P.; Viana, B.; Sanchez, C. *J. Sol–Gel Sci. Technol.* **2003**, *26*, 977; Nishide, H.; Cho, M. D.; Kaku, T.; Okamoto, Y. *Macromolecules* **1993**, *26*, 2377; Yoshino, N.; Paoletti, S.; Kido, J.; Okamoto, Y. *Macromolecules* **1985**, *18*, 1513.
15. (a) Gunnlaugsson, T.; MacDónaill, D. A.; Parker, D. *J. Am. Chem. Soc.* **2001**, *123*, 12866; (b) Gunnlaugsson, T. *Tetrahedron Lett.* **2001**, *42*, 8901.
16. Gunnlaugsson, T.; Leonard, J. P.; Mulready, S.; Nieuwenhuyzen, M. *Tetrahedron* **2004**, *60*, 105.
17. *Synthesis of 2-{4,7-bis-dimethylcarbamoylmethyl-10-[(2-methyl-quinolin-4-ylcarbamoyl)-methyl]-1,4,7,10-tetraaza-cyclododeca-yl}-N,N-dimethyl-acetamide* (**1**). Compound **1** (0.272 g, 0.636 mmol), Cs_2CO_3 (0.228 g, 0.7 mmol), KI (0.116 g, 0.7 mmol) and **3** (0.164 g, 0.7 mmol) were added to DMF (35 mL). The mixture was heated at 80 °C under an inert atmosphere for 72 h. The solution was filtered and the solvent removed under reduced pressure. A dark orange viscous residue was obtained (0.359 g, 0.57 mmol) which was purified by precipitation from diethyl ether to give a brown solid in 53% yield. Calculated for $C_{32}H_{51}N_9O_4$: $(M + H)^+$ *m/z*: 626.4142. Found: 626.4163; δ_H (400 MHz, $(CDCl_3)$ 10.5 (1H, s, N*H*), 8.75 (1H, d, $J = 8.5$, Ar-*H*), 7.93 (1H, s, Ar-*H*), 7.89 (1H, d, $J = 8.5$ Hz, Ar-*H*), 7.57 (1H, t, $J = 6.0$ Hz, Ar-*H*), 7.43 (1H, t, $J = 6.0$ Hz, Ar-*H*), 3.86 (2H, s, $HNCOCH_2$), 2.70 (43H, m, $N–CH_3$, $CH_2CON(CH_3)_2$, cyclen CH_2); δ_C (100 MHz, $(CDCl_3)$) 172.1, 170.4, 170.3, 158.3, 148.0, 141.8, 128.7, 127.7, 124.6, 123.4, 119.7, 112.6, 57.6, 54.5, 54.4, 35.7, 35.6, 35.0, 28.8, 26.5, 25.2; *m/z*: 626.33 $(M + H)^+$, 313.67 $(M + 2H/2)^+$.
18. *Synthesis of 2-{4,7-bis-dimethylcarbamoylmethyl-10-[(2-methyl-quinolin-4-ylcarbamoyl)-methyl]-1,4,7,10-tetraaza-cyclododeca-yl}-N,N-dimethyl-acetamide Eu(III)* (**1.Eu**). Compound **1** (0.095 g, 0.15 mmol) and Eu(III) trifluoromethane sulfonate (0.1 g, 0.16 mmol) were added to a 25 mL single neck round bottom flask that contained freshly dried MeCN (10 mL). After three freeze–pump–thaw cycles, the solution was placed under an argon atmosphere and left stirring at reflux for 24 h. The resulting solution was cooled to room temperature and then added dropwise to dry diethyl ether (100 mL) with stirring. The resulting precipitate was isolated to give **1.Eu** as a pale green solid in 84% yield. δ_H (400 MHz, CD_3OCD_3) 12.7, 10.4, 8.0, 6.9, 3.1, 2.2, 1.6, −5.5, −6.2, −7.0, −8.5; *m/z*: 463.5 $(M + [triflate]/2)^+$, 259.4 $(M/3)^+$, 388.6 $(M/2)^+$.

Towards the development of controllable and reversible *'on-off'* luminescence switching in soft-matter; synthesis and spectroscopic investigation of 1,8-naphthalimide-based PET (photoinduced electron transfer) chemosensors for pH in water-permeable hydrogels

Thorfinnur Gunnlaugsson,[a*] Colin P. McCoy,[b*] Ryan J. Morrow,[b] Caroline Phelan,[a] and Floriana Stomeo[a]

[a]Department of Chemistry, Centre for Synthesis and Chemical Biology, Trinity College Dublin, Dublin 2, Ireland and
[b]School of Pharmacy, Queen's University Belfast, 97 Lisburn Road, Belfast BT9 7BL, UK
E-mail: gunnlaut@tcd.ie

Dedicated to Professor Michael Anthony McKervey on his 65th birthday
(received 01 Mar 03; accepted 27 May 03; published on the web 30 May 03)

Abstract
The synthesis of the pH PET sensors **1** and **2** is described. These molecules display *'on-off'* switching in their fluorescence as a function of pH in aqueous solution. From the luminescent changes pK_a values of 8.4(±0.1) and 6.3(±0.1) were determined respectively. These compounds were incorporated into poly[methylmethacrylate-*co*-2-(hydroxyethylmethacrylate)]-based hydrogels and the luminescent properties of the resulting polymeric films were investigated using confocal laser-scanning microscopy. Both sensors showed substantial luminescent switching in the soft-matter, where the emission was *'switched off'* after treating the hydrogels with alkaline solution and *'switched on'* under acidic conditions.

Keywords: Fluorescent sensor, switches, pH, hydrogels

Introduction

There is currently great interest within the field of supramolecular chemistry in developing miniaturized molecular devices that mimic or mirror the action of macroscopic devices such as switches, motors and other machinery.[1] Supramolecular devices that show large changes in their so called *'off'* and *'on'* states, where their 'states' refer to their luminescence, magnetic, or electronic properties, are of particular interest as these can be modulated, or tuned, by employing external sources, or 'inputs', such as ions, molecules, light, *etc.*[2,3] A part of this rapidly emerging

field is the developments of simple chemical sensors and switches.[4] In recent times, the development of luminescent based chemosensors for medical application has become highly desirable, in particular for use in clinical diagnosis, for monitoring essential electrolytes and small molecules (such as oxygen, sugars, *etc.*) in so-called 'whole-blood' measurements.[5]

We are active in this field and have previously developed fluorescent switches and sensors where the fluorescence is modulated or switched *'on'* or *'off'* as a function of the analyte.[6] These types of sensor are based on the use of the *'fluorophore-spacer-receptor'* model developed by de Silva at Queen's University Belfast.[7] In this design the excited state of the fluorophore can be quenched by intermolecular electron transfer from the receptor to the fluorophore (or *vice versa*) prior to the recognition. Upon recognition of species such as cations, the oxidation potential of the receptor is increased and this causes the electron transfer to be *'switched off'* and in turn the emission to be *'switched on'*.[8] We have recently modified this design to allow the detection of anions (such as acetate and phosphate) and bis-anions (such as pyrophosphate, lactate *etc.*)[9] In these modified systems the emission is *'switched on'* prior to the anion recognition, but upon recognition the reduction potential of the receptor is increased giving rise to enhanced quenching and hence the emission is *'switched off'*.

Recently we have further extended this area of research by developing both colorimetic[10] and also 'delayed lanthanide luminescence' sensors, by employing Eu(III) and Tb(III) which emit at long wavelengths with characteristic line-like emissions. These sensors benefit from large signal to noise ratio and a high signal quality.[11] Such long-lived excited states (in the ms range), are highly desirable for *in vivo* sensing since they overcome short-lived (~ns) background emission or autofluorescence and light scattering from the active biological environment.

Another way of overcoming these features is to have fluorophores that absorb and emit at long wavelengths.[12] Specifically, 4- or 3-amino-1,8-naphthalimides are of particular interest in this respect.[5,12,13] They absorb around 450 nm and emit in the green, with λ_{max} ~ 550 nm and a high fluorescence quantum yield. Moreover, they are easily synthesized in bulk quantities as well as being well suited for incorporation into polymeric matrixes and onto solid-surfaces. These properties are essential when employing such devices in real-time and on-line analysis. However, such immobilization often decreases the efficiency of the sensors, in particular as they are often placed into organic phases or lipophilic membranes that effect the uptake of the aqueous based analyte, the response time and the photophysical properties of the solid state device are also affected.[5]

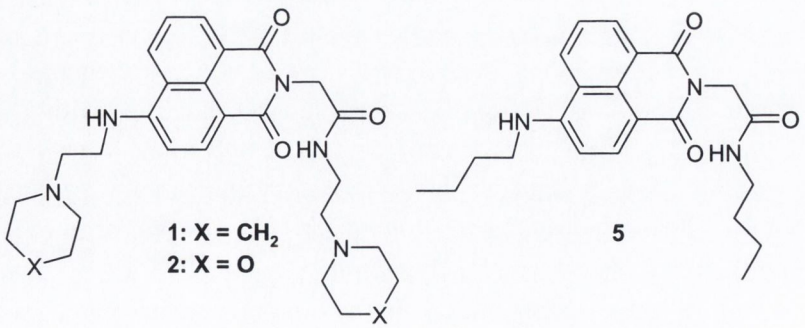

With this in mind we set out to develop novel fluorescent chemosensors based upon the amino-1,8-napthalimide structure and incorporate these into water-permeable hydrogels. Such hydrogels are easily handled and, when the composition is chosen judiciously, do not require that the sensor be covalently bonded to the polymeric matrix.[5,14,15] Compounds **1** and **2** are examples of our general design. In this paper we give account of our recent results on the synthesis of, as well as the solution and the soft-matter luminescent properties, of **1** and **2** as a function of pH.[§]

Results and Discussion

Design and synthesis of 1 and 2

The two chemosensors were designed for determining pH changes in the physiological pH range. As previously mentioned they are based on the *'fluorophore-spacer-receptor'* model developed by de Silva, where the 4-amino-1,8-naphthalimide moiety is the fluorophore and the piperidine and the morpholine amines are the proton acceptors. The ethylene spacer covalently separates the two units. In these particular cases, it was predicted that an electron transfer from the amine to the excited state of the fluorophore would quench fluorescence emission of the naphthalimide unit. This would represent the '*off-state*' as previously discussed.[16] In retrospect, the protonation of these amino moieties would increase the oxidation potential of the receptor, and as such, thermodynamically disallow the electron transfer.[16] Consequently the emission would be '*switched on*'. We chose piperidine and morpholine based amino derivatives to carry out this 'switching', but these two moieties have pKa's that overlap the physiological pH range.

As can be seen from these molecules, two amino moieties ('upper' and 'lower') were incorporated into the sensors. However, as demonstrated experimentally by de Silva *et al.*[16] only the receptor that is directly attached to the 4-amino moiety (the 'lower' moiety) is capable of quenching the excited state of **1** and **2**. This is due to the fact that molecules like **1** and **2**, have high exited state dipole moments that arise from their Internal Charge Transfer (ICT) excited state nature. In the case of **1** and **2** the amino moiety is acting as an electron donor, whereas the imide functions as an electron acceptor. Consequently, a push-pull mechanism is in operation, and due to charge repulsion, disallows the 'upper' amino to transfer an electron to the naphthalimide excited state. However, we predicted that the upper amine would substantially increase the water solubility of these molecules making them more acceptable to incorporation into hydrogels. This was indeed found to be the case as is discussed later.

The synthesis of **1** and **2** was achieved in two steps as shown in Scheme 1. The ester **4** was made in 77% yield by reacting the 4-chloro-1,9-naphthalic anhydride with glycine methyl ester in refluxing anhydrous toluene in the presence of triethyl amine. The desired product was isolated after treating it with aqueous acid, and recrystallization from methanol. The two chemosensors **1** and **2** were subsequently formed by reacting **4** in large excess of either 4-(2-aminoethyl)-piperidine or 4-(2-aminoethyl)-morpholine at 80°C for 12 hours. The resulting solutions were then cooled to room temperature before pouring them onto an ice water solution

with vigorous stirring. The two products were then isolated by filtration and washed several times with 1M HCl solution, affording the two products in 74 and 80% yield respectively. No further purification was necessary.

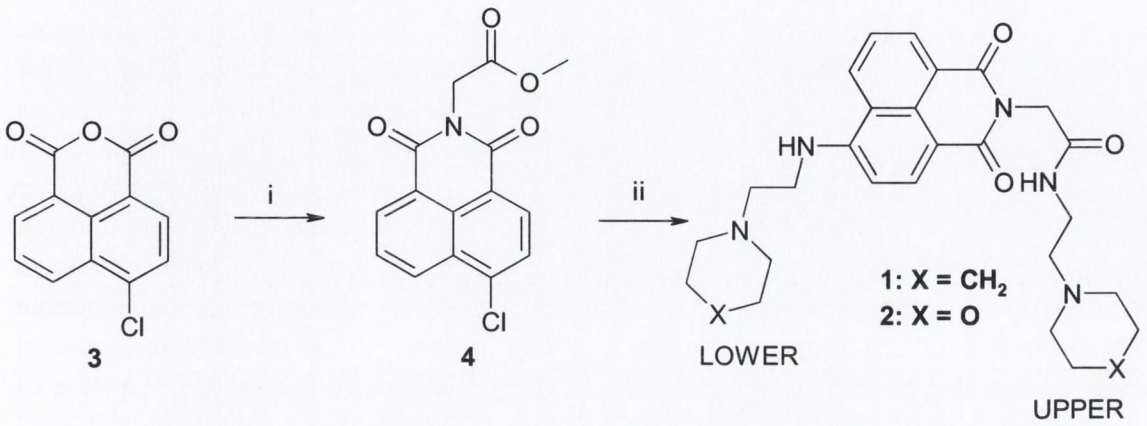

Scheme 1. i) Glycine methyl ester·HCl, toluene, triethyl amine, reflux 12 hours. ii) Neat amine, 80°C 12 hours.

The structures and purities of the desired products were confirmed by conventional techniques. For instance, in the ^{1}H NMR (400 MHz, $CDCl_3$) spectra a resonance at 6.56 ppm was observed. This is characteristic for the proton in position 3 of the naphthalimide ring. Furthermore, the protons for the two piperidine and the two morpholine moieties appear overlapped, but integrate to the correct number of protons for bi-substituted molecules. During the synthesis of **1** and **2**, no traces of the mono-substituted product were detected. Furthermore, the electro-spray mass spectrum contained the M^+ peaks at 492.3 and 495.8 and the $M+Na^+$ (due to complexation of Na+ form solvent during ionization) for **1** and **2** respectively, as well as showing some $M^+/2$ and $M+Na^+/2$ peaks, but no peaks attributed to the mono-substituted products.

Incorporation of 1 and 2 into hydrogels

In order to study the behaviour of **1** and **2** in a hydrogel matrix, **1** and **2** were effectively immobilized in a hydrogel comprising poly[methylmethacrylate-*co*-2-(hydroxyethylmethacrylate)] in a monomer ratio of 3:1 methylmethacrylate (MMA) to 2-(hydroxyethylmethacrylate) (HEMA) by weight, crosslinked with 1% by weight ethyleneglycol dimethacrylate and swollen to equilibrium in water. Hydrogels are, by definition, crosslinked polymers capable of taking up a significant proportion of their own weight of water while remaining insoluble in water.[17]

Amongst the most widely studied hydrogels are those based on poly(2(hydroxyethylmethacrylate)) (pHEMA).[18] pHEMA hydrogels swell markedly in water and swollen materials can comprise up to 70% water, depending on the quantity of crosslinker employed.[18,19] Such

hydrogels were found to be unsatisfactory for the current study as the permeability of the hydrogel was found to be such that immobilization of **1** and **2** was not permanent. To reduce the permeability, MMA was copolymerized with HEMA to give copolymers comprising a MMA/HEMA ratio of 3:1 (w/w). Using MMA as a comonomer contributes hydrophobic character to the resulting copolymer as homopolymeric pMMA takes up significantly less water than pHEMA. In order to achieve a homogeneous dispersion of **1** or **2** in the hydrogel, the appropriate sensor was dissolved in the monomer mixture prior to polymerization.

The mean equilibrium water content of the hydrogels studied was determined by measurement of loss in weight of three replicates of a sample following dehydration at 60°C for three days to constant weight. Hydrogels containing either 0.05% by weight **1** or **2** were found to comprise 10.1±0.6% by weight water. The equilibrium water content of the hydrogels was found to be pH independent, which is expected as the hydrogel contains no functional groups ionisable in the pH range studied. The immobilization of **1** or **2** was verified by allowing hydrogel segments to soak for 1 month in deionized water. This water was found to contain no trace of sensor as determined by UV-visible and fluorescence spectroscopies.

Ground and excited state investigation of 1 and 2 in solution

The photophysical properties of **1** and **2** were investigated in water, in the presence of 0.1M tetramethylammonium chloride (TMACl) to maintain constant ionic strength, prior to the incorporation into the hydrogels. Both compounds are highly coloured. When the UV-Visible spectra of **1** and **2** were recorded in alkaline solution at pH 12, a broad absorption was observed between 350 and 530 nm due to the ICT state (Figure 1), with λ_{abs} maximum at 450 nm. Upon acidification the band was blue shifted with small reductions in its maximum intensity at pH 6.42. However, upon further acidification the λ_{abs} became further blue shifted with small intensity enhancements. These changes can however, be considered to be only minor in comparison to the changes in the fluorescence spectra (see later). The reason for the blue shift is twofold. First, the protonation of the 'lower' tertiary amine will exert some weak charge repulsion on the 4-amino moiety of the fluorophores. However, the major reason is that in very acidic conditions the push-pull character of the ICT state is partially reduced due to the protonation of the 4-amino moiety itself (the pKa of this moiety is very low).

The fluorescence emission spectra of **1** and **2** were also recorded in water in the presence of 0.1M TMACl. In alkaline solution only a week emission was observed between 480 and 640 nm (Figure 2), with λ_{max} at *ca.* 550 nm. However, upon acidification the emission was gradually increased as demonstrated in Figure 2 for **2**. Similar results were found for **1**. After careful titration from pH 12 to 2.5, the emission maximal had shifted to *ca.* 535 nm, and the emission intensity had enhanced by over an order of magnitude. These changes are of such magnitude that they can be considered as representing two different 'states', where the fluorescence emission is *'switched off'* in alkaline solution and *'switched on'* in acidic solution. These changes are due to the protonation of the 'lower' amino moieties of the piperidine and the morpholine moieties. In

alkaline solution these moieties are engaged in PET quenching of the naphthalimide excited state, and upon protonation of these amines this quenching process in substantially removed.
As can be seen from Figure 2, some emission is observed in the alkaline solution. As the electron transfer is distance dependent (a function of $1/r^6$), for **1** and **2** the ethylene spacer gives rise to some deactivation of the excited state, even in alkaline solution, where it is in competition with PET.[20] However, it has recently been reported that the ethylene spacer shows greater biological resistance to degradation then a methylene spacer (which is commonly used),[7,8] which is important in the present context as these sensors are developed with the aim of continuous monitoring of pH in blood.[5]

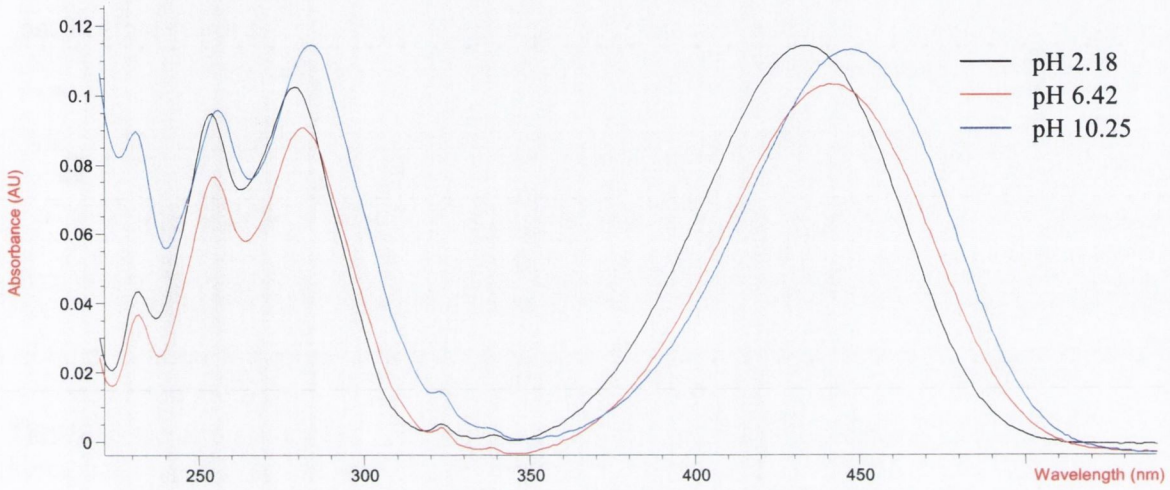

Figure 1. The UV-Visible spectra of **2** in water at three different pHs.

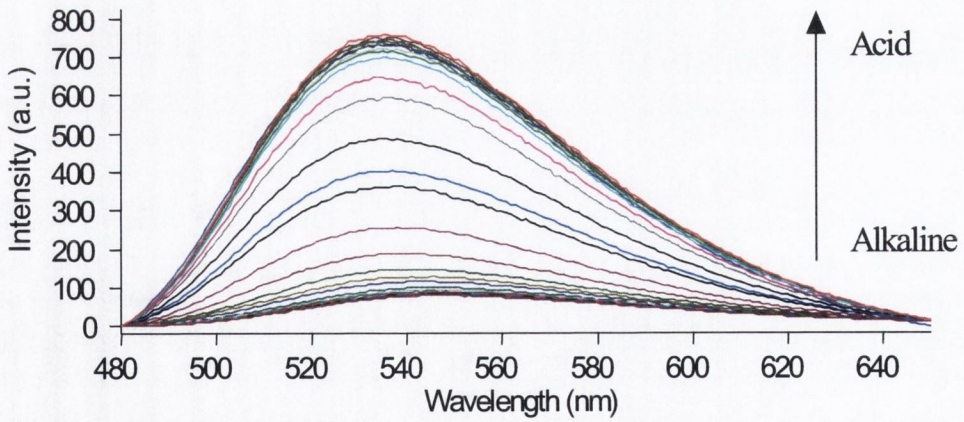

Figure 2. The changes in the fluorescence emission spectra of **2** as a function of pH in water. The pH range was from 12-2.5.

In contrast to the above results, compound **5**, which lacks the amino receptor, *did not show any changes* in emission properties as a function of pH except at very low pH where the 4-amino moiety was protonated. Compounds **1** and **2** are thus highly efficient *'off-on'* switches for pH. This switching process was also found to be reversible. From the changes in the fluorescence emission spectra as a function of pH, the pKa's of the two sensors can be determined. Figure 3, shows these changes when measured at 536 nm. From these changes the emission is *'switched off-on'* between *ca.* pH 7.5 and 9.5 for **1** and ca. 5.5 and 7.5 for **2**, which is an indication of 1:1 binding and simple equilibrium. From these changes a pKa values of 8.4(±0.1) and 6.3(±0.1) were determined. These results are consistent with compounds of similar nature that were developed by de Silva *et al.*[21] These pK_a values also indicate that these sensors, and in particularly **2**, would be well suited to monitor changes in the upper and the lower parts of the physiological pH range respectively.

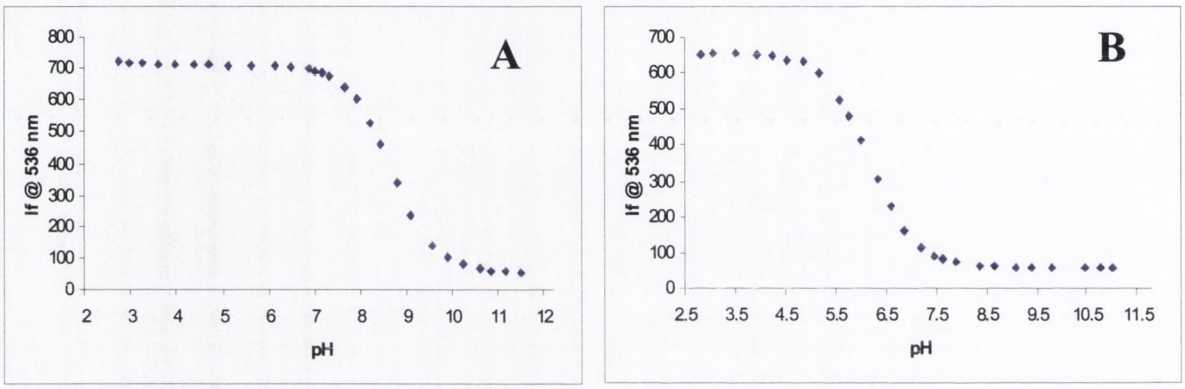

Figure 3. The changes in the fluorescence emission spectra of **1** (**A**) and **2** (**B**) at 536 nm as a function of pH.

Investigation of 1 and 2 after incorporation into hydrogels

As stated above the incorporation of these sensors into hydrogels was straightforward, as our design does not require the covalent incorporation into polymeric matrixes such as aminocellulose prior to the hydrogel formation.

As the hydrogel material used for immobilization of the sensors contains water, it was expected that the photophysical behaviour of **1** and **2** would be largely similar to that in solution. In order to characterize this behaviour, *in situ* fluorescence behaviour and distribution of **1** and **2** in the hydrogel matrices was examined using confocal laser-scanning microscopy (CLSM). CLSM allows direct, non-invasive measurement of fluorescence from the surface of a sample following excitation from an appropriate laser source.[22] To build up a single image, data is collected pixel by pixel with the laser rastering over the sample, with measurement of overall fluorescence intensity within a defined wavelength range being translated into a false colour for each pixel which correlates with that intensity.[23] Using this technique it is therefore possible to

obtain a spectrophotometric measurement of fluorescence emission from any defined area within a collected series of images. This allowed us to characterize both the distribution of the sensors within the hydrogel matrices and the fluorescence emission characteristics of the sensors on a macro (from square micron up to square millimetre) scale. Excitation was achieved using the 458nm line from a Ar/ArKr laser and monochromated xyλ data was collected as a series of scans with data being collected every 2.5nm with a bandwidth of 5nm over the range 465-750nm. A typical image showing emission integrated over the range 465-750nm is shown in Figure 4.

Figure 4. CLSM image of a typical section of hydrogel incorporating 0.05% w/w **2**, showing the homogeneity of the sensor within the hydrogel. This image was recorded at pH 2.5.

The xyλ data collected allowed fluorescence emission spectra from the surface of the bulk material in both acidic and basic media to be obtained. Figure 5 shows the fluorescence emission spectra obtained from a hydrogel containing **2** at pH values of 2.5 and 11.5.

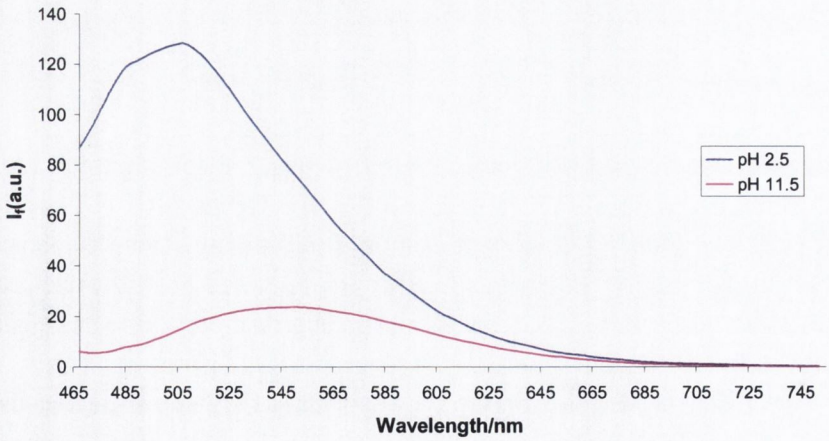

Figure 5. Fluorescence emission spectra obtained from a hydrogel containing 0.05% w/w **2** at pH values of 2.5 and 11.5.

As with solution measurements, the fluorescence behaviour of immobilized sensors was found to be strongly pH dependent, with a decrease in maximum intensity of emission of approximately an order of magnitude for a hydrogel at pH 11.5 compared to at pH 2.5. The emission maximum at pH 11.5 occurs at 550mn and at pH 2.5 at 510nm. This is consistent with the destabilization of the ICT excited state due to the proximity of the protonated amine to the partially positively charged end of the molecule at pH 2.5 as discussed for solution measurements. However, while the maximum at pH 11.5 occurs at almost the same wavelength as in solution (550nm), the maximum at pH 2.5 is further bathochromically shifted to 510nm compared to that observed in solution (532nm). This difference is attributable to the intermolecular forces between the sensors and the hydrophobic polymer chains, which further destabilize the polar excited state. We are currently carrying out further experiments on these compounds in hydrogels to quantify the effect of the adsorption of **1** and **2** on pHEMA chains. This work will be the subject of future publications.

Conclusions

In this paper we have given a comprehensive account of the design of two new pH PET sensors for monitoring pH changes in the physiological pH-range. The determined pK_a values for the two chemosensors **1** and **2** indicated that they would be able to monitor the necessary pH range. We incorporated these sensors into hydogels without having to covalently bind them to a resin or a polymeric support prior to incorporation. The luminescence properties of the resulting films were investigated using confocal laser-scanning microscopy. For both the emission was switched *'off'* or *'on'* as a function of pH, mirroring the behaviour in aqueous solution. We are currently investigating these features in much greater detail including developing films of different composition and thickness as well as incorporating chemosensors for other ions and molecules into these hydrogels.

Experimental Section

General Procedures. Melting points were determined using Electrothermal 1A9000 melting point apparatus. Infrared spectra were recorded on a Mattson Genesis II FTIR spectrophotometer equipped with a Gateway 2000 4DX2-66 workstation. Solid samples were dispersed in KBr and recorded as clear pressed discs. ^{1}H NMR spectra were recorded at 400 MHz using a Bruker Spectrospin DPX-400 instrument. ^{13}C NMR were recorded at 100 MHz using a Bruker Spectrospin DPX-400 instrument (both are referred to chloroform). Mass spectra were determined by detection using Electrospray on a Micromass LCT spectrometer, using a Waters HPLC. The whole system was controlled by MassLynx 3.5 on a Compaq Deskpro workstation. UV-Vis spectra were recorded on Shimadzu UV-2401 PC UV-Vis spectrometer (See Experimental Section).

Solution fluorescence emission spectra were recorded using Varian Cary Eclipse Fluorescence Spectrophotometer. Typically a solution of the sensor was made up with optical density of 0.2-0.25 in 50:50 MeOH:H_2O solvent systems containing the ionic strength. pH titrations were carried out by adjusting the pH of the above solution (10-20 ml) to high alkaline value (TBAOH or KOH) and aliquots of acid (HCl or TFA) were added. Determination of pKa and pM values was according to published proceadure.[17]

Hydrogel preparation

Crosslinked poly[methylmethacrylate-*co*-2-(hydroxyethylmethacrylate)] hydrogels were prepared by stirring a mixture of methylmethacrylate (7.35g), 2-(hydroxyethylmethacrylate) (2.45g), ethyleneglycol dimethacrylate (0.1g), azo-*bis*-isobutyronitrile (0.1g) and either sensor **1** or **2** (0.005g) until solution was complete, followed by injection of the monomer mixture into a 1mm mould with release liner. The mould was heated at 90°C for 6 hours and the resulting material washed thoroughly with deionised water and soaked in deionised water for 3 days.

Synthesis

***N*-(1-Methoxycarbonyl-methyl)-4-chloro-1,8-naphthalimide (4).** Glycine methyl ester hydro chloride (1.6 g, 12.7 mmol, 1.5 eq.), 4-chloro-1,8-naphthalic anhydride (2 g, 8.6 mmol, 1 eq.) and triethylamine (1.3 g, 1.8 ml, 12.7 mmol, 1.5 eq.) were refluxed in toluene (100 ml). After filtration through celite the mixture was reduced to dryness under reduced pressure. The resulting residue was dissolved in DCM and washed twice with 1.0 M HCl, once with water, dried over $MgSO_4$ and the solvent removed under reduced pressure, to give the desired product as a brown crystalline solid after recrystallisation from MeOH (2.0 g), in 77.0 % yield. m. p. 158 - 159°C; m/z found 304.0377 ($[M + H]^+$ $C_{15}H_{11}NO_4Cl$ requires 304.0371); δ_H (400 MHz, $CDCl_3$), 8.72 (1H, d, J = 7.5 Hz, Ar-H5), 8.58 (1H, d, J = 8.0 Hz, Ar-H7), 8.51 (1H, d, J = 7.5 Hz, Ar-H2), 8.1-7.9 (2H, m, Ar-H6, Ar-H3), 4.99 (2H, s, CH_2), 3.80 (3H, s, OCH_3); δ_c (100 MHz, $CDCl_3$), 168.4, 163.4, 139.6, 133.7, 132.4, 131.6, 131.5, 131.2, 131.1, 129.4, 129.3, 128.1, 127.9, 127.4, 122.6, 121.1, 52.5, 41.3; m/z: 327.2 $(M + Na)^+$, 329.2 630.5 $(2M + Na)^+$; ν_{max} (KBr)/cm^{-1} 1753, 1702, 1661. 1589, 1216, 1178.

General synthesis of 1 and 2 and related compounds

The 4-chloro-1,8-naphthalimide derivative (1 eq.) was suspended in excess amine. The resulting solution was heated to 80°C for 12 h. The product was precipitated out by pouring the resulting mixture onto an iced water solution with vigorous stirring. The product was filtered off and washed with 1N HCl solution. No further purification was necessary.

***N*-[1-(2-Piperidino-ethyl)-carboxamido-methyl]-4-(2-piperidino-ethylamino-1,8-naphthal-imide (1)** was synthesised by refluxing *N*-(1-methoxycarbonyl-methyl)-4-chloro-1,8-naphthal-imide, **3** (0.5 g, 1.6 mmol) in 4-(2-amino ethyl)-piperidine (2 ml) according to above procedure. The product was isolated after recrystallisation from EtOH as a bright orange powder (0.55 g, 74.3 % yield). m. p. 135 - 136°C; m/z: 492.2971 ($[M + H]^+$ $C_{28}H_{38}N_5O_3$ requires 492.2975); δ_H

(400 MHz, d_6-DMSO), 8.89 (1H, d, J = 8.5 Hz, Ar-H7), 8.44 (1H, d, J = 7.5 Hz, Ar-H5), 8.31 (1H, d, J = 8.5 Hz, Ar-H2), 7.99 (1H, t, J = 5.5 Hz, NH), 7.67 (1H, dd, J = 7.5, 8.0 Hz, Ar-H6), 7.62 (1H, t, J = 5.5 Hz, NH), 6.78 (1H, d, J = 8.5 Hz, Ar-H3), 4.62 (2H, s, CH_2CO), 3.51 (2H, q, J = 6.5, 6.0 Hz, CH_2), 3.31 (2H, q, J = 7.0, 6.0 Hz, CH_2), 2.58 (10H, m, (CH_2) x 5), 1.45-140 (14H, m, (CH_2) x 7); δ_c (100MHz, d_6-DMSO), 166.8, 163.6, 162.7, 150.6, 134.2, 130.6, 129.5, 128.4, 124.2, 121.8, 120.1, 107.5, 103.8, 57.5, 56.4, 54.1, 54.0, 41.9, 40.5, 36.3, 25.5, 25.4, 23.9; ν_{max} (KBr)/cm^{-1} 3396, 3381, 3300, 2937, 1693, 1653, 1589, 1397, 1106.

***N*-[1-(2-morpholino-ethyl)-carboxamido-methyl]-4-(2-morpholino-ethylamino)-1,8-naphthalimide (2)** was synthesised by refluxing *N*-(1-methoxycarbonyl-methyl)-4-chloro-1,8-naphthalimide, **3** (0.5 g, 1.6 mmol) in 4-(2-amino ethyl)-morpholine (2 ml) according to above procedure. The product was isolated after recrystallisation from DMF as a bright orange powder (0.62 g, 80 % yield). m. p. 242 - 243°C. Found: C, 62.80; H, 6.69; N, 14.09 %. $C_{26}H_{35}N_5O_5$ requires C, 62.76; H, 7.12; N, 14.07 %; δ_H (400 MHz, $CDCl_3$), 8.51 (1H, d, J = 7.5 Hz, Ar-H7), 8.44 (1H, d, J = 8.5 Hz, Ar-H5), 8.10 (1H, d, J = 8.5 Hz, Ar-H2), 7.62 (1H, dd, J = 8.0, 7.5 Hz, Ar-H6), 6.56 (1H, d, J = 8.0 Hz, Ar-H3), 6.45 (2H, br s, NH), 4.92 (2H, s, NCH_2), 3.78 (4H, s, $N(CH_2\underline{CH_2})_2O$), 3.50 (4H, s, $N(CH_2\underline{CH_2})_2O$), 3.46-3.43 (4H, br m, $NHCH_2$), 2.81 (2H, t, J = 5.5 Hz, CH_2N), 2.56 (4H, br s, $N(\underline{CH_2}CH_2)_2O$), δ 2.50 (2H, t, J = 5.5 Hz, CH_2N), 2.43 (4H, br s, $N(\underline{CH_2}CH_2)_2O$); δ_c (100 MHz, $CDCl_3$), 167.2, 164.0, 163.2, 149.5, 139.2, 137.6, 134.4, 131.0, 129.4, 126.2, 124.3, 121.9, 119.9, 108.9, 104.0, 66.6, 66.3, 56.2, 55.6, 52.8, 52.7, 42.6, 38.7, 35.2; m/z: 495.8 $(M)^+$, 517.8 $(M + Na)^+$; ν_{max} (KBr)/cm^{-1} 3374, 3300, 2942, 2825, 1691, 1652, 1588, 1397, 1109.

***N*-[1-(2-Butyl)-carboxamido-methyl]-4-(1-butylamino)-1,8-naphthalimide (5)** was synthesised by refluxing *N*-(1-methoxycarbonyl-methyl)-4-chloro-1,8-naphthalimide, **3** (0.3 g, 0.94 mmol) in *n*-butylamine (3 ml) according to the above procedure. The product was isolated after recrystallisation with DMF/water as a bright orange powder (0.25 g, 69.4 % yield). m. p. 239 - 240°C. Found: C, 68.54; H, 7.08; N, 10.87 %. $C_{22}H_{27}N_3O_3$ with 0.67 H_2O requires C, 68.46; H, 7.18; N, 10.89 %; δ_H (400 MHz, d_6-DMSO), 8.78 (1H, d, J = 8.5 Hz, Ar-H7), 8.44 (1H, d, J = 7.5 Hz, Ar-H5), 8.32 (1H, d, J = 8.5 Hz, Ar-H2), 8.01 (1H, br s, NH), 7.81 (1H, br s, NH), 7.67 (1H, t, J = 8.0 Hz, Ar-H5), 6.83 (1H, d, J = 9.0 Hz, Ar-H3), 4.56 (1H, s, CH_2CO), 3.42 (2H, q, J = 7.0, 6.0 Hz, $CONH\underline{CH_2}$), 3.10 (2H, q, J = 7.0, 6.0 Hz, $NHCH_2$), 1.67 (2H, quin, J = 7.0, 7.5 Hz, $CONHCH_2\underline{CH_2}$), 1.51 (4H, m, $CONH(CH_2)_2\underline{CH_2}$ and $NHCH_2\underline{CH_2}$), 1.33 (2H, sextet, J = 7.0, 7.5, 7.0 Hz, $NH(CH_2)_2\underline{CH_2}$), 1.03 (3H, t, J = 7.0 Hz, $CONH(CH_2)_3\underline{CH_3}$), 0.89 (3H, t, J = 7.0 Hz, $NH(CH_2)_3\underline{CH_3}$); δ_c (100MHz, d_6-DMSO), 166.7, 163.6, 162.7, 150.7, 134.2, 130.6, 129.6, 128.6, 124.1, 121.8, 120.1, 107.4, 103.7, 42.5, 41.9, 38.2, 31.1, 29.9, 19.7, 19.4, 13.7, 13.6; m/z: 382.1$(M)^+$, 309.0 $(M - NH(CH_2)_3CH_3)^+$; ν_{max} (KBr)/cm^{-1} 3443, 3316, 2955, 1690, 1664, 1629, 1583, 1534, 1377.

Acknowledgements

We thank Trinity College Dublin and Queen's University Belfast, National Pharmaceutical Biotechnology Centre, BioResearch Ireland, Centre for Synthesis and Chemical Biology, Kinerton Ltd and The Royal Society (for a University Research Fellowship to CPMcC) for financial support, Drs. Hazel M. Moncrieff and Frederick M. Pfeffer for helpful discussion and Dr. John E. O'Brien for assisting with NMR. We would particularly like to thank Professor A. P. de Silva, Queen's University of Belfast, and Dr. H. Q. Nimal Gunaratne, QUILL (Queen's University Ionic Liquid Laboratories), for their continuous support and friendship over the years.

References and Notes

[§] Parts of this work have been submitted as a communication.

1. (a) Rurack, K.; Resch-Genger, U.; *Chem. Soc. Rev.* **2002**, 116. (b) Lavigne J.J.; Anslyn E. V. *Angew. Chem. Int. Ed.* **2001**, *40*, 3119. (c) Amendola, V.; Fabbrizzi, L.; Mangano, C.; Pallavicini, P. *Acc. Chem. Res.* **2001**, *34*, 488. (d) de Silva, A. P.; Fox, D. B.; Huxley, A. J. M.; Moody, T. S. *Coord. Chem. Rev.* **2000**, *205*, 41.
2. (a) Fabbrizzi, L.; Licchelli, M.; Pallavicini, P. *Acc. Chem. Res.* **1999**, *32*, 846. (b) Czarnik, A.W. *Acc. Chem. Res.* **1994**, *27*, 302. (b) Raymo, F. M., *Adv. Mater.* **2002**, *14*, 401. (c) Raymo, F. M.; Giordani, S. *J. Am. Chem. Soc.* **2002**, *124*, 2004. (d) Raymo, F. M.; Giordani, S. *J. Am. Chem. Soc.* **2001**, *123*, 4651. (e) Balzani, V.; Credi, A.; Raymo, F. M.; Stoddart, J. F., *Angew. Chem. Int. Ed.* **2000**, *39*, 3348.
3. (a) Atwood, J. L.; Davies, J. E. D.; Macnicol D. D. *Comprehensive Supramolecular Chemistry,* Vögtle, F. Ed; Pergamon: England, 1996; Vol. 1, 2 and 10 (b) *Molecular Electronics and Molecular Electronic Devices*, Sienicki, K. Ed.; CRC Press: USA, 1993; Vol. 1-2. (c) Balzani V.; Scandola, F. *Supramolecular Photochemistry*, Ellis Horwood: Chichster, 1991.
4. (a) de Silva, A. P.; Gunaratne, H. Q. N.; Gunnlaugsson, T.; Huxley, A. J. M.; McCoy, C. P.; Rademacher J. T.; Rice, T. E. *Chem. Rev.* **1997**, *97*, 1515. (b) Fabbrizzi, L.; Licchelli, M.; Pallavicini, P. *Acc. Chem. Res.* **1999**, *32*. 846. (c) Licini, M.; Williams; J. A. G. *Chem. Commun.* **1999**, 1943.
5. He, H.; Mortellaro, M. A.; Leiner, M. J. P.; Young, S. T.; Fraatz, R. J.; Tusa, J. K. *Anal. Chem.* **2003**, *75*, 549, and references therein.
6. (a) Gunnlaugsson, T.; Nieuwnhuyzen, M.; Richard, L.; Thoss, V. *J. Chem. Soc. Peerkin 2,* **2002,** 141. (b) Gunnlaugsson T.; Bichell B.; Nolan C. *Tetrahedron Lett.* **2002**, *43*, 4989.
7. Bissell, R.A.; de Silva, A.P.; Gunaratne, H.Q.N.; Lynch, P.L.M.; Maguire, G.E.M.; McCoy C.P.; Sandanayake, K.R.A.S. *Top. Curr. Chem.* **1993**, *168*, 223.

8. (a) de Silva, A. P.; Fox. D. B.; Huxley, A. J. M.; McClenaghan, N. D.; Roiron, J. *Coord. Chem. Rev.* **1999**, *186*, 297. (b) de Silva, A. P.; Gunaratne, H. Q. N.; Gunnlaugsson, T.; Huxley, A. J .M.; McCoy, C. P.; Rademacher J. T.; Rice, T. E. *Chem. Rev.* **1997**, *97*, 1515.
9. (a) Gunnlaugsson, T.; Davis, A. P.; O'Brien, J.E.; Glynn, M. *Organic Lett.* **2002**, *4*, 2449. (b) Gunnlaugsson T.; Davis, A. P.; Glynn, M., *Chem. Commun.*, **2001**, 2556.
10. (a) Gunnlaugsson T.; Leonard *J. Chem. Soc. Perkin 2* **2002**, 1980. (b) Gunnlaugsson, T.; Nieuwnhuyzen, M.; Richard, L.; Thoss, V. *Tetrahedron Lett.* **2001**, *42*, 4725.
11. (a) Gunnlaugsson, T.; Harte, A. J.; Leonard, J. P.; Nieuwenhuyzen, M. *Supramol. Chem.* **2003**, *13*, in press. (b) Gunnlaugsson, T.; Harte, A. J.; Leonard, J. P.; Nieuwenhuyzen, M. *Chem. Commun.* **2002**, 2134. (c) Gunnlaugsson, T.; Mac Dónaill, D. A.; Parker, D. *J. Am. Chem. Soc.* **2001**, *123*, 12866. (d) Gunnlaugsson, T. Mac Dónaill D. A.; Parker, D. *Chem. Commun.* **2000**, 93. (e) Gunnlaugsson, T.; Parker, D. *Chem. Commun.* **1998**, 511.
12. (a) de Silva, A. P.; Gunaratne H.Q. N.; Lynch, P. L. M. *New. J. Chem.* **1996**, **20**, 871. (b) de Silva, A. P.; Gunaratne H.Q. N.; Rice, T. E. *Angew. Chem. Int. Ed. Engl.* **1996**, *35*, 2116.
13. (a) de Silva, A.P.; Rice, T.E. *Chem. Commun.,* **1999**, 163. (b) de Silva, A. P.; Gunaratne, H.Q.N.; Gunnlaugsson, T. *Tetrahedron Lett.* **1998**, *39*, 5077.
14. He, H.; Mortellaro, M. A.; Leiner, M. J. P.; Young, S. T.; Fraatz, R. J.; Tusa, J. K. *J. Am. Chem. Soc.* **2003**, *125*, 1468.
15. Recently, both Grabchev *et. al.* and Tian *et. al.* have developed polymers by incorporating 1,8-naphthalimide units covalently into the polymer backbone: (a) Grabchev, I.; Qian, X.; Xiao, Y.; Zhang, R. *New. J. Chem.* **2002**, *26*, 920. (b) Bojinov V.; Grabchev, I. *Dyes and Pigments* **2001**, *51*, 57. (c) Grabchev, I.; Bojinov, V.; Petkov, C. *Dyes and Pigm*ents **2001**, *51*, 1. (d) Grabchev, I. *Dyes and Pigments* **1998**, *38*, 219. (e) Tian, H.; Gan, J.; Chen, K.; He, K.; He, J.; Song, Q. L.; Hou, X. Y. *J. Mart. Chem.* **2002**, *12*, 1262. *Synthetic Metals* **2000**, *111*, 477.
16. de Silva, A. P.; Gunaratne H. Q. N.; McCoy, C. P. *Nature* **1993**, *364*, 42.
17. Lydon, M. J.; Minett, T. J.; Tighe, B. J. *Biomaterials* **1985**, *6*, 396.
18. (a) Wichterle, O.; Lim, D. *Nature* **1960**, *185*, 117. (b) Mack, E. J.; Okano, T.; Kim, S. W In Peppas, N. A. Ed. *Hydrogels in Medicine and Pharmacy, Volume 2: Polymers*, CRC Press: Boca Raton, **2000**, 65. (b) Peppas, N. A.; Bures, P.; Leobandung, W.; Ichikawa, H. *Eur. J. Pharm. Biopharm.* **2000**, *50*, 27.
19. (a) Rosiak, J. M.; Ulański, P.; Rzeźnicki, A. *Nucl. Instr. and Meth. in Phys. Res. B* **1995**, *105*, 335. (b) Rosiak, J. M.; Yoshii, F. *Nucl. Instr. and Meth. in Phys. Res. B* **1999**, *151*, 56.
20. Bissell, R.A.; de Silva, A.P.; Gunaratne, H.Q.N.; Lynch, P.L.M.; Maguire, G.E.M.; Sandanayake, K.R.A.S. *Chem. Soc. Rev.* **1992**, *21*,187.
21. de Silva, A. P.; Gunaratne, H.Q.N.; Habib-Jiwan, J.-L.; McCoy, C.P.; Rice, T.E.; Soumillion, J.-P. *Angew. Chem. Int. Ed. Engl.* **1995**, *34*, 1728.
22. (a) Paddock, S. W. *Biotechniques* **1999**, *27*, 992. (b) Wright, S. J.; Wright, D. J. *Methods in Cell Biol.* **2002**, *70*, 1. (b) Hanthamrongwit, M.; Wilkinson, R.; Osborne, C.; Reid, W. H.; Grant, M. H. *J. Biomed. Mater. Res.* **1996**, *30*, 331.
23. Paddock, S. W. *Mol. Biotechnol.* **2000**, *16*, 127.